THE
BENDIX
CORPORATION

GUIDANCE
SYSTEMS
DIVISION

TETERBORO,
NEW JERSEY 07608

SPACE CONSTRUCTION BASE CONTROL SYSTEM

FINAL REPORT

OCTOBER 27, 1978

PREPARED FOR:

GEORGE C. MARSHALL
SPACE FLIGHT CENTER
HUNTSVILLE, ALABAMA

NASA CONTRACT NO.
NAS8-32660

APPROVED BY:

D. A. Zomick

DR. D. A. ZOMICK
ENGINEERING MANAGER,
SYSTEMS ENGINEER AND
ANALYSIS

R. F. Kaczynski

R. F. KACZYNSKI
PROGRAM MANAGER

Stanley Seeb

S. SEEB
DIRECTOR OF ENGINEERING

FOREWORD

This Final Report is submitted in accordance with the Statement of Work, Exhibit "A" for Contract NAS8-32660. The study was directed from the Guidance Systems Division (GSD) of The Bendix Corporation. The program manager at this location for most of the contractural period was Mr. James Jennings. Contributors from GSD were Mr. Raymond Kaczynski (Sections 1 through 4) and Dr. Frederick Chichester (Section 7). Other tasks were completed by personnel from the Bendix Research Laboratories Division (BRL) and the Bendix Energy, Environment and Technology Office (BEETO). Material in Sections 5 and 6 was contributed by Dr. Kelvin Smith, Don Johnson and Dave Sidlosky. Mr. Art Cornell of BRL generated the dynamic mathematical models for the Space Construction Base and Mr. Donald Lipski of BRL wrote the programs for digital simulation. Mr. Calvin Rybak of BEETO wrote a technical paper which provides the basis for the material presented in Section 8. The guidance of Dr. Michael Borelli of MSFC throughout the study is gratefully achnowledged.

ABSTRACT

Many aspects of an attitude control system are studied and developed for a large space base that is structurally flexible and whose mass properties change rather dramatically during its orbital lifetime. Topics of discussion include the following:

a. Space base orbital pointing and maneuvering
b. Angular momentum sizing of actuators
c. Momentum desaturation selection and sizing
d. Multilevel control technique applied to configuration 1
e. One-dimensional model simulation
f. N-body discrete coordinate simulation
g. Structural analysis math model formulation
h. Discussion of control problems and control methods

TABLE OF CONTENTS

SECTION NO.	TITLE	PAGE NO.
	ABSTRACT	i
1.0	INTRODUCTION	1-1
1.1	OBJECTIVES	1-1
1.2	SCOPE	1-1
1.3	GENERAL	1-3
2.0	MISSION DEFINITION	2-1
2.1	PHYSICAL CONFIGURATION	2-1
2.1.1	MODULE DEFINITION	2-15
2.1.2	MASS PROPERTIES	2-18
2.2	ORBITAL PARAMETERS	2-23
2.3	OPERATIONAL REQUIREMENTS	2-24
2.3.1	MISSION TIMELINE	2-24
2.3.2	ATTITUDE POINTING AND MANEUVERING	2-24
2.3.3	GENERAL REQUIREMENTS	2-33
2.3.4	CONFIGURATION PECULIAR REQUIREMENTS	2-33
3.0	ACTUATOR SIZING	3-1
3.1	LONG TERM DISTURBANCES	3-1
3.1.1	GRAVITY GRADIENT	3-2
3.1.2	AERODYNAMIC	3-8
3.1.3	MAGNETIC	3-14
3.1.4	RADIATION	3-17
3.1.5	VEHICLE ROLL DURING X LOCAL VERTICAL ORIENTATION	3-27
3.1.6	SUMMARY	3-33
3.2	SHORT TERM DISTURBANCES	3-39

TABLE OF CONTENTS (CONT'D)

SECTION NO.	TITLE	PAGE NO.
3.2.1	CREW DISTURBANCES	3-40
3.2.2	DOCKING	3-46
3.3	MOMENTUM EXCHANGE ACTUATORS	3-48
3.3.1	ROLL AXIS MANEUVERING	3-50
3.3.2	ALTERNATE NON-ROLLING SOLAR POINTING APPROACH	3-53
3.4	REFERENCES	3-56
4.0	MOMENTUM DESATURATION	4-1
4.1	DESATURATION REQUIREMENTS	4-1
4.2	MAGNETIC DESATURATION	4-1
4.3	RCS DESATURATION	4-9
4.4	GRAVITY GRADIENT DESATURATION	4-9
4.5	SUMMARY	4-12
4.6	REFERENCES	4-15
5.0	CONTROL SYSTEM APPROACH	5-1
5.1	INTRODUCTION	5-1
5.2	CONTROL PROBLEMS AND APPROACH	5-3
5.3	CONTROL FUNCTIONS	5-3
5.4	SYSTEM CONCEPT	5-6
5.5	SPECIAL PROBLEM AREAS	5-8
5.6	APPENDAGE AND MODULE STABILIZING CONTROLS	5-10
5.7	VEHICLE CONTROL COORDINATOR	5-16
5.8	DISTRIBUTION OF SENSORS AND ACTUATORS	5-19
5.9	MULTIVARIABLE DESIGN ANALYSIS	5-21
6.0	DIGITAL SIMULATION	6-1
6.1	DESCRIPTION OF ONE-DIMENSIONAL MODELS	6-1
6.2	SOLAR WING DECOUPLING CONTROL STUDY USING THE ONE-DIMENSIONAL MODEL	6-12

TABLE OF CONTENTS (CONT'D)

SECTION NO.	TITLE	PAGE NO.
6.3	STUDIES WITH THREE-DIMENSIONAL MODELS	6-19
7.0	APPLICATION OF MULTILEVEL CONTROL TECHNIQUES TO SPACE CONSTRUCTION BASE	7-1
7.1	INTRODUCTION	7-1
7.2	GENERAL DECOMPOSED MODEL	7-2
7.2.1	BACKGROUND	7-2
7.2.2	DECOMPOSED TRANSLATIONAL STATE EQUATIONS	7-4
7.2.3	DECOMPOSED ROTATIONAL STATE EQUATIONS	7-10
7.3	CONSTRUCTION OF PERFORMANCE INDEX	7-17
7.4	FORMATION OF THE HAMILTONIAN	7-25
7.4.1	GENERAL DISCUSSION	7-25
7.4.2	HAMILTONIAN CORRESPONDING TO LOCAL VERTICAL STABILIZATION CONTROL	7-25
7.5	DEVELOPMENT OF COSTATE EQUATIONS	7-28
7.6	DEVELOPMENT OF CONTROL ALGORITHM	7-34
7.7	ADDITIONAL NECESSARY OPTIMALITY CONDITIONS	7-35
7.8	CONSTRUCTION OF SUBPROBLEM HIERARCHIES	7-39
7.9	REFERENCES	7-50
8.0	STRUCTURAL ANALYSIS TASK	8-1
8.1	INTRODUCTION	8-1
8.2	BACKGROUND	8-2
8.3	EQUATIONS OF MOTION FOR SINGLE CONNECTION POINT BETWEEN BODIES	8-6
8.4	EQUATIONS OF MOTION FOR MULTIPLE CONNECTION POINT BETWEEN BODIES	8-22
8.5	NOMENCLATURE	8-30

TABLE OF CONTENTS (CONT'D)

SECTION NO.	TITLE	PAGE NO.
9.0	CONCLUSIONS AND RECOMMENDATIONS	9-1
9.1	INTRODUCTION	9-1
9.2	MISSION PROFILE	9-1
9.3	ACTUATOR SIZING	9-1
9.4	MOMENTUM DESATURATION	9-2
9.5	CONTROL SYSTEM APPROACH	9-2
9.6	DIGITAL SIMULATION	9-4
9.7	MULTILEVEL CONTROL	9-4
9.7.1	RESULTS	9-4
9.7.2	RECOMMENDATIONS	9-6
9.8	STRUCTURAL ANALYSIS OF FLEXIBLE BODY CHARACTERISTICS	9-7

APPENDIX

A	DETAILED DESCRIPTION OF N-BODY MODEL
B	ALTERNATE FREQUENCY DOMAIN METHODS FOR THE ATTITUDE CONTROL OF A FLEXIBLE SPACE VEHICLE
C	COSTATE AND CONTROL EQUATIONS FOR MODIFIED SUBPROBLEM HIERARCHY WITH LOCAL VERTICAL ATTITUDE STABILIZATION CONTROL

LIST OF FIGURES

FIGURE NO.	TITLE	PAGE NO.
2-1	SPACE CONSTRUCTION BASE CONFIGURATION 1	2-2
2-2	SPACE CONSTRUCTION BASE CONFIGURATION 2	2-3
2-3	SPACE CONSTRUCTION BASE CONFIGURATION 3	2-4
2-4	SPACE CONSTRUCTION BASE CONFIGURATION 4	2-5
2-5	SPACE CONSTRUCTION BASE CONFIGURATION 5	2-6
2-6	SPACE CONSTRUCTION BASE CONFIGURATION 6	2-7
2-7	SPACE CONSTRUCTION BASE CONFIGURATION 7	2-8
2-8	SPACE CONSTRUCTION BASE CONFIGURATION 8	2-9
2-9	SPACE CONSTRUCTION BASE CONFIGURATION 9	2-10
2-10	SPACE CONSTRUCTION BASE CONFIGURATION 10	2-11
2-11	SPACE CONSTRUCTION BASE CONFIGURATION 11	2-12
2-12	SPACE CONSTRUCTION BASE CONFIGURATION 12	2-13
2-13	SPACE STATION CO-ORDINATE SYSTEM	2-19
2-14a	SPACE BASE TIMELINE	2-25
2-14b	SPACE BASE TIMELINE	2-26
3-1	GEOMETRY OF THE SPACE BASE IN EARTH ORBIT, Y_v SOLAR POINTING SHOWN	3-4
3-2	DEFINITION OF COORDINATE SYSTEMS AND ANGLES FOR X LOCAL VERTICAL ORIENTATION	3-28
3-3	VEHICLE ROLL ANGLE (ϕ) AND SOLAR PANEL ANGLE (δ) FOR ONE COMPLETE ORBIT AS A FUNCTION OF THE ORBIT PLANE TO SUN ANGLE	3-31
3-4	WALL PUSHOFF CREW DISTURBANCE	3-43
3-5	DOCKING DISTURBANCE	3-43
3-6	SOLAR POWER EFFICIENCY FOR X LOCAL VERTICAL ATTITUDE AS A FUNCTION OF β ANGLE AND NUMBER OF ADDITIONAL CMG UNITS REQUIRED	3-52
3-7	SOLAR POWER AVERAGE EFFICIENCY VS. BETA ANGLE FOR THE ALTERNATE NON-ROLLING APPROACH	3-54

LIST OF FIGURES (CONT'D)

FIGURE NO.	TITLE	PAGE NO.
4-1	BASIC ORIENTATION OF MAGNETIC TORQUERS	4-4
4-2	BLOCK DIAGRAM OF MAGNETIC TORQUING	4-5
5-1	SPACE BASE CONTROL CONCEPT	5-7
5-2	CONCEPT FOR MAIN BODY AND APPENDAGE ACTUATION	5-12
5-3	CONCEPT FOR DECOUPLING CONTROL	5-13
5-4	CONCEPT FOR ARTIFICIAL STIFFENING	5-14
5-5	CONCEPT FOR ARTIFICIAL DAMPING	5-15
5-6	BASIC VEHICLE COORDINATOR CONCEPT	5-17
5-7	VEHICLE CONTROL COORDINATOR WITH ON-BOARD IDENTIFICATION	5-18
5-8	STABILIZING CONTROL BASED ON LINEAR OPTIMAL CONTROL	5-22
5-9	DIGITAL CONTROL SYSTEM	5-23
5-10	STABILIZING CONTROL WITH PARTIAL DECOUPLING	5-27
5-11	SEPARATION OF DECOUPLING OPERATION	5-28
6-1	N-BODY, ONE-DIMENSIONAL MODEL	6-1
6-2	THREE BODY, ONE-DIMENSIONAL MODEL	6-6
6-3	VIBRATIONAL MODES	6-8
6-4	APPLICATIONS OF THE ONE-DIMENSIONAL MODEL	6-9
6-5	DECOUPLING CONTROL	6-13
6-6	DECOUPLING PERFORMANCE, TORSIONAL AXIS OF SOLAR WING	6-15
6-7	DECOUPLING PERFORMANCE, NORMAL AXIS OF SOLAR WING	6-16
6-8	DECOUPLING PERFORMANCE, LATERAL AXIS OF SOLAR WING	6-17
6-9	N-BODY MODEL OF SPACE BASE	6-20

LIST OF FIGURES (CONT'D)

FIGURE NO.	TITLE	PAGE NO.
7-1	TOPOLOGICAL TREE OF SPACE BASE RIGID BODIES	7-3
7-2	OVERALL CONTROL PROBLEM STRUCTURE	7-4
7-3	TRANSLATIONAL SUBPROBLEM HIERARCHY WITHOUT CONTROL	7-9
7-4	BODY i TRANSLATIONAL SUBPROBLEM HIERARCHY FOR i=1,8	7-10
7-5	ROTATIONAL SUBPROBLEM HIERARCHY WITHOUT CONTROL	7-15
7-6	BODY i ROTATIONAL SUBPROBLEM HIERARCHY FOR i=1,2,...,n	7-16
7-7	SUBPROBLEM HIERARCHY FOR MULTILEVEL LOCAL VERTICAL ATTITUDE STABILIZATION CONTROL WITHOUT TRANSLATIONAL EQUATIONS	7-41
7-8	SUBPROBLEM HIERARCHY FOR MULTILEVEL LOCAL VERTICAL ATTITUDE STABILIZATION CONTROL WITH TRANSLATIONAL EQUATIONS	7-44
7-9	REDUCED SUBPROBLEM HIERARCHY FOR MULTILEVEL LOCAL VERTICAL ATTITUDE STABILIZATION CONTROL WITH TRANSLATIONAL EQUATIONS	7-47
8-1	VEHICLE CONFIGURATION	8-7
8-2	TYPICAL CONNECTION POINT BETWEEN BODIES "j" AND "ℓ"	8-23

LIST OF TABLES

TABLE NO.	TITLE	PAGE NO.
2-1	MODULE ACRONYMS	2-14
2-2	SPACE CONSTRUCTION BASE / DIMENSION SUMMARY	2-20
2-3	ELEMENTS OF THE INERTIA MATRIX	2-22
2-4	CREW REQUIREMENTS FOR THE SCB MISSION	2-27
2-5	POINTING AND MANEUVERING REQUIREMENTS FOR THE SPACE CONSTRUCTION BASE	2-28
2-6	GENERAL REQUIREMENTS FOR THE SCB MISSION	2-29
2-7	CONFIGURATION PECULIAR REQUIREMENTS FOR THE SCB MISSION	2-30
3-1	ANGULAR MOMENTUM REQUIREMENTS DUE TO GRAVITY GRADIENT TORQUES	3-7
3-2	ATMOSPHERIC MASS DENSITY	3-11
3-3	MAGNETIC TORQUES AND ANGULAR MOMENTUM FOR THE SPACE BASE	3-16
3-4	RADIATION FORCES ON LARGE SURFACES OF SPACE BASE	3-21
3-5	INTENSITY OF RADIATION FOR INERTIAL XPOP ORIENTATION	3-23
3-6	INTENSITY OF RADIATION FOR X LOCAL VERTICAL ORIENTATION	3-23
3-7	RADIATION FORCES AND ANGULAR MOMENTUM	3-24
3-8	ANGULAR MOMENTUM DUE TO RADIATION FORCES	3-25
3-9	ANGULAR ROLL RATE AND MOMENTUM REQUIREMENTS	3-32
3-10	SUMMARY OF ANGULAR MOMENTUM DUE TO LONG TERM CYCLIC TORQUES	3-35
3-11	SUMMARY OF ANGULAR MOMENTUM DUE TO LONG TERM BIAS TORQUES	3-37

LIST OF TABLES (CONT'D)

TABLE NO.	TITLE	PAGE NO.
3-12	DISTURBANCE LOCATIONS ON THE SCB	3-41
3-13	PHYSICAL CHARACTERISTICS OF SCB VEHICLE DISTURBANCE LOCATIONS	3-44
3-14	PHYSICAL CHARACTERISTICS OF DISTURBANCE LOCATIONS FOR SCB BODIES	3-45
3-15	NUMBER OF DGCMG UNITS REQUIRED FOR ANGULAR MOMENTUM ENVELOPE	3-49
4-1	SCB REQUIREMENTS FOR MOMENTUM DESATURATION	4-2
4-2	MAGNETIC TORQUING CHARACTERISTICS	4-7
4-3	RCS CHARACTERISTICS	4-8
4-4	RELATIVE DISADVANTAGES OF THE DESATURATION SCHEMES CONSIDERED FOR THE SPACE CONSTRUCTION BASE	4-13
4-5	RECOMMENDATIONS FOR MOMENTUM MANAGEMENT	4-14
5-1	CONTROL SYSTEM DESIGN TRADES AND CONSIDERATIONS	5-9
5-2	CONSIDERATIONS FOR SENSOR AND ACTUATOR DISTRIBUTION	5-20
6-1	ONE DIMENSIONAL MODEL PARAMETERS FOR CONFIGURATION I	6-10
6-2	DECOUPLING CONTROL GAINS	6-14
6-3	TYPICAL FINGE POINT CHECK	6-21
6-4	TYPICAL COMPARISON OF RESULTS BETWEEN THE THREE DIMENSIONAL AND ONE DIMENSIONAL MODELS FOR THE TORSIONAL MODE	6-22

LIST OF TABLES (CONT'D)

TABLE NO.	TITLE	PAGE NO.
7-1	NUMBER OF RIGID BODIES PER CONFIGURATION	7-2
7-2	DEGREES OF FREEDOM	7-4
7-3	NUMBERS OF SCALAR EQUATIONS TO BE SOLVED FOR LOCAL VERTICAL ATTITUDE STABILIZATION CONTROL	7-48

SECTION 1

1.0 INTRODUCTION

This report is submitted in compliance with the Statement of Work contract NAS8-32660 Exhibit "A." The period of performance covered by the report is the calendar year of July 27, 1977 to July 27, 1978. The submission and approval of this report constitute the successful completion of the Exhibit "A" portion of the contract. Additional studies, basically a continuation of the present work effort, will be conducted under an Exhibit "B" Scope of Work.

1.1 OBJECTIVES

The sections that follow summarize the effort expended on the Space Construction Base (SCB) Control System Study contract. The topics discussed are diverse in content but all represent a portion of the overall study. The primary objective of the study was to develop a control system and flexible control techniques that will stabilize a large and growing space station of the future.

1.2 SCOPE

The thrust of the program occurred in several unique directions. A hypothetical space mission was developed using the basic information generated by NASA, and requirements and timeline were formulated. From this initial baseline the effort branched into several categories:

1. Defining a mathematical model to be used in an all up and limited stability model.
2. Investigation of modern control techniques as an integral part of the control system.
3. Development of a mathematical model that would describe the flexible structure characteristics of a large vehicle assuming the model characteristics of the individual pieces are known.
4. Determine sizing requirements for a momentum storage system taking into account gravity gradient, magnetic, aerodynamic and radiation torques. Requirements were determined for:

    a. All configurations, various orientations (X-POP, X-LV, XP-POP, etc.)
    b. Inertial pointing modes anywhere in the celestial sphere (configurations 4 through 7).
    c. Earth pointing modes (configuration 12).

The results of these studies have become the bas s for the development of the control system. At presen t, the simulation effort is in progress and is expected to continue into the extension effort. The structural math model effort will also be continued. An attempt will be made to validate the model by using known spacecraft data. Other tasks such as the mission profile, multilevel analysis and angular momentum sizing are essentially complete in themselves, and will be used only as reference material during the continuation.

1.3 GENERAL

Several appendices containing detailed equations and modeling are included at the end of the report. When necessary, sequences of equations are included in the body of the report.

The RFQ requested that the International System of units (designated as SI) be used in the program and in any reporting. Expression in customary units would be acceptable if it is useful to the primary recipients, but SI should be stated first with the customary units afterwards, in parenthesis. In the report, SI units are often used (magnetic and radiation); torques, angular momentum, moments of inertia and distances, however, are stated in English units since this was the method used in presenting all of the data in the RFQ.

A liberal approach was also taken in the numbering of SCB configurations. The RFQ initially used Roman numerals, but the text here uses Arabic numerals in most cases -- except where material is reprinted from the RFQ.

SECTION 2

2 0 MISSION DEFINITION

A mission profile is defined which identifies those parameters which are the necessary inputs to the control system definition. Those parameters are defined in reference 2-1 using information obtained from

a. the RFP data package (reference 2-2)
b. conversation with MSFC and others
c. best estimates.

2.1 PHYSICAL CONFIGURATION

The Space Construction Base concept consists of a baseline configuration shown in Figure 2-1. This configuration, which is later expanded, includes a Habitability Module (crew quarters), Subsystem Module (control center), Turret Assembly (rotating member and structural support for the solar wings), Solar Wings A and B, and a Docking Module. The docking module plays a major role in the buildup to a larger structure since, in many configurations, it becomes the attachment point for the next module.

The space base modules are transported to orbit by the Shuttle Orbiter. The Orbiter Remote Manipulator System extracts the payloads from the orbiter payload bay and aids in the docking (berthing) and connect on of the modules.

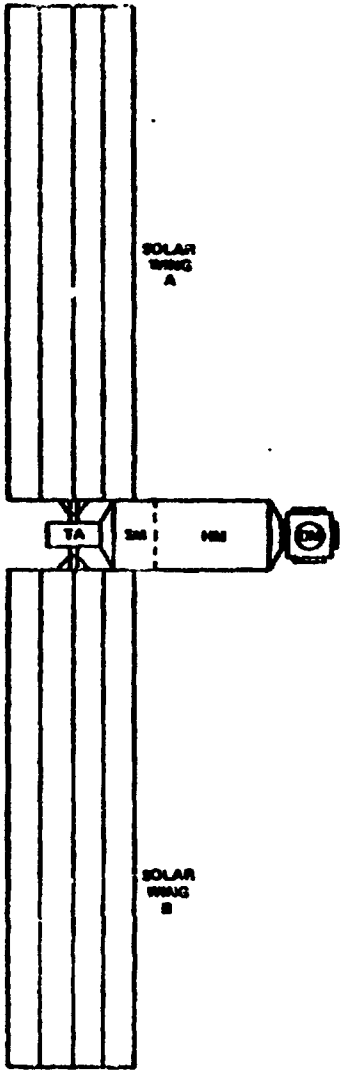

FIGURE 2-1
SPACE CONSTRUCTION BASE-CONFIGURATION 1

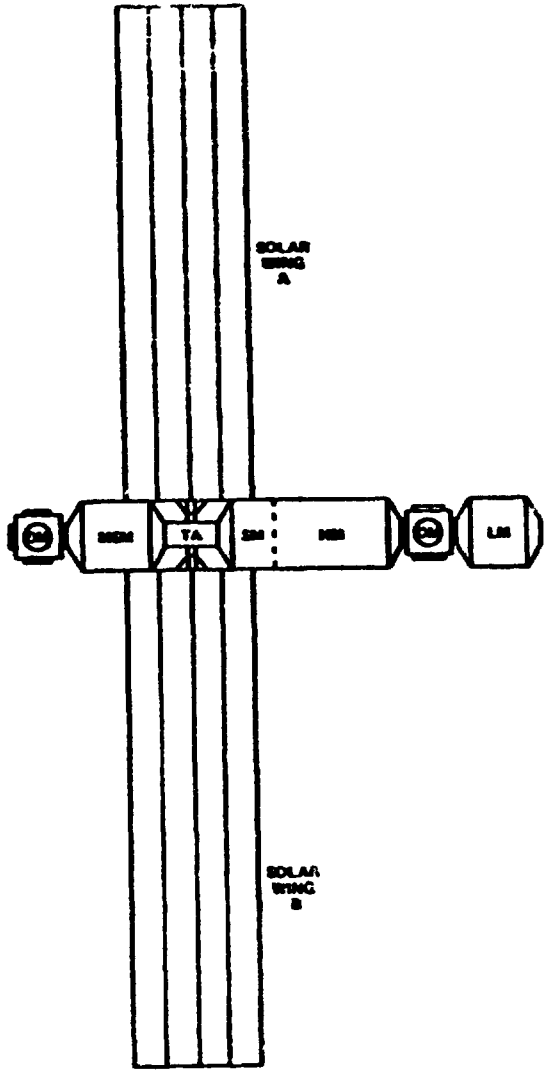

FIGURE 2-2

SPACE CONSTRUCTION BASE-CONFIGURATION 2

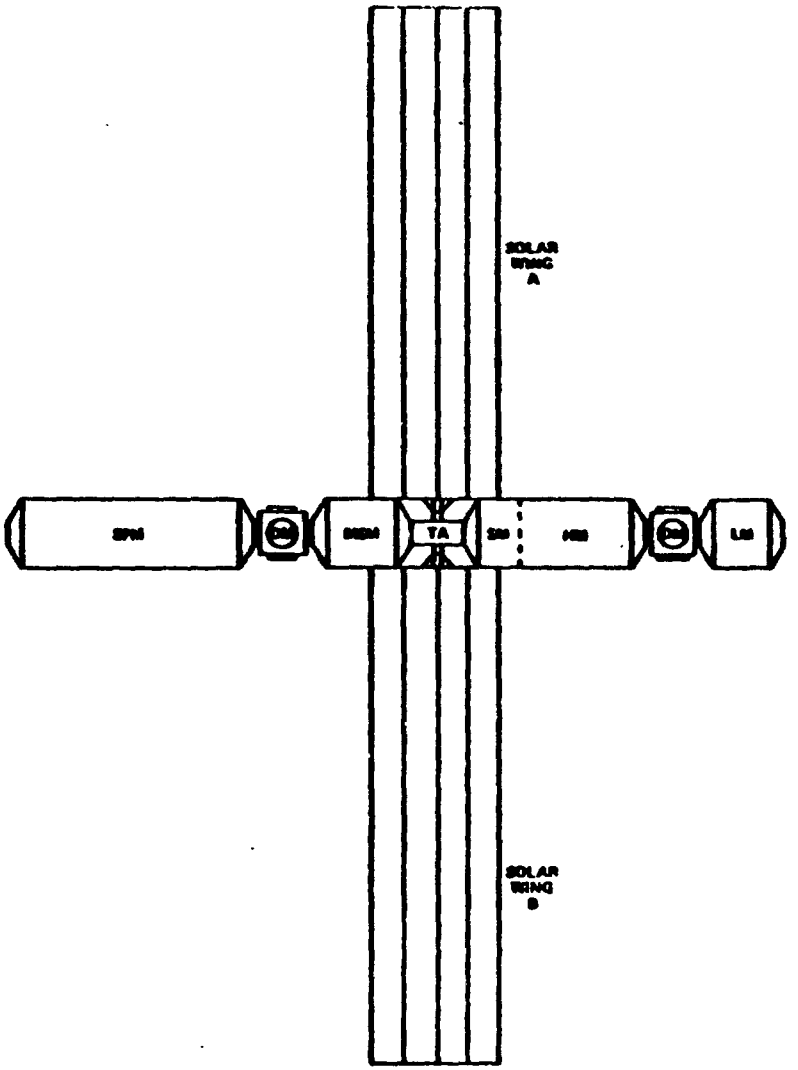

FIGURE 2-3

SPACE CONSTRUCTION BASE-CONFIGURATION 3

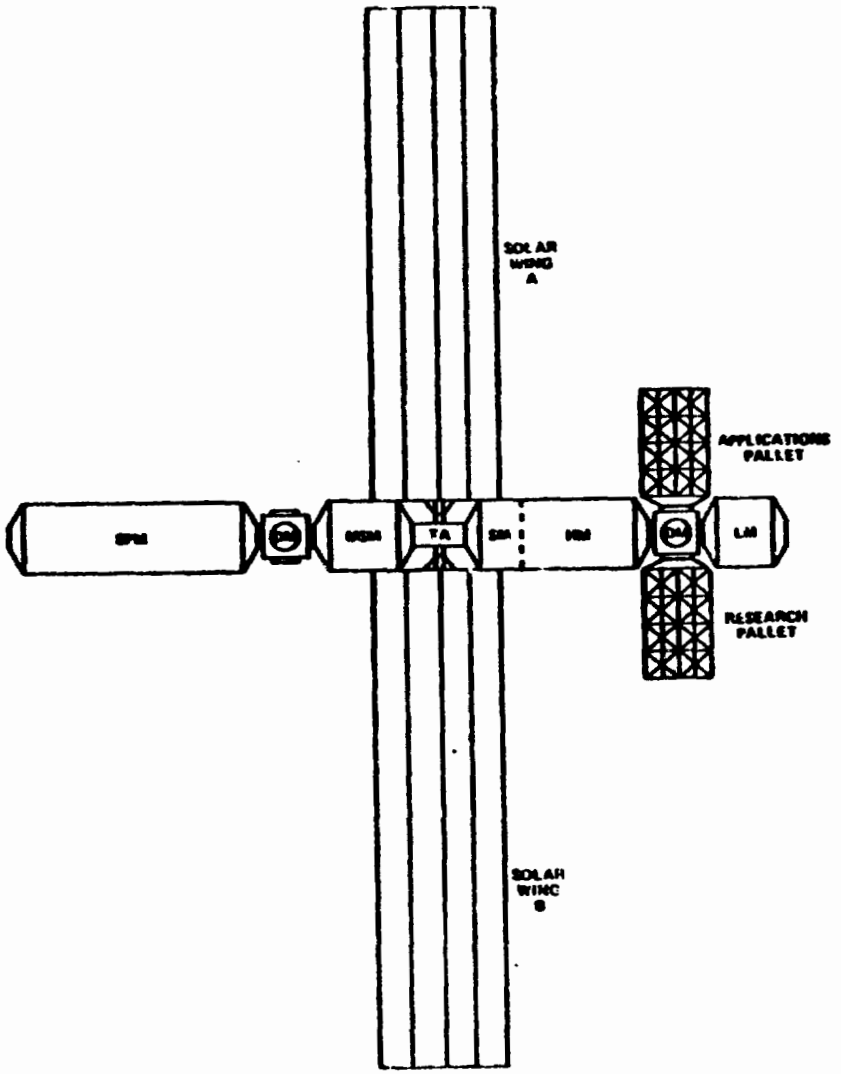

FIGURE 2-4

SPACE CONSTRUCTION BASE-CONFIGURATION 4

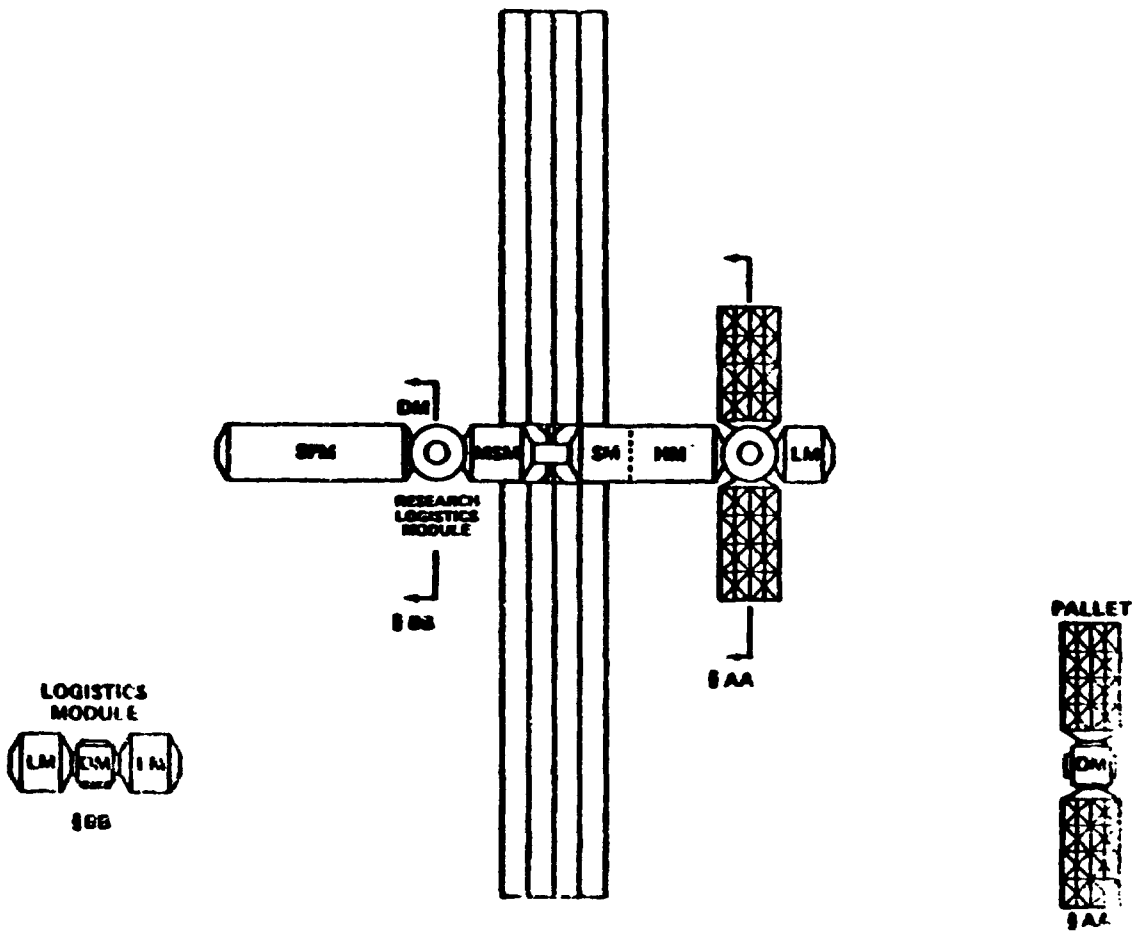

FIGURE 2-5

SPACE CONSTRUCTION BASE-CONFIGURATION 5

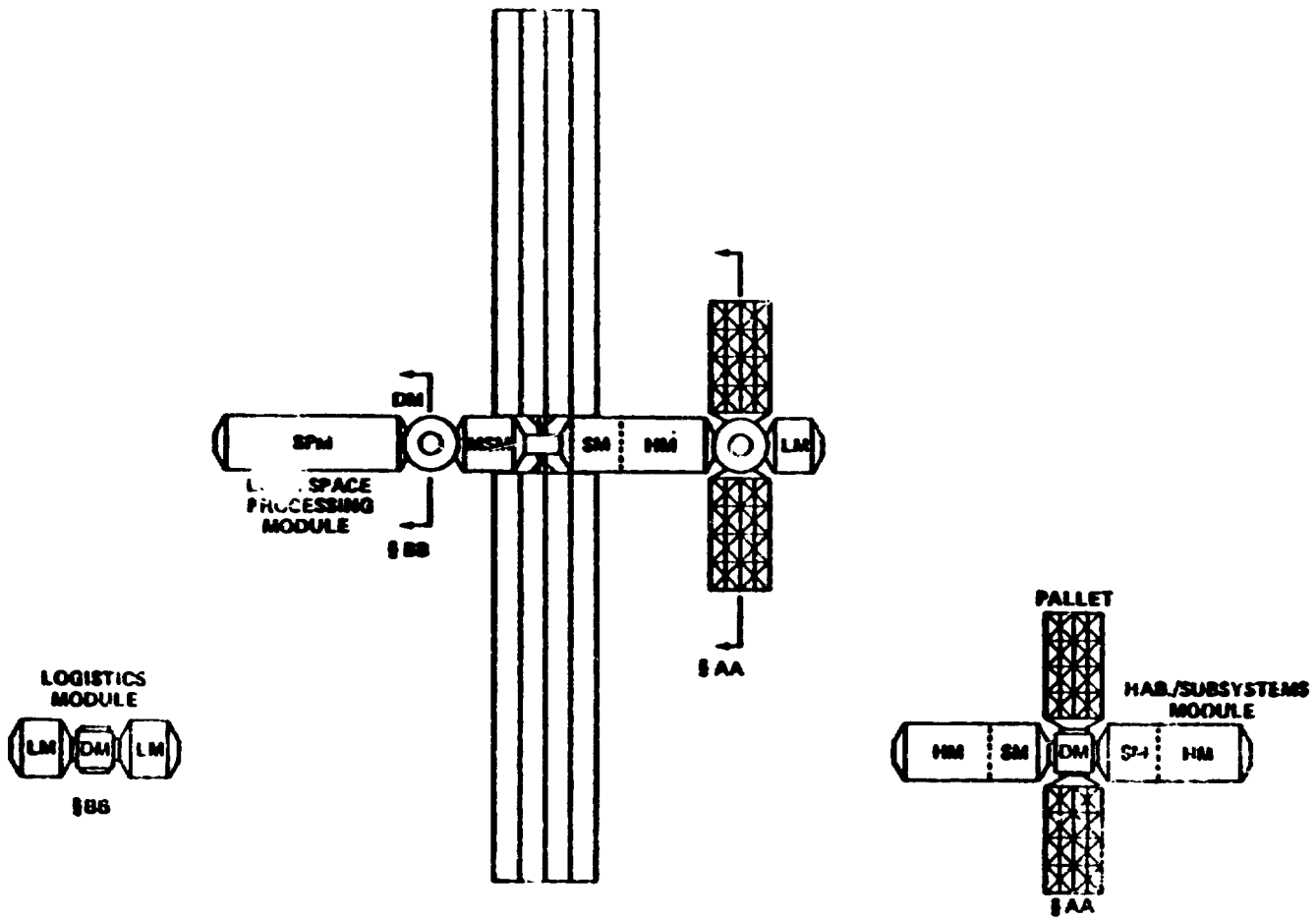

FIGURE 2-6

SPACE CONSTRUCTION BASE-CONFIGURATION 6

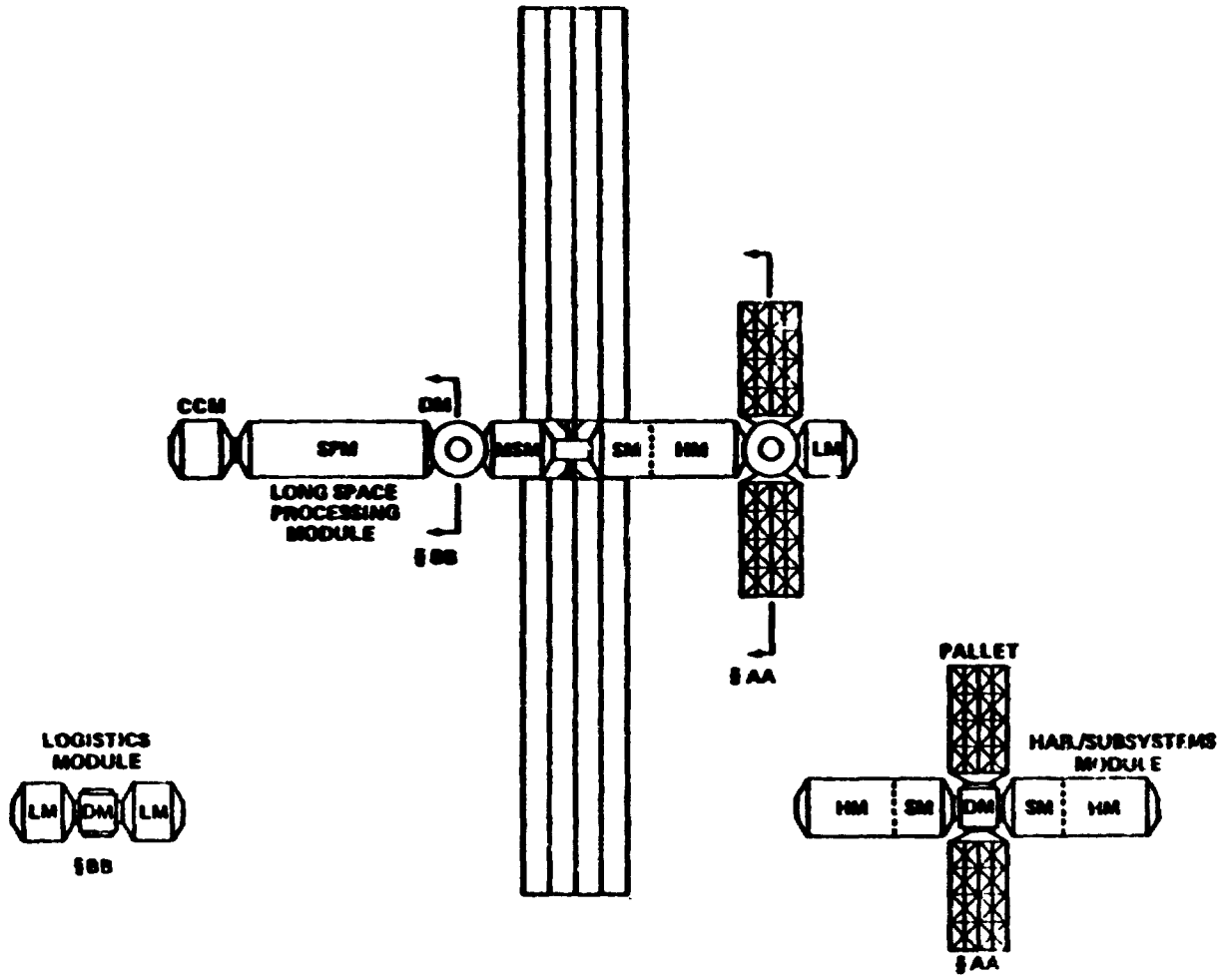

FIGURE 2-7

SPACE CONSTRUCTION BASE-CONFIGURATION 7

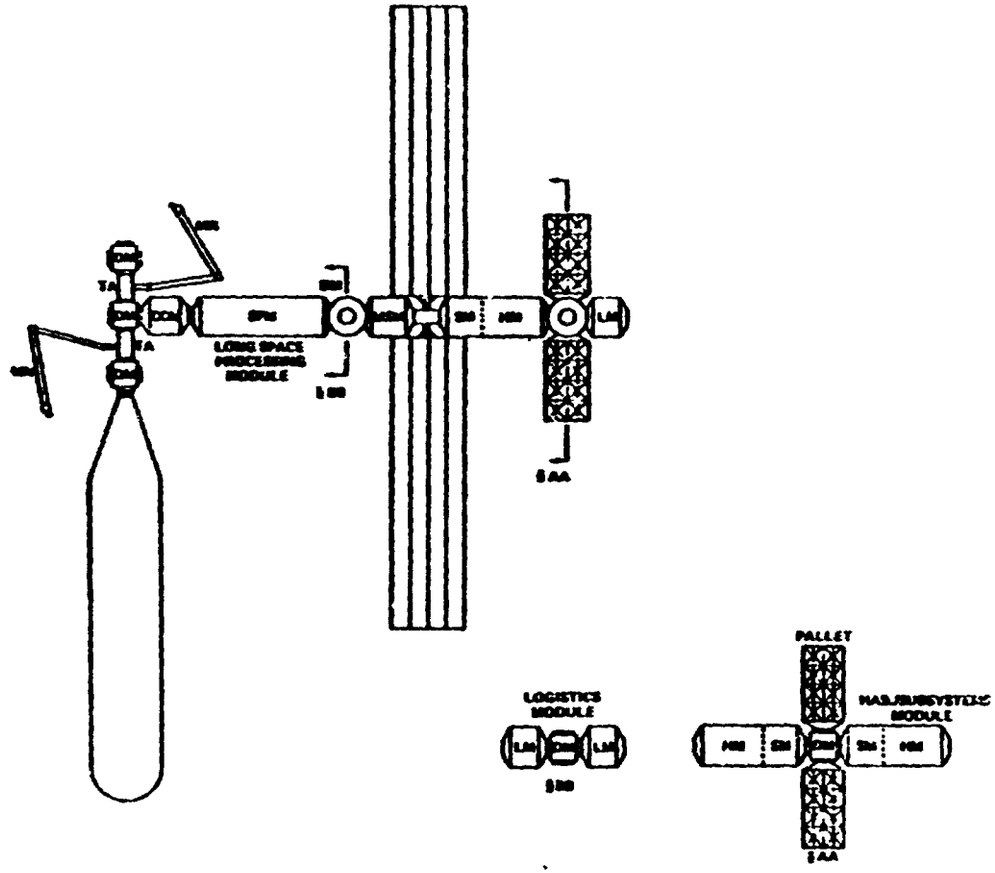

FIGURE 2-8

SPACE CONSTRUCTION BASE-CONFIGURATION 8

FIGURE 2-9
SPACE CONSTRUCTION BASE-CONFIGURATION 9

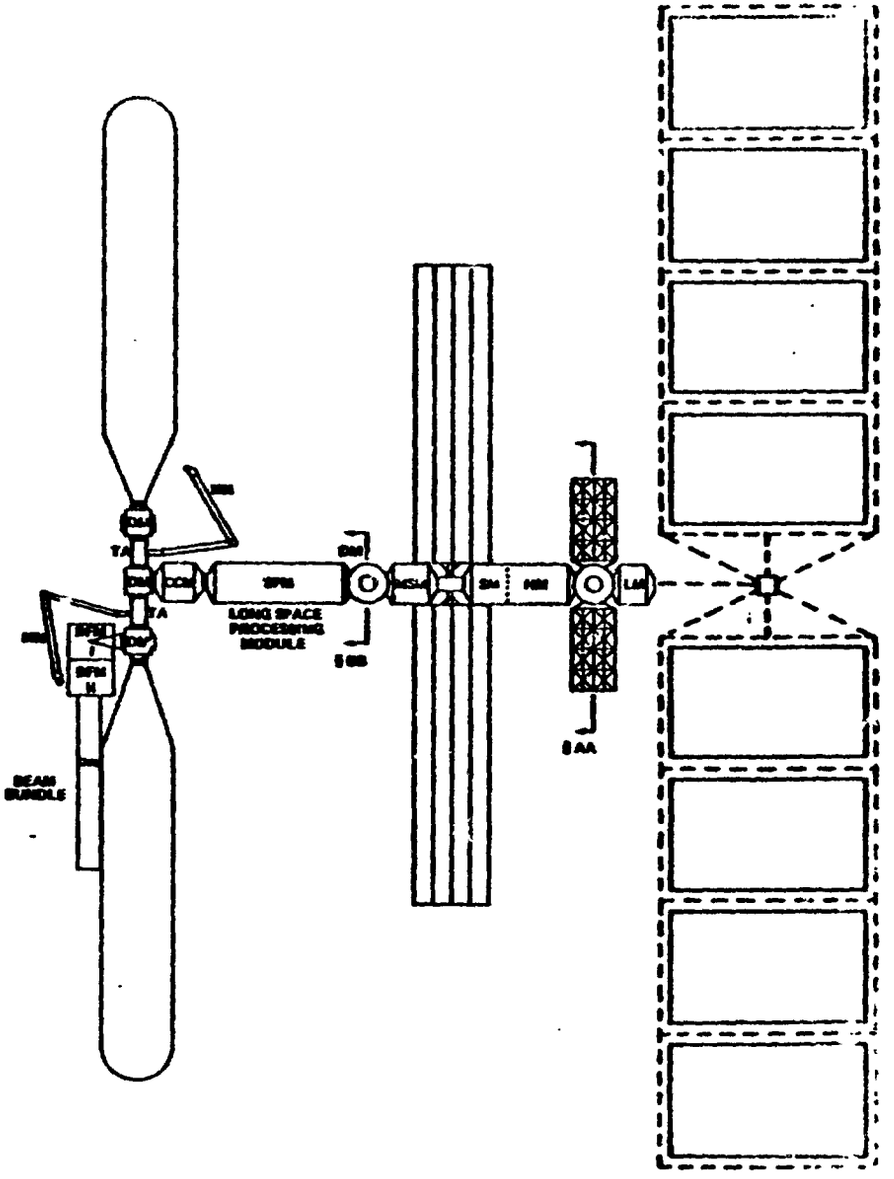

FIGURE 2-10
SPACE CONSTRUCTION BASE-CONFIGURATION 10

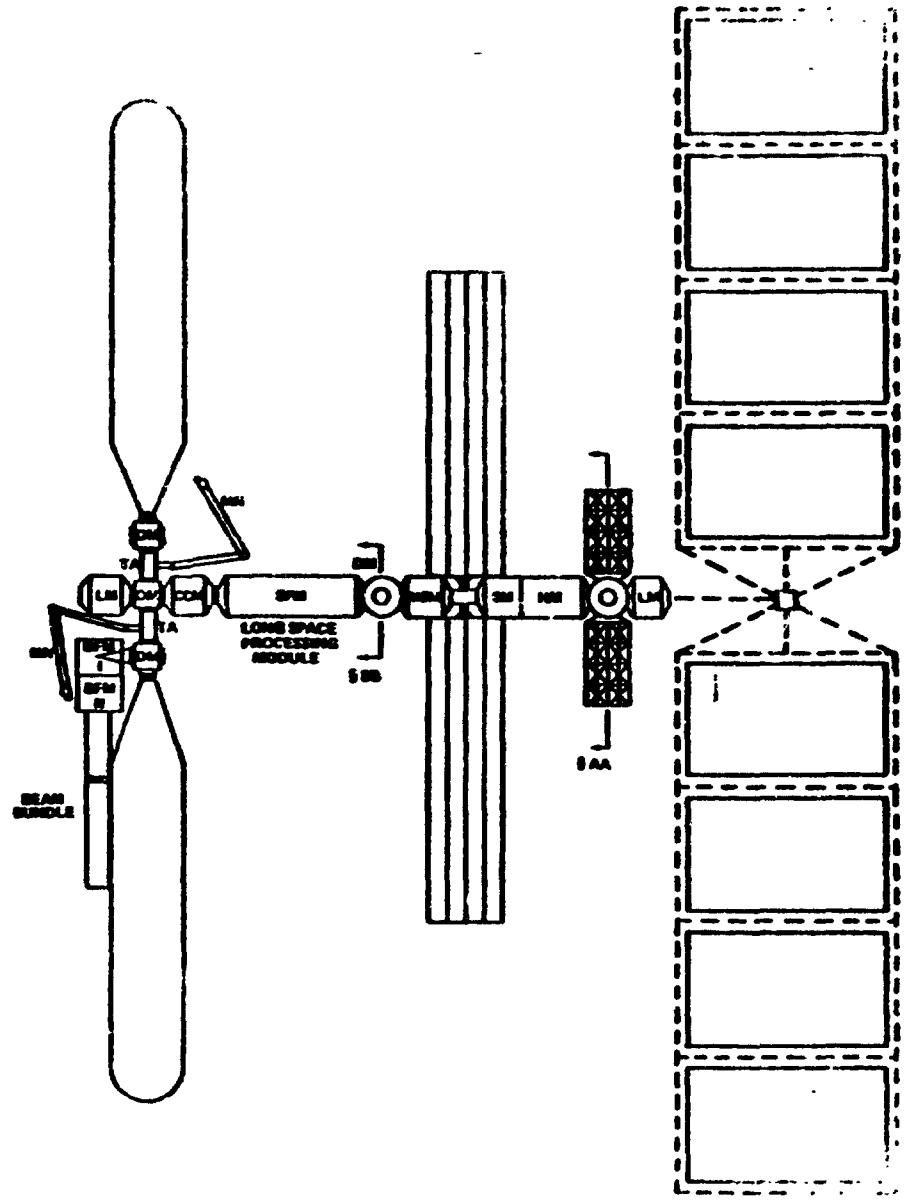

FIGURE 2-11

SPACE CONSTRUCTION BASE-CONFIGURATION 11

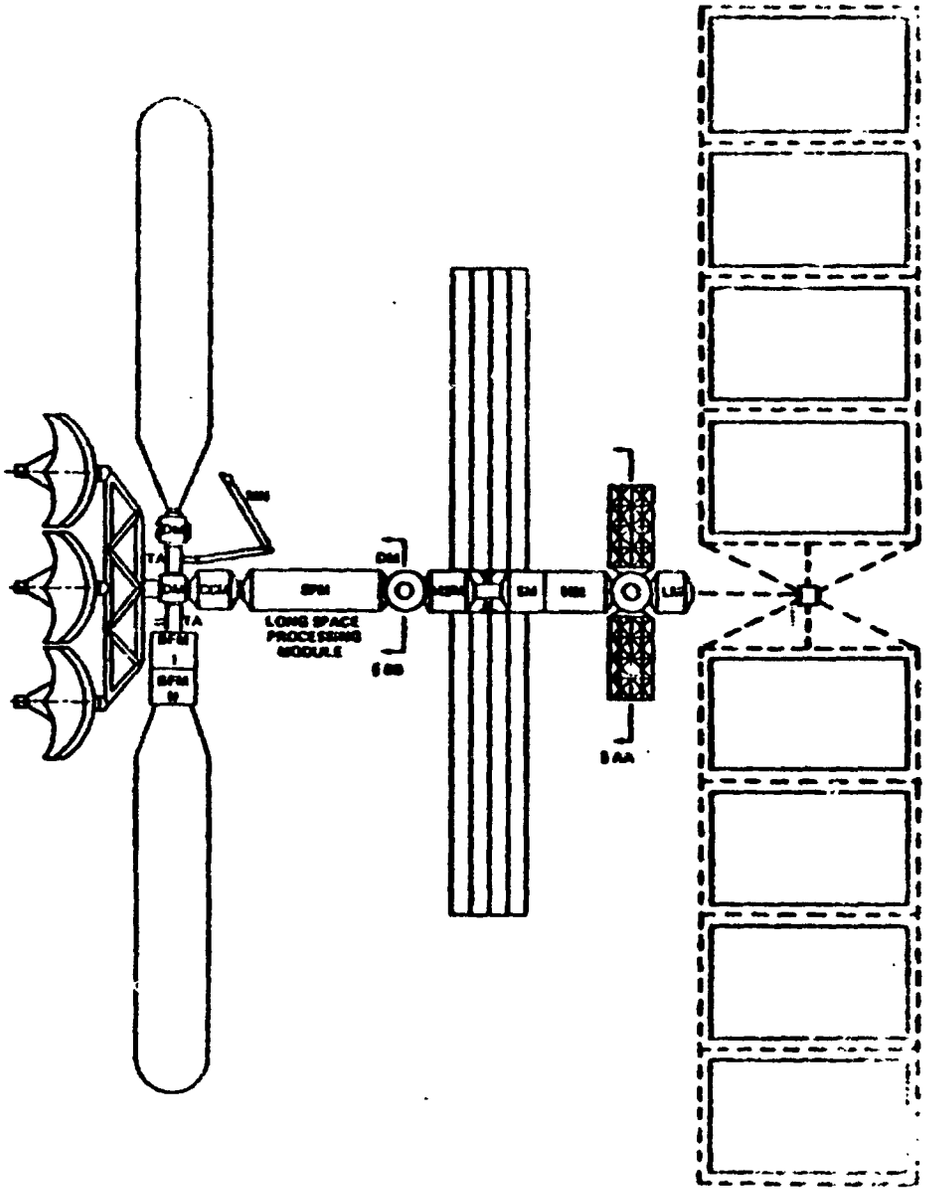

FIGURE 2-12

SPACE CONSTRUCTION BASE-CONFIGURATION 12

TABLE 2-1
MODULE ACRONYMS

AP	-	Applications Pallet
BFM	-	Beam Fabrication Module
CCM	-	Construction Control Module
DM	-	Docking Module
HAB	-	Habitability Module
HM	-	Habitability Module
LM	-	Logistics Module
MM	-	Manipulator Module
MSM	-	Mission Support Module
PSP	-	Public Service Platform
RP	-	Research Pallet
SM	-	Subsystem Module
SPM	-	Space Processing Module
SW	-	Solar Wing
SWA	-	Solar Wing Array
TA	-	Turret Assembly

Figures 2-2 through 2-12 identify the buildup beyond the initial configuration to the final Space Base. It should be noted that for each configuration there is a period of time in which the Orbiter is either docked or connected to the base via the RMS. For these cases it should be assumed that the Orbiter Reaction Control System (RCS) provides the stabilization and control of the entire structure. Prior to attachment the Space Base/Orbiter configuration will be maneuvered to a minimum momentum buildup orientation based upon the selected attach point. This orientation will be accomplished by the Base and the Orbiter separately prior to docking, in order to minimize Orbiter RCS usage.

2.1.1 Module Definition

The basic modules associated with the space base are described briefly. Acronyms for each are listed in Table 2-1.

- Subsystem Module - basically, the control center for the spacecraft operations. It houses all life support, communications and other electronic equipment. Fully habitable.

- Habitability Module - Provides crew quarters, exercise facilities, health, sleeping and dining facilities.

- Turret Assembly - The electromechanical structure for mounting the solar panels. Assume it has full freedom about the Z_V axis and can be servoed to a sun sensor

null. This structure also contains a pressurized passageway to interconnect adjacent modules.

- Solar Wings A&B - Solar panel assemblies that will provide all space base power requirements until the beam building equipment is utilized (configuration 10). Assume 50% occultation will provide adequate power.

- Docking Module - Simply, a structure that will allow a maximum of six separate modules to be attached in different directions. This module contains pressurized passageways for crew operations. The docking ports on this module shall be considered to be flexible and shall be simulated by a hinge-spring joint. Axial rotation shall also be considered in the control system.

- Mission Support Module - A module that contains additional equipment such as experimental hardware, consumables, spare subsyste- equipment, repair shop, test facility.

- Logistics Module - A pressurized habitable module containing consumable provisions and equipment for furthering the space base buildup.

- Space Processing Module - A laboratory setup for the experimentation of manufacturing hardware and pharmaceuticals in a zero gravity environment.

- Application Pallet - This module is essentially a storage unit for equipment necessary in furthering the function of the Space Processing Module. The equipment is externally fastened to a structure whose outline is cylindrical (to be compatible with the Orbiter). The pallet equipment must be retrieved by Extra Vehicular Activity (EVA).

- Research Pallet - Similar to the Applications Pallet but essentially holds equipment for further space experimentation. It could include a gimballed or floating structure for deep space telescope (high energy, UV) experiments.

- Construction Control Module - This module is defined as the control center for the construction phase of the large antenna array system.

- Manipulator - During the main stages of actual construction of structures in space the Orbiter supplies the space base with two structures identified as Manipulators. These manipulators are viewed as mechanical arms that have full rotational freedom about the X_V axis and 90° of "L-BOW" motion. The X_V rotational freedom is supplied by two identical turret assemblies like those supporting the solar wings. These Manipulators are controlled through the Construction Control Module.

- External Tanks - During the latter stages of base buildup two Orbiter booster tanks are added to the configuration. These tanks are empty, uninhabitable and serve only as strongbacks (support structures) for the construction of beams.

- Beam Fabrication Module - The Beam Fabrication Module contains the raw materials and machinery for the beam manufacturing. It is assumed that the space base crew operates the equipment from within the module and stores th sections externally, on the external tanks until final assembly begins.

- 150KW Arrays - These are large solar arrays that will provide the power necessary to operate the beam construction equipment and ultimately the final space base configuration. Assume the structure has unlimited freedom about Z_V and can be sun servoed.

- Public Service Platform - The Public Service Platform is the antenna communication array along with other equipment capable of monitoring items such as hurricanes, earthquakes, weather traffic control, personal communication, etc.

2.1.2 Mass Properties

The coordinate system to be used for analysis and definition purposes is shown in Figure 2-13. It is right-handed, with the origin being placed at the Subsystem Module/Habitability Module interface.

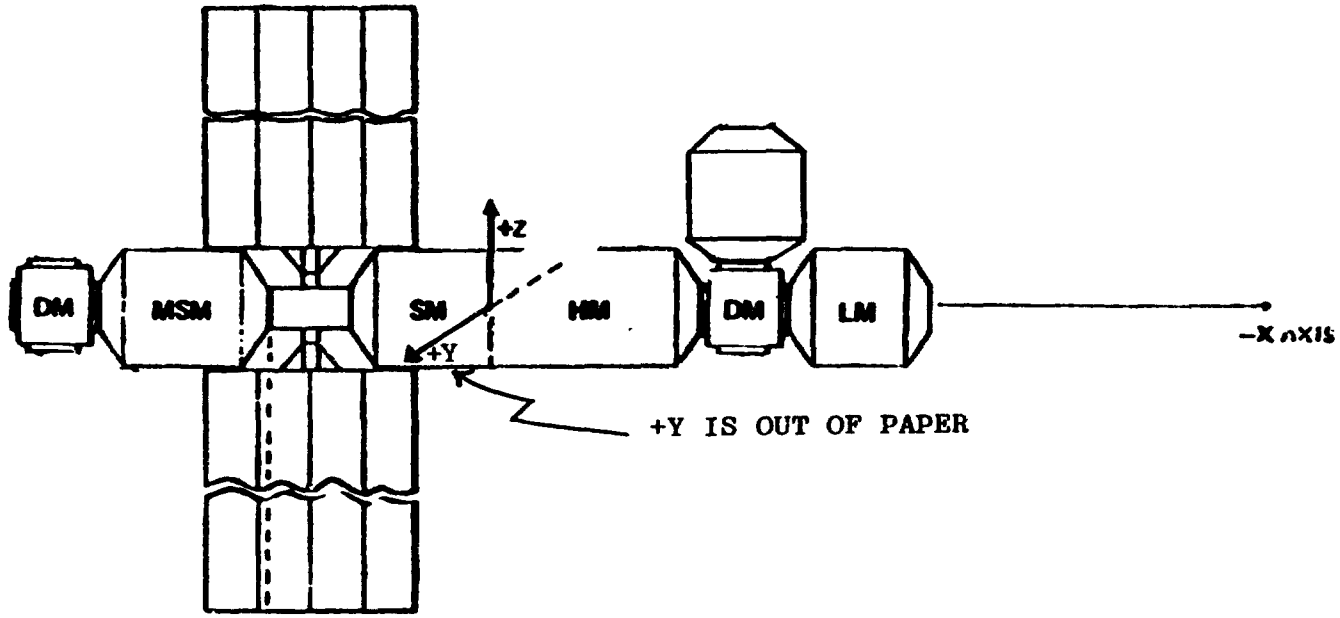

FIGURE 2-13
SPACE STATION CO-ORDINATE SYSTEM

TABLE 2-2

SPACE CONSTRUCTION BASE MASS/DIMENSION SUMMARY

	MASS(#)	SIZE (FT) L W T	LOCATION (INCHES) X	Y	Z
SUBSYSTEM MODULE	16,440	11' x 14.5'D	65	0	0
HABITABILITY MODULE	16,487	26' x 14.5'D	-156	0	0
TURRET ASSEMBLY	650	11' x 8.75'D	198	0	0
SOLAR WING A	951	104' x 26' x	198	0	715
SOLAR WING B	851	104' x 26' x	198	0	-715
DOCKING MODULE	5,625	10.8' x 11.7' x 11.7'	-377	0	0
MISSION SUPPORT MODULE	13,697	20.8' x 14.5'D	389	0	0
DOCKING MODULE	5,625	10.8' x 11.7' x 11.7'	578	0	0
LOGISTICS MODULE	20,575	17.5' x 14.5'D	-546	0	0
SPACE PROCESSING MODULE	25,794	51.5' x 14.5'D	952	0	0
APPLICATIONS PALLET	16,400	25' x 14'D	-377	0	220
RESEARCH PALLET	16,400	25' x 14'D	-377	0	-220
RESEARCH LOGISTICS MODULE	20,575	17.5' x 14.5'D	578	175	0
RESEARCH LOGISTICS MODULE	20,575	17.5' x 14.5'D	578	-175	0
HABITABILITY MODULE	16,487	26' x 14.5'D	-377	358	0
SUBSYSTEMS MODULE	16,440	11' x 14.5'D	-377	136	0
HABITABILITY MODULE	16,487	26' x 14.5'D	-377	-358	0
SUBSYSTEMS MODULE	16,440	11' x 14.5'D	-377	-136	0
CONSTRUCTION CONTROL MODULE	13,670	17.5' x 14.5'D	1366	0	0
DOCKING MODULE	5,625	11.7' x 10.8' x 11.7'	1541	0	250
TURRET ASSEMBLY	650	8.75'D x 11'*	1541	0	125
DOCKING MODULE	5,625	11.7' x 10.8' x 11.7'	1541	0	0
TURRET ASSEMBLY	650	8.75'D x 11'	1541	0	-125
DOCKING MODULE	5,625	11.7' x 10.8' x 11.7'	1541	0	-250
MANIPULATOR	805	43' x 1.5'D	1360	0	125
MANIPULATOR	805	43' x 1.5'D	1723	0	-125
(EXTERNAL TANK A)	(75,000)	(27.6'D x 154')	1541	0	-1237
BEAM FABRICATION MODULE A	35,020	15'D x 13'	1791	0	-250
(EXTERNAL TANK B)	(75,000)	(27.6'D x 154)	1541	0	1237

*WHEN DIAMETER APPEARS FIRST, IT IMPLIES DIAMETERS LIE IN PLANE ⊥ TO X-Y PLANE

TABLE 2-2 (CONTINUED)

	MASS(#)	SIZE (FT) L W T	LOCATION (INCHES) X	Y	Z
BEAM FABRICATION MODULE B	35,020	15'D x 15'	1791	0	-406
("150 KW" ARRAY WING A)	(8,276)	(82' x 190' x 21')	-1143	0	1294
("150 KW" ARRAY WING B)	(8,276)	(82' x 190' x 21')	-1143	0	-1294
("150 KW" SUBSYSTEMS)	(45,615*)	(5'D x 5')	-1143	0	0
CONSTRUCTION LOGISTICS MODULE	20,575	17.5' x 14.5'D	1716	0	0
(PUBLIC SERVICE PLATFORM A)	(21,600)	(105' x 440' x 312')	1889	0	0

*ENERGY STORAGE IN CONSTRUCTION CONTROL MODULE (ASSUMPTION)

TABLE 2-3

ELEMENTS OF THE INERTIA MATRIX

- o GIVEN IN VEHICLE COORDINATES (XV, YV, ZV)
- o $I_{XY} = I_{YX}$, $I_{YZ} = I_{ZY}$, $I_{ZX} = I_{XZ}$

CONFIG. NO.	WEIGHT (LBS)	ON-AXIS (DIAGONAL) TERM ($SLUG-FT^2$)			PRODUCT OF INERTIA TERMS ($SLUG-FT^2$)		
	W	I_{XX}	I_{YY}	I_{ZZ}	I_{XY}	I_{YZ}	I_{ZX}
1	40904.	.26620E6	.53219E6	.29685E6	0	0	0
2	80801.	.29815E6	.27208E7	.24854E7	0	0	0
3	106595.	.31920E6	.73281E7	.70927E7	0	0	0
4	139395.	.68683E6	.93917E7	.88138E7	0	0	0
5	180545.	.99243E6	.11383E8	.11077E8	0	0	0
6	246399.	.20896E7	.14562E8	.15299E8	0	0	0
7	260069.	.21008E7	.19630E8	.20367E8	0	0	0
8	354854.	.22031E8	.75525E8	.56566E8	0	0	+.21268E8
8A	354854.	.16802E8	.88217E8	.74487E8	0	0	0
9	464874.	.52726E8	.13463E9	.85231E8	0	0	+.19761E7
10	562061.	.61369E8	.19729E9	.13928E9	0	0	+.58867E7
11	582636.	.61393E8	.20261E9	.14459E9	0	0	+.56941E7
12	588637.	.70445E8	.20090E9	.20986E9	-.34308E7	+.10579E7	+.59784E7

Table 2-2 lists the module dimensions, weight and center of mass for each component. More detailed moment of inertia properties for each module is given in reference 2-2.

Moments and products of inertia and the weight of each configuration are listed in Table 2-3. Reference 2-2 is the source of more detailed configuration information. It lists the configuration breakdown summaries, including radius of gyration (K), total weight, configuration CG with respect to the coordinate system origin, vehicle axis moments of inertia, principal axis moments of inertia, direction cosines and angles between the vehicle axes and principal axes.

2.2 ORBITAL PARAMETERS

The initial Space Base configuration will be launched into a 270 nautical mile orbit of either 28.5 or 55 degree inclination. The entire mission of buildup and operation will be in Low Earth Orbit (LEO). Orbit decay may require periodic reboost but this problem shall not be addressed in this study. The orbit will be assumed to be circular. If we then assume a spherical earth, the orbital period will be 5668.2 seconds. The corresponding orbital rate will be 1.10850×10^{-3} rad/sec. The linear velocity for this altitude is approximately 24,975 ft/sec.

2.3 OPERATIONAL REQUIREMENTS

Operational Requirements of the Space Construction Base were non-existent in the data package compiling the study contract. In order to determine a feasible control system for the SCB, certain assumptions will be made regarding its operation and mission accuracies. All of these assumptions are listed here. As the study progresses, these parameters may be altered based upon new information or driven by other constraints.

2.3.1 Mission Timeline

The period of buildup and operation of the Space Base is shown in Figures 2-14 a and b. This timeline is hypothetical but can be used as a baseline for consideration in determining duration of each configuration in orbit and the orbital maintenance and lifetime of subsystem components. The lifetime of configuration 12 can be eventually considered open-ended for purposes of the study. Note that each configuration is expected to have a lifetime of approximately 4 months.

Along with the timeline presented, the crew is expected to grow in numbers as shown in Table 2-4.

2.3.2 Attitude Pointing and Maneuvering

Attitude pointing and maximum slewing requirements are listed in Table 2-5 as a function of configuration number. The maximum slewing rates are reduced for later configurations to bound the angular momentum requirements.

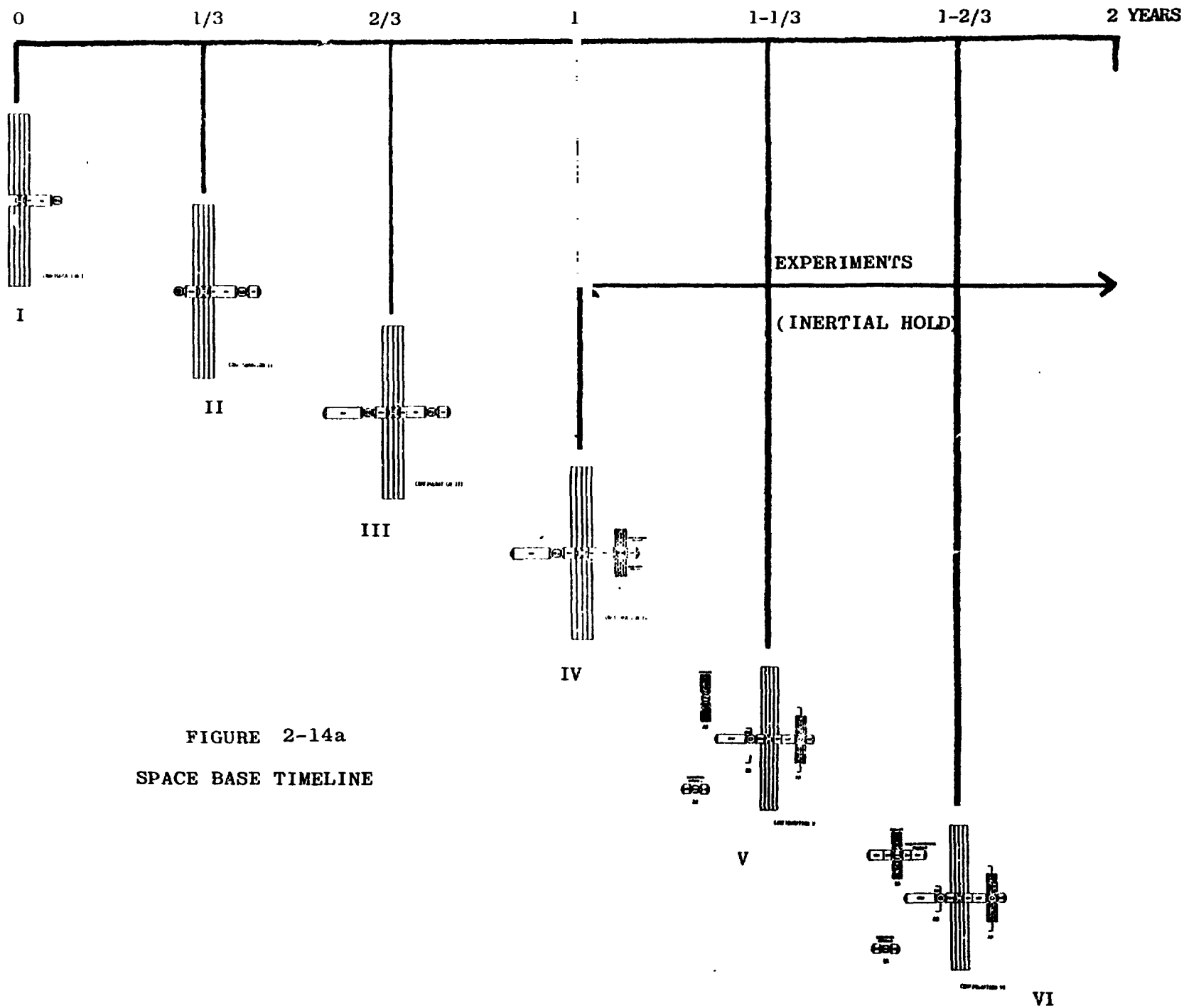

FIGURE 2-14a

SPACE BASE TIMELINE

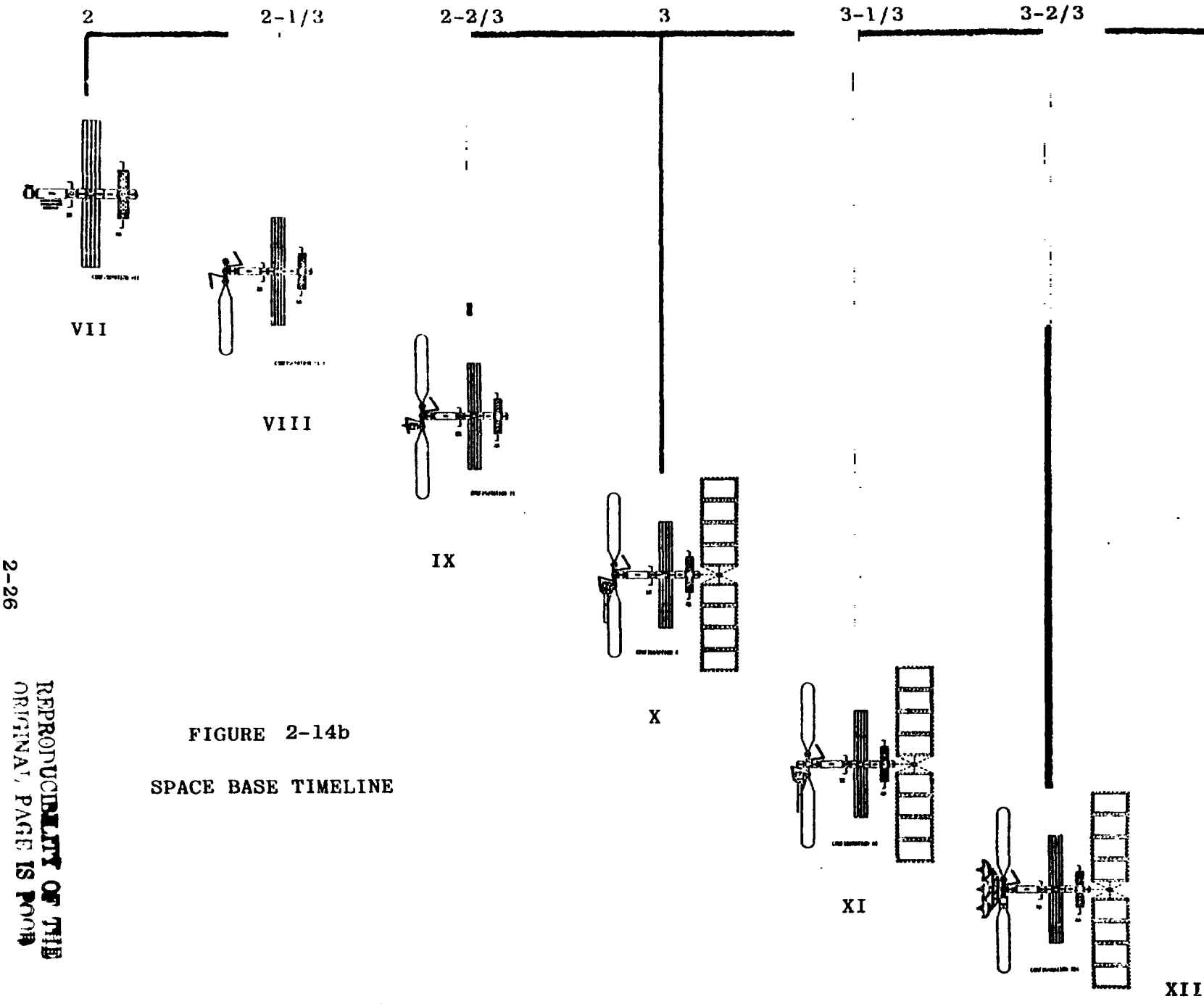

FIGURE 2-14b

SPACE BASE TIMELINE

TABLE 2-4

CREW REQUIREMENTS
FOR THE SCB MISSION

CONFIGURATION	CREW
1	3
2	3
3	6
4	6
5	9
6	9
7	9
8	9
9	9
10	12
11	12
12	12

TABLE 2-5

POINTING AND MANEUVERING REQUIREMENTS FOR THE SPACE CONSTRUCTION BASE

CONFIGURATION	POINTING ACCURACY		POINTING STABILITY		INERTIAL MODE DURATION HRS. PER DAY	SLEW RATE °/SEC	COMMENTS
	COARSE (DEG)	FINE (MIN)	COARSE (MIN)	FINE (SEC)			
1	±0.5	±1.0	10.0	10.0	N/A	0.10	
2	±0.5	±1.0	10.0	10.0	N/A	0.10	
3	±0.5	±1.0	10.0	10.0	N/A	0.10	
4	±0.5	±1.0	10.0	10.0	4 HR/DAY CONSECUTIVE	0.10	
5	±0.5	±1.0	10.0	10.0	4 HR/DAY CONSECUTIVE	0.10	Research Pallet has its own Fine Pointing System for experiments (3 arc sec for 4 hour intervals)
6	±0.5	±1.0	10.0	10.0	4 HR/DAY CONSECUTIVE	0.10	
7	±0.5	±1.0	10.0	10.0	4 HR/DAY CONSECUTIVE	0.10	
8	±0.5	N/A	10.0	N/A	N/A	0.05	Slew Rate Reduced
9	±0.5	N/A	10.0	N/A	N/A	0.05	
10	±0.5	N/A	10.0	N/A	N/A	0.05	
11	±0.5	N/A	10.0	N/A	N/A	0.05	
12	±0.5	N/A	10.0	N/A	N/A	0.05	

TABLE 2-6

GENERAL REQUIREMENTS
FOR THE SCB MISSION

- Both turret assemblies have full freedom about Z_V and can be servoed to the sunline.
- Assume 50% of solar panel area can be occulted without loss of required power to spacecraft functions.
- There is no requirement for periodic rotation of the spacecraft about any axis for the purpose of thermal control (no "barbecue" mode).
- Every docking module joint is to be considered "flexible" (simulated by a spring-hinge).
- Solar panel bending modes are estimated by using the results of a study of the SEPS Solar Array Dynamic Analysis (May 1976).
- It is most likely that docking will be refined to "berthing" in which the impulse imparted to the spacecraft will be less than the present docking forces. However, we will use docking data for analyses since it will be worst case data.

TABLE 2-7

CONFIGURATION PECULIAR REQUIREMENTS
FOR THE SCB MISSION

o IN ADDITION TO GENERAL REQUIREMENTS

CONFIGURATION	REQUIREMENTS
1	a) Entire configuration is prefab and delivered to orbit by the shuttle orbiter. Solar panels unfold. b) Turret assembly joint to spacecraft main body should be considered to be identical to a docking module joint.
2	a) No peculiar requirements.
3	a) Space processing module added; crew may double in size (from 3 to 6 men). b) Assume that electromechanical equipment can impart impulses to the spacecraft of 100 times a typical crew motion (wall push-off).
4	a) Assume Research Pallet contains a separately stabilized experiment. b) This is the first configuration to require inertial pointing capability. c) Must consider solar panel occultation by Research and Application Pallets.
5	a) First configuration with modules placed in $Y_V Z_V$ plane.
6	a) Additional modules in $Y_V Z_V$ plane. b) Assume additional crew members (max of nine).

TABLE 2-7 (Cont'd)

CONFIGURATION	REQUIREMENTS
7	a) No additional special requirements.
8	a) Major imbalance in vehicle axis inertias. b) Tank is a strongback. c) Consider an alternate configuration where the single tank is placed along $-X_V$ direction until the second tank is added. d) Building manipulator arms appear.
9	a) Second tank is added. b) Solar panel occultation may be significant to alter the main vehicle orientation.
10	a) Large solar arrays are added. b) Assume same articulation as smaller solar arrays. c) Assume large solar arrays supplement smaller units. d) Assume large array connection to main spacecraft body is a spring-hinge joint.
11	a) Beam construction begins for large antenna structure of 12.

TABLE 2-7 (Cont'd)

CONFIGURATION	REQUIREMENTS
12	a) Antenna structure is completed. b) Subsystems are added for information gathering and transmission. c) Assume antenna structure is earth pointing continuously. d) Examine a configuration where the X principal axis of inertia is the controlled axis. e) The combination of the antenna structure and subsystems module equipment form the "Public Service Platform".

The time duration for inertial hold modes during configurations 4, 5, 6 and 7 may be limited by the capability of selected momentum exchange actuators and the desaturation system.

2.3.3 General Requirements

The general requirements for the SCB mission are listed in Table 2-6. It should be noted that these general requirements apply to all configurations unless otherwise stated.

2.3.4 Configuration Peculiar Requirements

In addition to the general requirements, Table 2-7 lists requirements which are peculiar to individual configurations.

2.4 REFERENCES

2-1 Jennings, J., MT-40,801, Definition of Space Base Buildup, 21 October 1977

2-2 Space Construction Base Buildup Summary, Data Package Attachment to Exhibit A Scope of Work, Request for Quotation 1-7-ED-07552-AP131D, Marshall Space Flight Center, 10 March 1977

SECTION 3

3.0 ACTUATOR SIZING

It is presumed that the SCB actuator system is composed of momentum exchange devices; in particular, double gimbal control moment gyros (DGCMG's). One inherent advantage is the spherical angular momentum envelope. Modified SKYLAB-type DGCMG's are assumed: 2300 ft-lb-sec each and with gimbal stops removed. The number of DGCMG units required will be a function of a momentum profile based on the magnitude of disturbance torques to which the SCB is subjected. In general, this CMG requirement is based upon the long term cyclic variation in angular momentum disturbances. The angular momentum buildup due to bias disturbance torques will be used to size and select momentum desaturation schemes in Section 4 for the various SCB configurations.

Both long and short term disturbances on the SCB will be defined in the following paragraphs, with CMG sizing being primarily a function of the long term effects.

3.1 LONG TERM DISTURBANCES

Most of the long term angular momentum variations are caused by torques due to gravity gradient and aerodynamic effects on the SCB. These are described in references 3-1 and 3-2, respectively. Other less important sources are magnetic and radiation torques, which are described in references 3-3 and 3-4. Each will be described and then combined into a composite angular momentum requirement for each configuration.

3.1.1 Gravity Gradient

The largest torques, which a spacecraft is subjected at the altitude of interest, are ordinarily those due to forces from earth gravitational effects. Various space base orientations are also examined to determine those which are more practical with respect to minimizing the gravity gradient angular momentum requirements. These gravity gradient torques are obtained for all twelve space base configurations for the following orientations:

1. X-POP (X_V perpendicular to the orbital plane)

2. Y-POP

3. Z-POP

4. Y_V Solar Inertial (worst case $\beta = 45^{\circ}$)

The last listed orientation was included to obtain a worst case inertial pointing requirement for space base configurations 4, 5, 6 and 7. Pointing experiments from the Application Pallet or the Research Pallet will probably be most expedient at these times. From configurations 8 and on, the space base becomes cumbersome and the many large appendages may occult the field of view of any pointing experiments. It is assumed that for these experiments, the $\pm Z_V$ axes may be called upon to point anywhere in the celestial sphere; and item (4) above is a worst case orientation with respect to gravity gradient bias torques.

The geometry of the space base in earth orbit is shown in Figure 3-1; the orientation shown is Y_V solar inertial. Some of the assumptions used in computing gravity gradient torques were the following:

1. Orbital altitude - 270 N.mi.
2. Orbital inclinations up to 55 degrees
3. Spherical earth (non-oblate)
4. Circular orbit

One other assumption is used for determining feasibile space base orientations:

Solar wings and the 150 KW Solar Arrays are rotatable about the Z_V axis.

Space base mass data is available in Section 2. It is presented in the following form:

1. Moments of inertia about the three vehicle axes (X_V, Y_V, Z_V).
2. Principal moments of inertia.
3. Transformation ${}_pC_V$ from vehicle to principal axis.

Vehicle moment of inertia matrix I_V is obtained by using the following similarity transformation:

$$I_V = {}_pC_V{}^T \; I_P \; {}_pC_V \qquad (3\text{-}1)$$

where each term is a 3x3 matrix, and I_p is a diagonal matrix of the principal moments of inertia. The resulting

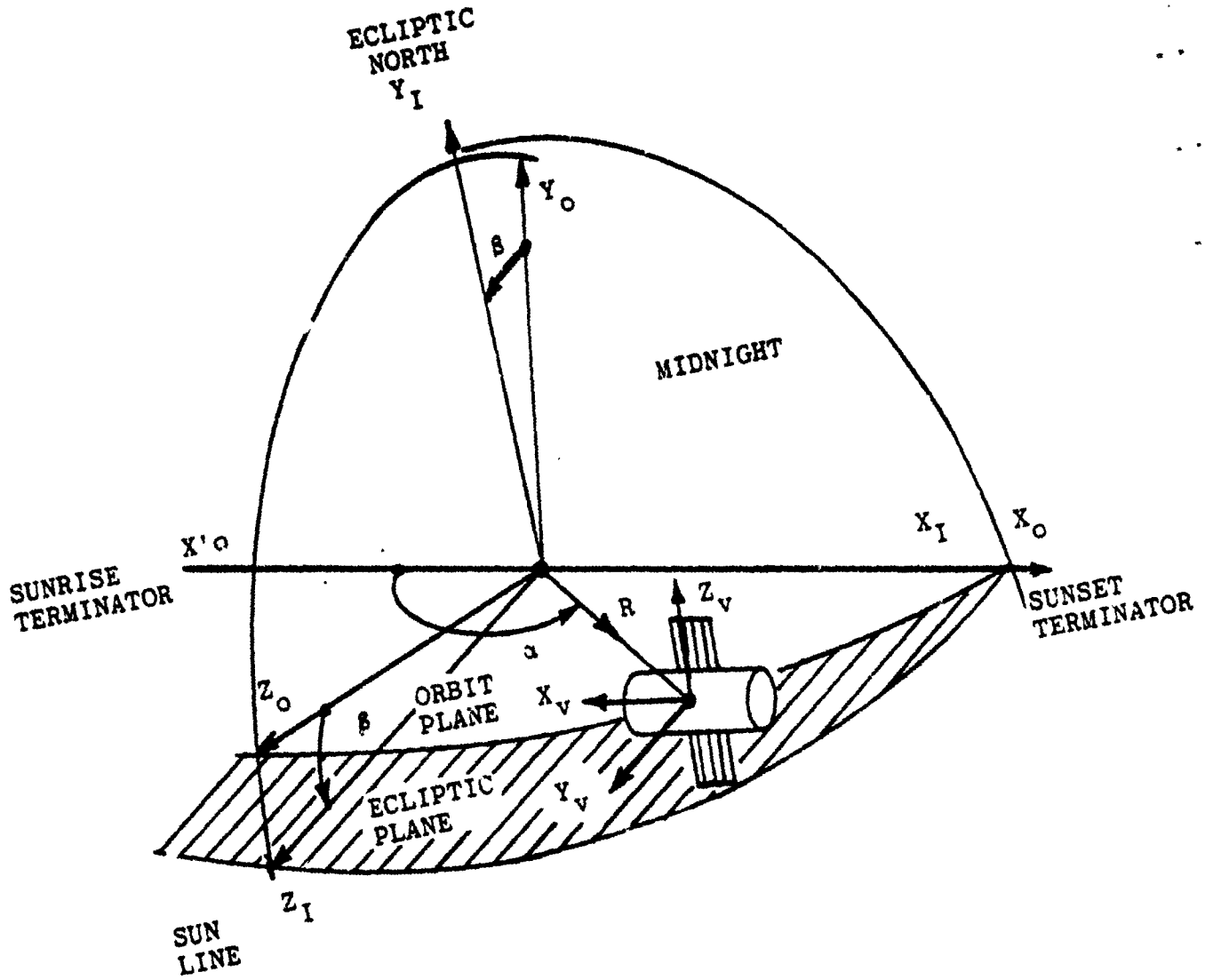

FIGURE 3-1 GEOMETRY OF THE SPACE BASE IN EARTH ORBIT, Y_V SOLAR POINTING SHOWN

moment of inertia matrix will be:

$$I_V = \begin{bmatrix} I_{XX} & I_{XY} & I_{XZ} \\ I_{YX} & I_{YY} & I_{YZ} \\ I_{ZX} & I_{ZY} & I_{ZZ} \end{bmatrix} \qquad (3\text{-}2)$$

where $I_{YX} = I_{XY}$

$I_{ZY} = I_{YZ}$

$I_{XZ} = I_{ZX}$

The gravity gradient torques about the vehicle axes were calculated using the following expressions from reference 3-5:

$$L_{gx} = \frac{3k}{R^3}\left[(I_{zz} - I_{yy})a_y a_z + I_{yz}(a_y^2 - a_z^2) + I_{xz}a_x a_y - I_{xy}a_x a_z\right]$$

$$L_{gy} = \frac{3k}{R^3}\left[(I_{xx} - I_{zz})a_z a_x + I_{zx}(a_z^2 - a_x^2) + I_{yx}a_y a_z - I_{yz}a_y a_x\right] \qquad (3\text{-}3)$$

$$L_{gz} = \frac{3k}{R^3}\left[(I_{yy} - I_{xx})a_x a_y + I_{xy}(a_x^2 - a_y^2) + I_{zy}a_z a_x - I_{zx}a_z a_y\right]$$

where

k is the gravitational constant = 1.407654×10^{16} ft^3/sec^2

R is the distance from the planet mass center to the spacecraft mass center = $R_o + h$

I_{ij} with i, j = x, y, z are the components of the inertial dyadic

a_i with i = x,y,z are the direction cosines of the vector R with respect to the X_v, Y_v, Z_v coordinate frame (see Figure 3-1)

and

R_o = earth's radius = 3440.0756 N.mi (mean)

h = 270 N.mi.

The magnitude of R is thus obtained,
$R = R_o + h = 3710.076$ N.mi $= 2.254285 \times 10^7$ ft
The coefficient outside the bracket of (3-3)can also be defined as:

$$\frac{3k}{R^3} = 3W_o^2 \qquad (3\text{-}4)$$

where W_o = orbital rate = 1.10850×10^{-3} rad/sec

The orbital period T_o is also obtained and calculated as 5668.2 seconds.

The equations of (3-3) were implemented on the digital computer for X-POP, Y-POP and Z-POP orientations and were also integrated as a function of time to obtain angular momentum changes due to gravity gradient torques. The angular momentum was then expressed in cyclic and bias buildup terms.

An additional configuration was added by eliminating the asymmetry of the single external tank of configuration 8. The tank was temporarily repositioned along the $+X_v$

TABLE 3-1

ANGULAR MOMENTUM REQUIREMENTS
DUE TO GRAVITY GRADIENT TORQUES

- ORIENTATION: Y_V LOCAL VERTICAL WITH $\beta = 45^\circ$
- ALTITUDE: 270 N. Mi.
- $H_T = (H_X^2 + H_Y^2 + H_Z^2)^{\frac{1}{2}}$ AT EACH INSTANT OF TIME, MAXIMUM MAGNITUDE IS PRESENTED

SPACE BASE CONFIGURATION NO.	BUILDUP H (FT-LB-SEC/ORBIT)				CYCLIC H (FT-LB-SEC)			
	H_X	H_Y	H_Z	H_T	H_X	H_Y	H_Z	H_T
4	3017.	0	0	3017.	240.0	4778.	5117.	7001.
5	1598.	0	0	1598.	127.2	5929.	6109.	8513.
6	3852.	0	0	3852.	306.6	7766.	7332.	10680.
7	3852.	0	0	3852.	306.5	10735.	10305.	14884.

axis by using the middle docking module. The mass characteristics were recomputed and the symmetric structure is designated as configuration 8A. All of these results are tabulated in reference 3-1 and the X-POP orientation was selected for configuration 1 through 11. It is presently planned that configuration 12 will operate in the X_v local vertical orientation with the microwave antennas pointing towards earth.

The angular momentum magnitudes for the selected orientations are summarized in 3.1.6. Angular momentum magnitudes are shown in Table 3-1 for a Y_v solar inertial orientation for configurations 4, 5, 6 and 7. The β angle was a worst case of 45^o. This, of course, is not a preferred orientation. If the sizing of the CMG system is based upon a preferred, low torque orientation, its capacity may not be quite enough to handle this worst case Y_v solar orientation - - except for a very limited time.

3.1.2 Aerodynamic

Aerodynamic forces, torques about the c.m. and angular momentum are obtained for each for all twelve orbital configurations. This effort was concentrated on those vehicle modules having large surface areas at some distance from the overall center of mass (c.m.). The portions of the vehicle in this classification are the following: the solar wings, the solar arrays and the external tanks. The tank(s) are included in configurations 10, 11 and 12.

Worst case aerodynamic torques are obtained using the "free molecular flow" theory which is recommended fcr altitudes above 65 N.mi. (120 KM). Normal forces on flat areas (solar wings and arrays) are then obtained. Angles of attack on flat surfaces, and "shading" effects are much more complex and are not included in this report.

In an atmospheric environment, the aerodynamic force would be

$$F = q\ C_D\ A \qquad (3\text{-}5)$$

where

F = the aerodynamic force

C_D = drag coefficient for the body of the interest

A = projected area of the space base element normal to the incident flow.

$q = \frac{1}{2}\ \rho V^2$ = dynamic pressure

ρ = mass density of the atmosphere

V = space base velocity, or relative velocity of the space base element relative to the local atmosphere

Reference 3-6 includes a table for determining the C_D for several basic body shapes in a hyperthermal free molecular flow condition. C_D is also a function of the speed of reemitted molecules and whether a diffused reemission or a specular reflection occurs. The worst case was taken and C_D is conservatively specified as being 2.6 for a flat plate and 2.5 for a cylinder.

The flat plate areas for the two solar wings and the two solar arrays are 5,408 ft^2 and 31,160 ft^2, respectively. The cylinder side area per external tank is 4250.4 ft^2 each. For a 270 N.mi (500 Km) orbit, the space base velocity is 24,975 ft/sec, and the worst case mass density (reference 3-7) is 1.53×10^{-14} slugs/ft^3. A listing of mass densities as a function of night and day and also high/low solar activity is given in Table 3-2.

Using (3-5) for the worst case atmospheric density,
$F = (4.772 \times 10^{-6}\ lb/ft^2)\ C_D A$

For flat plates,
$F = (1.241 \times 10^{-5}\ lb/ft^2)\ A$

For cylinders,
$F = (1.193 \times 10^{-5} lb/ft^2)A$

Using these expressions,
F = 0.0671 lb (solar wings)
F = 0.3866 lb (solar arrays)
F = 0.0507 lb (each external tank)

Both the solar wings and solar arrays were assumed to be rotatable around the Z_V axis. With the panels facing towards the forward velocity and the initial Y_V axis, the moments would be as follows:

L_{XV} = 0 (because of balancing aero forces, except for configuration 8)

TABLE 3-2

ATMOSPHERIC MASS DENSITY

- ALTITUDE OF 270 Naut. Mi (500 KM)
- FROM NASA SP-8021, MODEL OF THE EARTH'S ATMOSPHERE

CONDITIONS		ATMOSPHERIC MASS DENSITY	
		SLUGS/FT^3	NORMALIZED TO MAXIMUM
HIGH SOLAR ACTIVITY	NIGHT	1.53×10^{-14}	1
	DAY	9.70×10^{-15}	1/1.58
LOW SOLAR ACTIVITY	NIGHT	2.44×10^{-16}	1/62.7
	DAY	6.40×10^{-17}	1/239

$L_{YV} = 0$
L_{ZV} = very high

With all solar panels facing towards the original $\pm X_V$ axis with edges into the relative "wind",

$L_{XV} \cong 0$ (except for configuration 8)
$L_{YV} \cong 0$
$L_{ZV} \cong 0$

The effort here will therefore concentrate on the former case where L_{ZV} becomes very high. In general,

$$-L_{ZV} = \Sigma F_{YV} \times (X_{CP} - X_{CM}) \qquad (3\text{-}6)$$

where
F_{YV} = each vector force parallel to the Y_V axis
X_{CP} = each aerodynamic center of pressure location in the X_V direction
X_{CM} = the vehicle center of mass location along the X_V axis

The angular momentum can then be computed as follows:

$$H_{ZV} = \int L_{ZV}\, dt \qquad (3\text{-}7)$$

For a solar inertial condition, the L_{ZV} torque will be cyclic and

$$H_{ZV}(PEAK) = (T_o/4\pi)\, L_{ZV}(PEAK) \qquad (3\text{-}8)$$

where

T_o = orbital period = 5668.2 sec

For an X_V local vertical condition the momentum on the solar wings and arrays will be as in (3-8); but for the external tanks:

$$H_{ZV} \text{ (BUILD UP PER ORBIT)} = T_o L_{ZV}(\text{BIAS}) \qquad (3\text{-}9)$$

The assumptions for these aerodynamic characteristics are reiterated as follows:

(a) Only space base modules with large surface areas at a large moment arm from the c.m. are considered
(b) No "shading" of the airstream by one section of the vehicle on another is considered
(c) Aerodynamic force computations are based on a space base velocity along its Y_V axis (assumes the sun is also along this axis)
(d) Surface drag coefficients used were for the worst case hyperthemal free molecular flow
(e) Worst case atmospheric density was assumed (high solar activity at nighttime).

With regard to this last item, it must be pointed out that the atmospheric mass density (ρ) can also be approximately 240 times less than that used in the calculations of aerodynamic force. For low solar activity at daytime, all computed forces, torques and angular momentum magnitudes would be reduced by a factor of about 240.

The (X_{CP} - X_{CM}) radius arms, aerodynamic forces, L_{ZV} torques and H_{ZV} angular momentum levels for the solar wings, solar arrays and the external tanks are tabulated in reference 3-2. The composite aerodynamic angular momentum magnitudes are summarized in section 3.1.6. The results are given for the worst case atmospheric density (high solar activity at night) and also when normal (actually minimum when low solar activity and in daytime).

3.1.3 Magnetic

The peak cyclic magnetic torques are obtained using the following vector expression:

$$\underline{L} = \underline{\mu} \times \underline{B} \qquad (3\text{-}10)$$

where

$\underline{L}$ = torque vector (N-m)
$\underline{\mu}$ = spacecraft magnetic moment vector (A-m^2)
$\underline{B}$ = peak of the earth's flux density (tesla or webers/m^2) above the magnetic poles

Reference (3-8) presents an approach for estimating μ, the magnitude of a spacecraft's magnetic moment, on the basis of two factors:

1. The degree of control over current loops, magnetic materials, quality control of potential moment sources, test and magnetic compensation.

2. The size of the vehicle, specifically its mass.

Minimal control of (1) above is designated Class III. An estimate of the dipole magnetic moment per unit mass for a Class III spacecraft would be approximately 0.01A-m^2/KG.

A model of the earth's magnetic field (B) in orbit is available in reference (3-9). The magnetic flux is given in terms of a spherical harmonic expansion series. Only the first term or so is required to obtain an estimate of the maximum magnetic torques. At an orbit altitude of 270 N.mi., the magnitude over the magnetic poles is approximately 0.60 gauss or 6×10^{-5} tesla in the vertical direction. The magnitude at the magnetic equator is 0.30 gauss or 3×10^{-5} tesla, and the direction of the flux is horizontal to the earth's surface towards the south magnetic pole. An orbit parallel to the plane of the magnetic equator would therefore result in a constant spacecraft torque for an inertially oriented vehicle. A higher torque is possible over the magnetic poles, but the result is cyclic.

The peak magnetic torque is calculated above the magnetic poles for each space base configuration for the following assumptions:

a. The orbit passes over the magnetic poles
b. The space base magnetic moment magnitude is 0.01A-m^2/KG; and the direction is always normal to B in the magnetic polar region.

TABLE 3-3

MAGNETIC TORQUES AND ANGULAR MOMENTUM

FOR THE SPACE BASE

- SPACE BASE MAGNETIC MOMENT IS BASED ON CLASS III OF NASA SP-8018 (SPACECRAFT MAGNETIC TORQUES) $\mu = .01 A\text{-}m^2/KG$
- EARTH'S MAGNETIC FIELD IN MAGNETIC POLAR REGION AT 270 N.MI. ALTITUDE IS .60 GAUSS, OR 6×10^{-5} TESLA
- SPACE BASE IS INERTIALLY ORIENTED IN AN ORBIT OVER THE MAGNETIC POLES

CONFIG. NO.	WEIGHT W (LBS)	MASS M (KG)	MAGNETIC MOMENT μ ($A\text{-}M^2$)	PEAK MAGNETIC TORQUE $L = \mu \times B$ (N-M)	(FT-LB)	PEAK ANGULAR MOMENTUM H_{CYCLIC} (FT-LB-SEC)
1	40904	18554	185.5	.0113	.00821	3.70
2	80801	36651	366.5	.0220	.0162	7.32
3	106595	48351	483.5	.0290	.0214	9.65
4	139395	63228	632.3	.0379	.0280	12.62
5	180545	81894	818.9	.0491	.0362	16.35
6	246399	111765	1117.6	.0671	.0495	22.31
7	260069	117965	1179.6	.0708	.0522	23.55
8	354854	160959	1609.6	.0966	.0712	32.13
9	464874	210863	2108.6	.1265	.0933	42.09
10	572061	259482	2594.8	.1557	.1148	51.80
11	582636	264279	2642.8	.1586	.1170	52.75
12	588637	267001	2670.0	.1602	.1182	53.30

The calculated cyclic magnetic torques and angular momentum are listed in Table 3-3.

For the unique condition of having an orbit parallel to the magnetic equator, the steady magnetic torque can be calculated by multiplying each torque item in Table 3-3 by one-half. The magnetic angular momentum buildup per orbit can be obtained by multiplying each H_{CYCLIC} in Table 3-3 by 2π. This was done in summary tabulations given in section 3.1.6.

The results indicate that magnetic contributions are negligible and will not have to be considered for simulation modeling or for sizing attitude control actuators and momentum exchange systems. If a magnetic desaturation system is used on the space base, any residual magnetic moment dipole will be automatically compensated.

3.1.4 Radiation

Sources of electromagnetic radiation that cause forces and possible torques to act on the space base (reference 3-10) are the following:

1. Direct solar photon radiation
2. Solar radiation reflected by the earth and its atmosphere
3. Radiation directly from the earth and its atmosphere
4. Radiation from portions of the space base itself.

The most important cause of radiation is (1) above. The intensity of the radiation, or solar flux, is given in terms of energy per unit time through a cross-sectional unit area:

$I_1 = 1353 \text{ w/m}^2 \pm 3.3\%$

The percentage is not a tolerance, but a seasonal variation because of the earth's orbit about the sun. The worst case magnitude is then $I_1 = 1398 \text{ w/m}^2$. The forces caused by other sources are usually at least an order of magnitude smaller.

Radiation due to the earth's reflectance is maximum at the subsolar point (high noon). It reduces to zero on the night side. The peak magnitude when at 270 N.mi. (500 Km) and assuming the earth's planetary albedo of 0.34 is

$I_2 = 600 \text{ w/m}^2$ (peak)

The mean magnitude of I_2 for a 50% daylight orbit is approximately 191 w/m^2.

Radiation directly from the earth and its atmosphere at sea level has a mean emission intensity of 243 w/m^2. With clear skies and at the lower latitudes, the worst case intensity at a 270 N.mi. orbit is

$I_3 = 150 \text{ w/m}^2$.

Radiations and reflections from the space base itself, item (4), are the least important and will be assumed as negligible.

For each of the (1) through (3) radiation sources, the radiation force is calculated as a function of whether the radiation is

a. Completely absorbed
b. Completely specularly reflected
c. Completely diffusely reflected.

The worst case turns out to be when the surface is such that a complete specular reflection is obtained. The expression defining this force (reference 3-10) is

$$F = \frac{I}{c}\left[-(1+c_{rs})\cos\theta\underline{n}+(1-c_{rs})\sin\theta\underline{s}\right](\cos\theta)A \qquad (3\text{-}11)$$

where

I = radiation intensity
c = speed of light = 2.997925×10^8 m/s
c_{rs} = coefficient of reflectivity, assumed to be 1 for the worst case
θ = angle between the surface normal and the direction of radiation
$\underline{n}$ = unit normal vector
$\underline{s}$ = unit vector along the surface
A = area of the surface

For $c_{rs} = 1$,

$F_N = 2AI/c$ = normal force when θ is zero (3-12)

$F_N = 6.671281 \times 10^{-9}$ AI (3-13)

Using the numerical value of flux intensity estimated for I_1, I_2 and I_3, the normal forces are

$F_1 = 9.3265E\text{-}6$ A

$F_2 = 4.0028E\text{-}6$ A(peak)

$F_3 = 1.0007E\text{-}6$ A(worst case)

where F is in newtons and A is in m^2 units.

F_1, F_2 and F_3 are computed for the surfaces of three vehicle modules: the solar wings, solar arrays and external tank(s). All other module surfaces are smaller and/or are at a shorter moment arm, and are assumed to be negligible in computing torquing moments.

Table 3-4 is a listing of maximum F_1, F_2 and F_3 forces for each of the three modules. The numerical magnitudes are given in pounds. The areas for the solar wings, solar arrays and for one external tank are A_w, A_a and A_t, respectively:

$A_w = 2 \times 2704\ ft^2 = 5408\ ft^2$

$A_a = 2 \times 15580\ ft^2 = 31160\ ft^2$

A_t (projected) = 4250.4 ft^2 (each)

Table 3-4

Radiation Forces

on

Large Surfaces of Space Base

- All forces given in lbs
- Forces normal to plane surfaces or projection of non-planar bodies

Radiation Type N	Solar Wings (s)	Solar Arrays (a)	External Tank (One) (t)	External Tanks (tt)
1	1.0534E-3	6.0696E-3	8.2793E-4	1.6559E-3
2	4.5211E-4	2.6050E-3	3.5533E-4	7.1066E-4
3	1.1302E-4	6.5122E-4	8.8831E-5	1.7766E-4

$F_N = 2.03341 \times 10^{-9}$ AI (pounds)

$I_1 = 1398 w/m^2 = 95.794$ lb/ft-sec

$I_2 = 600 w/m^2 = 41.113$ lb/ft-sec

$I_3 = 150 w/m^2 = 10.278$ lb/ft-sec

For two external tanks, A_{tt} = 8500.8 ft^2

Radiation torques are computed for two vehicle orientations: XPOP inertial and X local vertical. Intensity of radiations causing both bias and cyclic torques are given in Tables 3-5 and 3-6 for the two orientations. In some cases, these would modify the forces given in Table 3-4.

Peak torques, L_1, L_2 and L_3 are computed using moment arms available from Section 2. These are listed in Table 3-7 for each section of the space base. The moment arm in each case is $X_{CP}-X_{CM}$, where

X_{CP} = center of radiation pressure on the module of interest along the vehicle's X axis

X_{CM} = space base center of mass location along the X axis

Bias and cyclic angular momentum components can then be computed from these torques. For the XPOP inertial orientation, all maximum torques would be about the Z axis. The Z axis angular momentum components would then be as follows:

$$H_{BIAS} = T_o \left[L_1 + L_2/\pi \right] \quad (3\text{-}14)$$

$$H_{CYCLIC} = (T_o/2\pi) \left[L_2/2 + L_3 \right] \quad (3\text{-}15)$$

where L_1, L_2 and L_3 are torques for solar wings, solar arrays and external tanks as each are included in a vehicle configuration.

Table 3-5

Intensity of Radiation

for

Inertial XPOP Orientation

- All units in w/m^2
- Results in Z axis torques

Radiation Source	Magnitude Used for Computation:	
	Bias Torques	Cyclic Torques
I_1	1398 for panels	-
	1398 for tanks	-
I_2	191 for panels	$\pm$300 for panels
	191 for tanks	$\pm$300 for tanks
I_3	-	$\pm$150 for panels
	-	$\pm$150 for tanks

Table 3-6

Intensity of Radiation

for

X Local Vertical Orientation

- All units in w/m^2
- Results in maximum Z axis to. ues

Radiation Source	Magnitude Used for Computation:	
	Bias Torques	Cyclic Torques
I_1	1398 for panels(β=90°)	$\pm$1398 for panels(β=0°)
	1398 for tanks "	$\pm$1398 for tanks "
I_2	191 for panels	$\pm$300 for panels
	0 for tanks	0 for tanks
I_3	-	$\pm$150 for panels
	-	0 for tanks

Table 3-7

Radiation Forces and Angular Momentum

- Orbit Period (T_o) is 5668.2 seconds for 270 N.mi. orbit

Module Surface	Config.	Arm $X_{CP}-X_{CM}$ (ft)	Peak Torques (ft-lb) $L_i=(X_{CP}-X_{CM}) \times F_i$			Angular Momentum (ft-lb-sec) H_{BIAS} $T_o(L_1+L_2/\pi)$	H_{CYCLIC} $\frac{T_o}{2\pi}(L_1+L_2/2+L_3)$	$\frac{T_o}{2\pi}(L_1)$
			L_1	L_2	L_3			
SOLAR WINGS (s)	1	+22.90	+.0241	+.01035	+.00259	+155	±28.8	±21.8
	2	22.48	.0237	.0102	.00254	153	28.2	21.4
	3	1.83	.00193	.00083	.00021	12.4	2.3	1.7
	4	12.68	.0134	.00573	.00143	86.0	15.9	12.0
	5	2.57	.0027	.00116	.00029	17.4	3.2	2.4
	6	14.69	.0155	.00664	.00166	99.7	18.5	14.0
	7	8.80	.00927	.00398	.0010	124.3	11.1	8.4
	8	-23.44	-.0247	-.0106	-.00265	-159	29.4	22.3
	8a	-40.26	-.0424	-.0182	-.00455	-273	50.6	38.3
	9	-45.95	-.0484	-.0208	-.00519	-312	57.7	43.7
	10	-33.92	-.0357	-.0153	-.00383	-250	42.6	32.2
	11	-37.18	-.0392	-.0168	-.00420	-252	46.7	35.3
	12	-36.27	-.0382	-.0164	-.00410	-246	45.6	34.5
SOLAR ARRAYS (a)	10	-145.67	-.884	-.379	-.0949	-5696	1054	798
	11	-148.93	-.904	-.388	-.0970	-5824	1078	816
	12	-148.02	-.898	-.386	-.0946	-5788	1071	810
EXT.TANK (t)	8*	+88.48	+.0733	+.0314	+.00786	+472	87.4	66.1
	8a	151.59	.1255	.0539	.0135	809	150	113
EXTERNAL TANKS (tt)	9	+71.66	+.1187	+.0509	+.0127	+764	142	107
	10	78.	.1292	.0554	.0139	832	154	117
	11	74.73	.1237	.0531	.0133	797	148	112
	12	75.65	.1253	.0538	.0134	807	149	113

*$Z_{CP}-Z_{CM}$=-81.30 ft

Table 3-8

Angular Momentum

Due to

Radiation Forces

- Space Construction Base Surfaces Considered are Solar Wings, Solar Arrays and External Tank(s)

CONFIG.	H_Z ANGULAR MOMENTUM			
	XPOP INERTIAL		X LOCAL VERTICAL	
	H_{BIAS} (FT-LB-SEC/ORBIT)	H_{CYCLIC} (FT-LB-SEC)	H_{BIAS} (FT-LB-SEC/ORBIT	H_{CYCLIC} (FT-LB-SEC)
1	+155	$\pm$7.00	+155	$\pm$28.8
2	153	6.87	153	28.3
3	12.4	0.56	12.4	2.30
4	86.0	3.88	86.0	15.9
5	17.4	0.78	17.4	3.22
6	99.7	4.49	99.7	18.5
7	124.	2.69	124.	11.1
8*	313.	28.4	256.	95.5
8a	535.	48.8	438.	164.
9	453.	48.5	361.	165.
10	-5114.	305.	-5214.	1213.
11	-5279.	310.	-5375.	1235.
12	-5227	308.	-5324.	1230.

*H_X, H_Y are also possible because of asymmetric configuration. For XPOP: H_{BIAS} = 288., H_{CYCLIC} = $\pm$26.1 ft-lb-sec. For X Local Vertical: H_{BIAS} = 288., H_{CYCLIC} = $\pm$87.8 ft-lb-sec.

For an X local vertical orientation, the external tanks will not contribute to a Z axis torque for radiations from the earth (I_2 and I_3). The Z axis angular momentum components were based on vehicle and solar panel orientations as determined in reference 3-4 . The resulting components, therefore, are the following:

$$H_{BIAS} = T_o \left[L_1 + L_2/\pi\right] - T_o \left[L_2/\pi\right]_{TANKS} \qquad (3\text{-}16)$$

where the first term includes contributions from solar wings, solar arrays and the tanks. Also

$$H_{CYCLIC} = (T_o/2\pi)\left[L_1 + L_2/2 + L_3\right] - (T_o/2\pi)\left[L_2/2 + L_3\right]_{TANKS} \qquad (3\text{-}17)$$

where the first term again includes all contributions.

The results of equations (3-14) through (3-17) are illustrated in Table 3-8 for all space construction base configurations. These angular momentum magnitudes are included in the summaries given in Section 3.1.6.

Although these momentum levels are less than gravity gradient and worst case aerodynamic angular momentums, radiation effects appear to be greater than those obtained from magnetic torques. For a sizing estimate of a momentum exchange or a momentum desaturation system, torques and angular momentum caused by radiation may be considered negligible.

3.1.5 Vehicle Roll During X Local Vertical Orientation

During a local vertical orientation of an orbital vehicle, it is necessary to rotate the vehicle about its vertical axis if solar panels are articulated about a single axis. This provides the solar panels with what is effectively "two-axis pointing".

An X local vertical vehicle is illustrated in Figure 3-2, each coordinate space is defined as follows:

- O orbital coordinates, Y_o defines the orbit and X_oZ_o are in the orbital plane
- I inertial coordinates, where X_I points toward the sun
- V vehicle coordinates, where X_V is the roll axis
- S solar panel coordinates, where Y_S is the axis normal to plane of the panels

The angles shown are defined as follows:

- α_Y vehicle position in orbit, defined as zero when X_V is parallel with X_o
- β_Z rotation about Z_o defining the solar angle between X_o and X_I
- ϕ_x vehicle roll angle about X_v, where zero is defined when Y_v is parallel to Y_o
- δ_z solar panel angle about Z_v, where zero is defined when Y_s is parallel to Y_v

Angular rotations from O to I or S are indicated on the figure where an interim coordinate system is defined:

U vehicle coordinate system anywhere in the orbit where $\phi_x = 0$

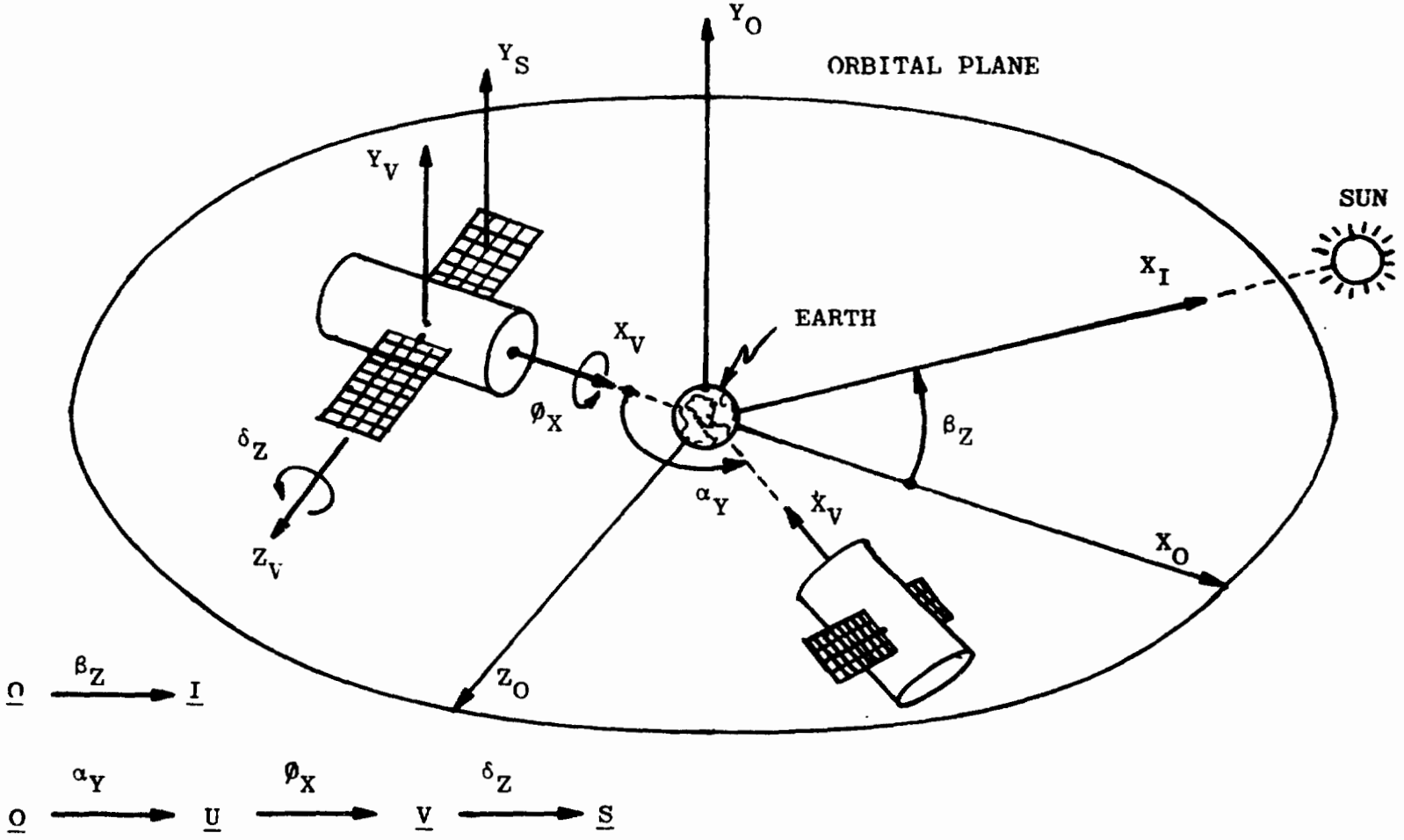

FIGURE 3-2 DEFINITION OF COORDINATE SYSTEMS AND ANGLES FOR X LOCAL VERTICAL ORIENTATION

Transformations may then be generated between the S and I coordinate systems as a function of the angles. In order for the solar panels to point towards the sun, the following must be true:

$$Y_S \cdot X_I = 1 \tag{3-18}$$

Other relationships which also must be true are

$$\begin{aligned} X_S \cdot X_I &= 0 \\ Z_S \cdot X_I &= 0 \\ Y_S \cdot Y_I &= 0 \\ Y_S \cdot Z_I &= 0 \end{aligned} \tag{3-19}$$

The roll angle ϕ and the solar panel angle δ was then determined in reference 3-11 using the functions of (3-18) and (3-19):

$$\tan\phi = \frac{\sin\alpha}{\tan\beta} \tag{3-20}$$

$$\sin\delta = -\cos\alpha \cos\beta \tag{3-21}$$

where the notation was simplified by eliminating the angle subscripts:

$$\begin{aligned} \alpha &= \alpha_y \\ \beta &= \beta_z \\ \phi &= \phi_x \\ \delta &= \delta_z \end{aligned}$$

Equations (3-20) and (3-21) are plotted in Figure 3-3 as a function of the position in orbit (α) and the angle between the ecliptic and the orbital plane (β). For a circular orbit, α is directly proportional to time.

Observation of Figure 3-3 for very small β angles indicates a potential problem. Theoretically, the vehicle must roll 180° about X_v in a very short period of time. If the moment of inertia of the vehicle about X_v is appreciable, extremely high changes of angular momentum will be required twice per orbit - once positive and then negative. The angular momentum swing about the X axis of configuration 12 is listed in Table 3-9 as a function of the β angle. The amplitude of the angular momentum is defined by the following:

$$H_x = I_{xx} \dot{\phi}_{MAX} \qquad (3\text{-}22)$$

where $\dot{\phi}_{MAX}$ is obtained by taking the time derivative of (3-20):

$$\dot{\phi}_{MAX} = \pm W_o / \tan\beta \qquad (3\text{-}23)$$

and W_o = orbital rate for the 270 N.mi. orbit = 1.1085×10^{-3} rad/sec.

Table 3-9 indicates the consequence of having a single axis articulation of the solar panels when the β angle has a small magnitude: the requirement for extremely

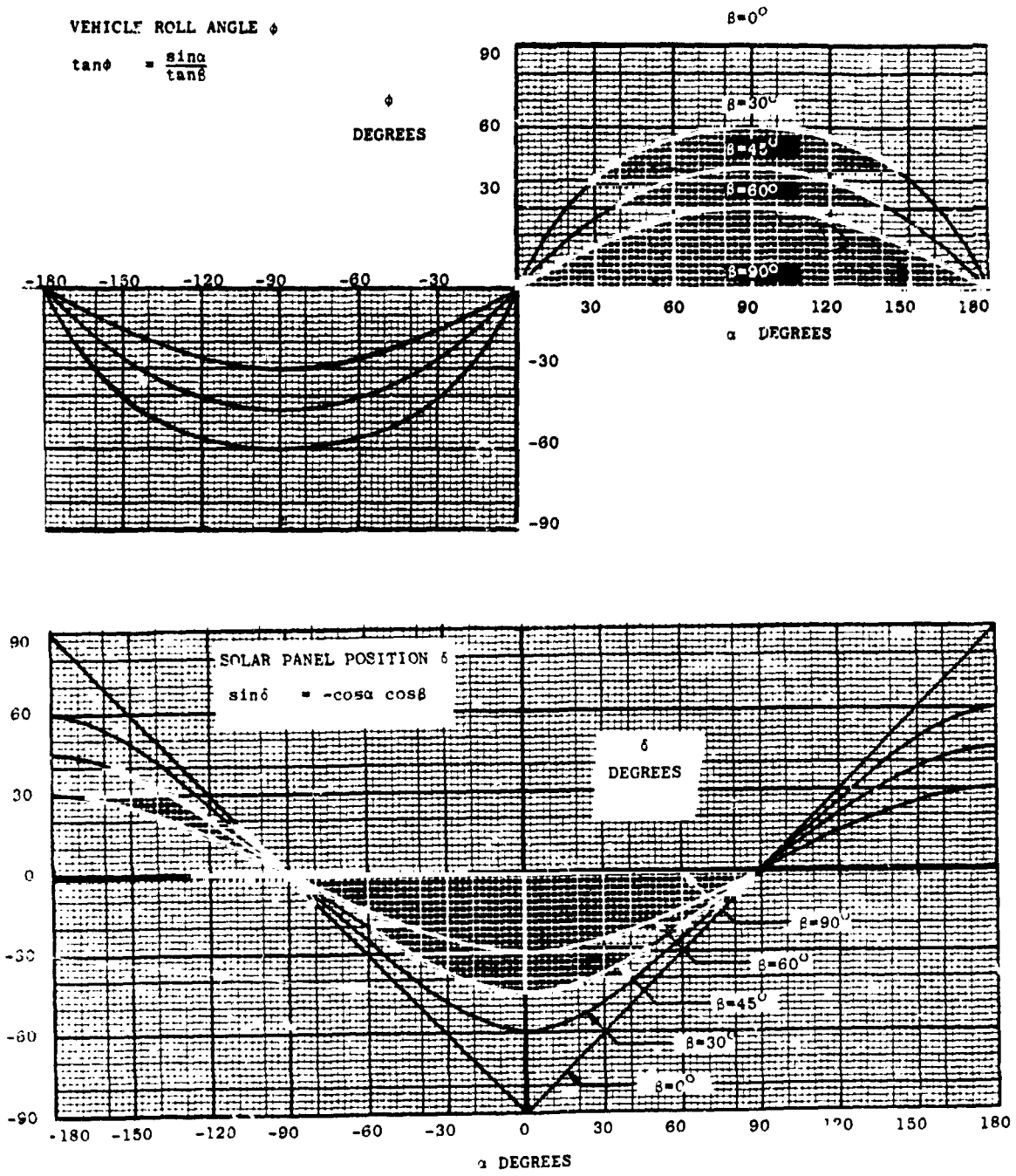

FIGURE 3-3 VEHICLE ROLL ANGLE (ϕ) AND SOLAR PANEL ANGLE (δ) FOR ONE COMPLETE ORBIT AS A FUNCTION OF THE ORBIT PLANE TO SUN ANGLE (β)

Table 3-9

ANGULAR ROLL RATE
AND MOMENTUM REQUIREMENTS

- X local vertical orientation
- I_{xx} = 7.044512x10^{7} Ft-Lb-Sec^{2} for configuration 12
- An equivalent CMG unit has an angular momentum of 2300 Ft-Lb-Sec
- Assumes sun line is perfectly normal to the solar panels for all β angles

$\pm\beta$	$\dot{\phi}_{MAX}$	MAGNITUDE OF MAX. ROLL RATE	EQUIVALENT NUMBER OF
(DEG)	(RAD/SEC)	(DEG/SEC)	CMG UNITS
0	∞	∞	∞
1	0.0635	3.64	1950.
10	0.00629	0.360	192.7
20	0.00305	0.1745	93.4
30	0.00192	0.110	58.8
45	0.0011085	0.0635	34.0
51.79	0.0008726	0.050	29.4
60	0.000640	0.0367	19.6
70	0.000400	0.0229	12.35
80	0.000196	0.0112	6.0
90	0.0	0.0	0.0

high magnitudes of angular momentum about the X axis. Solutions to this problem of small β angles, which should be considered are one of the following:

1. Double axis articulation of the solar panels.

or

2. Set a fixed $\phi = \pm 90$ degrees with the Z axis perpendicular to the orbit (see Figure 3-2) and with δ being controlled by sun sensors to keep Y_S aligned as close as possible to X_I (rotating once per orbit) for small β angles.

The problem with 1. is the complexity of the additional solar panel control hardware. The disadvantage of 2. is the loss of some solar power: e.g., to 86.6% of nominal for $\beta = 30$ deg or 70.7% of nominal for $\beta = 45$ deg. This power reduction can be minimized by adding dedicated control or momentum exchange devices for the X_V vehicle axis (reaction wheels) such that two axis pointing can be resumed for β angles less than 30 degrees.

3.1.6 Summary

All long term angular momentum requirements are combined to determine:

- o A total momentum envelope for prospective momentum exchange devices
- o Maximum momentum buildups due to bias torque for sizing momentum desaturation devices in Section 4.

Angular momentum requirements for gravity gradients, aerodynamic, magnetic and radiation torques were determined in sections 3.1.1 through 3.1.4, respectively. These are combined on a vehicle-axis basis to determine maximum components of total angular momentum vectors.

A summary of cyclic angular momentum requirements are given in Table 3-10 for all twelve space construction base configurations. The recommended attitude orientation for each configuration is given. Alternate, modified orientations are also listed for configurations 8 through 11 where 8M, 9M, 10M and 11M are rotated slightly about the YV axis (from the nominal XPOP attitude) until the XP axis (principal X axis) is normal to the orbital plane. 12M is an alternate to configuration 12 (XV local vertical) where the XP axis is always along the local vertical. Alphabetical symbols after numerical magnitudes identify the source of the angular momentum contribution:

A Aerodynamic torque
G Gravity gradient torque
M Magnetic torque
R Radiation torque

Maximum components along each of the vehicle's axes are labelled as H_x, H_y and H_z. The magnetic angular momentum, which is computed as a direct function of the vehicle mass, is given as a spherical component H_{xyz} since the magnetic moment of the vehicle has no preferred orientation.

Table 3-10

Summary of Angular Momentum

Due to Long Term Cyclic Torques

● Max Total is for Period of High Solar Activity

CONFIG.	ATTITUDE	ANGULAR MOMENTUM (FT-LB-SEC)					
		MAX COMPONENTS				TOTALS	
		H_X	H_Y	H_Z	H_{XYZ}	MAX	NORMAL
1	XPOP	194.G	0	693.A 7.R	4.M	730.	198.
2	XPOP	196.G	0	680.A 7.R	7.M	721.	203.
3	XPOP	196.G	0	56.A 1.R	10.M	215.	206.
4	XPOP	480.G	0	384.A 4.R	13.M	630.	493.
5	XPOP	254.G	0	78.A 1.R	16.M	282.	270.
6	XPOP	613.G	0	445.A 5.R	22.M	782.	635.
7	XPOP	613.G	0	266.A 3.R	23.M	692.	636.
8	XPOP	(t)A	0	1310.A 28.R	25000.G 32.M	26371.	25065.
8' (I)	XPOP	7340.G (t)A	0	1310.A 28.R	32.M	7494.	7372.
8A	XPOP	11415.G	0	2350.A 49.R	32.M	11696.	11447.
9	XPOP	41100.G	0	1890.A 48.R	42.M	41188.	41142.
9M (II)	XPOP	40970.G	0	1890.A 48.R	42.M	41053.	41012.

(Continued)

Table 3-10 (Continued)

CONFIG.	ATTITUDE	ANGULAR MOMENTUM (FT-LB-SEC)					
		MAX COMPONENTS				TOTALS	
		H_X	H_Y	H_Z	H_{XYZ}	MAX	NORMAL
10	XPOP	484[illegible].G	0	22900.A 305.R	52.M	53790.	48524.
10M (II)	XPOP	47860.G	0	22900.A 305.R	52.M	53241.	47914.
11	XPOP	48450.G	0	23700.A 310.R	53.M	54126.	48505.
11M (II)	XPOP	47910.G	0	23700.A 310.R	53.M	53643.	47965.
12	XLV	0 (IV)	0	23400.A 1230.R	∿0	24630. (IV)	1328. (IV)
12M (III)	XP-LV	0 (IV)	0	23400.A 1230.R	∿0	24630. (IV)	1328. (IV)

(t) a minor trace of angular momentum exists

(I) $\phi_Y \stackrel{\sim}{=} 25^O$ to put the XP axis normal to the orbit plane

(II) $\phi_Y < 5^O$ to put the XP axis normal to the orbit plane

(III) $\phi_{TOTAL} < 10^O$ to put the XP axis along the local vertical

(IV) This entry does NOT include an H_X component required for maneuvering about the X axis.

TABLE 3-11

SUMMARY OF ANGULAR MOMENTUM

DUE TO LONG TERM BIAS TORQUES

● MAX TOTAL IS FOR PERIOD OF HIGH SOLAR ACTIVITY

CONFIG.	ATTITUDE	ANGULAR MOMENTUM (FT-LB-SEC/ORBIT)					
		MAX COMPONENTS				TOTALS	
		H_X	H_Y	H_Z	H_{XYZ}	MAX	NORMAL
1	XPOP	-	-	200.AB 155.R	25.M	380.	181
2	"	-	-	215.AB 153.R	45.M	413.	199.
3	"	-	-	18.AB 12.R	60.M	90.	72.
4	"	-	-	125.AB 86.R	80.M	291.	167.
5	"	-	-	25.AB 17.R	100.M	142.	117.
6	"	-	-	140.AB 100.R	145.M	385.	246.
7	"	-	-	85.AB 124.R	150.M	359.	274.
8	"	(t)AB	220000.G	415.AB 313.R	200.M	220200.	220200.
8M (I)	"	(t)AB	0	415.AB 313.R	200.M	930.	517.
8A	"	0	0	715.AB 535.R	200.M	1450.	738.
9	"	-	20650.G	600.AB 453.R	260.M	20937.	20915.
9M (II)	"	-	0	600.AB 453.R	260.M	1313.	716.

(Continued)

TABLE 3-11 (Continued)

CONFIG.	ATTITUDE	ANGULAR MOMENTUM (FT-LB-SEC/ORBIT)					
		MAX COMPONENTS				TOTALS	
		H_X	H_Y	H_Z	H_{XYZ}	MAX	NORMAL
10	XPOP	-	61520.G	7290.AB 5114.R	315.M	63073.	62050.
10M (II)	"	-	0	7290.AB 5114.R	315.M	12719.	5459.
11	"	-	59490.G	7540.AB 5279.R	340.M	61195.	60067.
11M (II)	"	-	0	7540.AB 5279.R	340.M	13159.	5650.
12	XLV	-	124900.G	71680.G 43500.A 7450.AB 5324.R	350.M	179158.	147191.
12M (III)	XP-LV	-	0	43500.A 7450.AB 5324.R	350.M	56624.	5886.

(t) a minor trace of angular momentum exists

(I) $\phi_Y \tilde{=} 25^\circ$ to put the XP axis normal to the orbit plane

(II) $\phi_Y < 5^\circ$ to put the XP axis normal to the orbit plane

(III) $\phi_{TOTAL} < 10^\circ$ to put the XP axis along the local vertical

AB caused by half-wave rectification of aerodynamic cyclic torques

The magnitudes listed under components are for maximum aerodynamic torques obtained for the rare, periodic occasions of high solar activity which results in maximum atmospheric densities (at nighttime). Totals are listed for this maximum and also the normal, where aerodynamic torques are at their normal levels.

Angular momentum buildups due to bias torques are presented in a similar manner in Table 3-11. Here

AB Represents aerodynamic bias torques cause by rectification of cyclic torques, where the vehicle is in daytime or nighttime for one-half of the orbit, the difference in air density causing an apparent half-wave rectification of aero torques.

The resulting angular momentum listings given in Tables 3-9 and 3-10 will be used to select actuator groupings in 3.3, while those listed in Table 3-11 will be used for determining a momentum desaturation system in Section 4.

3.2 SHORT TERM DISTURBANCES

Short term disturbances were defined mainly as forcing functions for the computer simulation of the SCB. Disturbances being considered are crew disturbances and Shuttle Orbiter docking. These disturbances can also be used in sizing the torque capability of the attitude actuator system.

Other disturbances which cannot and will not be considered at this time are:

a. Moving parts of equipment (such as cameras, manipulator arms)
b. Rotational wheel unbalances
c. Attitude control system noise from sensors, quantization, etc.

Locations of disturbances to be applied to the SCB simulations are listed in Table 3-12. All possible docking and/or crew disturbance force directions are noted on the table. Module locations and section numbers were defined in Section 2.

3.2.1 Crew Disturbances

Crew disturbance torques are basically caused by forces generated at a radius arm from the vehicle body center of mass. In vector form,

$$\underline{L} = \underline{R} \times \underline{F} + \underline{M} \qquad (3\text{-}24)$$

where

$\underline{L}$ = resultant torque disturbance
$\underline{R}$ = radius arm from the center of mass to the point of application of the crew disturbance force
$\underline{F}$ = crew disturbance force
$\underline{M}$ = any disturbance moment generated as a couple.

TABLE 3-12

DISTURBANCE LOCATIONS ON THE SCB

MODULE	BODY SECTION	DISTURBANCES		FORCE AXES	CONFIGURATIONS FOR DOCKING	
		CREW	DOCKING		FROM	TO
DM1	1	✓	✓	x	1	1
		✓	✓	y	1	5
		✓	✓	z	1	3
DM2	6	✓	✓	x	2	2
		✓	✓	y	2	4
		✓	✓	z	2	12
DM3	7	✓	✓	x	8	10
		✓	✓	y	8	12
		✓		z	-	-
DM4	10	✓	✓	x	8	12
		✓	✓	y	8	12
		✓	✓	z	8	8
HM3 (at the end in the -y direction)	1	✓		x	(6)*	(12)*
		✓		y	(6)*	(12)*
		✓		z	(6)*	(12)*

*crew disturbances only

A time history of a "wall push off" crew disturbance force is shown in Figure 3-4; this was obtained from reference 3-12. The force can be restricted as being along the vehicle X, Y or Z axis, and the resulting scalar equations are

$$L_X = R_Y F_Z - R_Z F_Y + M_X$$

$$L_Y = R_Z F_X - R_X F_Z + M_Y \qquad (3\text{-}25)$$

$$L_Z = R_X F_Y - R_Y F_X + M_Z$$

Radius arm components (R_X, R_Y, R_Z) were obtained from Section 2, and are listed in Tables 3-13 and 3-14. The conditions in Table 3-13 are for an ideally rigid SCB while Table 3-14 represents a flexible vehicle where modules are divided into bodies as in reference 3-13. Each body normally contains one or more modules. Table 3-14 also lists the body number, SCB configuration number, body mass and the moment of inertia about its center of mass. Each body moment of inertia was computed about its i-th axis as follows:

$$J_{ii} = m \left[(K_i)^2 + (r_j - c_j)^2 + (r_k - c_k)^2 \right] \qquad (3\text{-}26)$$

where

m = the body mass
K_i = radius of gyration about the i-th axis
r_j, r_k = module location along j-th and k-th axes with respect to the origin of SCB axis definition

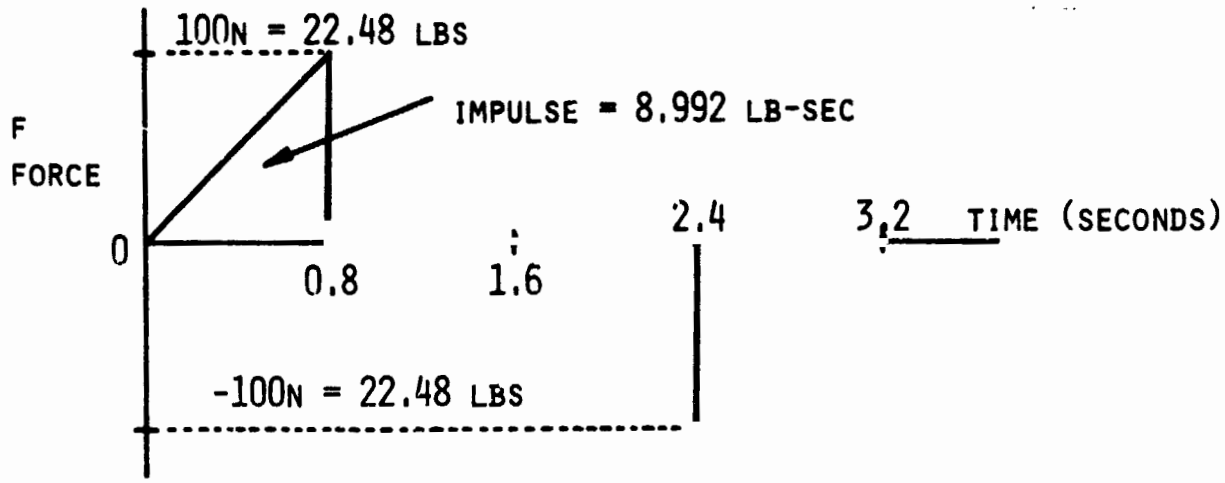

FIGURE 3-4 WALL PUSHOFF CREW DISTURBANCE

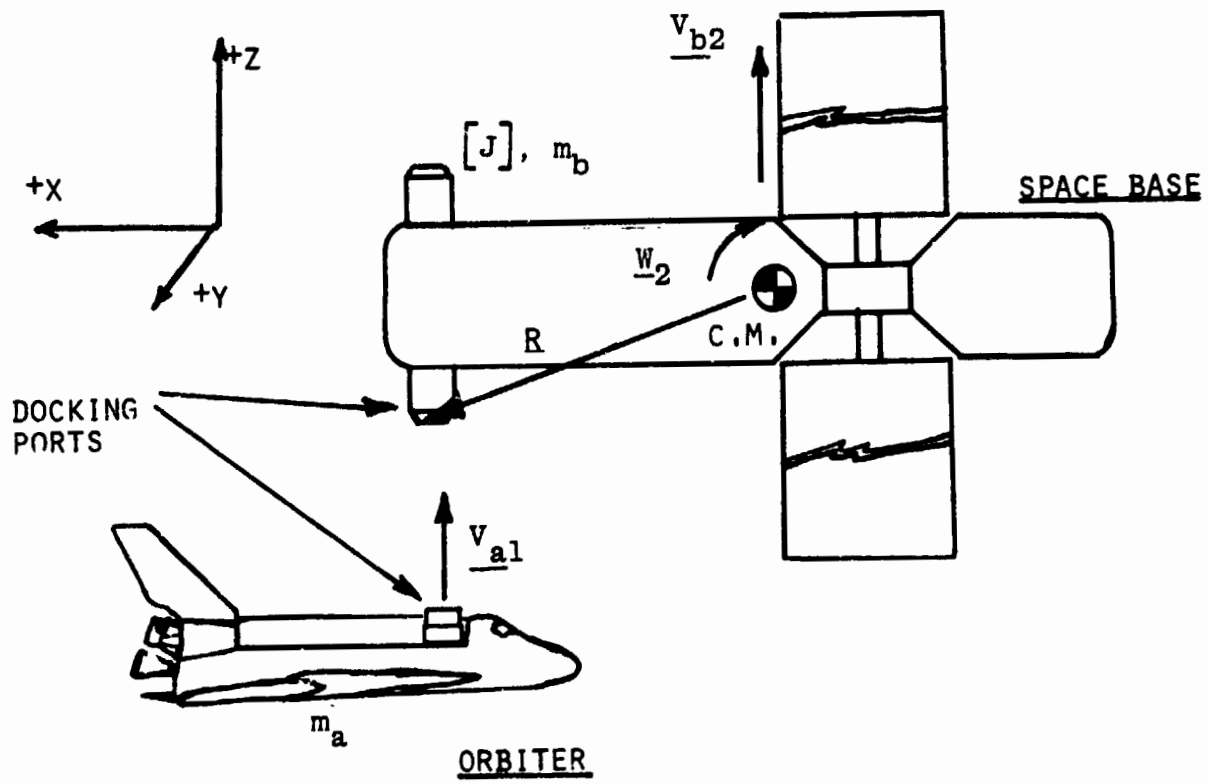

FIGURE 3-5 DOCKING DISTURBANCE

TABLE 3-13

PHYSICAL CHARACTERISTICS OF SCB VEHICLE

DISTURBANCE LOCATIONS

o RIGID BODY

o i = x, y, z AXES

DISTURBANCE LOCATION		VEHICLE CENTER	R_i	gm_b	J_{ii}	VEHICLE
MODULE	POSITION (IN)	OF MASS (IN)	RADIUS ARM (FT)	WEIGHT (LBS)	MOMENT OF INERTIA (SLUGS)	CONFIG. APPLICABLE
DM1	-377	-76.8	-25.0	40,904	2.6620E5	1
	0	0	0		5.3219E5	
	0	0	0		2.9685E5	
DM2	578	633.2	-4.60	588,637	7.0445E7	12
	0	29.7	-2.475		2.0090E8	
	0	-48.1	4.0083		2.0986E8	
DM3	1541	"	75.65	"	"	12
	0		-2.475			
	0		4.0083			
DM4	1541	"	75.65	"	"	12
	0		-2.475			
	250		24.842			
DM3	-377	"	-84.183	"	"	12
	-514.2		-45.325			
	0		4.0083			

TABLE 3-14

PHYSICAL CHARACTERISTICS OF DISTURBANCE LOCATIONS FOR SCB BODIES

o FLEXIBLE BODY

o i = x, y, z AXES

DISTURBANCE LOCATION			BODY CENTER OF MASS (IN)	R_i RADIUS ARM (FT)	gm_b WEIGHT (LBS)	J_{ii} MOMENT OF INERTIA INERTIA (SLUG-FT^2)	BODY CONFIG. APPLICABLE	
MODULE	BODY	POSITION (IN)					FROM	TO
DM1	1	-377 0 0	-88.742 0 0	-24.011 0 0	39,202	3.1021E4 2.6466E5 2.6466E5	1	1
DM2	6	578 0 0	535.191 0 0	3.567 0 0	60,472	3.3632E5 1.3981E5 4.2742E5	5	12
DM3	7	1541 0 0	1150.995 0 0	32.5 0 0	45,089	3.5866E4 7.4545E5 7.[illegible]73E5	8	12
DM4	10	1541 0 250	1541 0 1145.65	0 0 -74.971	82,080	[illegible]42E[illegible] [illegible] 2.[illegible]	9	12
HM3	1	-377 -514.2 0	-321.92 0 25.403	-4.59 -42.85 -2.1[illegible]7	142,031	1.3691E6 1.5339E6 2.1758E6	6	12

c_j, c_k = locations of the center of mass of the body along the j-th and k-th axes with respect to the origin of the SCB axis definition

Also,
$$c = \frac{\sum_{n=1}^{N}(m_n r_{ni})}{m} \qquad (3\text{-}27)$$

and
$$m = \sum_{n=1}^{N} m_n \qquad (3\text{-}28)$$

where n = module number

N = total number of modules forming the body of interest

3.2.2 Docking

Docking disturbances to SCB will be as an initial condition of angular rate, $\underline{W}(o)$. Equations for the solution of $\underline{W}(o)$ are generated in reference 3-14 utilizing Figure 3-5. A generalized scalar equation to be simulated for each case follows:

$$W_x(o) = \frac{R_y V_z - R_z V_y}{J_{xx}/m_a + R_y^2 + R_z^2}$$

$$W_y(o) = \frac{R_z V_x - R_x V_z}{J_{yy}/m_a + R_z^2 + R_x^2} \qquad (3\text{-}29)$$

$$W_z(o) = \frac{R_x V_y - R_y V_x}{J_{zz}/m_a + R_x^2 + R_y^2}$$

where

V_x, V_y, V_z = linear relative velocity of the docking vehicle along the SCB X, Y, Z axes

m_a = mass of the docking vehicle

J_{xx}, J_{yy}, J_{zz} = the moments of inertia of the space base about the vehicle or section of interest, about the center of mass of the vehicle or its section of interest

Equation 3-29 assumes that the impact of docking is completely inelastic due to the operation of the docking latching mechanism. Also, the docking vehicle is assumed to be a point mass (or particle) once it is docked to the space base. A more complete derivation of these equations would have included inertia dyadics for both bodies and the inertial translational and rotational velocities at the instant of impact. The resulting equations, however, would then be extremely complex. The docking condition would be assumed for a fully loaded Shuttle Orbiter at a relative velocity of 0.5 ft/sec. The orbiter mass, m_a, will be assumed to be 7200 slugs (equivalent to a weight of approximately 230,000 lbs.). The magnitudes of J_{ii}, R_j and R_k can be found in Tables 3-13 or 3-14, dependent upon whether a rigid or flexible SCB is being simulated. Based upon conditions shown in Table 3-12, only one component, either V_j or V_k, can exist during docking. This can further simplify equation (3-29) by eliminating one of the terms in the numerator.

If translational docking disturbances on a body are of interest, the initial condition of a SCB linear velocity can be defined as:

$$\underline{V}_c(o) = \left[\frac{m_a}{m_a + m_b}\right] \underline{V} \qquad (3\text{-}30)$$

Components of the $\underline{V}_2$ vector are scaled to $\underline{V}$ in a proportionate manner as shown in (3-30)

where

m_b = mass of the space base

$$\underline{V} = \left[V_x \; V_y \; V_z\right]^T$$

3.3 MOMENTUM EXCHANGE ACTUATORS

On the basis of data presented in Sections 3.1.5 and 3.1.6, the number and size of momentum exchange actuators can now be determined. An ideal momentum exchange actuator for a vehicle and mission of this type would be a double-gimbal control moment gyro (DG CMG). Each CMG unit would have a spherical momentum envelope, with modifications previously recommended to remove all gimbal stops. Assuming the same type as used for Skylab, the angular momentum for each DG CMG is 2300 ft-lb-sec. The number of DG CMG units required for each configuration is given in Table 3-15. The largest number of DG CMG units in the Table is 24 for configurations 10 and 11. All 24 of these CMG units would also

C-2

TABLE 3 -15

NUMBER OF DGCMG UNITS REQUIRED FOR ANGULAR MOMENTUM ENVELOPE

- CMG H = 2300 FT-LB-SEC EACH
- ASSUMES NO REDUNDANCY
- SPHERICAL CMG ENVELOPE

CONFIG.	ATTITUDE	DGCMG UNITS	
		MAXIMUM	NORMAL
1	XPOP	2*	2*
2	"	2*	2*
3	"	2*	2*
4	"	2*	2*
5	"	2*	2*
6	"	2*	2*
7	"	2*	2*
8	"	12	11
8M	XP-POP	4	4
8A	XPOP	6	5
9	"	18	18
9M	XP-POP	18	18
10	XPOP	24	22
10M	XP-POP	24	21
11	XPOP	24	22
11M	XP-POP	24	21
12	XLV	11#	2*#
12M	XP-LV	11#	2*#

*MINIMUM REQUIRED FOR CONTROL OF VEHICLE

DOES NOT INCLUDE ANGULAR MOMENTUM REQUIREMENTS FOR ROLL AXIS MANEUVERING WHICH IS NECESSARY FOR POINTING SOLAR WINGS AND ARRAYS DIRECTLY AT THE SUN

be available for configuration 12, although only 11 units would be required for the worst case conditions.

3.3.1 ROLL AXIS MANEUVERING

The additional 13 units would be available for assistance in cycling the roll axis of the vehicle about the vertical axis for accurate pointing of solar panels throughout each orbit, if desirable.

Reference to Table 3-9, however, indicates that a total of 59 or 34 equivalent CMG units would be required for vehicle roll about the local vertical with β angles of 30 and 45 degrees, respectively. For β=45 degrees, the additional angular momentum about the X axis can be in the form of 10 reaction wheels (2300 ft-lb-sec), 10 single gimbal (SG) CMG units or 10 additional DG CMG units. The reaction wheels (RW's) would extend the momentum envelope of the system to the equivalent of 34 CMG's in the $\pm$ X direction, while 24 actual CMG's would still be available for control about the Y and Z axes.

If 10 single gimbal CMG units were used, needless momentum would be available for the Y and Z axes (beyond the 24 DG CMG units which are already redundant). The 10 SG CMG units would weigh more than the 10 RW's because of the gimbals and gimbal servos. Also, additional software would be required for the RW steering control laws.

If 10 additional DG CMG units were added to the system, they would weigh more than the RW's or the SG CMG units because of the gimballing and controls. The steering

control law software, however, is easily integrated into the software existing (reference 3-15) for the original 24 DG CMG units. The full spherical momentum envelope of 34 DG CMG units would then be available and no additional steering control laws would be required. On that basis, the addition of the 10 DG CMG units appears to be the most attractive approach.

The fixed roll angle approach (with the Y vehicle axis IN the Orbital Plane and with the Z axes NORMAL to the Orbital Plane) would be used for β angles less than 45 degrees. For a β angle just slightly less than 45 degrees, only 71% of the solar power would be available at the solar panels. For smaller β angles, the efficiency would improve up to 100% when $\beta = 0$. For β angles larger than $\pm$ 45 degrees, the roll about vertical maneuvering would be required and 100% of the solar panel electrical power would be available.

If the roll control transition is to take place at β=30 degrees, then the minimum solar power efficiency would be improved to 86.6%; but 35 additional DG CMG units (or SG CMG's or RW's) would be required for configuration 12. Figure 3-6 summarizes the trade off between solar power efficiency and the number of additional DG CMG units as a function of the β angle. The horizontal straight line is when the vehicle maneuvers in roll about the local vertical. The curved portion (actually a cosine β function) is for when the roll angle is fixed and the Z, or solar drive, axis is normal to the orbital plane.

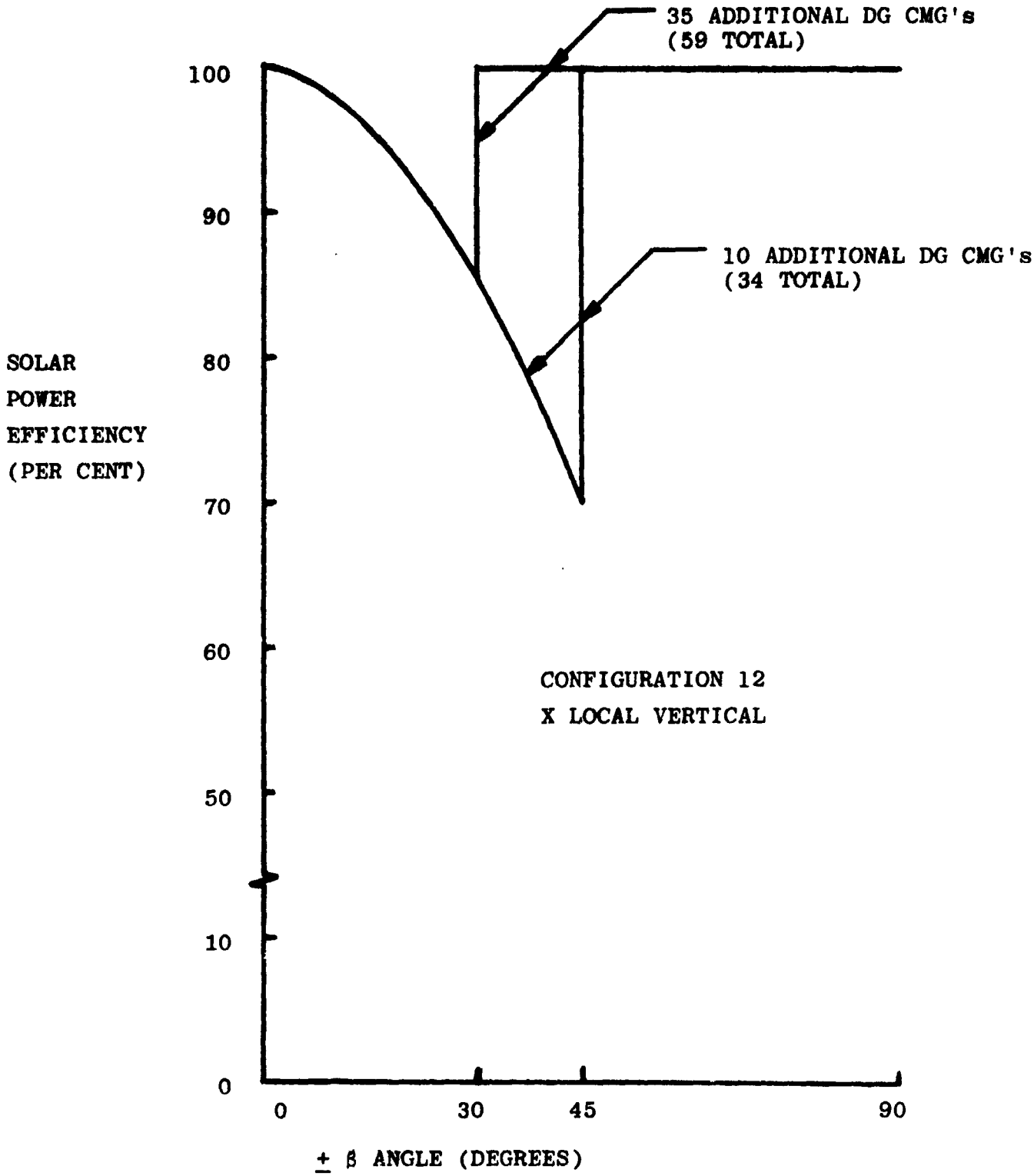

FIGURE 3-6 SOLAR POWER EFFICIENCY FOR X LOCAL VERTICAL ATTITUDE AS A FUNCTION OF β ANGLE AND NUMBER OF ADDITIONAL CMG UNITS REQUIRED

3.3.2 ALTERNATE NON-ROLLING SOLAR POINTING APPROACH

An alternate approach would completely eliminate roll maneuvers around the local vertical for all β angles -- with a slight increase in the average solar power efficiency. For β angles with magnitudes less than 36 degrees, the same technique as previously described would be used: the vehicle roll angle would be set at 90 degrees (relative to that shown in Figure 3-2) and the solar panels would be controlled to point towards the X_o axis on the diagram. The efficiency would then be equal to cosβ.

For β angles larger than 36.1 degrees, the vehicle roll angle would be set to 0 degrees (Y axis normal to the orbit plane) and the solar panel drive would attempt to point towards the sun (maximize $Y_S \bullet X_I$). This can be accomplished by using solar aspect sensors on the solar panels to set $X_S \bullet X_I = 0$. Ordinarily the solar power efficiency would vary in a cyclic manner as a function of orbit position angle α. The resulting instantaneous solar power efficiency would be

$$\eta = Y_S \bullet X_I = \left[1 - (\cos\beta \sin\alpha)^2\right]^{\frac{1}{2}} \qquad (3\text{-}31)$$

Also,

$$\tan\delta = \frac{\cos\alpha}{\tan\beta} \qquad (3\text{-}32)$$

where δ = solar panel position angle.

An expression can also be generated for the <u>average</u> solar power efficiency as a function of the β angle using (3-31):

$$\bar{\eta} = \frac{2}{\pi} \int_0^{\pi/2} \eta \, d\alpha \qquad (3\text{-}33)$$

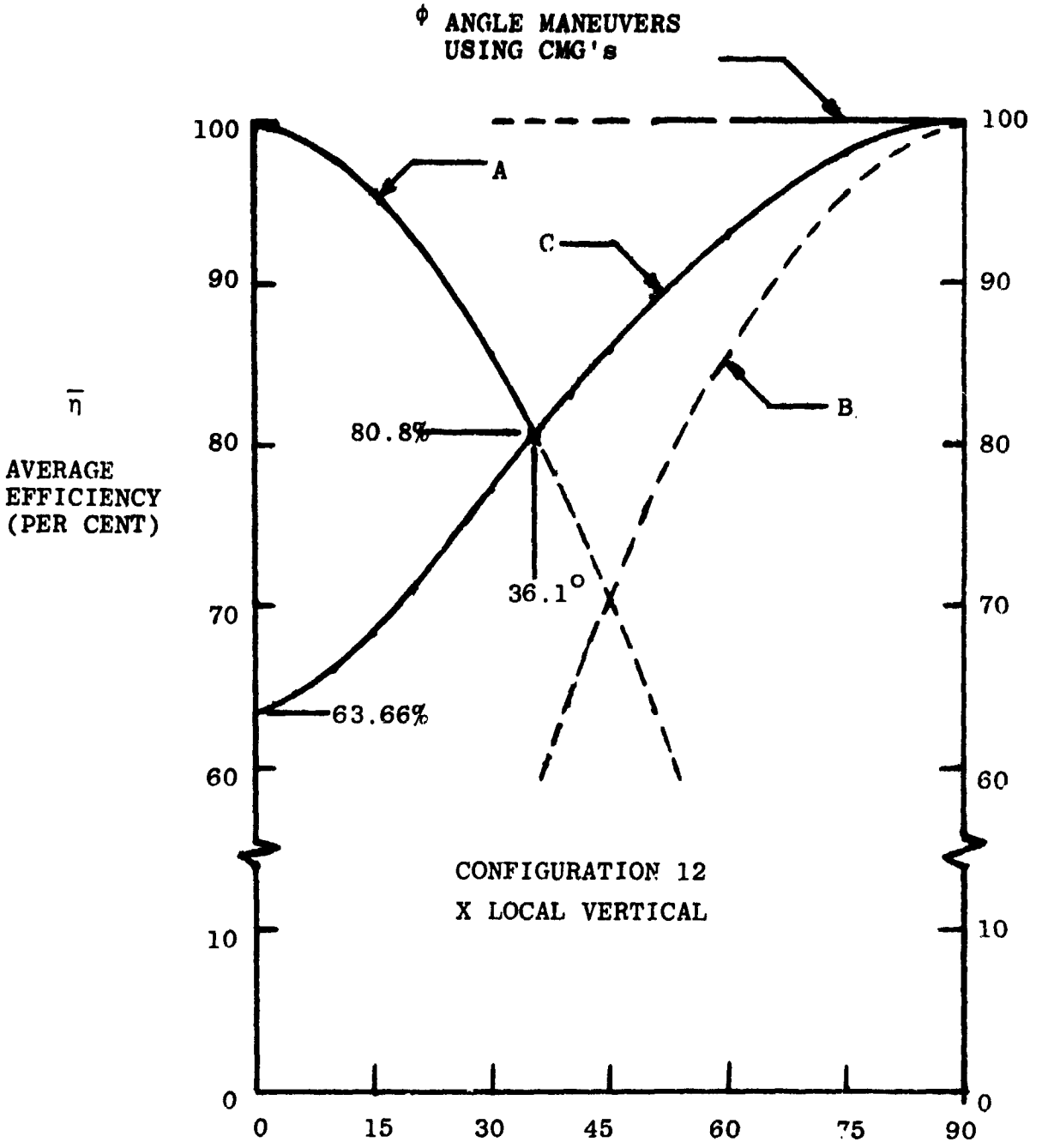

A: $\phi = 90^{o}$ (ZPOP), SOLAR DRIVE OPERATIONAL (POINTING TO X_O)
B: $\phi = 0^{o}$ (YPOP), SOLAR DRIVE FIXED ($\delta = 0$ or 180^{o})
C: $\phi = 0^{o}$ (YPOP), SOLAR DRIVE OPERATIONAL ($X_S \bullet X_I = 0$)

FIGURE 3-7 SOLAR POWER AVERAGE EFFICIENCY vs. BETA ANGLE FOR THE ALTERNATE NON-ROLLING APPROACH

The integral portion of (3-33) (tabular data was obtained in reference 3-16) is an elliptic integral which results in curve C of Figure 3-7. Curve A is for the case when the solar panels point towards X_o (when $\phi = 90^o$ or the Z axis of the vehicle is perpendicular to the orbit plane). A composite of curves A and C would then be utilized; they cross at $\beta=36.1^o$ where the average solar power efficiency is approximately 80.8%. This is an apparent improvement over the method described in 3.3.1 since no continuous roll axis maneuvering or additional CMG units are required. This should be the preferred approach. The CMG units indicated in Table 3-15 would then apply.

3.4 REFERENCES

3-1 Kaczynski, R. F., Space Base Angular Momentum Requirements for Gravity Gradient Torques, MT 40,802, 24 October 1977

3-2 Kaczynski, R. F., Space Base Angular Momentum Requirements for Aerodynamic Torques, MT 40,803, 17 November 1977

3-3 Kaczynski, R. F., Space Base Angular Momentum Requirements for Magnetic Torques, MT 40,804, 22 November 1977

3-4 Kaczynski, R. F., Space Base Angular Momentum Requirements for Radiation Torques, MT 40,805, February 1, 1978

3-5 NASA SP-8024, Spacecraft Gravitational Torques, NASA Space Vehicle Design Criteria (Guidance and Control), May 1969

3-6 NASA SP-8058, Spacecraft Aerodynamic Torques, Anon., January, 1971

3-7 NASA SP-8021, Model of the Earth's Atmosphere, Anon., May, 1969

3-8 NASA SP-8018, Spacecraft Magnetic Torques, Anon., March 1969.

3-9 NASA SP-8017, Magnetic Fields - Earth and Extra-terrestial, Anon., March 1969

3-10 NASA SP-8027, Spacecraft Radiation Torques, October 1969

3-11 Kaczynski, R. F., Solar Panel Position and Vehicle Roll Orientation During X Local Vertical Mode, MT 40,806, February 1978

3-12 Fritz, C. G.; Howell, J. T.; Nicaise, P. D. and Parker, J. R., NASA TM X-64972, A Miniaturized Pointing Mount for Spacelab Missions, November 25, 1975

3-13 Cornell, G. A., Space Base Mathematical Model, Bendix Research Laboratories Report, Program BRL-SB-1, December 14, 1977

3-14 Kaczynski, R. F., Short Term Disturbances on the Attitude of the Space Construction Base, MT 40,809, May 8, 1978

3-15 Kennel, H. F., Steering Law for Parallel Mounted Double-Gimballed Control Moment Gyros, NASA TM X-64930, February 1975.

3-16 CRC Standard Mathematical Tables, 18th Edition, The Chemical Rubber Co., 1970 (see page 537).

SECTION 4

4.0 MOMENTUM DESATURATION

4.1 DESATURATION REQUIREMENTS

Desaturation requirements are based upon the longterm bias torques determined in the preferred orientations of each SCB configuration. The requirements for momentum desaturation are listed in Table 4-1. The worst case average torque for one orbital period is also tabulated. Almost all of the disturbance torque is about the space construction base (SCB) Z axis for all twelve configurations. All of these are summarized in reference 4-1.

Magnetic torquing, reaction control (RCS) and gravity gradient (GG) desaturation were evaluated for the XPOP orientations and also for the X local vertical alignment for configuration 12M. Characteristics of these approaches were independently determined in reference 4-2. They will be reviewed in the following paragraphs and then compared at the end of this section.

4.2 MAGNETIC DESATURATION

A counteracting magnetic torque $\underline{L}_m$ is generated on the vehicle by $\underline{M}$, a torque coil system magnetic moment, interacting with the earth's magnetic field $\underline{B}$ according to the physical law given by:

$$\underline{L}_m = \underline{M} \times \underline{B} \qquad (4\text{-}1)$$

where each vector in (4-1) can be put in vehicle coordinates. SI units for L_m, M and B are N-m, A-m^2 and tesla, respectively. The average L_m torque vector per orbit should be equal and opposite to the average disturbance torque of the previous orbit, as measured from the momentum exchange control system.

TABLE 4-1

SCB REQUIREMENTS FOR MOMENTUM DESATURATION

- MAXIMUM MOMENTUM AND TORQUE ARE FOR MAXIMUM SOLAR ACTIVITY
- ALMOST ALL MOMENTUM AND TORQUE ARE ABOUT THE VEHICLE'S Z AXIS
- ORBITAL PERIOD IS 5668 SECONDS

CONFIGURATION		ANGULAR MOMENTUM (FT-LB-SEC/ORBIT)		AVERAGE BIAS TORQUE (FT-LB)	
NO.	ATTITUDE	MAXIMUM	NORMAL	MAXIMUM	NORMAL
1	XPOP	380	181	.0670	.0319
2	"	413	199	.0729	.0351
3	"	90	72	.0159	.0127
4	"	291	167	.0513	.0295
5	"	142	117	.0251	.0206
6	"	385	246	.0679	.0434
7	"	359	274	.0633	.0483
8M	XP-POP	930	517	.164	.0912
9M	"	1313	716	.232	.126
10M	"	12719	5459	2.24	.963
11M	"	13159	5650	2.32	.997
12M	XP-LV	56624	5886	9.99	1.04

A basic orientation of four magnetic torques relative to vehicle axes is given in Figure 4-1. If λ is set at 35.26 degrees, each component of the magnetic momemt vector $\underline{m} = \begin{bmatrix} m_1 & m_2 & m_3 & m_4 \end{bmatrix}^T$ has direction cosines of equal magnitude with the X, Y and Z axes. A block diagram for the typical implementation of a magnetic torquing system is shown in Figure 4-2. Both the minimum energy (ME) and cross product control laws are described. The cross product law is easier to comprehend and implement, but the ME law is expected to use less electrical energy and could be a candidate for the SBC application.

An explanation of some of the symbols follows:

$\underline{B}$ = predicted magnetic field of the earth at the instantaneous location of the SCB in orbit, in vehicle coordinates (tesla)

$\underline{B}_a$ = actual B (tesla)

$\underline{B}_m$ = measured B (tesla)

$\underline{L}_{AVG}$ = average bias torque (previous or presently predicted orbit) in vehicle coordinates (N-m)

$\underline{L}_m$ = generated magnetic torque in vehicle coordinates (N-m)

$\underline{m}, \underline{m}_c$ = actual and commanded magnetic moments, respectively, in coil coordinates ($A\text{-}m^2$)

$\underline{M}, \underline{M}_c$ = actual and commanded magnetic moments, respectively, in vehicle coordinates ($A\text{-}m^2$)

T = time period of ME control law solution (sec)

ΔH = angular momentum vector change (or commanded dump) over the period T (N-m-sec)

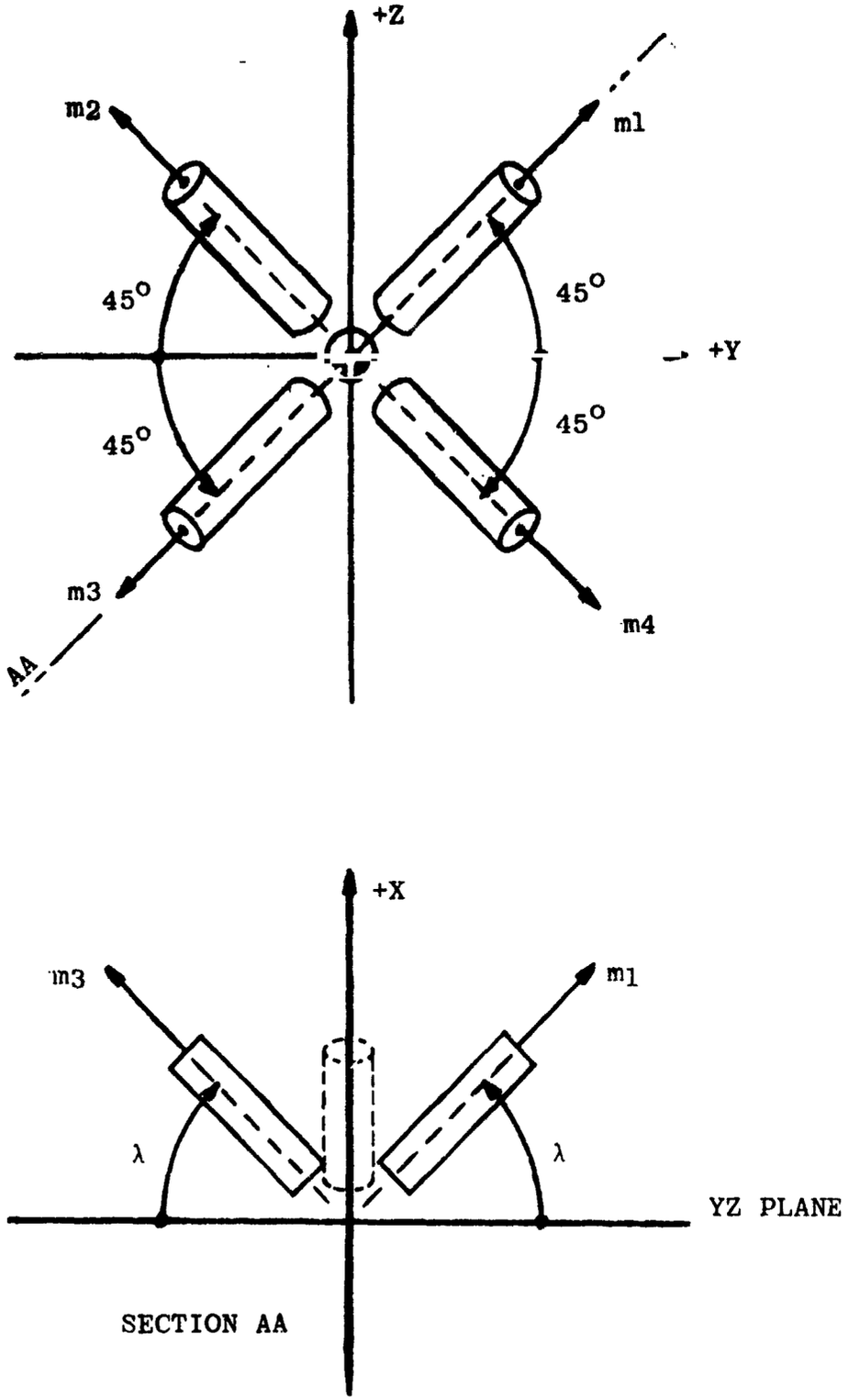

BASIC ORIENTATION OF MAGNETIC TORQUERS

FIGURE 4-1

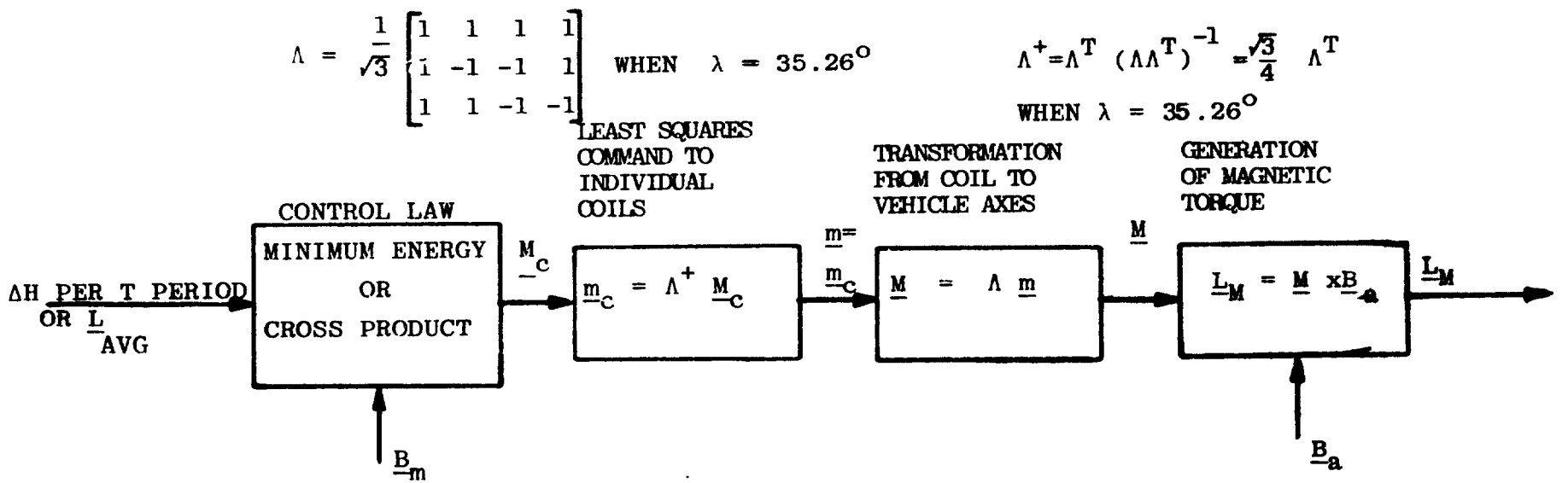

CONTROL LAWS

MINIMUM ENERGY:

$$\underline{M}_c = \underline{B}_m \times \left[\int_0^T [B]\, dt \right]^{-1} \underline{\Delta H} \qquad \text{WHERE } [B] \triangleq -\begin{bmatrix} x \\ B \end{bmatrix}\begin{bmatrix} x \\ B \end{bmatrix}$$

CROSS PRODUCT:

$$\underline{M}_c = \frac{\underline{B}_m \times \underline{L}_{AVG}}{B_m^2}$$

$$\text{AND } \begin{bmatrix} x \\ B \end{bmatrix} \triangleq \begin{bmatrix} o & -Bz & By \\ Bz & o & -Bx \\ -By & Bx & o \end{bmatrix}$$

BLOCK DIAGRAM OF MAGNETIC TORQUING

FIGURE 4-2

Note that the diagram assumes $\underline{m} = \underline{m}_c$. The first two blocks on the diagram must be implemented in the computer, while the second two blocks are inherent to the individual orientations and the operation of the torquer coils.

Table 4-2 is a summary of the magnetic torquing system characteristics. An average earth's magnetic field flux magnitude of 0.1×10^{-4} tesla is assumed to be available on either the vehicle X or Y axis. This is a fairly conservative estimate for all orbits.

From the block diagram we see that

$$L_{MZ} = 0.577 \, (m_1 + m_2 + m_3 + m_4) \, B = 2.3094mB \qquad (4\text{-}2)$$

gives the Z-axis magnetic torque if the directions of the magnetic moments are properly obtained from the control law. Utilizing the torque requirements from Table 4-1, the required magnetic moment per coil (m) was calculated. It was also recalculated for the case when one coil (as shown in Figure 4-1) has malfunctioned. A magnetic torquer size of 3300 A-m^2 was selected for configurations 1 through 7.

Each coil is estimated to be 84 inches long and 3.1 inches in diameter. The weight of each magnetic torquer will be 90 pounds and will require 22.5 watts for a maximum magnetic moment.

The magnetic torquing system was tripled for configurations 8M and 9M, and multiplied by another tenfold for configurations 10M and 11M. If magnetic torquing were to be used for configuration 12M (X local vertical) without any additional gravity gradient or RCS assistance, the system would have to be multiplied 130-fold when compared to the original system for the earlier configurations, the reason for this being the large solar panel surfaces being located so far from the center of mass.

TABLE 4-2

MAGNETIC TORQUING CHARACTERISTICS

- COILS IN PYRAMID CONFIGURATION ABOUT THE X AXIS, 45° BETWEEN Y AND Z AXES
- λ = 35.26 DEG
- ASSUME AVERAGE EARTH FIELD = 0.1×10^{-4} TESLA ON ANY ONE AXIS

CONFIG.	MAGNETIC MOMENT-m ($A\text{-}m^2$ PER COIL) REQUIRED NORMAL	REQUIRED ONE FAILURE	ACTUAL	NO. OF MAG. TORQUING COILS PER ORIENTATION	TOTAL	CAPABILITY ACTUAL/REQ'D	WEIGHT (LBS)	PEAK POWER (WATTS) ½ COILS	ALL COILS
1	2140	2850	3300	1	4	1.16	360	22.5	90
2	2328	3104	"	1	4	1.06	"	"	"
3	508	677	"	1	4	4.87	"	"	"
4	1638	2185	"	1	4	1.51	"	"	"
5	802	1069	"	1	4	3.09	"	"	"
6	2169	2890	"	1	4	1.14	"	"	"
7	2022	2696	"	1	4	1.22	"	"	"
8M	5238	6984	9900	3	12	1.42	1080	67.5	270
9M	7409	9879	"	3	12	1.002	"	"	"
10M	71540	95390	99000	30	120	1.04	10800	675	2700
11M	74095	98790	"	30	120	1.002	"	"	"
12M	319050	425400	429000	130	520	1.01	46800	2925	11700

TABLE 4-3

RCS CHARACTERISTICS

- $L_Z = RF_Y$
- CONFIGURATION TIME PERIOD IS 4 MONTHS EACH (Δt)
- $W = 2\Delta t\ F_Y/I_{SP} \quad 2\ \Delta t\ L_Z/(I_{SP}\ R)$
- I_{SP} IS ASSUMED TO BE 300 SEC
- WEIGHT DOES NOT INCLUDE TANKAGE, VALUES, PIPING, THRUSTERS

CONFIG.	L_Z AVG. BIAS TORQUE (FT-LB)	THRUSTER LOCATIONS +X MODULE	THRUSTER LOCATIONS -X MODULE	COUPLE ARM(R) (FT)	AVG FORCE F_Y (LBS)	W PROPELLANT WEIGHT (LBS) PER CONFIG.	W PROPELLANT WEIGHT (LBS) ACCUMULATED TOTAL
1	.0670	-	DM1 377"+5.4'	30.4*	.0022	77.3	77.3
2	.0729	DM2 578"+5.4'	LM1 5'+6'+8.75'	107.8	.000676	47.4	124.7
3	.0159	SPM 952"+25.75'	LM1 5'+6'+8.75'	159.3	.0000998	6.99	131.7
4	.0513	SPM "	LM1 "	"	.000322	22.6	154.3
5	.0251	SPM "	LM1 "	"	.000158	11.0	165.3
6	.0679	SPM "	LM1 "	"	.000426	29.9	195.2
7	.0633	CCM 1366"+8.75'	LM1 "	176.8	.000358	25.1	220.3
8M	.164	CCM "	LM1 "	"	.000928	65.1	285.4
9M	.232	CCM "	LM1 "	"	.00131	91.9	377.3
10M	2.24	CCM "	LM1 "	"	.0127	890	1267.3
11M	2.32	CCM "	LM1 "	"	.0131	921	2188.3
12M	9.99	PSP 1889"	LM1 "	211.6	.0472	3310	5498.3

*Thruster at - X end only, C.M. is at -76.8 in. for Configuration 1.

4.3 RCS Desaturation

An RCS desaturation system would be operated on demand, i.e. whenever the momentum envelope of the CMG system is approached or whenever the opportunity exists. RCS thruster locations are assumed to be available at the largest radius arms along the X-axis and to operate as a couple (for all except configuration 1). A specific impulse I_{SP} was assumed to be 300 seconds. The time period Δt for each configuration was assumed to be four months each, also the worst case average torque was assumed to exist over the complete Δt period of operation. The propellant weights per configuration and the total accumulation were then computed. All of these characteristics were tabulated in Table 4-3. Although the propellant weights do not include tankage, valving, piping and thrusters, they appear to be very competitive with magnetic torque desaturation. The weight numbers are quite low considering that the fuel is consumed over a four year period.

4.4 Gravity Gradient Desaturation

Whenever the SCB is not in a precise pointing period during its mission, it can be tilted slightly from its nominal orientation to generate a gravity gradient torque which is equal and opposite to the cumulative bias effects of aerodynamic, radiation, magnetic and also gravity gradient disturbances. For example, in the XPOP mode a slight tilt about the Y or Z vehicle axes will generate desired gravity gradient bias torques about the Y and Z axes, respectively. Torques may also be generated about the X axes through a combination of Y and Z axes tilts; this effect, however, will be much weaker because of the actual inertia properties of the SCB. The approximate (small angle) gravity gradient bias torque equations, which assume a circular orbit and neglect product of inertia terms, follows:

$$L_x = K_x \text{ SIN } \theta \text{ SIN } \Psi$$

$$L_y = K_y \text{ SIN } \theta \qquad (4.3)$$

$$L_z = K_z \text{ SIN } \Psi$$

where $K_x = 3W_o^2 (I_{zz} - I_{yy}) / 2$

$K_y = 3W_o^2 (I_{xx} - I_{zz}) / 2$

$K_z = 3W_o^2 (I_{yy} - I_{xx}) / 2$

I_{xx}, I_{yy}, I_{zz} = moments of inertia about vehicle axes

W_o = orbital rate (rad/sec)

θ, Ψ = small tilt angles about the vehicles Y and Z axes, respectively.

A similar relationship also exists for the X local vertical attitude during configuration 12.

Ordinarily, the tilt angles will be constant over the whole orbit and will be updated every orbit or so. But when an inertial orientation is required for celestial viewing, there are some problems in using gravity gradient desaturation:

(a) Large angular momentum build-ups may require large tilt angles during occulted portions of the orbit.

(b) An additional momentum capability would be required for slewing through large angle maneuvers.

(c) Most of the disturbance bias torques will be due to gravity gradient and aerodynamic effects; if the aerodynamic bias torques change appreciably for large tilt angles, it is possible that an angular momentum buildup may not be bounded by simple gravity gradient control.

(d) More complex software.

For the reasons stated above, it is recommended that another desaturation scheme (magnetic) be available for SCB configurations requiring orientations other than XPOP or X local vertical. Gravity gradient desaturation, however, does have some advantages for these preferred orientations:

(a) It is virtually weightless and requires no power (no additional hardware).

(b) Software for continuous tilting is fairly simple

(c) No contaminants are released in the immediate vicinity of the vehicle.

4.5 Summary

The three desaturation schemes which were discussed may be compared by listing some of the disadvantages of each as listed in Table 4-4. The magnetic torquing system appears to be the most flexible approach. For the last few configurations (10M, 11M, 12M), however, the magnetic system gets extremely heavy in weight. For configurations 10M and 11M RCS thrusters may be mounted on the CCM and LM1 modules. The RCS will then be the primary desaturation approach for 10M and 11M, with some assistance from the magnetic torquing system. It would actually be recommended that the RCS system be installed prior to configuration 8M or 9M and be available as a backup or for an emergency desaturation condition.

No additional desaturation equipment would be required for configuration 12M, since a "fixed" gravity gradient tilt angle from the local vertical can be used to counteract a long term angular momentum buildup. One additional complication with 12M, however, is the continual cyclic rolling about the local vertical for β angles greater than 30 or 40 degrees. The CMG angular momentum buildup should be separable from the cyclic momentum for controlling the roll angle about the local vertical; this buildup would be an input signal to the gravity gradient moment management control law.

A summary of recommendations for SCB momentum management is shown in Table 4-5. A magnetic torquing system can be used for configurations 1 through 9M, with the RCS system used as a backup for 8M and 9M. The logistics of propellant fuel replenishment and thruster relocation for an RCS desaturation system is thus circumvented for the first seven configurations.

TABLE 4-4

RELATIVE DISADVANTAGES OF THE DESATURATION SCHEMES CONSIDERED FOR THE SPACE CONSTRUCTION BASE

MAGNETIC	RCS	GRAVITY GRADIENT
o HEAVIEST, PARTICULARLY FOR LATER CONFIGURATIONS	o RELEASE OF CONTAMINANTS	o UNIQUE ORIENTATIONS OR TILTS MAY COMPROMISE POINTING REQUIREMENTS.
o SOME COMPLEX SOFTWARE	o LOGISTICS OF - RESUPPLY - REPOSITIONING OR ADDING OF THRUSTERS FOR SOME CONFIGURATIONS	o TILTING MAY ALSO CHANGE AERODYNAMIC TORQUES
	o PULSING MAY EXCITE BENDING MODES	o INERTIA PROPERTIES REQUIRED (MAY BE DIFFICULT TO DEFINE FOR A LARGE FLEXIBLE VEHICLE)
	o MAY REQUIRE SOME CREW WORKLOAD	o COMPLEX SOFTWARE IF TILT MANEUVERING IS REQUIRED.
		o SOME CREW WORKLOAD MAY BE REQUIRED.
		o MANEUVER ACCELERATIONS AND DECELERATIONS MAY EXCITE BENDING MODES

TABLE 4-5

RECOMMENDATIONS FOR MOMENTUM MANAGEMENT

SCB CONFIGURATION	DESATURATION	
	PRIMARY	BACKUP OR ASSIST
1 THRU 7	MAGNETIC TORQUING	NONE
8M AND 9M	MAGNETIC TORQUING	RCS BACKUP
10M AND 11M	RCS	MAGNETIC TORQUING ASSIST
12M	GRAVITY GRADIENT, FIXED TILT	RCS & MAGNETIC TORQUING BACKUP

Rather than a tenfold increase of the magnetic torquers for configurations 10M and 11M, the RCS system can become the primary desaturation system at that point. Progressing to configuration 12M would ordinarily require a larger increase in propellant weight. But fortunately configuration 12M is in an X local vertical orientation. A fixed small tilt angle from local vertical can be utilized such that a fixed gravity gradient torque cancels the large Z axis aerodynamic torque. The twelve magnetic torquers and the existing RCS thrusters can be used for backup and for short term assistance in desaturation.

4.6 References

4-1 Kaczynski, R. F., Bendix MT-40,807, Total Angular Momentum Requirements for the Space Construction Base, March 17, 1978.

4-2 Kaczynski, R.F., Bendix MT-40810, Angular Momentum Desaturation of the Space Construction Base, August, 1978.

SECTION 5

5.0 CONTROL SYSTEM APPROACH

5.1 INTRODUCTION

This section is part of a study of control system concepts for the Space Construction Base. This effort is directed to investigate control during buildup, i.e., while the Space Construction Base is being assembled in low earth orbit. Study emphasis is on coupling control and control coordination since these are identified as problem areas peculiar to this application. This section presents a clarification of anticipated design problems and control concepts.

Within the next 10 years, earth satellites are expected to include a new breed of large structures constructed in space. Each one may serve a wide range of functions from scientific experiments to manufacturing in the zero-g environment. Others may have special purposes such as collecting solar energy and either retransmitting it to earth via microwave or servicing other space systems. Many of these satellites will be constructed from sections transported by the Space Shuttle.

These large structures introduce new challenges to control system design. The changing physical structure during construction affects the optimum distribution of sensors, the control system structure, and control parameters. The large size and requirements for minimizing weight can bring structural modes within the control system bandwidth - resulting in stability problems and coupling effects.

The Space Construction Base provides a conceptual baseline for various system studies related to these large space structures. It is of "intermediate size" with outer dimensions of 320 by 420 ft. It is conceived to be constructed in a sequence of twelve configurations over a period of four years or longer.

The objective of the study described in this section is to investigate Space Construction Base control problems throughout buildup and during any dynamic testing while in low earth orbit (LEO). The control system must maintain overall stability, include vernier control for at least one element or module, and provide maneuvering capability.

The emphasis in this work is on those control problems which are peculiar to vehicles such as the Space Construction Base. This includes appendage and module stabilizing control in which the coupling between modules and appendages, shape of individual modules or appendages, and the damping of structural modes are controlled. This also includes the vehicle control coordinator which must vary control parameters and select sensors according to configuration and performance changes. Special problems also include model uncertainty and reliability.

5.2 CONTROL PROBLEMS AND APPROACH

Eventually, it is desired to define a control system concept which will stabilize the Space Construction Base attitude, in whole and in part, and provide vernier, maneuvering, and momentum management capability. Such a system must be designed in light of model uncertainty, adapt to configuration changes, function in the presence of strong intermodule interactions and low structural damping, and have a high degree of system integrity with respect to possible component failures.

The Space Construction Base concept introduces a special set of control problems. The control system must accommodate itself to changes in the structure during buildup. It must be relatively insensitive to uncertainties in the structural dynamics since they will not be known precisely. The structure must be regarded as being flexible due to its large size and due to the need to minimize its weight. It must be recognized that the Space Construction Base will be used for a wide variety of purposes.

The purpose of this section is to outline a control system concept for the Space Construction Base. Emphasis is given to those elements which are peculiar to this application. The categories of control and control requirements are discussed in Section 5.3. This is followed in Section 5.4 by a description of the overall control system concept. Important problems special to the Space Construction Base are outlined in Section 5.5. Sections 5.6 and 5.7 outline approaches for two control functions of importance for large spacecraft.

5.3 CONTROL FUNCTIONS

As a convenience, the control of the Space Construction Base may be divided into several functional areas:

A. Appendage and module stabilizing control includes coupling control, shape control, and artificial damping of structural modes. Coupling control ranges from complete decoupling to artificial stiffening in which one module is slaved to another. These functions must be accomplished while the Space Shuttle is docking, station-keeping or maneuvering. This functional area is somewhat analogous to the stability augmentation function of an aircraft.

B. Attitude control holds a given overall orientation of the spacecraft. This would be referenced to an inertial frame or local vertical. Typical accuracy requirements would be on the order of 0.5 deg.

C. Vernier control holds an instrument, element, or module to a precise attitude. Typical accuracy requirements are 1 to 10 arc-s.

D. Maneuvering control changes the overall orientation of the Space Construction Base such as required for docking or for minimizing gravity gradient torque after a module has been added.

E. Momentum desaturation is required with moment exchange devices such as reaction wheels (RWs) and control moment gyros (CMGs). Thus, secondary actuators are used along with CMGs and RWs.

The functional structure of the control system design reflects the philosophy and complexity of the control system. It must express the delegation of computer authority, a definition of control loops, and guidelines for sensor and actuator distribution. Further definition of the functional design would include control loop parameters such as gain factors, filter constants and sensor and actuator dynamic requirements (bandwidth, position and rate limits, etc.)

The delegation of computer authority is tied to the use of centralized or decentralized control. The viewpoints of hierarchical and multilevel control may be adapted to this application. Decentralization has

be·ome more attractive for digital control systems recently with the growth of microcomputer technology. Intervention from ground control should be an integral part of the concept.

The extent of coupling among control loops is an important part of the functional design. Artificial stiffening is an attempt to force the space vehicle to act as a single rigid body, i.e., control action substitutes for a very heavy rigid structure. Complete decoupling is an attempt to cancel interactions between the control loops. Partial decoupling limits the interactions to assume sufficient stability margins. Artificial stiffening between modules would be desirable during maneuvering so as to rotate the vehicle as a unit. Decoupling control, however, may be more desirable while holding a given attitude so as to minimize the coupling of disturbances. Notch filters serve to decrease the interactions between control loops and the structural modes but make the design sensitive to model uncertainties.

Guidelines should be established for sensor and actuator distribution. These will establish the relationship of location selection to mode shapes, function of the given module, and center of gravity. The number of sensors and actuators on a given module also depends on these considerations. The possibility of including more sensor locations than actuators should also be considered since many sensors are of lighter weight and lower cost than the actuators. Also, optimum sensor locations may then be selected according to changes in structural modes.

The mechanization concept would include many hardware selections. For example, there would be some consideration of using digital or analog computers at each level of control. Sensor choices may include different classes of gyros and accelerometers, as well as strain gages. Actuators may include CMGs, torquers/motors, and/or reaction jets. Possibly the earth's magnetic field combined with local electromagnets may be used for momentum management.

5.4 SYSTEM CONCEPT

Figure 5-1 illustrates a functional concept for the Space Construction Base control system. It is intended to fulfill all of the categories of control outlined in Section 5.3. Each block will be changed as the Space Construction Base is assembled.

The Vehicle Control Coordinator would change control parameters as the configuration changes. The selected parameters may be predetermined nominal values corresponding to each configuration, values based on sensed behavior of the system, and/or values remotely commanded by a ground station. It would also be capable of selecting or weighting sensor outputs based on estimated modal shapes. The coordinator may include an identifier for estimating the dynamics of the vehicle. The identifier may simulate an adjustable model which is updated based on observations of the actuator commands and sensor outputs. Some of the coordinator functions may be performed in a ground computer. The vehicle control coordinator is discussed further in Section 5.7.

The Vehicle Attitude Reference Unit may be located in the Habitability Module or the Subsystems Module since these are included in all configurations. It would include gyros, a fixed reference system such as a star tracker, and a computer (or computer segment) for strapdown guidance computations.

The Vehicle Manuevering and Attitude Control unit seeks to maintain a desired overall vehicle attitude or slew rate. Primary control will likely be achieved through use of the double gimbal control moment gyros (DGCMGs).

The primary actuators for momentum management are assumed to be electromagnetic. Thrusters should provide backup. A magnetometer is likely needed to determine ambient magnetic field so that electromagnetic requirements may be computed to achieve a given moment.

Vernier controls are separate functions. A separate set of sensors, control logic and CMGs is required. These would be localzed to vehicle elements such as the research pallet.

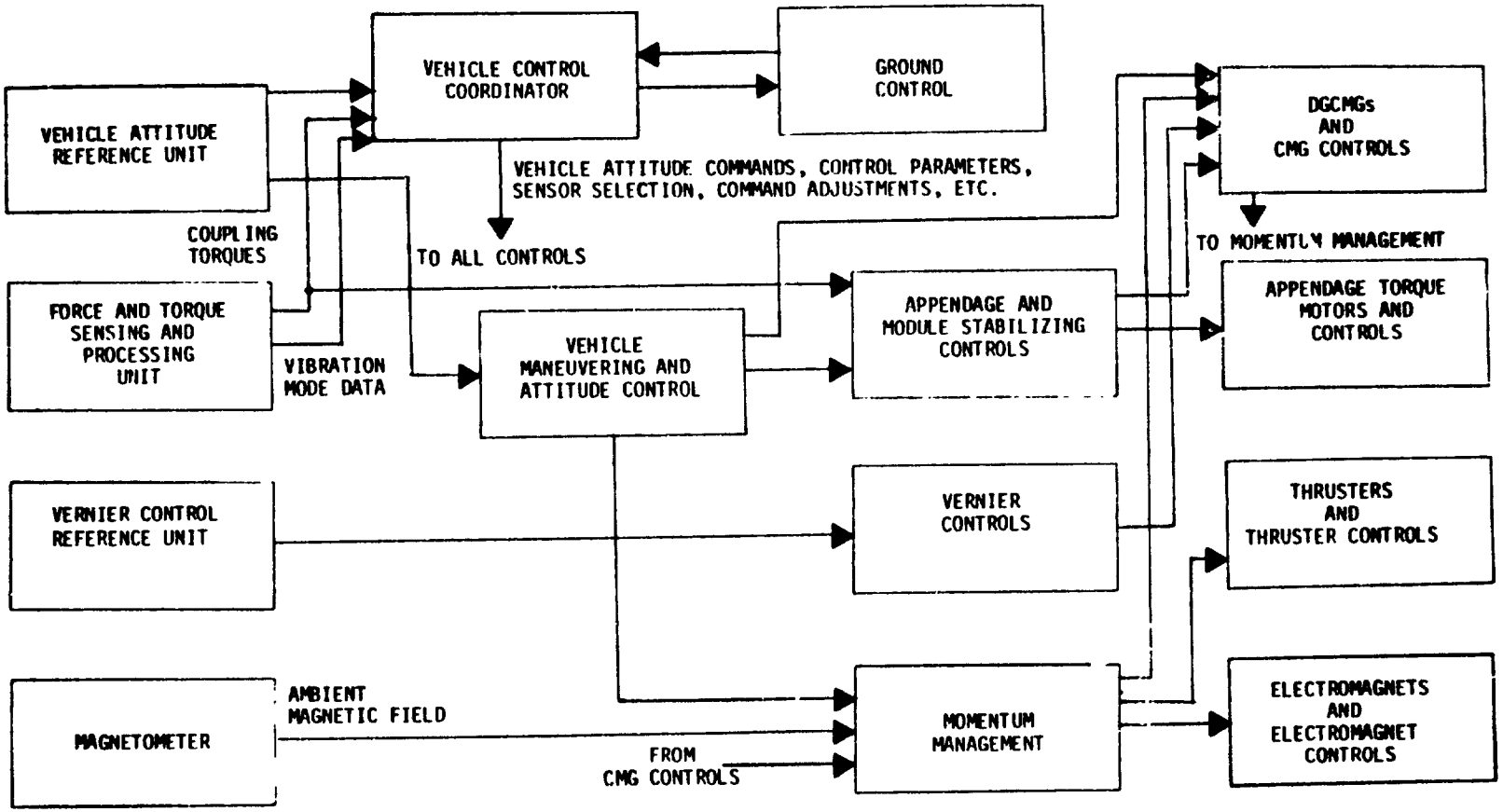

Figure 5-1 - Space Base Control Concept

The control concepts described in the above discussion are similar to those found on many existing spacecraft. The coordinator functions are probably more important and complicated than in many other space vehicles. However, the newest feature is the Appendage and Module Stabilizing Control (or just stabilizing control). This feature is discussed in Section 5.6 with supporting simulation and analysis results given in Section 6.

The Force and Torque Sensing and Processing Units provide primary inputs to the stabilizing controls. The applicable sensors are strain gages from which coupling torques and relative angles are computed. The coupling torques are at the interconnections between modules and between modules and appendages such as the solar panels, external tanks, and antenna support structure. The strain gages will also be used to provide vibration modal data for the Vehicle Control Coordinator and Ground Control. The number of sensor locations may be limited by such considerations as computer capacity and calibration requirements. Alternate sensors such as optical devices may also be considered for stabilizing control.

The primary actuators for the coupling control function of the stabilizing controls are appendage torque motors. Shape control and artificial damping may also be accomplished with torque motors. For larger appendages such as the large solar panels, CMGs may be used for actuation providing there is another type of actuator for momentum desaturation and for balancing large constant torques.

5.5 SPECIAL PROBLEM AREAS

Because of its large size and its buildup in orbit, the Space Construction Base presents special control problems. These must be considered in any trade studies and in design development.

One of the primary considerations is model uncertainty. It is not practical to conduct meaningful preflight dynamic tests of the entire structure. In fact, the final configuration may be unknown when the first sections are placed in orbit. Modes of multiple-connected

Table 5-1 - Control System Design Trades and Considerations

Functional Elements	Design Feature Trades	Considerations
Vehicle Control Coordinator	Functional assignments to ground control or vehicle which control parameters should be adjustable which sensors should be selectable	Space computer requirements Response time Flexibility in adapting to configuration and operational changes Reliability Design sensitivity to model uncertainties Capability to influence dynamic performance Cost
Actuators	Application of rotary actuators versus CMGs to appendage and module stabilizing Actuators for desaturation of CMGs (passive devices versus mass expulsion thrusters)	Capability to improve dynamic behavior Availability of appropriate actuators Power requirements Size and weight Reliability Cost Desaturation requirements Resupply requirements
Sensors	Strain gages versus optical devices for relative angle data	Size and weight Accuracy Sensitivity to model uncertainties (including modal shapes) Dynamic response Linearity Range Reliability Cost Calibration requirements Multiple usage capability Power distribution requirements
Appendage and Module Stabilizing Controls	where to insert coupling controls where to insert shape controls where to insert artificial damping	Capability to improve dynamic behavior Reliability Cost Actuator requirements Power requirements Sensor requirements Sensitivity to model uncertainties

large structures cannot be accurately predicted analytically. Also, the analytical models used in control system design are necessarily simplified. The control system must be designed to satisfy performance requirements in spite of these uncertainties.

Another consideration is that the control configuration will change as modules are added. Control of a given module may require sensor data from other modules leading to greater complexity as others are added. Actuator requirements on a given module may depend on the number and size of other modules, as well as local weight and weight distribution. The control of a given module must adapt to disturbances propagated from other modules. As modules are added, new structural modes are added and others shifted. Fixed sensor and actuator locations on a given module may not be optimum for all configurations.

Even if the configuration of the Space Construction Base were constant, there would still be special control problems. Strong interaction among the modules may lead to a need for some degree of decoupling. Since a complex control system can be highly susceptible to component failures, the system integrity must allow satisfactory performance of many functions in spite of some loop failures. Control system computational requirements must also be considered. There are restrictions on locating actuators. For example, the small solar panels will unlikely support the mass of control moment gyros (CMGs).

Table 5-1 is a summary of some control system design considerations for the Space Construction Base.

5.6 APPENDAGE AND MODULE STABILIZING CONTROLS

The controls under discussion in this section include coupling controls, shape control and artificial damping. They serve to stabilize the Space Construction Base by controlling either module interactions or individual modules directly.

Potential actuators include rotary torquers, control moment gyros (CMGs), and motor driven cable winches. The rotary torquers would be placed at the joints between modules and used primarily for coupling control. Some rotary actuators will be free to rotate to large angles - e.g., a solar wing must rotate to maintain pointing toward the sun. CMGs may be used for any of the above functions but must be supplemented with other actuators for momentum desaturation. Cable winches may be used in coupling or shape control if the dynamic response requirements are minimal. For example, such a situation would exist if there is a large constant torque required to maintain a desired shape (to overcome a spring restoring torque).

Coupling control may accomplish either decoupling or stiffening at the points between modules and between module and appendages. Both characteristics may be obtained through control mode switching. Decoupling control would be applied when it is desired to minimize the transfer of disturbances. On the other hand, artificial stiffening may be applied during maneuvers so that the structure will rotate as a whole.

Figure 5-2 illustrates how a rotary actuator may be interfaced to an appendage hinge joint with the main body. Double Gimbaled Control Moment Gyros (DGCMGs) are assumed to be controlling the main body. As shown, the rotary actuator will apply a torque to both the main body and appendage. The reaction torque on the main body may be cancelled with a command to the DGCMGs. Alternately, the attitude control on the main body could be allowed to make the necessary corrections.

Decoupling control is shown in Figure 5-3. The main body and appendage each has its own control loop (via $K_{\theta 1}$ and $K_{\theta 2}$) for stabilization. The decoupling serves to cancel or partially cancel the coupling terms shown in Figure 5-2. The extent of decoupling is governed by the gain factors, K_{C1} and K_{C2} $(0 \leq K_{Ci} \leq 1)$.

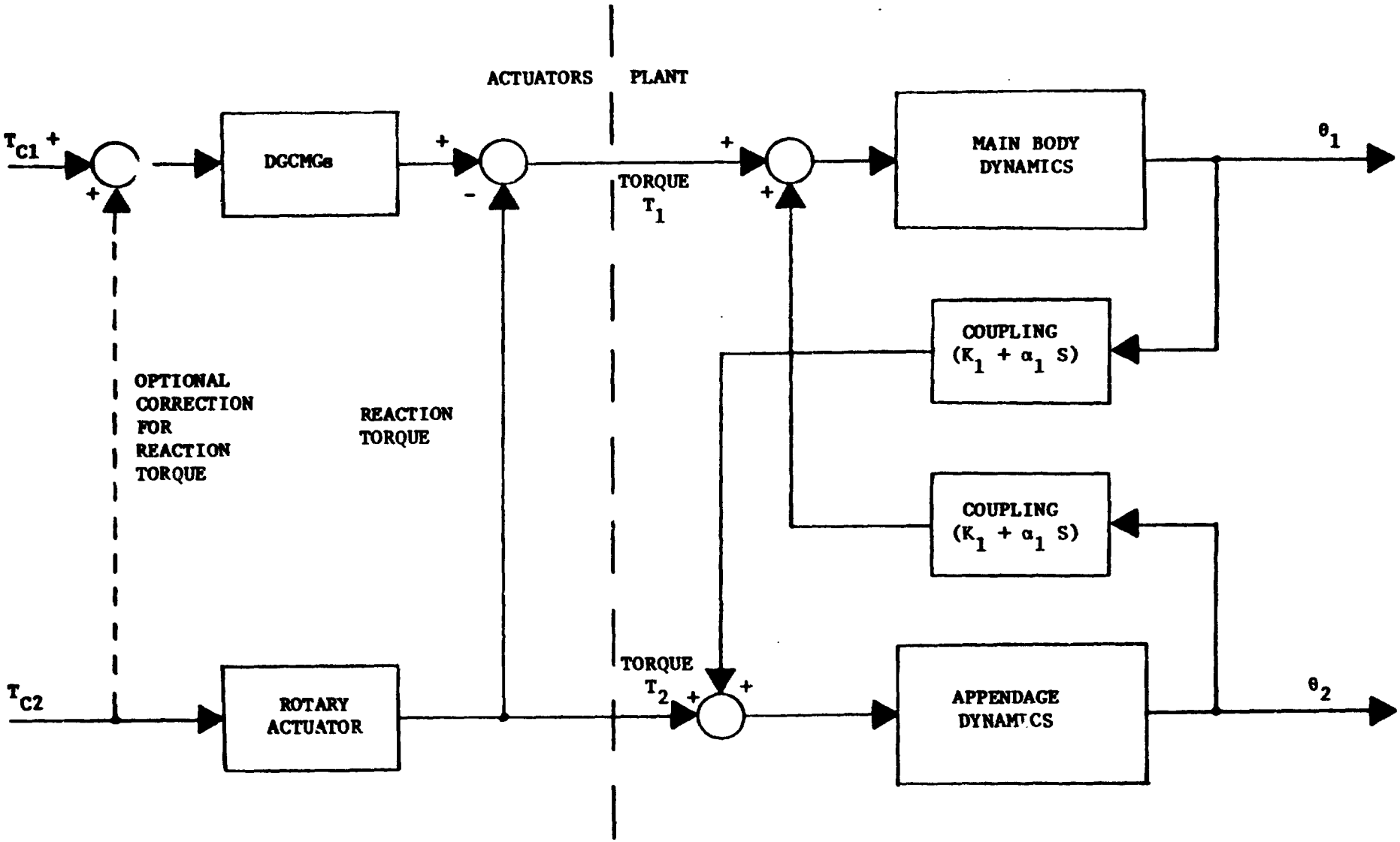

Figure 5-2 - Concept for Main Body and Appendage Actuation

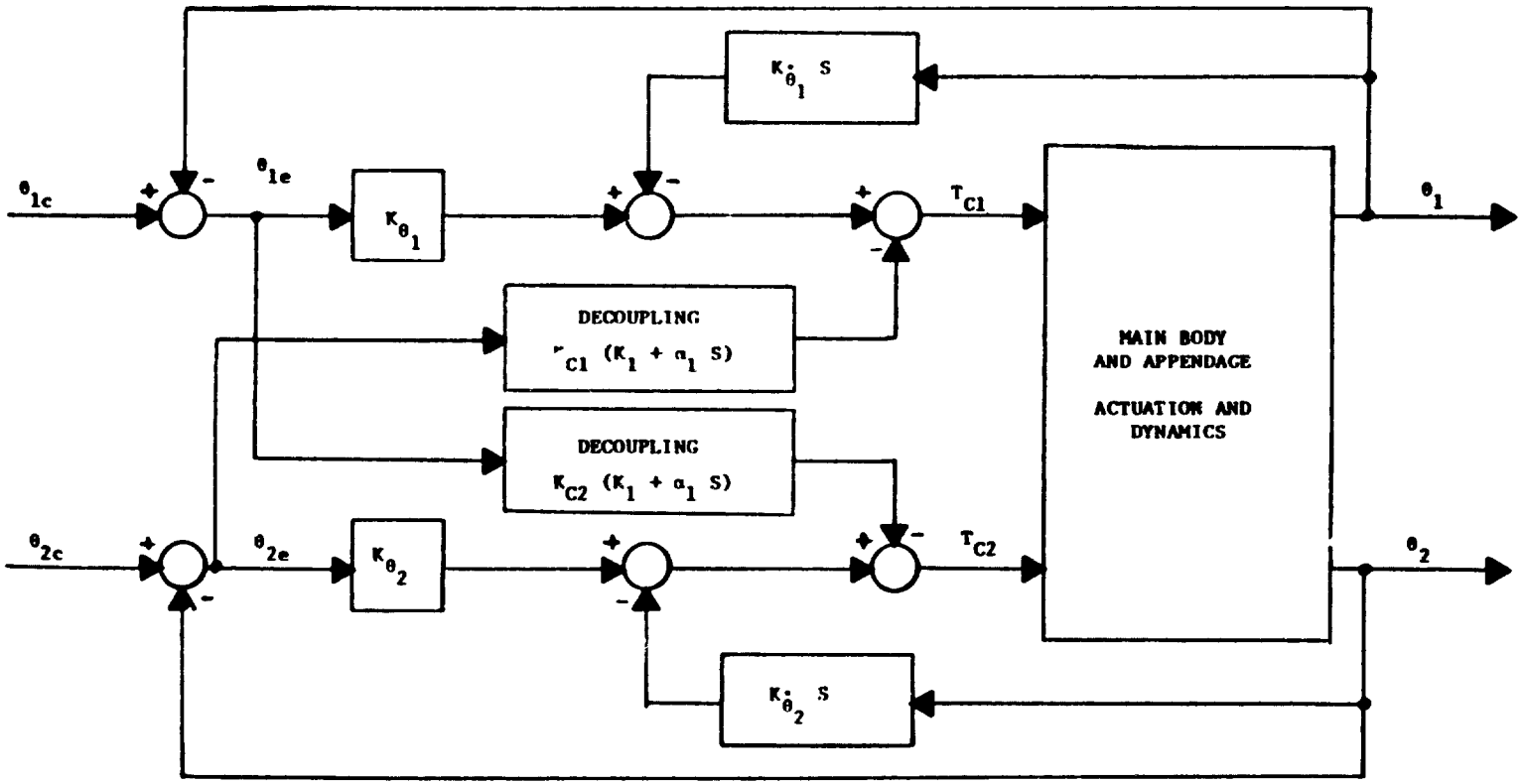

Figure 5-3 - Concept for Decoupling Control

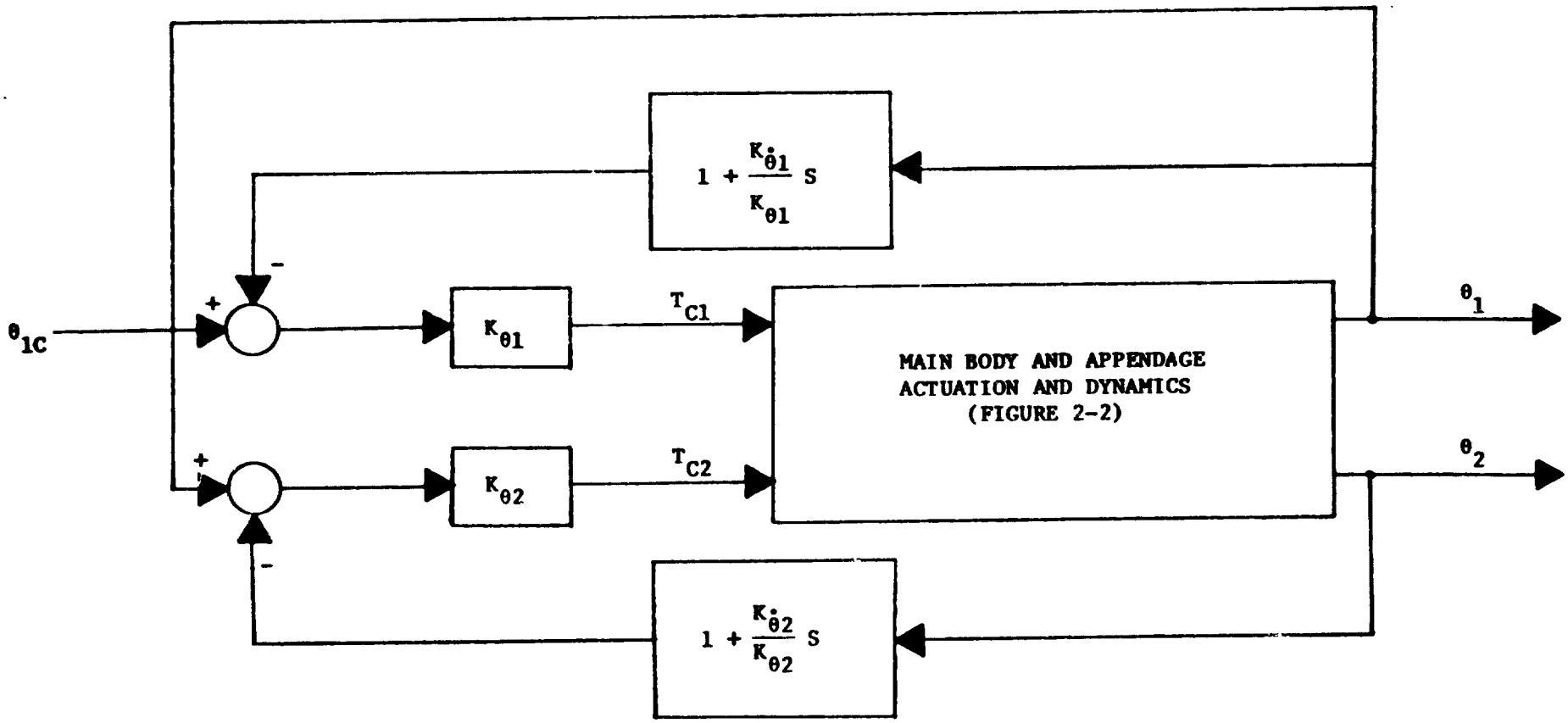

Figure 5-4 - Concept for Artificial Stiffening

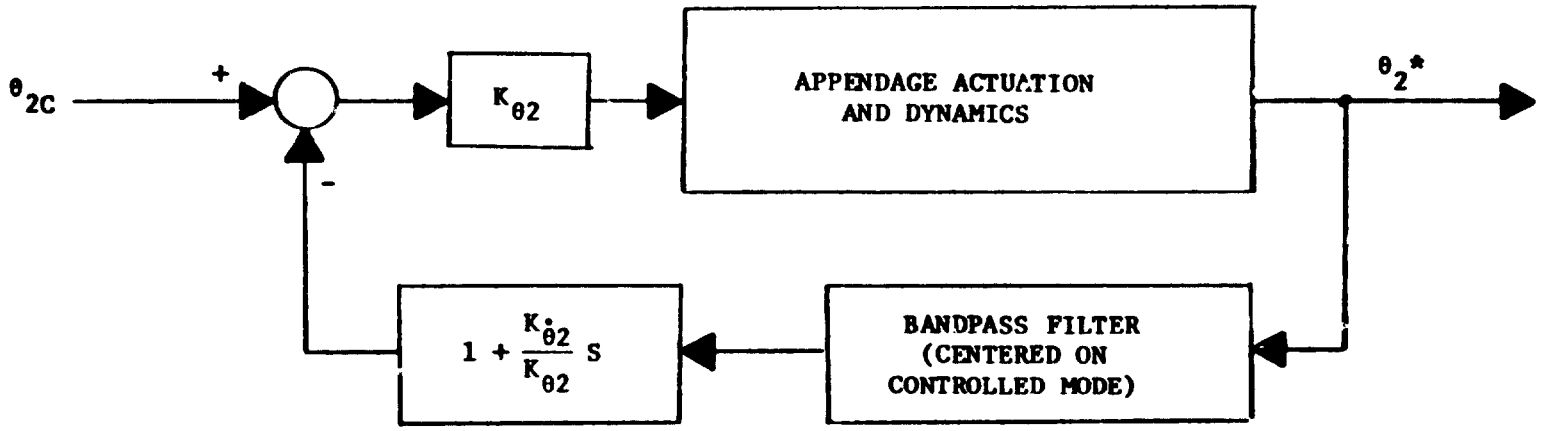

*θ_2 = ANGLE OF APPENDAGE MEASURED CLOSE TO ACTUATOR

Figure 5-5 - Concept for Artificial Damping

Artificial stiffening control is illustrated in Figure 5-4 In this case, the appendage attitude command is set to the main body angle. There is no decoupling and the control parameters will generally have different values than with decoupling control. The objective is to slave the appendage angle to that of the main body. This would be desirable during any maneuver.

Both the decoupling control and artificial stiffening include an appendage control loop with the paramters $K_{\theta 2}$ and $K_{\dot{\theta} 2}$. This configuration has been found convenient for the study of decoupling and artificial stiffening controls, but it is not necessarily the best for the damping of structural modes. Therefore, alternate configurations such as that of Figure 5-5 should be investigated. The concept shown includes a bandpass filter to isolate the mode being damped and has a higher gain to be responsive to the controlled mode.

The use of coupling control will certainly be selective. That is, for a given appendage and axis of rotation, the coupling may be left uncontrolled. For example, the couplings from the solar wings to the main body about the Z-axis (wing torsion) will probably be uncontrolled ($K_{C1} = 0$ in Figure 5-3 . This is because a motion of a solar wing about this axis will have little effect on the main body due to the large difference in moments of inertia. However, coupling from the main body to each solar wing about the Z-axis will probably be controlled ($K_{C2} > 0$) since any disturbance on the main body will otherwise propagate to the solar wing.

5.7 VEHICLE CONTROL COORDINATOR

Due to its large size and the buildup process, the Space Construction Base control system will require some means to adjust control parameters and select sensors. These functions are achieved through the Vehicle Control Coordinator with some interaction with Ground Control.

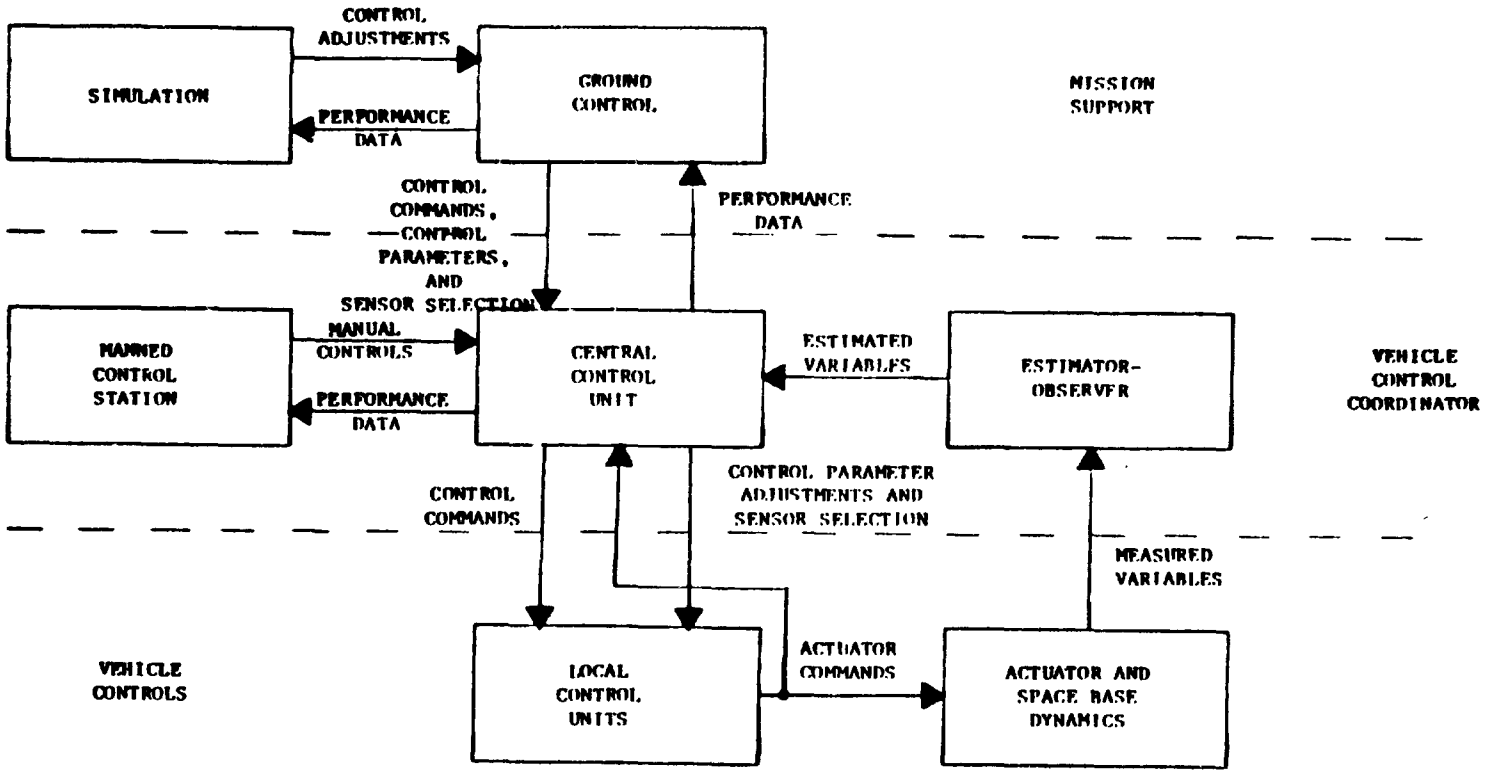

Figure 5-6 - Basic Vehicle Coordinator Concept

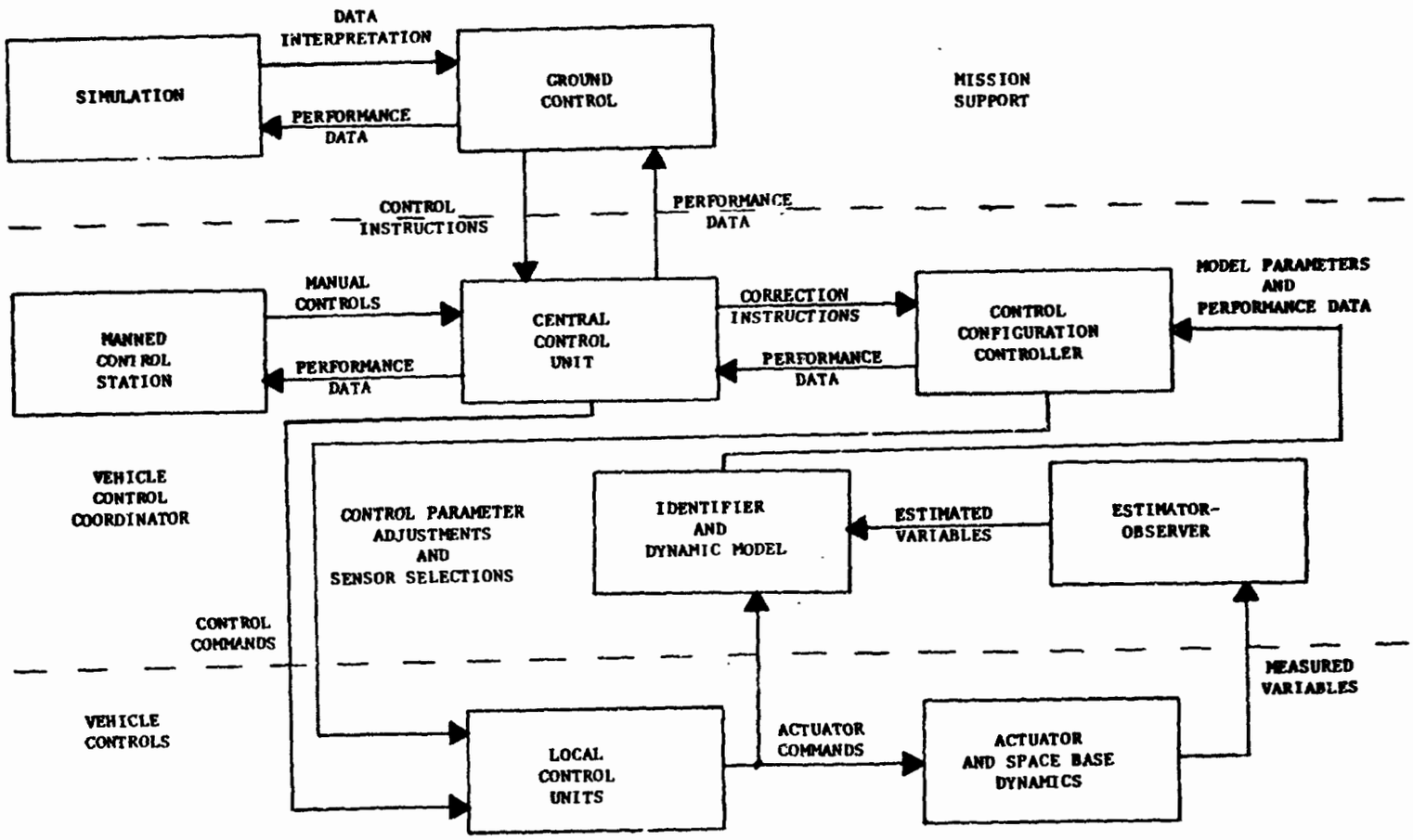

Figure 5-7 - Vehicle Control Coordinator With
On-Board Identification

Two concepts for making these adjustments are discussed briefly in this section. These represent two extremes in the level of complexity of the spaceborne control system. The actual configuration may include features of each concept but will probably be closer to the simpler approach of Figure 5-6.

Figure 5-6 illustrates a concept with a minimum level of on-board capability. All of the central parameter and sensor selections are determined on the ground through the mission support function. The ground simulation is updated based on performance data received from the spacecraft and is used for determining desirable control parameters and sensor locations. The central control unit functions primarily as memory so as to minimize radio communication requirements. There is some capability for manual intervention by space personnel. Those variables which have errors characterized as stochastic are estimated with a Kalman Filter or Extended Kalman Filter. Those which are characterized as deterministic are computed with an Observer.

Figure 5-7 shows a concept with extensive on-board capability. The control parameter and sensor selections are determined primarily from on-board computations in the Vehicle Control Coordinator. The ground simulation serves to interpret performance data transmitted from the spacecraft. Ground Control provides overall instructions such as maneuvering and docking commands. Ground Control may also provide a backup to space computations. The Control Configuration Controller, Identifier, on-board dynamic model simulation, and estimator-observer provide adaptive control capability. The identifier compares the system performance with the dynamic model and adjusts the model accordingly. The comparisons may be made using test signal inputs or be based on the response to normal disturbances.

5.8 DISTRIBUTION OF SENSORS AND ACTUATORS

A basic part of the control system design will be the selection of actuator and sensor types and locations. This will be based partly on the determination of torque requirements for countering disturbances such as gravity gradient and aerodynamic drag.

Table 5-2 lists some of the trades associated with sensor and actuator distribution. The extent to which performance such as stability and pointing accuracies can be improved over uncontrolled behavior is of fundamental importance. Certain locations such as the small solar wings are not feasible for relatively large and heavy actuators such as CMGs and the accompanying momentum desaturation actuators. Structural modal shapes must be considered so as to avoid strong actuator interactions and large sensor errors.

Table 5-2 - Considerations for Sensor and Actuator Distribution

Item Under Consideration	Alternatives	Considerations
1. Actuator Locations	Modules on main body On appendages At appendage hinge joints At module interconnections	Performance requirements Effectiveness in obtaining desired moment or force Size and weight Structure modal shapes Safety Access for maintenance Power distribution requirements Momentum desaturation requirements
2. Sensor Locations	Modules on main body On appendages	Size and weight Sensitivity to desired measurements Structural modal shapes Power distribution requirements Access for maintenance

5.9 MULTIVARIABLE DESIGN ANALYSIS

Although the primary tool for control system design is computer simulation, there are some analytical approaches that are useful in the design derivation. Most of the single-loop methods are well known and do not require review here.

Multivariable or multiple-loop control, however, is an area of continuous research - warranting more discussion. Multivariable analytical approaches include:

A. Multilevel Control - This is a viewpoint of systems as consisting of layers of decision levels. An overall system is divided (or decomposed) into a hierarchy of goal-seeking subsystems or decision problems.

B. Linear Quadratic Regulator (LQR) - This approach, also known as Linear Optimal control, views the system as a whole with the performance specified in terms of a single index.

C. Multivariable Nyquist Array (MNA) - This is an extension of frequency response methods to multivariable control systems and includes the concept of partial decoupling.

D. Characteristic Loci - This is another extension of frequency response methods to multivariable control systems. It is analogous to the root locus technique and does not require partial decoupling as a separate step.

E. Other Algebraic Techniques - Pole/zero placement and matrix transfer functions may be analyzed from a variety of alternate viewpoints which have appeared recently in the literature.

Figure 5-8 shows a typical application of linear optimal control. The design procedure is conceptually straightforward using available computer programs. The gain matrix is often taken as a steady-state constant matrix, but it must be changed as modules are added to space

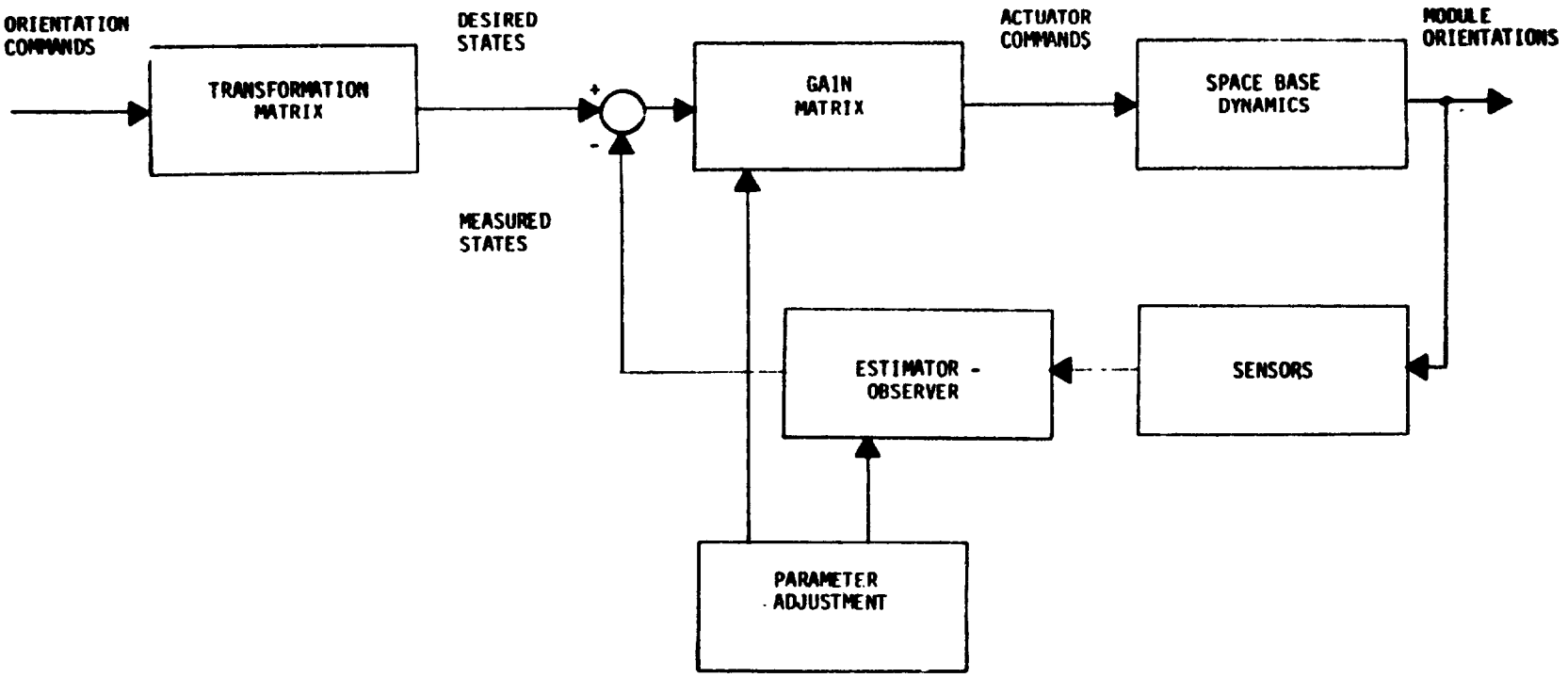

Figure 5-8 - Stabilizing Control Based On Linear Optimal Control

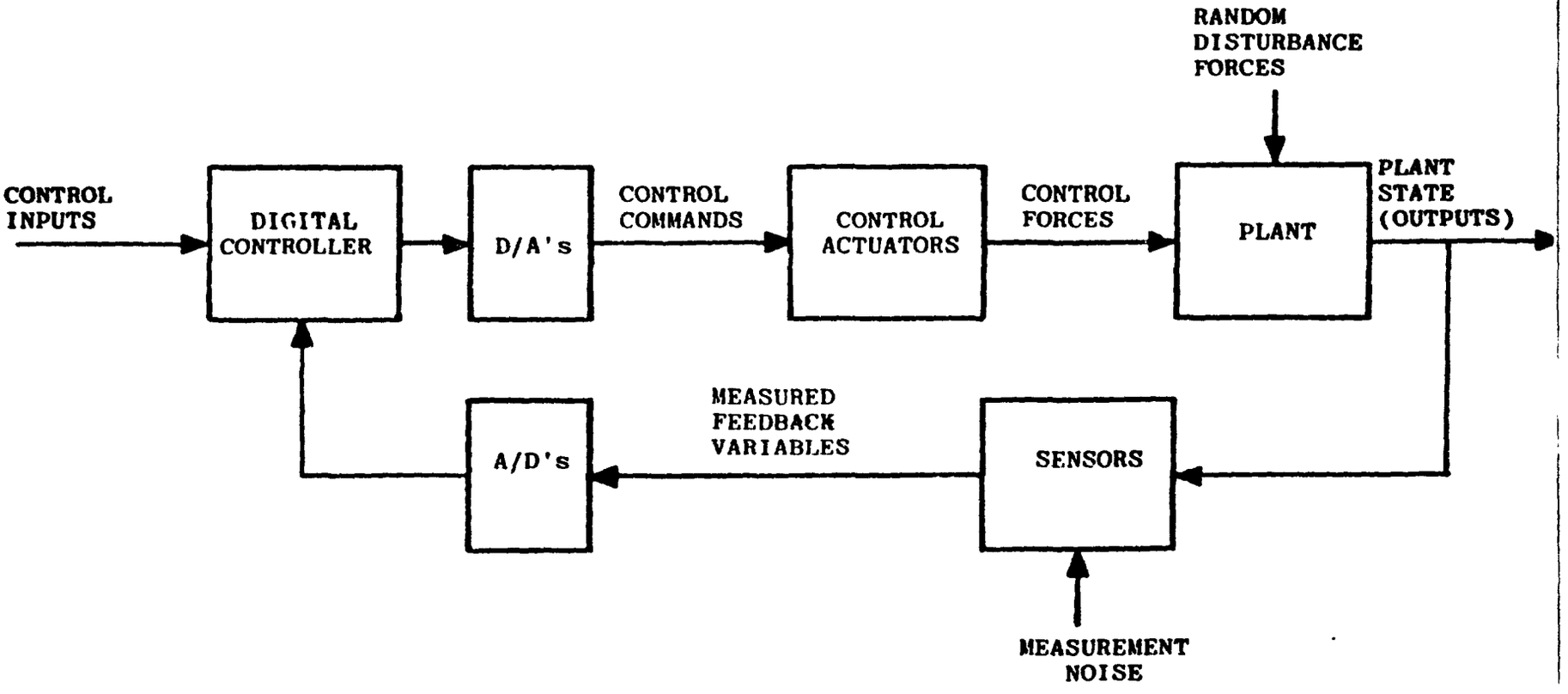

Figure 5-9 - Digital Control System

base. An estimation is required if the measurement noise and disturbances are modeled as random processes. An observer is applicable to deterministic systems which have some states that cannot be measured directly.

In practice, the design procedure is iterative. First, the choice of an approximate linear model must be made. Second, a performance index with desired weighting factors on each state and control variable must be selected. For stochastic representations, the statistics must be determined, although they are generally unknown. After a design has been computed, the result should be evaluated on a more exact, possible nonlinear simulation. Since that result is unlikely to satisfy the designer, the procedure must be repeated with different performance weighting or a different linear model.

Figure 5-9 shows a digital control representation of the overall space construction base control system - linearized about some reference condition. The control parameters for the "digital controller" may be derived using the LQR method. The first step would be to derive a continuous model for each configuration of the control actuators (e.g., CMG servo loops), the overall space base dynamics, and the sensors. Each model must be linearized and simplified for representation of perturbations about some reference point. Each model will have a separate set of control parameters, i.e., an LQR design.

Each continuous model must be converted to a discrete model. This may be accomplished once a sample rate has been selected. The state transition matrix is obtained by summing matrices obtained from a truncated exponential series expansion (of e^{AT} where A = continuous plant matrix and T = sample period). For disturbances and noise, the covariance matrices are converted by dividing by the sample period.

The objective of the control system design is to minimize a performance criterion:

$$J_N = E\left[\sum_{i=1}^{N} \{x^T(i)\ F(i)\ x\ (i) + u^T(i-1)\ G(i-1)\ u(i-1)\}\right]$$

where

X(i) = column state vector at i'th sample time (n components)

u(i - 1) = column control vector at (i - 1)st sample time (r components)

F(i) = n x n symmetric positive semi-definite matrix (plant state variable weightings)

G(i) = r x r symmetric positive semi-definite matrix (control variable weightings)

E(Y) = expected value of Y

In order to solve the optimal control problem, it is first necessary to select the performance weighting matrices, F and G. A convenient way for doing this is to start with the identity matrices of state and control orders. Each diagonal element is normalized by dividing each by the square of the maximum expected value of the corresponding state, error, or control variable. These weighting matrices are normally diagonal matrices since any off-diagonal terms would lack physical meaning. The normalized weighting matrix for the state variables is multiplied by one constant and the weighting matrix for the control is multiplied by another constant. The ratio of these constants then determines the ratio of control activity to state variable variation.

Once the solution is obtained for several sets of performance index parameters, it is necessary to test the resulting system design in a nonlinear simulation. The performance of the simulated system is compared as the performance index parameters are varied. Thus the optimal control approach reduces the problem from trial and error variation of control parameters to variation of the ratio between control and state variable weighting. The linear model dimensions may also be varied for evaluation through simulation.

The Multivariable Nyquist Array (MNA) method results in a system such as shown in Figure 5-10. The control would serve to provide sufficient decoupling between modules to provide a given stability margin. This function is labeled "partial decoupling" and is derived to achieve a property called diagonal dominance. The actuator commands into the "Space Base dynamics" may each influence the orientation of more than one module. On the other hand, the vector components into the "Partial Decoupling" each has primary influence on a single module. Thus, once partial decoupling is inserted, the "Individual Loop Controllers" may be each designed separately as independent control loops. This could be applicable to the analysis of stabilizing control for the Space Construction Base.

Thus, in the MNA analysis, the selection of control parameters is divided into two problems (see Figure 5-11). The first is the partial decoupling of otherwise strongly interacting loops. This is accomplished through the proper selection of the parameters, ℓ_{ij}. Once this is accomplished, each loop is analyzed individually to select the parameters, f_{ii}.

The control inputs to the plant, u_1 and u_2, each affect both outputs, θ_1 and θ_2. Partial decoupling through the proper selection of ℓ_{11}, ℓ_{12}, ℓ_{21}, and ℓ_{22}, weaken the links between u_1' and θ_2 and u_2' and θ_1. That is, u_1' mainly affects θ_1 and u_2' mainly affects θ_2. The extent of decoupling defined in Figure 5-11 for the 2-loop case, is based on a theorem by Gershgorin.

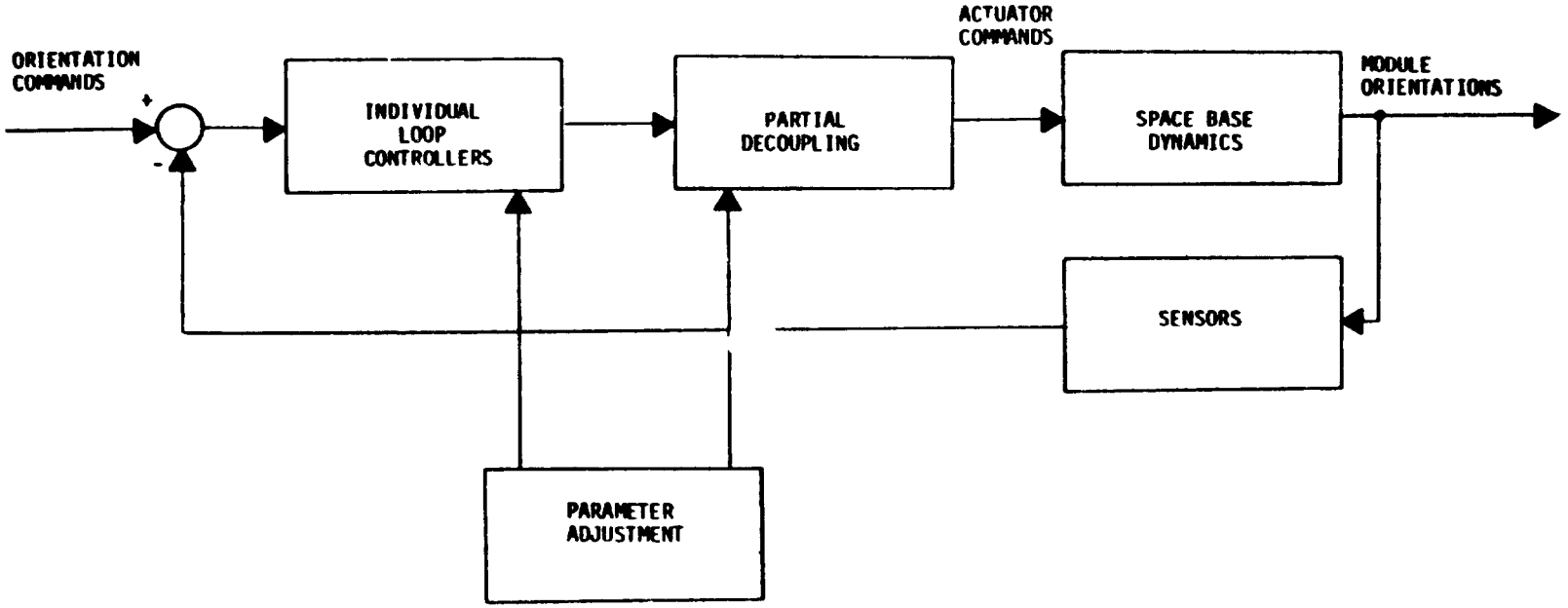

Figure 5-10 - Stabilizing Control With Partial Decoupling

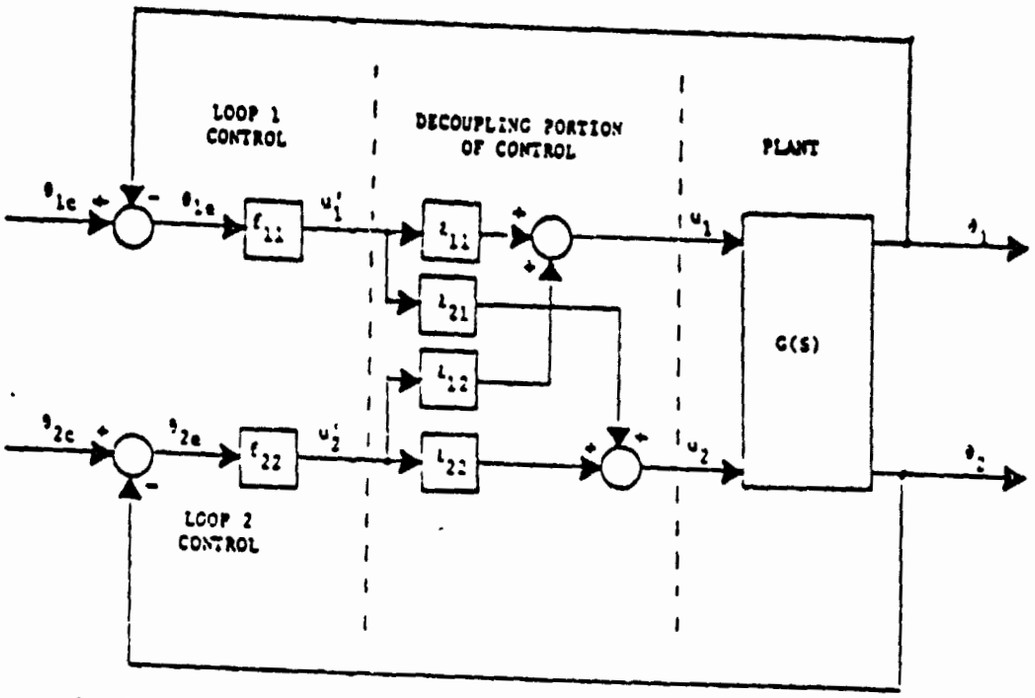

$$\theta = G(S)\, L\, F\, \theta_a$$

$$= \begin{pmatrix} g_{11}(S) & g_{12}(S) \\ g_{21}(S) & g_{22}(S) \end{pmatrix} \begin{pmatrix} l_{11} & l_{12} \\ l_{21} & l_{22} \end{pmatrix} \begin{pmatrix} f_{11} & 0 \\ 0 & f_{22} \end{pmatrix} \begin{pmatrix} \theta_{a1} \\ \theta_{a2} \end{pmatrix}$$

$$GL = \begin{pmatrix} q_{11}(S) & q_{12}(S) \\ q_{21}(S) & q_{22}(S) \end{pmatrix}$$

where:

$$q_{11} = g_{11}\, l_{11} + g_{12}\, l_{21}$$

$$q_{12} = g_{11}\, l_{12} + g_{12}\, l_{22}$$

$$q_{21} = g_{21}\, l_{11} + g_{22}\, l_{21}$$

$$q_{22} = g_{21}\, l_{12} + g_{22}\, l_{22}$$

DIAGONAL DOMINANCE OF GL:
SELECT l_{ij} SUCH THAT

$$|q_{12}(S)| < |q_{11}(S)| \qquad |q_{21}(S)| < |q_{11}(S)|$$

$$|q_{21}(S)| < |q_{22}(S)| \quad \underline{\text{OR}} \quad |q_{12}(S)| < |q_{22}(S)|$$

(ROW DOMINANCE) (COLUMN DOMINANCE)

FOR $S = j\omega$ OVER THE FREQUENCY RANGE OF INTEREST.

Figure 5-11 - Separation of Decoupling Operation

SECTION 6

6.0 DIGITAL SIMULATION

Two modeling approaches have been adopted for this study. A simple one dimensional simulation is used for preliminary design development and initial prediction of performance. A more detailed, three dimensional n-body simulation has also been developed for futher evaluation of expected performance. Selected situations have been simulated on both programs and compared.

The purpose of this section is to describe the one dimensional model and some preliminary results from its application.

6.1 DESCRIPTION OF ONE-DIMENSIONAL MODELS

The n-body, one dimensional system is illustrated in Figure 6-1. It consists of masses (J_1, J_2, ... J_n) connected by massless rods having spring constants (K_1, K_2, ... K_{n-1}) and viscous damping (α_1, α_2, ... α_{n-1}). Torques are applied to the masses (T_1, T_2, ... T_n), which are each a sum of disturbance and control torques. This model may be easily adapted to represent as many masses as desired.

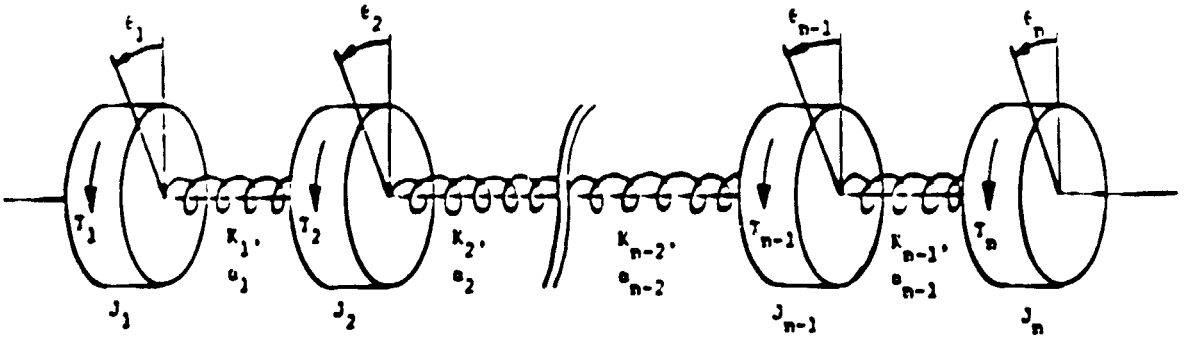

Figure 6-1 N Body, One Dimensional Model

The equations of motion are:

$$J_1 \ddot{\theta}_1 = -K_1 \theta_1 + K_1 \theta_2 - a_1 \dot{\theta}_1 + a_1 \dot{\theta}_2 + T_1$$

$$J_2 \ddot{\theta}_2 = K_1 \theta_1 - (K_1 + K_2) \theta_2 + K_2 \theta_3 + a_1 \dot{\theta}_1 - (a_1 + a_2) \dot{\theta}_2$$

$$+ a_2 \dot{\theta}_3 + T_2 \qquad (6\text{-}1)$$

$$\vdots$$

$$J_{n-1} \ddot{\theta}_{n-1} = K_{n-2} \theta_{n-2} - (K_{n-2} + K_{n-1}) \theta_{n-1} + K_{n-1} \theta_n$$

$$+ a_{n-2} \dot{\theta}_{n-2} - (a_{n-2} + a_{n-1}) \dot{\theta}_{n-1} + a_{n-1} \dot{\theta}_n + T_{n-1}$$

$$J_n \ddot{\theta}_n = K_{n-1} \theta_{n-1} - K_{n-1} \theta_n + a_{n-1} \dot{\theta}_{n-1} - a_{n-1} \dot{\theta}_n + T_n$$

For this study, a three body one dimensional model was extensively used. With n = 3 in equations (3-1):

$$J_1 \ddot{\theta}_1 = -K_1 \theta_1 + K_1 \theta_2 - a_1 \dot{\theta}_1 + a_1 \dot{\theta}_2 + T_1$$

$$J_2 \ddot{\theta}_2 = K_1 \theta_1 - (K_1 + K_2) \theta_2 + K_2 \theta_3 + a_1 \dot{\theta}_1 - (a_1 + a_2) \dot{\theta}_2 \qquad (6\text{-}2)$$

$$+ a_2 \dot{\theta}_3 + T_2$$

$$J_3 \ddot{\theta}_3 = K_2 \theta_2 - K_2 \theta_3 + a_2 \dot{\theta}_2 - a_2 \dot{\theta}_3 + T_3$$

A corresponding state variable representation is:

$$\theta_1 = X_1,\ \dot{X}_1 = X_2$$

$$\dot{X}_2 = [T_1 - \alpha_1 (X_2 - X_4) - K_1(X_1 - X_3)]/J_1$$

$$\theta_2 = X_3,\ \dot{X}_3 = X_4$$

$$\dot{X}_4 = [T_2 + \alpha_1(X_2 - X_4) + K_1(X_1 - X_3) - \alpha_2(X_4 - X_6) \quad (3\text{-}3)$$

$$- K_2(X_3 - X_5)]/J_2$$

$$\theta_3 = X_5,\ \dot{X}_5 = X_6$$

$$\dot{X}_6 = [T_3 + \alpha_2(X_4 - X_6) + K_2(X_3 - X_5)]/J_3$$

In vector form, equations (3-3) may be expressed:

$$\begin{bmatrix} \theta_1 \\ \theta_2 \\ \theta_3 \end{bmatrix} = [C_{ij}] \begin{bmatrix} X_1 \\ X_2 \\ X_3 \\ X_4 \\ X_5 \\ X_6 \end{bmatrix}$$

$$\begin{bmatrix} \dot{X}_1 \\ \dot{X}_2 \\ \dot{X}_3 \\ \dot{X}_4 \\ \dot{X}_5 \\ \dot{X}_6 \end{bmatrix} = [a_{ij}] \begin{bmatrix} X_1 \\ X_2 \\ X_3 \\ X_4 \\ X_5 \\ X_6 \end{bmatrix} + [b_{ij}] \begin{bmatrix} T_1 \\ T_2 \\ T_3 \end{bmatrix}$$

where

$$A = [a_{ij}] = \begin{bmatrix} 0 & 1 & 0 & 0 & 0 & 0 \\ -\frac{K_1}{J_1} & -\frac{\alpha_1}{J_1} & \frac{K_1}{J_1} & \frac{\alpha_1}{J_1} & 0 & 0 \\ 0 & 0 & 0 & 1 & 0 & 0 \\ \frac{K_1}{J_2} & \frac{\alpha_1}{J_2} & \frac{-(K_1 + K_2)}{J_2} & \frac{-(\alpha_1 + \alpha_2)}{J_2} & \frac{K_2}{J_2} & \frac{\alpha_2}{J_2} \\ 0 & 0 & 0 & 0 & 0 & 1 \\ 0 & 0 & \frac{K_2}{J_3} & \frac{\alpha_2}{J_3} & -\frac{K_2}{J_3} & -\frac{\alpha_2}{J_3} \end{bmatrix}$$

and

$$B = [b_{ij}] = \begin{bmatrix} 0 & 0 & 0 \\ 1 & 0 & 0 \\ 0 & 0 & 0 \\ 0 & 1 & 0 \\ 0 & 0 & 0 \\ 0 & 0 & 1 \end{bmatrix} \qquad C = [c_{ij}] = \begin{bmatrix} 1 & 0 & 0 & 0 & 0 & 0 \\ 0 & 0 & 1 & 0 & 0 & 0 \\ 0 & 0 & 0 & 0 & 1 & 0 \end{bmatrix}$$

The three body one dimensional model is illustrated in block diagram form in Figure 6-2. This shows the open loop second order transfer function for each body as well as the dynamic coupling between bodies.

The above combination of three representations of the one dimensional model provides the opportunity for analyzing the control system from a variety of viewpoints. The state space representation, for example, may be used in the application of linear optimal control. A generalized control equation has been formulated, which in vector form is:

$$\begin{bmatrix} T_{1C} \\ T_{2C} \\ T_{3C} \end{bmatrix} = - \begin{bmatrix} k_{ij} \end{bmatrix} \begin{bmatrix} \theta_1 \\ \theta_2 \\ \theta_3 \end{bmatrix} - \begin{bmatrix} d_{ij} \end{bmatrix} \begin{bmatrix} \dot{\theta}_1 \\ \dot{\theta}_2 \\ \dot{\theta}_3 \end{bmatrix} + \begin{bmatrix} C_1 \\ C_2 \\ C_3 \end{bmatrix} \theta_C$$

$$= - \begin{bmatrix} k_{11} & d_{11} & k_{12} & d_{12} & k_{13} & d_{13} \\ k_{21} & d_{21} & k_{22} & d_{22} & k_{23} & d_{23} \\ k_{31} & d_{31} & k_{32} & d_{32} & k_{33} & d_{33} \end{bmatrix} \begin{bmatrix} X_1 \\ X_2 \\ X_3 \\ X_4 \\ X_5 \\ X_6 \end{bmatrix} + \begin{bmatrix} C_1 \\ C_2 \\ C_3 \end{bmatrix} \theta_C$$

and

$$\begin{bmatrix} T_1 \\ T_2 \\ T_3 \end{bmatrix} = \begin{bmatrix} T_{1C} \\ T_{2C} \\ T_{3C} \end{bmatrix} + \begin{bmatrix} T_{1d} \\ T_{2d} \\ T_{3d} \end{bmatrix}$$

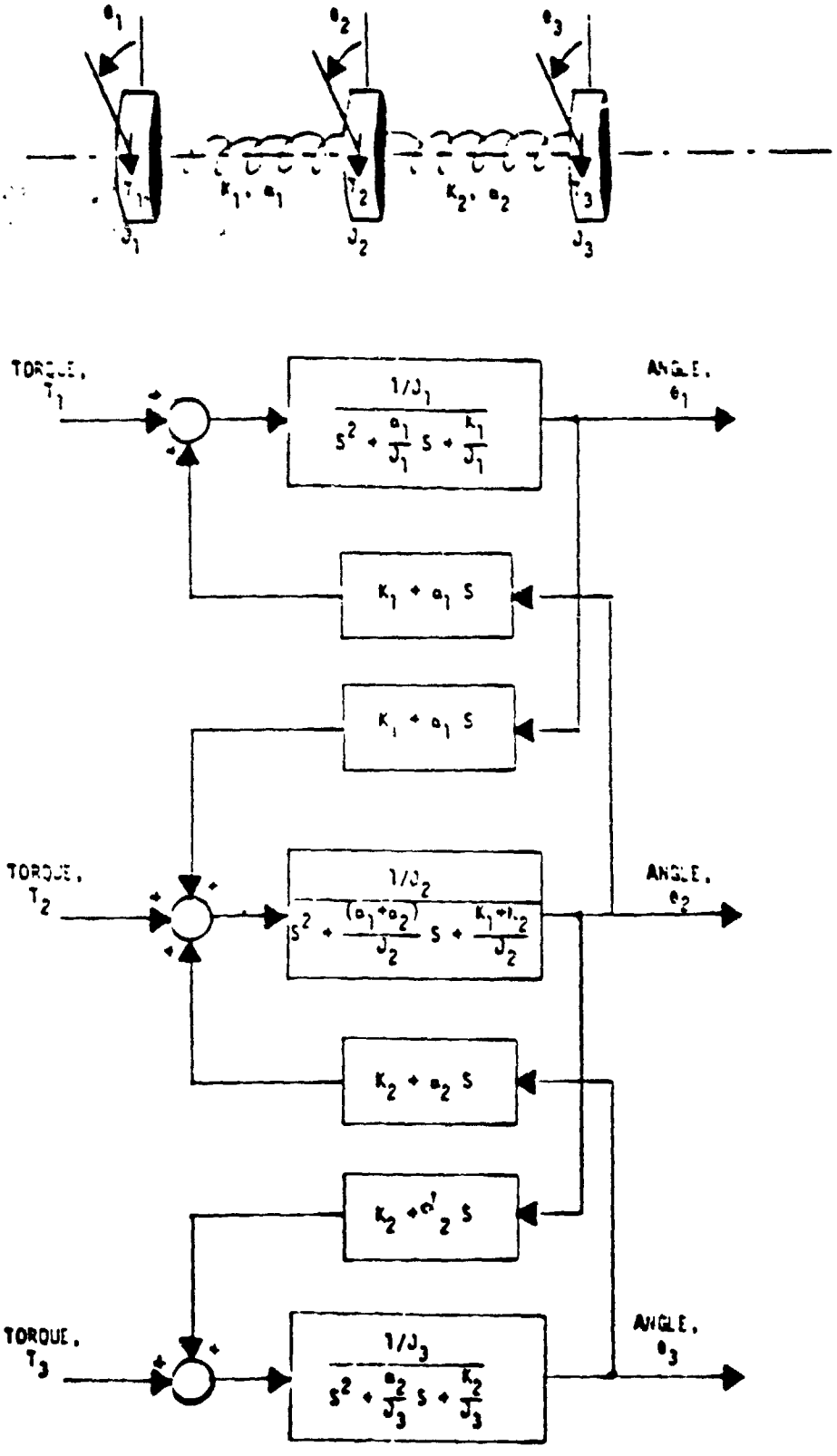

Figure 6-2 - Three Body, One Dimensional Model

where

T_{id} = disturbance torque

T_{ic} = control torque

d_{ij} = rate feedback gain

k_{ij} = position feedback gain

Depending on the control gains(k_{ij}, d_{ij}) selected, a variety of control loop configurations may be realized.

Figure 6-3 illustrates the vibrational modes of the three dimensional model. Dynamic rotation about each of the three axes may be studied individually, using the one dimensional model. The two modal frequencies associated with each axis were chosen to be representative of dynamics of Configuration I of the Space Construction Base.

In order to relate the three dimensional model parameters to the one dimensional model, it is necessary to compute the effective moment of inertia of each body or appendage. These inertias are referred to the actuation point. The spring and damping constants were calculated by deriving expressions for the eigenvalues of $[a_{ij}]$ of the one dimensional model, and equating these to the desired values.

One dimensional model parameters used to represent Configuration I are summarized in Table 6-1.

A five body, one dimensional model has also been developed for this study. Figure 6-4 shows various applications of the one dimensional model. The three body one dimensional model has been used to represent each axis of the main body and one solar wing of Configuration I. The wing is divided into two bodies to represent two modal frequencies (6-4a). Four modal frequencies of the solar wing may be represented by using the five body version of the one dimensional model (6-4b). Also, the five body model may be used to represent the main body with both solar wings present (6-4c).

SOLAR WING MODES
(RADIANS/SECOND)

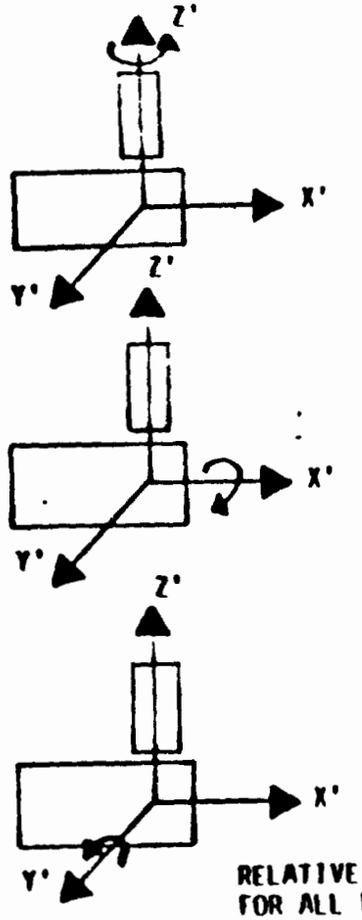

TORSIONAL

ω_1 = 0.32

ω_2 = 1.0

NORMAL

ω_1 = 0.13

ω_2 = 1.1

LATERAL

ω_1 = 2.5

ω_2 = 19.0

RELATIVE DAMPING RATIO
FOR ALL MODES = 0.005

CONFIGURATION 1 OF SPACE CONSTRUCTION BASE

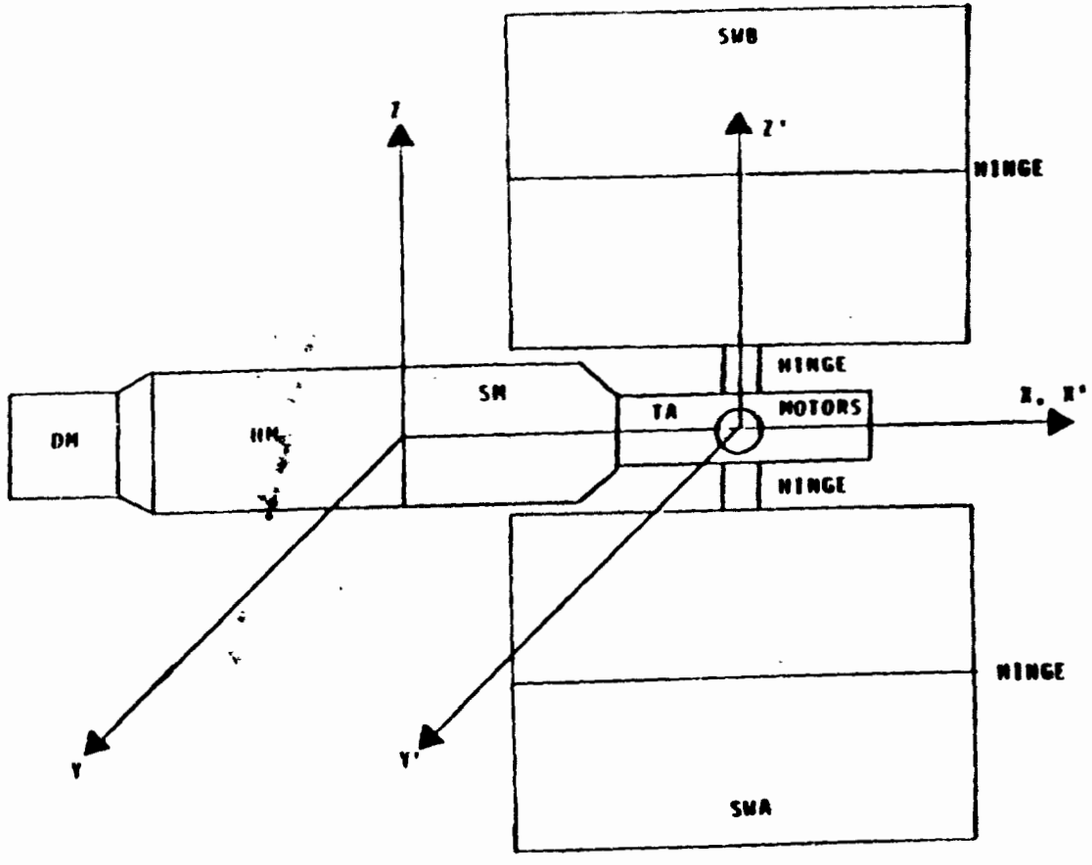

Figure 6-3- Vibrational Modes

TORSIONAL MODEL

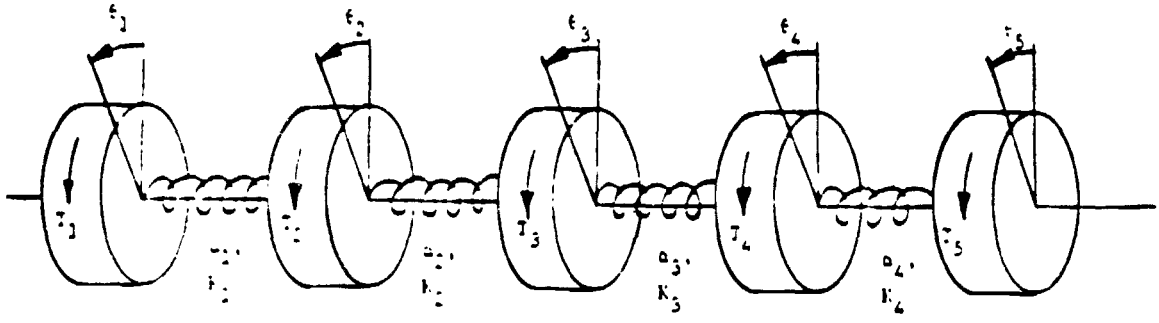

APPLICATIONS

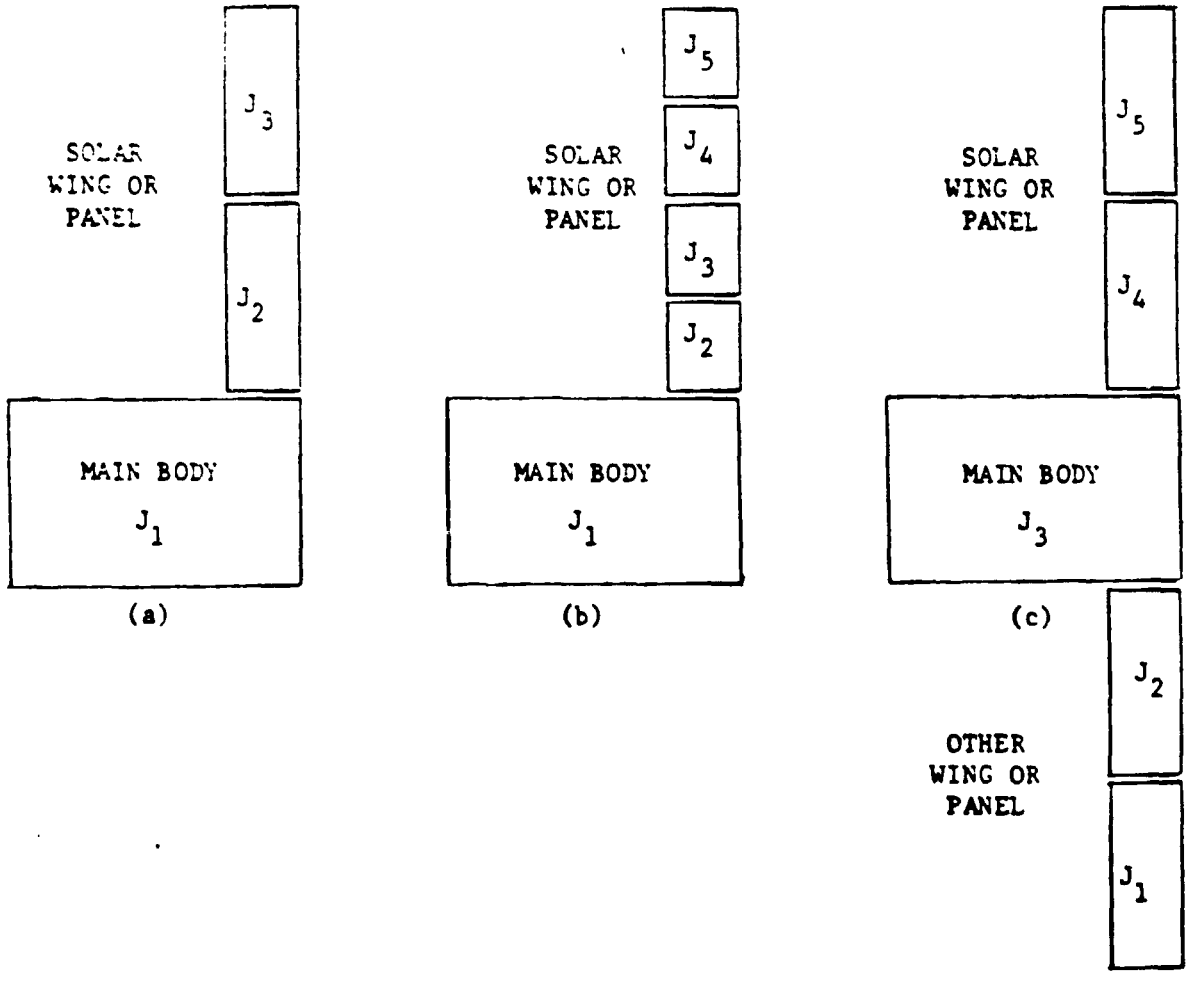

Figure 6-4 - Applications of the One Dimensional Model

Table 6-1 - One Dimensional Model Parameters for Configuration I

Axes	Modes (radians/s)	Moments of Inertia ($ft\text{-}lb\text{-}s^2$)	Spring Constants (ft-lb/radian)	Viscous Damping Const. (ft-lb/radian per s)
Torsional (Z-Axis)	$\omega_1 = 0.32$ $\omega_2 = 1.0$	$J_1 = 960550$ $J_2 = 757.25$ $J_3 = 757.25$	$K_1 = 655.72$ $K_2 = 89.549$	$\alpha_1 = 3.5879$ $\alpha_2 = 3.2039$
Normal (X'-Axis)	$\omega_1 = 0.13$ $\omega_2 = 1.1$	$J_1 = 31045.0$ $J_2 = 17800.0$ $J_3 = 99500.0$	$K_1 = 19668.3$ $K_2 = 1841.4$	$\alpha_1 = 36.216$ $\alpha_2 = 155.00$
Lateral (Y'-Axis)	$\omega_1 = 2.5$ $\omega_2 = 19.0$	$J_1 = 960550.0$ $J_2 = 18600.0$ $J_3 = 100400.0$	$K_1 = 5998410.0$ $K_2 = 702403.0$	$\alpha_1 = 267.7730$ $\alpha_2 = 3148.03$

Represents rotational motion about each of three axes for one solar wing and main body.

These one dimensional models may also be used to represent the large solar panels of Configurations X, XI, and XII of the Space Construction Base. In this case, one or both of the solar panels may be represented, with the remainder of the structure lumped into the 'main body.'

6.2 SOLAR WING DECOUPLING CONTROL STUDY USING THE ONE-DIMENSIONAL MODEL

During periods when the Space Construction Base (SCB) is being held at constant attitude, the decoupling control decreases the propagation of disturbances between the solar wings and main body. The three body one dimensional model has been used for this portion of the study. Figure 6-5 illustrates the decoupling control concept. Momentum exchange devices in the main body of the SCB are represented by torque T_{C1}. Torque motors located at the hinge point between the main body and solar wing are represented by torque T_{C2}. Actuators cannot be placed on the outer section of the solar wing (represented by mass J_3), hence $T_{C3} = 0$, and has been omitted from the illustration. A constant attitude is held when θ_{1C} and θ_{2C} are constant. With $K_{C1} = K_{C2} = 1.0$, complete decoupling of the bodies occurs; however, due to imperfect sensors and actuators, this may not be possible to do in practice.

The rate and position feedback gains ($K_{\dot{\theta}1}$, $K_{\dot{\theta}2}$, $K_{\theta 1}$, $K_{\theta 2}$) were calculated assuming that the controlled body is completely decoupled from the rest of the structure. A control loop bandwidth of 0.3 radians/s and a damping of 0.7 were chosen for this control. The gains were calculated from:

$$
\begin{aligned}
K_{\theta 1} &= \omega_{n1}^{2}\ J_1 \text{ FT-LB/RADIAN} \\
K_{\dot{\theta}1} &= 2\zeta\omega_{n1}\ J_1 \text{ FT-LB/RADIAN/S} \\
K_{\theta 2} &= \omega_{N2}^{2}\ J_2 \text{ FT-LB/RADIAN} \\
K_{\dot{\theta}2} &= 2\zeta\omega_{n2}\ J_2 \text{ FT-LB/RADIAN/S}
\end{aligned}
\qquad (6\text{-}4)
$$

The resulting gains for the torsional, normal, and lateral axis controls are summarized in Table 6-2.

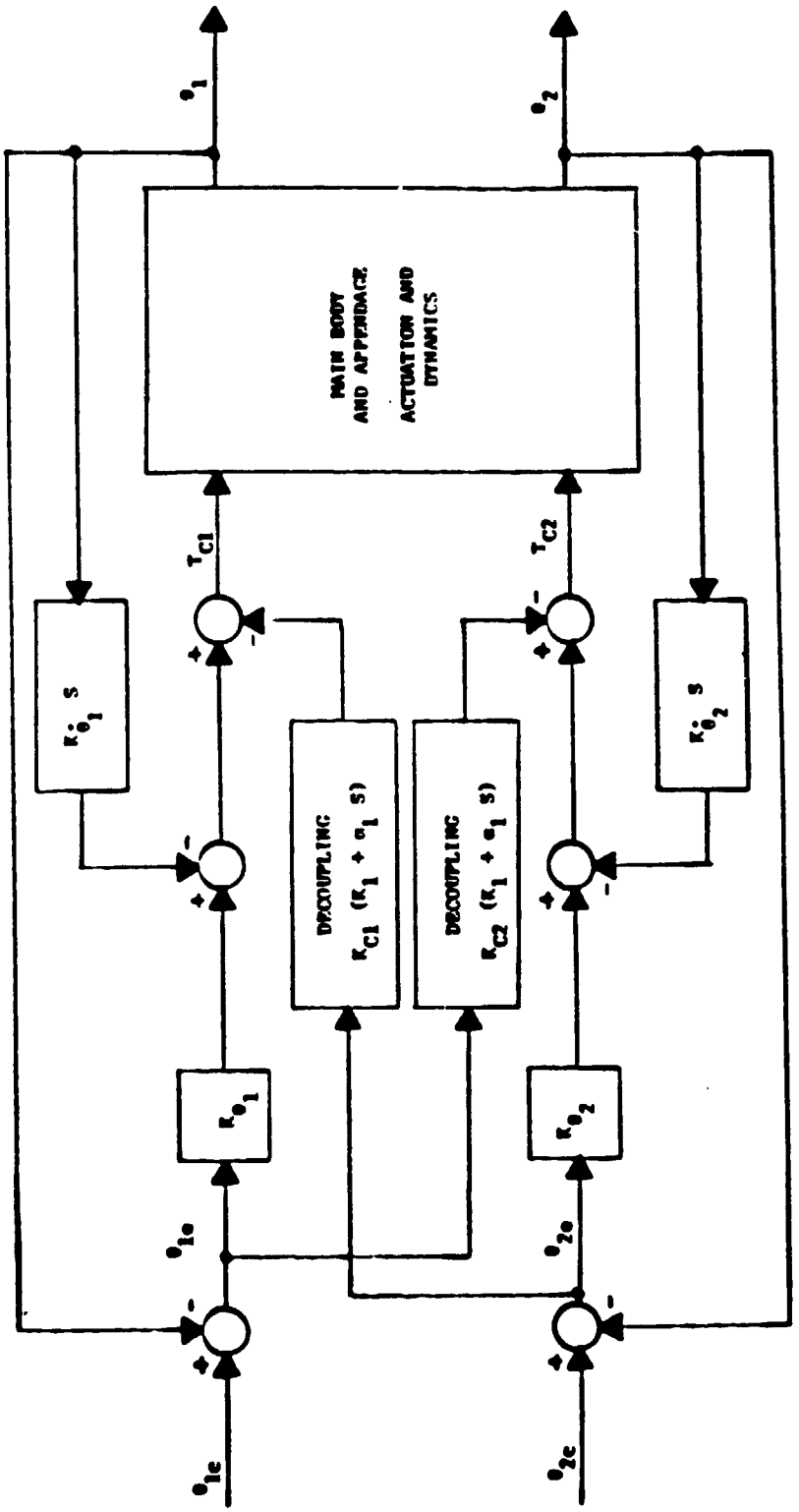

FIGURE 6-5 DECOUPLING CONTROL

TABLE 6-2 DECOUPLING CONTROL GAINS

AXIS	$K_{\theta 1}$	$K_{\dot{\theta} 1}$	$K_{\theta 2}$	$K_{\dot{\theta} 2}$
TORSIONAL	86449.5	403431.	68.152.	318.045
NORMAL	2794.05	13038.9	1602.0	7476.0
LATERAL	86449.5	403431.	1674.0	7812.0

For comparison purposes, a performance index has been defined for each angle of the one dimensional model.

$$(PI)_j = \frac{10}{\theta_{10}} \int_0^T |\theta_j| dt \qquad (6\text{-}5)$$

where

$(PI)_j$ = performance index for the j'th angle

θ_j = value of the j'th angle, in radians

T = duration of computer run, in seconds

θ_{i0} = initial condition of a selected angle, in radians

For this part of the study, perfect actuators and sensors are assumed. In further work, realistic models for these will be incorporated into the simulation. Disturbances are represented by an initial condition on one of the masses (θ_{i0} in equation 6-5) for the decoupling study.

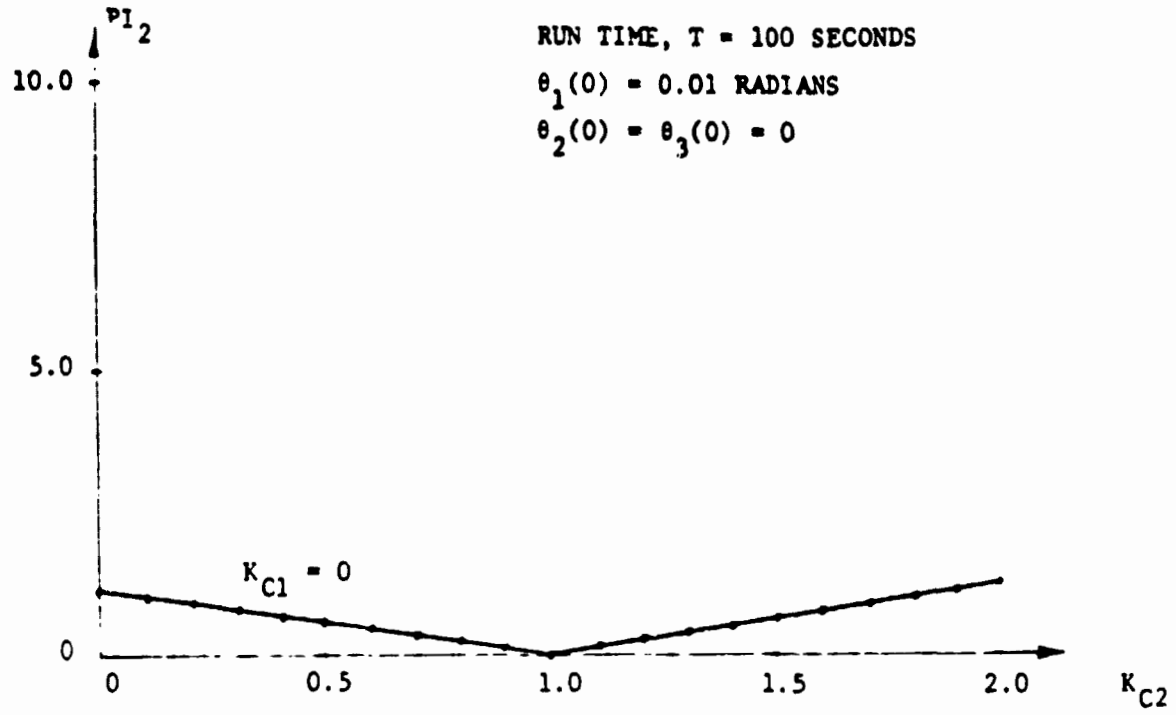

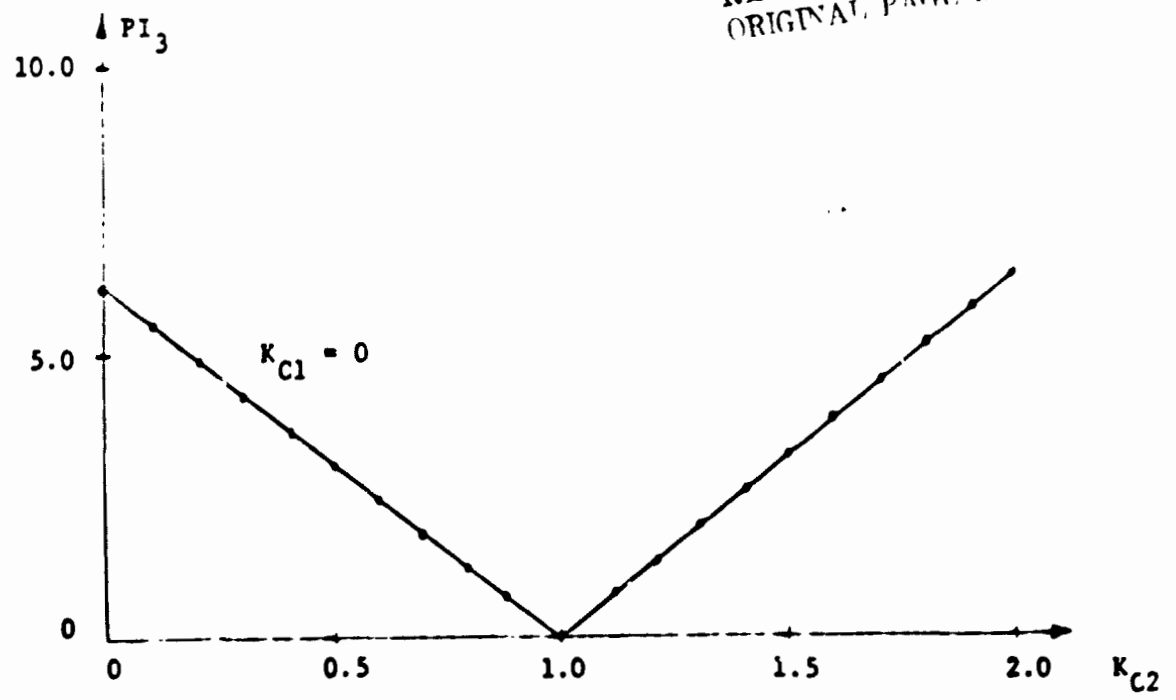

Figure 6-6 - Decoupling Performance, Torsional Axis of Solar Wing

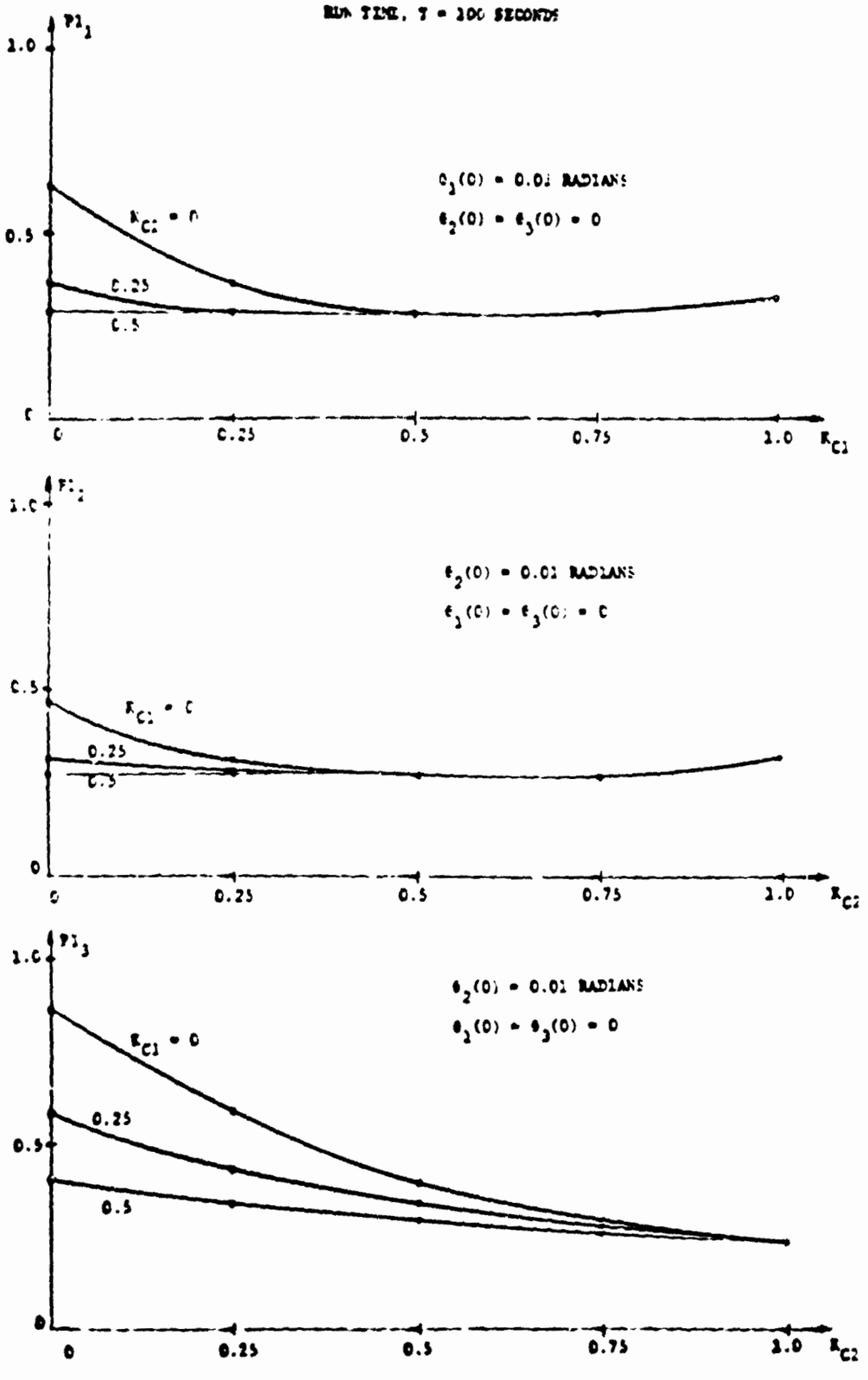

FIGURE 6-7 DECOUPLING PERFORMANCE, NORMAL AXIS OF SOLAR WING

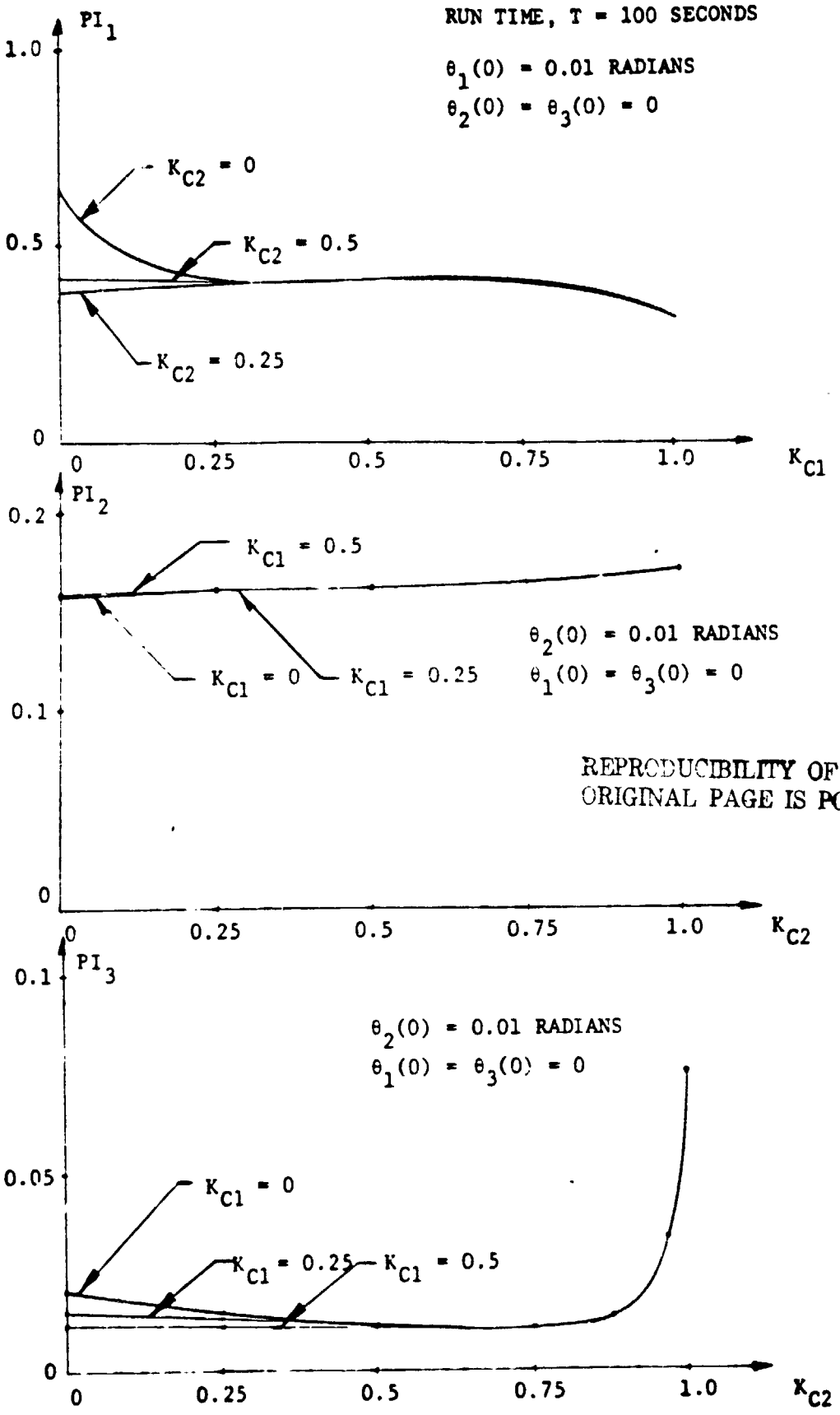

Figure 6-8 - Decoupling Performance, Lateral Axis of Solar Wing

In the case of the torsional axis, $J_1 >> J_2$ and $J_1 >> J_3$, so that movements of J_2 have little effect on J_1. For this reason, it was decided that J_1 not be decoupled from J_2 ($K_{C1} = 0$). Decoupling of disturbances propagating from J_1 to J_2 is provided for, the amount of decoupling determined by gain K_{C2}. A series of computer simulations were done, varying K_{C2} from 0 to 2.0, the results of which are shown in Figure 6-6.

Performance indices PI_2 and PI_3 take on their largest value when $K_{C2} = 0$. This is the case where no decoupling torque in applied and the greatest disturbance transfer occurs.

The indices increase linearly with K_{C2}. This range of gains represents the case where too much decoupling torque is provided. The indices decrease linearly until $K_{C2} = 1.0$, where $PI_2 = PI_3 = 0$, corresponding to complete decoupling. As K_{C2} is increased from 1.0 to 2.0, the indices increase linearly with K_{C2}. This range of gains represents the case where too much decoupling torque is provided.

A similar control was applied to the normal axis. Due to the fact that J_1, J_2, and J_3 are of comparable size, there is a strong coupling of disturbances between them. Therefore, it was decided to decouple J_2 from J_1 as well as to decouple J_1 from J_2. A series of computer simulations were done, varying K_{C1} and K_{C2} over a range of 0 to 1.0. The results are shown in Figure 6-7. Good performance is achieved for gains from 0.5 to 1.0, indicating that complete decoupling is not necessary for this axis.

In the lateral axis, masses J_1, J_2, and J_3 are again of comparable size, J_3 being the largest. This presents a particularly difficult control problem, since J_3 cannot be controlled. Simulation of the J_1 and J_2 controls for the lateral axis were done, again varying K_{C1} and K_{C2} over a range of 0 to 1.0, the results of which are shown in Figure 6-8. Variations in these control gains have little effect on PI_1 and PI_2. Index PI_3 shows only slight changes up to the point where $K_{C2} = 1.0$, where it sharply increases. It is not understood at this time why this is so. The effect of the outer control loops (rate & position feedback) on the decoupling control has not been determined as yet, and this may explain this result. This work will be done in the future.

6.3 STUDIES WITH 3-DIMENSIONAL MODELS

A simulation is in the development process for representing each configuration of the Space Construction Base (Figure 6-9). It has been organized to limit the maximum number of rigid bodies to 20. Except for the Research Pallet, the bodies are assumed to be connected by hinges. Each hinge has three dimensional freedom in angular rotation. The Research Pallet has the added feature of being free to translate independently in three directions.

The digital computer simulation has been developed for configuration I and it is in process of final verficiation. Each hinge point has been tested separately in the torsional, lateral and normal vibrational modes. Applying appropriate initial conditions allowed one to neglect the effect of all bodies except the two on either side of any hinge. The relative inertias of the two remianing bodies were forced to differ by several orders of magnitude so that one body could be deflected and allowed to oscillate about the other. Table 6-3 shows selected analytical results from one such oscillation along with the corresponding simulation results for a typical hinge check.

Since there exists a direct relationship between the one dimensional and three dimensional models in the torsional mode, comparisons were also made to check higher order oscillations in the latter model. A typical comparison is shown in Table 6-4.

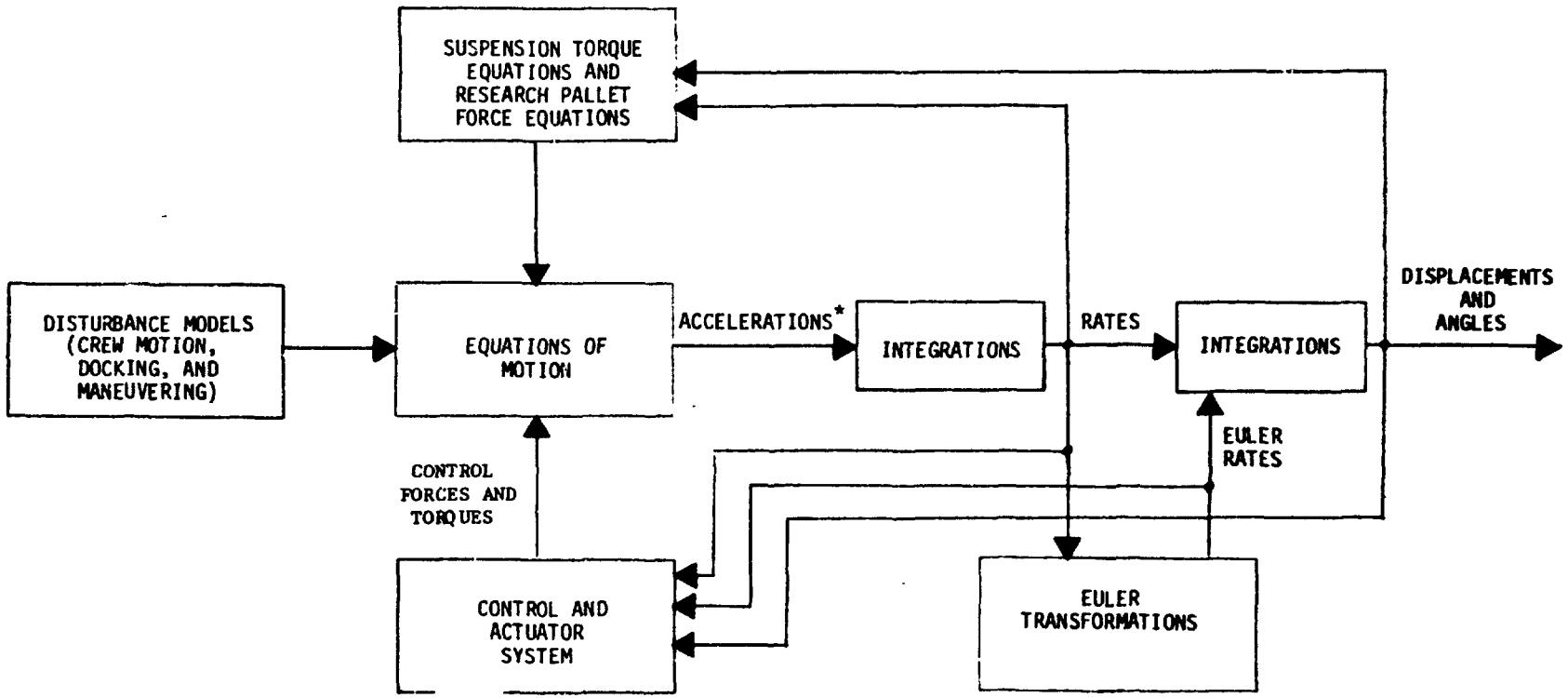

*ACCELERATIONS INCLUDE THE SYSTEM TRANSLATIONAL ACCELERATION, RESEARCH PALLET TRANSLATIONAL ACCELERATION, AND THE ANGULAR ACCELERATIONS OF ALL MODULES AND APPENDAGE SEGMENTS.

Figure 6-9 - N-Body Model of Space Base

Table 6-3 - Typical Hinge Point Check

Time (Seconds)	Analytical Solution (Radians)	Simulation Result (Radians)
0.00	0.0100000	0.0100000
0.15	0.0051247	0.0051246
0.30	-0.0039420	-0.0039420
0.45	-0.0079993	-0.0079993
0.60	-0.0038890	-0.0038890
0.75	0.0033448	0.0033449
0.90	0.0063922	0.0063921
1.05	0.0029400	0.0029399
1.20	-0.0028254	-0.0028255
1.35	-0.0051025	-0.0051025
1.50	-0.0022131	-0.0022129
1.65	0.0023772	0.0023773
1.80	0.0040688	0.0040688
1.95	0.0016578	0.0016577
2.10	-0.0019929	-0.0019930

Table 6-4 - Typical Comparison of Results Between the Three Dimensional and One Dimensional Models for the Torsional Mode

Time (Seconds)	Relative Angle Between Bodies One and Two (Radians)		Relative Angle Between Bodies Two and Three (Radians)	
	1-Dimensional	3-Dimensional	1-Dimensional	3-Dimensional
0.00	0.0100000	0.0100000	0.0000000	0.0000000
0.15	0.0036347	0.0036347	0.0037235	0.0037235
0.30	-0.0037967	-0.0037967	0.0038721	0.0038721
0.45	-0.0049997	-0.0049997	0.0001943	0.0001943
0.60	-0.0016310	-0.0016310	-0.0026968	-0.0026968
0.75	0.0016090	0.0016090	-0.0027087	-0.0027087
0.90	0.0021514	0.0021514	-0.0009910	-0.0009910
1.05	0.0007222	0.0007222	0.0003906	0.0003906
1.20	-0.0006698	-0.0006699	0.0005240	0.0005240
1.35	-0.0009142	-0.0009142	-0.0001073	-0.0001073
1.50	-0.0003096	-0.0003096	-0.0006176	-0.0006176
1.65	0.0002869	0.0002869	-0.0006090	-0.0006090
1.80	0.0003954	0.0003954	-0.0002813	-0.0002813
1.95	0.0001386	0.0001386	-0.0000114	-0.0000114
2.10	-0.0001179	-0.0001179	0.0000294	0.0000294

SECTION 7

7.0 APPLICATION OF MULTILEVEL CONTROL TECHNIQUES TO SPACE CONSTRUCTION BASE

7.1 INTRODUCTION

This section begins with a presentation of a state variable form of the sixty-six degree of freedom mathematical model, comprised of discrete rigid bodies, of the Space Construction Base described by Cornell (7-1)* of Bendix Research Laboratories in his memorandum of December 14, 1977. This state variable model was decomposed into a set of decoupled first order scalar differential equations to render it more amenable to the application of hierarchical multilevel control techniques.

In a prior memorandum by Chichester (7-2) of Bendix Guidance Systems Division, multilevel techniques were demonstrated by applying them to the optimal control of a single axis torsional model to which control had been applied previously by Porcelli (7-3) using another method. The overall multilevel approach was described in terms of the following sequence of steps.

1. Express mathematical model of plant, (system to be controlled), in state variable form.
2. Decompose mathematical model of plant into set of decoupled equations.
3. Construct performance index.
4. Form Hamiltonian.
5. Develop costate equations with associated coordination equations.
6. Develop control algorithm.
7. Construct subproblem hierarchy.
8. Discretize equations of each subproblem in the hierarchy.

* These numbers refer to references listed at the end of Section 7.

This section summarizes the application of the first seven steps of this sequence, and an additional step, to the twelve configurations of the mathematical model of the Space Construction Base documented in the memorandum by Cornell (7-1). The additional step cited here is the incorporation of special necessary conditions for optimality in the costate and control equations due to the non-separability of the performance index required for multilevel local vertical attitude control of the Space Construction Base.

7.2 GENERAL DECOMPOSED MODEL

7.2.1 background

Figure 1 and Tables 7-1 and 7-2 are reproduced from Cornelli's memorandum (7-1). Figure 7-1 presents a topological tree that shows how the rigid bodies comprising the mathematical model are connected. A single line represents a three degree of freedom spring hinge suspension while a double line represents a six degree of freedom suspension. Table 7-1 lists the number of rigid bodies associated with each configuration of the model. Table 7-2 lists the numbers of degrees of freedom associated with each of the twelve configurations.

As indicated by Figure 7-2, the equations comprising the overall control problem in state variable form may be assembled into two related subproblem hierarchies, the translational hierarchy and the rotational hierarchy.

TABLE 7-1

CONFIGURATION	NUMBER OF RIGID BODIES
1	5
2	6
3	7
4	8
5	8
6	8
7	8
8	10
9	10
10	19
11	20
12	20

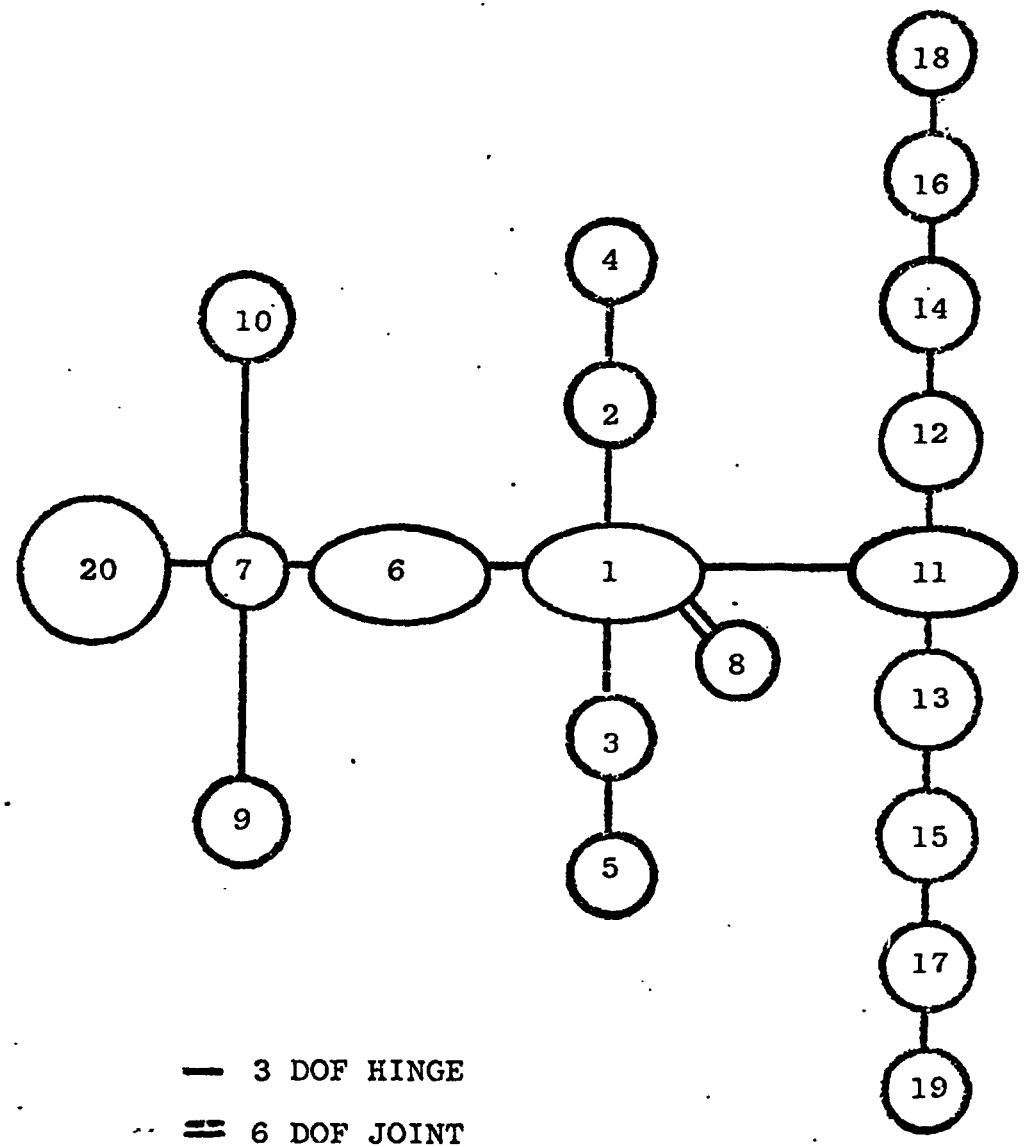

Figure 7-1. Topological Tree of Space Base Rigid Bodies

TABLE 7-2 - Degrees of Freedom

Configuration	Degrees of Freedom Translational	Rotational	Total
1	3	15	18
2	3	18	21
3	3	21	24
4	6	24	30
5	6	24	30
6	6	24	30
7	6	24	30
8	6	30	36
9	6	30	36
10	6	57	63
11	6	60	66
12	6	60	66

7.2.2 Decomposed Translational State Equations

The decomposed translational equations for configurations 1 through 12 may be written in the form of equations (1) through (12) with the aid of equations (13) through (43). It should be noted that the state variables, R_{ix}, R_{iy} and R_{iz}, are scalar components along the Space Base axes of the translational displacement vector of the ith rigid body of the body and the state variables V_{Tix}, V_{Tiy} and V_{Tiz} are the corresponding scaler components of the translational velocity vector where, in this instance, i = 1,8.

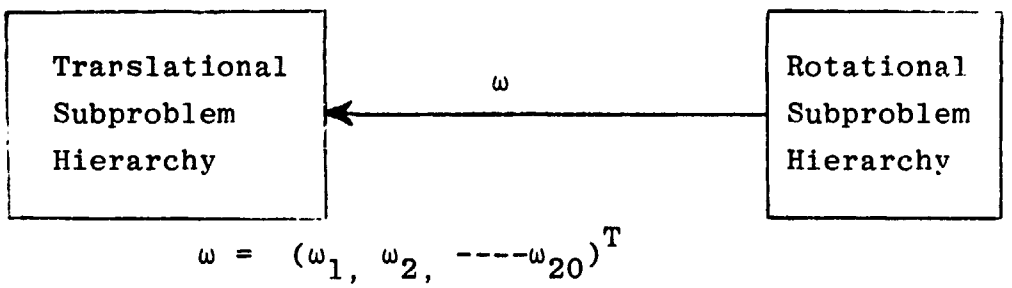

Figure 7-2. Overall Control Problem Structure

Decomposed Translational State Equations

Scalar State Equations

$$\dot{R}_{1x} = \hat{S}_{T1x} \tag{1}$$

$$\dot{V}_{T1x} = \frac{\Sigma F_x}{\Sigma M} + S_{T1x} \tag{2}$$

$$\dot{R}_{1y} = \hat{S}_{T1y} \tag{3}$$

$$\dot{V}_{T1y} = \frac{\Sigma F_y}{\Sigma M} + S_{T1y} \tag{4}$$

$$\dot{R}_{1z} = \hat{S}_{T1z} \tag{5}$$

$$\dot{V}_{T1z} = \frac{\Sigma F_z}{\Sigma M} + S_{T\ z}$$

$$\dot{R}_{8x} = \hat{S}_{T8x} \tag{7}$$

$$\dot{V}_{T8x} = \frac{F_{8x}}{m_8} + S_{T8x} \tag{8}$$

$$\dot{R}_{8y} = \hat{S}_{T8y} \tag{9}$$

$$\dot{V}_{T8y} = \frac{F_{8y}}{m_8} + S_{T8y} \tag{10}$$

$$\dot{R}_{8z} = \hat{S}_{T8z} \tag{11}$$

$$\dot{V}_{T8z} = \frac{F_{8z}}{m_8} + S_{T8z} \tag{12}$$

where:

$$\Sigma M = \sum_{\substack{i=1 \\ i \neq 8}}^{n} m_i \tag{13}$$

$$\Sigma F_x = \sum_{\substack{i=1 \\ i\neq 8}}^{n} \Sigma F_{ix} \tag{14}$$

$$\Sigma F_y = \sum_{\substack{i=1 \\ i\neq 8}}^{n} \Sigma F_{iy} \tag{15}$$

$$\Sigma F_z = \sum_{\substack{i=1 \\ i\neq 8}}^{n} \Sigma F_{iz} \tag{16}$$

$$F_i = (F_{ix},\ F_{iy},\ F_{iz})^T \tag{17}$$

The upper limit of the summations in equations (13) through (17), n, varies between 5 and 20 according to the specific configuration of the space base being modeled as shown in Table 7-1. It also may be seen in Table 7-1, that for configurations 1, 2 and 3, the translational equations of rigid body 8 are omitted.

The following coordination equations are defined for each of the decomposed translational state equations.

$$\hat{S}_{T1x} = V_{T1x} \tag{18}$$

$$S_{T1x} = \frac{-1}{\Sigma M}(L_x + N_x) \tag{19}$$

$$\hat{S}_{T1y} = V_{T1y} \tag{20}$$

$$S_{T1y} = \frac{-1}{\Sigma M}(L_y + N_y) \tag{21}$$

$$\hat{S}_{T1z} = V_{T1z} \tag{22}$$

$$S_{T1z} = \frac{-1}{\Sigma M}(L_z + N_z) \tag{23}$$

$$\hat{S}_{T8x} = V_{T8x} \tag{24}$$

$$S_{T8x} = \frac{S_{18x}}{m_8} \tag{25}$$

$$\hat{S}_{T8y} = V_{T8y} \tag{26}$$

$$S_{T8y} = \frac{S_{18y}}{m_8} \tag{27}$$

$$\hat{S}_{T8z} = V_{T8z} \tag{28}$$

$$S_{T8z} = \frac{S_{18z}}{m_8} \tag{29}$$

where:

$S_{18} = (S_{18x}, S_{18y}, S_{18z})^T$ is the vecter representing the suspension force exerted on body 1 by body 8.

$L = (L_x, L_y, L_z)^T$ is the aggregation of terms linear in $\dot{\omega}_i$ resulting from the summation of the translational equations of all of the rigid bodies of the model except body 8.

N_x, N_y, N_z are components of terms along the space base axes each of which is quadratic in ω_{ix}, ω_{iy} and ω_{iz}.

$$L_x = \sum_{\substack{i=1 \\ i\neq 8}}^{20} b_{Txi} \dot{\omega}_i \tag{30}$$

where:

$$\dot{\omega}_i = (\dot{\omega}_{ix}, \dot{\omega}_{iy}, \dot{\omega}_{iz})^T \tag{31}$$

$$b_{Txi} = (b_{Txix}, b_{Txiy}, b_{Txiz})^T \tag{32}$$

$$L_y = \sum_{\substack{i=1 \\ i\neq 8}}^{20} b_{Tyi} \dot{\omega}_i \tag{33}$$

where:

$$b_{Tyi} = (b_{Tyix},\ b_{Tyiy},\ b_{Tyiz})^T \tag{34}$$

$$L_z = \sum_{\substack{i=1 \\ i\neq 8}}^{20} b_{Tzi}\ \dot{\omega}_i \tag{35}$$

where:

$$b_{Tzi} = (b_{Tzix},\ b_{Tziy},\ b_{Tziz})^T \tag{36}$$

$$N_x = \sum_{\substack{i=1 \\ i\neq 8}}^{20} \omega_i^T\ A_{Txi}\ \omega_i \tag{37}$$

$$\omega_i = (\omega_{ix},\ \omega_{iy}\ \omega_{iz})^T \tag{38}$$

$$A_{Txi} = \begin{bmatrix} 0 & \frac{1}{2}a_{Txixy} & \frac{1}{2}a_{Txixz} \\ \frac{1}{2}a_{Txixy} & a_{Txiyy} & 0 \\ \frac{1}{2}a_{Txixz} & 0 & a_{Tzizz} \end{bmatrix} \tag{39}$$

$$N_y = \sum_{\substack{i=1 \\ i\neq 8}}^{20} \omega_i^T\ A_{Tyi}\ \omega_i \tag{40}$$

$$A_{Tyi} = \begin{bmatrix} a_{Tyixx} & \frac{1}{2}a_{Tyixy} & 0 \\ \frac{1}{2}a_{Tyixy} & 0 & \frac{1}{2}a_{Tyiyz} \\ 0 & \frac{1}{2}a_{Tyiyz} & a_{Tyizz} \end{bmatrix} \tag{41}$$

$$N_z = \sum_{\substack{i=1 \\ i \neq 8}}^{20} \omega_i^T A_{Tzi} \omega_i \qquad (42)$$

$$A_{Tzi} = \begin{bmatrix} a_{Tzixx} & 0 & \frac{1}{2}a_{Tzixz} \\ 0 & a_{Tziyy} & \frac{1}{2}a_{Tziyz} \\ \frac{1}{2}a_{Tzixz} & \frac{1}{2}a_{Tziyz} & 0 \end{bmatrix} \qquad (43)$$

The subproblem hierarchy corresponding to the decomposed translational state equations, (1) through (12), and the translational state coordination equations, (19) through (29) is shown in Figures 7-3 and 7-4. It should be noted that this subproblem hierarchy corresponds to the decomposed model without the application of control.

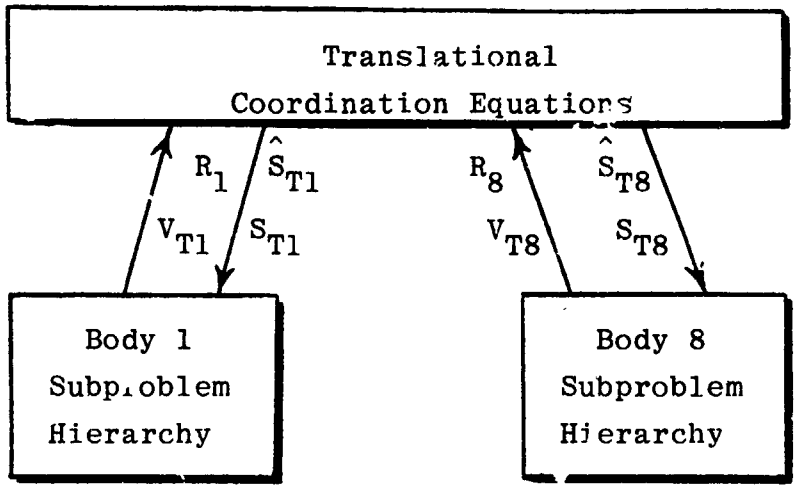

Figure 7-3. Translational Subproblem Hierarchy Without Control

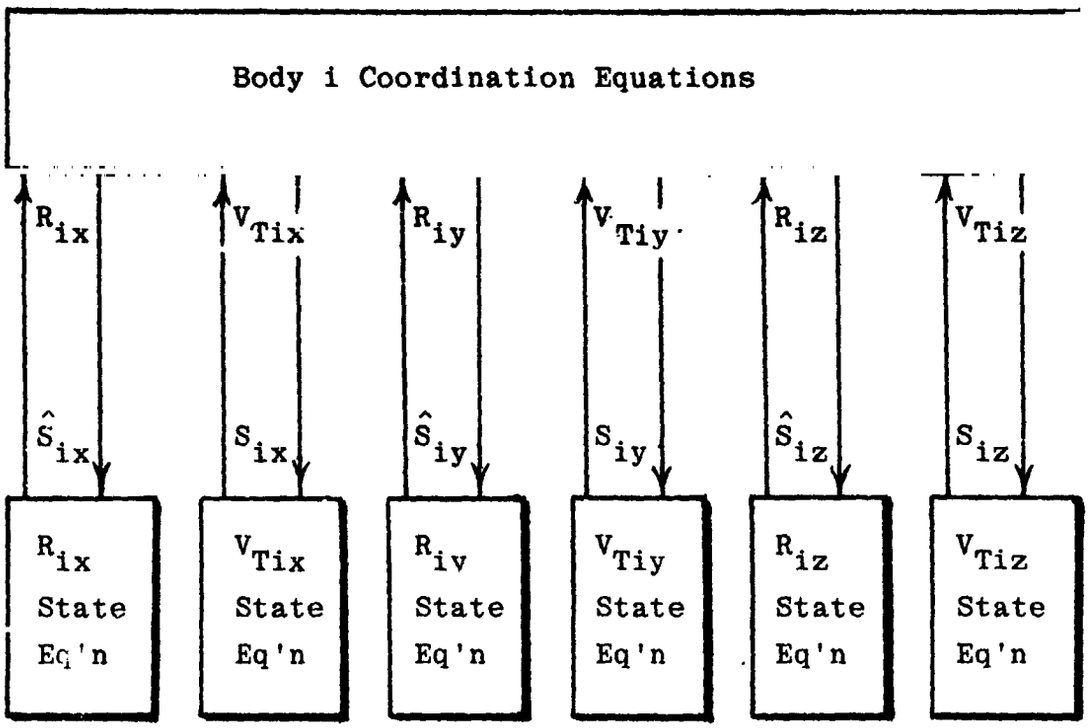

Figure 7-4. Body i Translational Subproblem Hierarchy for i=1,8

7.2.3 Decomposed Rotational State Equations

The decomposed rotational state equations for configurations (1) through (12) may be written in the form of equations (44) through (49) with the aid of rotational state coordination equations (50) through (55) and equations (58) through (63). Here it should be noted that the state variables ϕ_i, θ_i and ψ_i are the Euler angles of the ith rigid body with respect to the space base coordinate axes and the state variables ω_{ix}, ω_{iy}, and ω_{iz} are the scaler components with respect to the space base axes of the angular rates of the ith rigid body where in this instance i=1,2,---,n, the value of n depending upon the particular configuration being modeled as shown in Table 7-1.

$$A'_{ix,j} = \begin{bmatrix} 0 & \frac{1}{2}a_{ix,jx,jy} & \frac{1}{2}a_{ix,jx,jz} \\ \frac{1}{2}a_{ix,jx,jy} & a_{ix,jy,jy} & \frac{1}{2}a_{ix,jy,jz} \\ \frac{1}{2}a_{ix,jx,jz} & \frac{1}{2}a_{ix,jy,jz} & a_{ix,jz,jz} \end{bmatrix} \quad (61)$$

$$A'_{iy,j} = \begin{bmatrix} a_{iy,jx,jx} & \frac{1}{2}a_{iy,jx,jy} & \frac{1}{2}a_{iy,jx,jz} \\ \frac{1}{2}a_{iy,jx,jy} & 0 & \frac{1}{2}a_{iy,jy,jz} \\ \frac{1}{2}a_{iy,jx,jz} & \frac{1}{2}a_{iy,jy,jz} & a_{iy,jz,jz} \end{bmatrix} \quad (62)$$

$$A'_{iz,j} = \begin{bmatrix} a_{iz,jx,jx} & \frac{1}{2}a_{iz,jx,jy} & \frac{1}{2}a_{iz,jx,jz} \\ \frac{1}{2}a_{iz,jx,jy} & a_{iz,jy,jy} & \frac{1}{2}a_{iz,jy,jz} \\ \frac{1}{2}a_{iz,jx,jz} & \frac{1}{2}a_{iz,jy,jz} & 0 \end{bmatrix} \quad (63)$$

$$\bar{A}_{ix,j} = \begin{bmatrix} \bar{a}_{ix,jx,jx} & \frac{1}{2}\bar{a}_{ix,jx,jy} & \frac{1}{2}\bar{a}_{ix,jx,jz} \\ \frac{1}{2}\bar{a}_{ix,jx,jy} & \bar{a}_{ix,jy,jy} & \frac{1}{2}\bar{a}_{ix,jy,jz} \\ \frac{1}{2}\bar{a}_{ix,jx,jz} & \frac{1}{2}\bar{a}_{ix,iy,iz} & \bar{a}_{ix,jz,jz} \end{bmatrix} \quad (64)$$

$$\bar{A}_{iy,j} = \begin{bmatrix} \bar{a}_{iy,jx,jx} & \frac{1}{2}\bar{a}_{iy,jx,jy} & \frac{1}{2}\bar{a}_{iy,jx,jz} \\ \frac{1}{2}\bar{a}_{iy,jx,jy} & \bar{a}_{iy,jy,jy} & \frac{1}{2}\bar{a}_{iy,jy,jz} \\ \frac{1}{2}a_{iy,jx,jz} & \frac{1}{2}\bar{a}_{iy,jy,jz} & \bar{a}_{iy,jz,jz} \end{bmatrix} \quad (65)$$

$$\bar{A}_{iz,j} = \begin{bmatrix} \bar{a}_{iz,jx,jx} & \frac{1}{2}\bar{a}_{iz,jx,jy} & \frac{1}{2}\bar{a}_{iz,jx,jz} \\ \frac{1}{2}\bar{a}_{iz,jx,jy} & \bar{a}_{iz,jy,jy} & \frac{1}{2}\bar{a}_{iz,jy,jz} \\ \frac{1}{2}\bar{a}_{iz,jx,jz} & \frac{1}{2}\bar{a}_{iz,jy,jz} & \bar{a}_{iz,jz,jz} \end{bmatrix} \quad (66)$$

The subproblem hierarchy corresponding to the decomposed rotational state equations, (44) through (49) and the rotational state coordination equations, (50) through (66) is shown in Figures 7-5 and 7-6. As was the case with the subproblem hierarchies in Figures 7-3 and 7-4 for the translational equation, these hierarchies also correspond to the uncontrolled case.

Inspection of the state equations (45), (47) and (49) reveals that they are quadratic in the state variables ω_{ix}, ω_{iy} and ω_{iz}. Since the traditional development of multilevel control techniques has been concentrated on the control of linear systems, this form of the state equations poses a special problem in such application. Pontryagin's maximum principle, upon which multilevel optimization is based, does not preclude the control of nonlinear systems and some recent papers by Hassan and Singh (7-4), (7-5), (7-6) and (7-7) describe some potentially useful approaches for effecting such control by multilevel techniques.

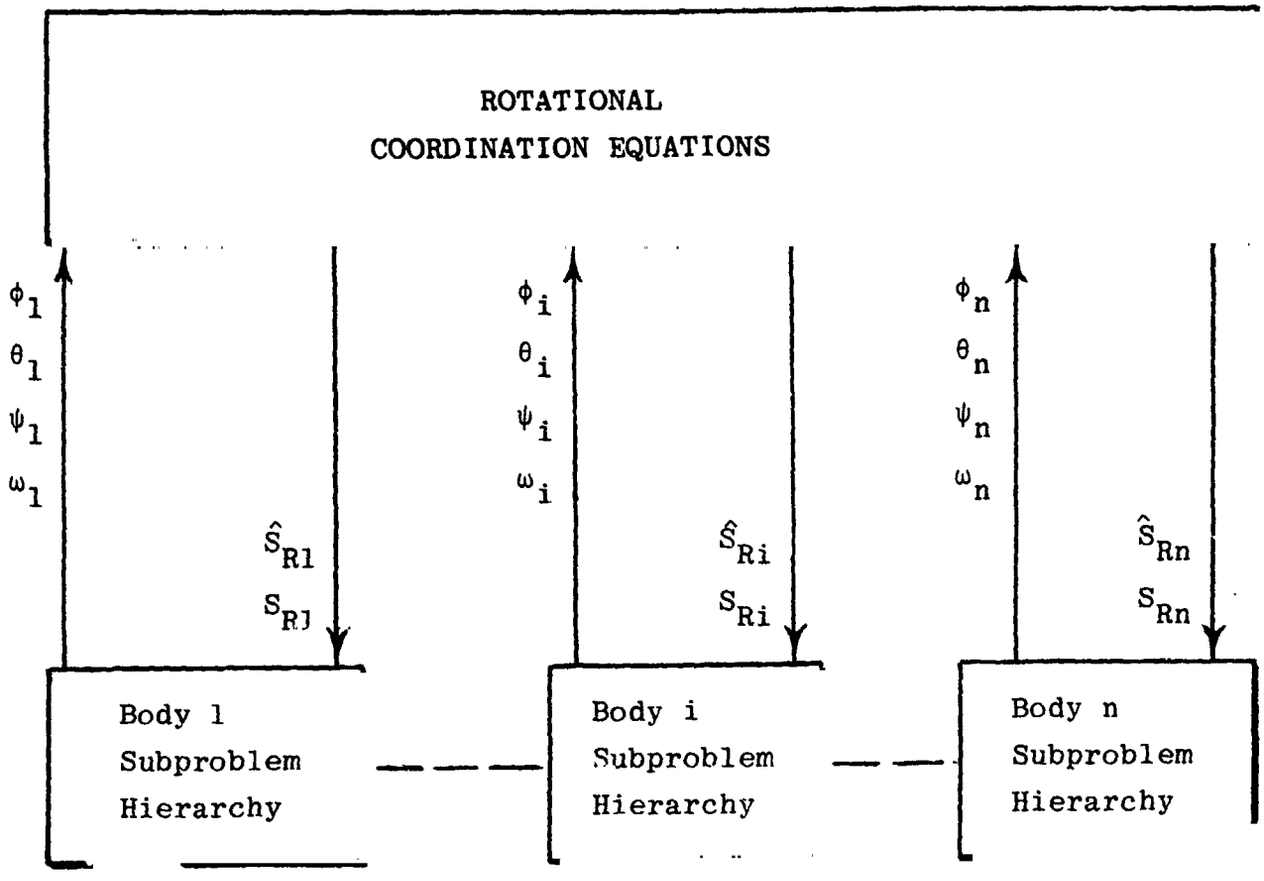

Figure 7-5. Rotational Subproblem Hierarchy Without Control

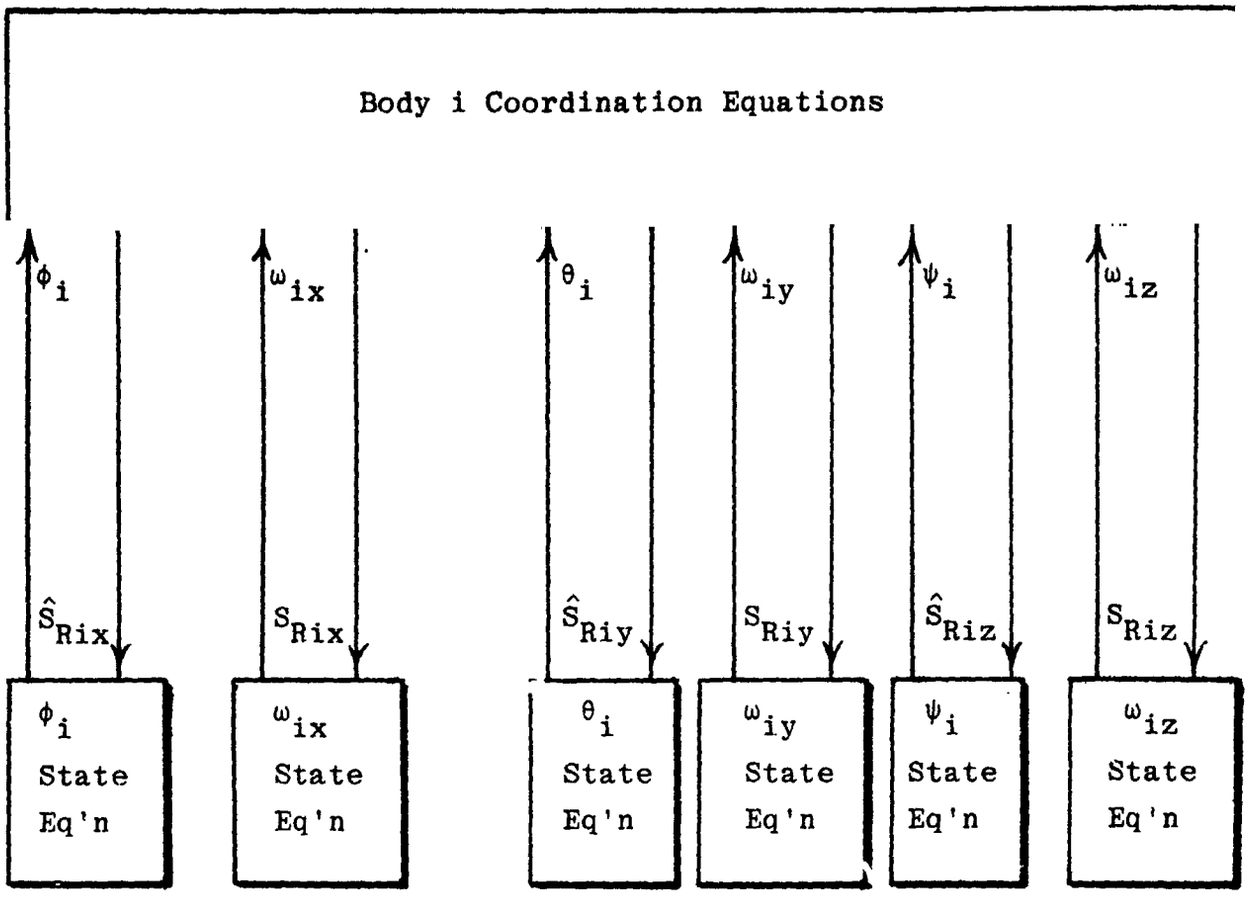

Figure 7-6. Body i Rotational Subproblem Hierarchy for i = 1, 2, --- n.

7.3 CONSTRUCTION OF PERFORMANCE INDEX

7.3.1 General Discussion

After the state equations for the uncontrolled system (plant) have been decomposed, i.e., decoupled, the next step in the application of hierarchical multilevel optimal control is the formulation of a performance index functional that provides a measure of the departure of the system's operation from the optimal condition. The most distinctive characteristic of a performance index utilized in the application of multilevel control techniques is that it must be either decomposed at the ontset in the same manner as the state equations of the plant or amenable to such decomposition.

The specific form of the performance index and the variables utilized in it depend upon the type of control to be effected and the relative importance of such factors as the polarity of errors and minimization of the energy expended in effecting control in comparison with minimization of error. In the present section the formulation of a performance index for local vertical attitude stabilization involves only the rotational state variables of those rigid bodies of the mathematical model to which torque is applied.

7.3.2 Performance Index for Local Vertical Attitude Stabilization

Since the performance index of this section pertains only to attitude control, it is not a function of any of the translational state variables. The following assumptions were utilized in constructing this performance index.

1) The differences (errors) between the actual and specified Euler angles of body 1, $\phi_1-\phi_1^*$, $\theta_1-\theta_1^*$ and $\psi_1-\psi_1^*$, respectively, are to be minimized. (The convention adopted here and later in this section is that x^* is the specified or optimal value of x.)

2) The differences between the actual and specified body rate components of body 1, $\omega_{1x} - \omega_{1x}^*$, $\omega_{1y} - \omega_{1y}^*$ and $\omega_{1z} - \omega_{1z}^*$ are also to be minimized.

3) The Euler angle errors $\phi_8 - \phi_8^*$, $\theta_8 - \theta_8^*$ and $\psi_8 - \psi_8^*$, and body rate errors, $\omega_{8x} - \omega_{8x}^*$, $\omega_{8y} - \omega_{8y}^*$ and $\omega_{8z} - \omega_{8z}^*$, are similarly to be minimized if body 8 is present in the configuration being controlled.

4) The relative Euler angles and body rate components with respect to body 1 of the remaining bodies comprising the mathematical model are to be minimized.

5) Departures from specified or optimal values of the state variables are equally important for either polarity of the same magnitude.

6) Control is effected only by the application of torque to each of the rigid bodies of the model.

7) Control actuator torque is applied to each solar wing only at its interface with the rest of the space base.

8) Control energy is proportional to the square of the torque applied to each rigid body of the model.

9) Each error term and each control energy term is multiplied by a constant coefficient, $W_{i,j}$, representing the relative significance of that term in the performance index.

10) The time interval over which the performance index is to be optimized extends from t_o to t_f.

The performance index resulting from the application of the above assumptions is the following:

$$
\begin{aligned}
P=\int_{t_o}^{t_f} \Big\{ & W_{1,1}\,(\phi_1-\phi_1^*)^2+W_{1,2}(\omega_{1x}-\omega_{1x}^*)^2+W_{1,3}T_{a1x}^2 \\
& + W_{1,4}(\theta_1-\theta_1^*)^2 + W_{1,5}(\omega_{1y}-\omega_{1y}^*)^2+W_{1,6}\,T_{a1y}^2 \\
& +W_{1,7}\,(\psi_1-\psi_1^*)^2+W_{1,8}(\omega_{1z}-\omega_{1z}^*)^2+W_{1,9}T_{a1z}^2 \\
+ \sum_{i=2,3,6,11} & \Big[W_{i,1}(\phi_i-\phi_1)^2+W_{i,2}(\omega_{ix}-\omega_{1x})^2+W_{i,3}T_{aix}^2 \\
& +W_{i,4}(\theta_i-\theta_1)^2+W_{i,5}(\omega_{iy}-\omega_{1y})^2+W_{i,6}T_{aiy}^2 \\
& +W_{i,7}(\psi_i-\psi_1)^2+W_{i,8}(\omega_{iz}-\omega_{1z})^2+W_{i,9}T_{aiz}^2\Big] \\
& +W_{7,1}(\phi_7-\phi_6)^2+W_{7,2}(\omega_{7x}-\omega_{1x})^2+W_{7,3}\,T_{a7x}^2 \\
& +W_{7,4}(\theta_7-\theta_6)^2+W_{7,5}(\omega_{7y}-\omega_{1y})^2+W_{7,6}\,T_{a7y}^2 \\
& +W_{7,7}(\psi_7-\psi_6)^2+W_{7,8}(\omega_{7z}-\omega_{6z})^2+W_{7,9}\,T_{a7z}^2 \\
& +W_{8,1}(\phi_8-\phi_8^*)^2+W_{8,2}(\omega_{8x}-\omega_{8x}^*)^2+W_{8,3}\,T_{a8x}^2 \\
& +W_{8,4}(\theta_8-\theta_8^*)^2+W_{8,5}(\omega_{8y}-\omega_{8y}^*)^2+W_{8,6}\,T_{a8y}^2 \\
& +W_{8,7}(\psi_8-\psi_8^*)^2+W_{8,8}(\omega_{8z}-\omega_{8z}^*)^2+W_{8,9}T_{a8z}^2 \\
+ \sum_{i=12,13} & \Big[W_{i,1}(\phi_i-\phi_{11})^2+W_{i,2}(\omega_{ix}-\omega_{11x})^2+W_{i,3}T_{aix}^2 \\
& + W_{i,4}(\theta_i-\theta_{11})^2+W_{i,5}(\omega_{iy}-\omega_{11y})^2+W_{i,6}T_{aiy}^2 \\
& +W_{i,7}(\psi_i-\psi_{11})^2+W_{i,8}(\omega_{iz}-\omega_{11z})^2+W_{i,9}T_{aiz}^2\Big]
\end{aligned}
\tag{67}
$$

$$+\sum_{i=9,10,20}\Big[W_{i,1}(\phi_i-\phi_7)^2+W_{i,2}(\omega_{ix}-\omega_{7x})^2+W_{i,3}T_{aix}^2 + W_{i,4}(\phi_i-\phi_7)^2+W_{i,5}(\omega_{iy}-\omega_{7y})^2+W_{i,6}T_{aiy}^2 +W_{i,7}(\psi_i-\psi_7)^2+W_{i,8}(\omega_{iz}-\omega_{7z})^2+W_{i,9}T_{aiz}^2\Big]\Big\}\,dt \qquad (67)$$

Cont'd.

A similar performance index could be constructed for inertially referenced optimal attitude control. It would differ from that shown in equation (67) in that $\phi_1^*=\theta_1^*=0$ and $\omega_{1x}^*=\omega_{1y}^*=\omega_{1z}^*=0$. Neither of these performance indexes is separable in this form due to the generation of cross products of the state variables by the error terms. Hence, neither of them can be utilized directly in the application of multilevel control techniques. A paper by Singh and Hassan (7-7), however, presents an approach to multilevel optimization that utilizes non-separable performance index or cost functions that are transformed to quasi-separable forms. The corresponding form of the local vertical attitude control performance index of equation (67) is presented in equations (68) through (118).

$$P=\int_{\text{to}}^{t_f}\Big\{\sum_{i=1}^{20}\Big[u_{ix}(T_{aix}-T_{aix}^*)^2+u_{iy}(T_{aiy}-T_{aiy}^*)^2 \qquad i\neq 4,5,14,15,16,17,18,19$$

$$+u_{iz}(T_{aiz}-T_{aiz}^*)^2+\sum_{j=1}^{6}p_{i,j}\Big] +G(\phi_i^*,\theta_i^*,\psi_i^*,\omega_{ix}^*,\omega_{iy}^*,\omega_{iz}^*)\Big\}\,dt \qquad (68)$$

The terms and coefficients introduced in equation (68) are defined in equations (69) through (118)

$$G(\phi_i^*, \theta_i^*, \psi_i^*, \omega_{ix}^*, \omega_{iy}^*, \omega_{iz}^*)$$

$$=-2\Bigg[\sum_{i=1,2,3,6,11}(W_{i,1}^*\phi_1\phi_i^* + W_{i,2}\omega_{1x}^*\omega_{ix}^* + W_{i,4}\theta_1^*\theta_i^*$$

$$+W_{i,5}\ \omega_{1y}^*\omega_{iy}^* + W_{i,7}\psi_1^*\psi_i^* + W_{i,8}\omega_{1z}^*\omega_{iz}^*)$$

$$+W_{7,1}\phi_6^*\phi_7^* + W_{7,2}\omega_{6x}^*\omega_{7x}^* + W_{7,4}\theta_6^*\theta_7^* + W_{7,5}^*\omega_{6y}^*\omega_{7y}^*$$

$$+W_{7,7}\psi_6^*\psi_7^* + W_{7,8}\omega_{6z}^*\omega_{7z}^* + W_{8,1}(\phi_8^*)^2 + W_{8,2}(\omega_{8x}^*)^2$$

$$+W_{8,4}(\theta_8^*)^2 + W_{8,5}(\omega_{8y}^*)^2 + W_{8,7}(\psi_8^*)^2 + W_{8,8}(\omega_{8z}^*)^2$$

$$+\sum_{i=9,10,20}(W_{i,1}\phi_7^*\phi_i^* + W_{i,2}\omega_{7x}^*\omega_{ix}^* + W_{i,4}\theta_7^*\theta_i^*$$

$$+W_{i,5}\omega_{7y}^*\omega_{iy}^* + W_{i,7}\psi_7^*\psi_i^* + W_{i,8}\omega_{7z}^*\omega_{iz}^*)$$

$$+\sum_{i=12,13}(W_{i,1}\phi_{11}^*\phi_i^* + W_{i,2}\omega_{11x}^*\omega_{ix}^* + W_{i,4}\theta_{11}^*\theta_i^*$$

$$+W_{i,5}\omega_{11y}^*\omega_{iy}^* + W_{i,7}\psi_{11}^*\psi_i^* + W_{i,8}\omega_{11z}^*\omega_{iz}^*)\Bigg] \qquad (69)$$

$$p_{1,1} = W'_{1,1}\phi_1^2 + W_{1,1}(\phi_1^*)^2 \qquad (70)$$

$$p_{1,2} = W'_{1,2}\omega_{1x}^2 + W_{1,2}(\omega_{1x}^*)^2 + W_{1,3}T_{1x}^2 \qquad (71)$$

$$P_{1,3} = W'_{1,4}\theta_1^2 + W_{1,4}(\theta_1^*)^2 \qquad (72)$$

$$p_{1,4} = W'_{1,5}\omega_{1y}^2 + W_{1,5}(\omega_{1y}^*)^2 + W_{1,6}T_{1y}^2 \qquad (73)$$

$$P_{1,5} = W'_{1,7}\psi_1^2 + W_{1,7}(\psi_1^*)^2 \qquad (74)$$

$$P_{1,6} = W'_{1,8}\omega_{1z}^2 + W_{1,8}(\omega_{1z}^*)^2 + W_{1,9}T_{1z}^2 \qquad (75)$$

For i=2,3,9.10,12,13,20:

$$p_{i,1}=W_{i,1}\phi_i^2 \tag{77}$$

$$p_{i,2}=W_{i,2}\omega_{ix}^2+W_{i,3}T_{ix}^2 \tag{78}$$

$$p_{i,3}=W_{i,4}\theta_i^2 \tag{79}$$

$$p_{i,4}=W_{i,5}\omega_{iy}^2+W_{i,6}T_{iy}^2 \tag{80}$$

$$p_{i,5}=W_{i,7}\psi_i^2 \tag{81}$$

$$p_{i,6}=W_{i,8}\omega_{iz}^2+W_{i,9}T_{iz}^2 \tag{82}$$

For i=6,7,11:

$$p_{i,1}=W'_{i,1}\phi_i^2 \tag{83}$$

$$p_{i,2}=W'_{i,2}\omega_{ix}^2+W_{i,3}T_{ix}^2 \tag{84}$$

$$p_{i,3}=W'_{i,4}\theta_i^2 \tag{85}$$

$$p_{i,4}=W'_{i,5}\omega_{iy}^2+W_{i,6}T_{iy}^2 \tag{86}$$

$$p_{i,5}=W'_{i,7}\psi_i^2 \tag{87}$$

$$p_{i,6}=W'_{i,8}\omega_{iz}^2+W_{i,9}T_{iz}^2 \tag{88}$$

$$p_{8,1}=W_{8,1}\left[\phi_8^2+(\phi_8^*)^2\right] \tag{89}$$

$$p_{8,2}=W_{8,2}\left[\omega_{8x}^2+(\omega_{8x}^*)^2\right]+W_{8,3}T_{8x}^2 \tag{90}$$

$$p_{8,3}=W_{8,4}\left[\theta_8^2+(\theta_8^*)^2\right] \tag{91}$$

$$p_{8,4}=W_{8,5}\left[\omega_{8y}^2+(\omega_{8y}^*)^2\right]+W_{8,6}T_{8y}^2 \tag{92}$$

$$p_{8,5}=W_{8,7}\left[\psi_8^2+(\psi_8^*)^2\right] \tag{93}$$

$$p_{8,6}=W_{8,8}\left[\omega_{8z}^2+(\omega_{8z}^*)^2\right]+W_{8,7}T_{8z}^2 \tag{94}$$

$$W'_{1,1}=W_{1,1}+W_{2,1}+W_{3,1}+W_{6,1}+W_{11,1} \quad (95)$$

$$W'_{1,2}=W_{1,2}+W_{2,2}+W_{3,2}+W_{6,2}+W_{11,2} \quad (96)$$

$$W'_{1,4}=W_{1,4}+W_{2,4}+W_{,3,4}+W_{6,4}+W_{11,4} \quad (97)$$

$$W'_{1,5}=W_{1,5}+W_{2,5}+W_{3,5}+W_{6,5}+W_{11,5} \quad (98)$$

$$W'_{1,7}=W_{1,7}+W_{2,7}+W_{3,7}+W_{6,7}+W_{11,7} \quad (99)$$

$$W'_{1,8}=W_{1,8}+W_{2,8}+W_{3,8}+W_{6,8}+W_{11,8} \quad (100)$$

$$W'_{6,1}=W_{6,1}+W_{7,1} \quad (101)$$

$$W'_{6,2}=W_{6,2}+W_{7,2} \quad (102)$$

$$W'_{6,4}=W_{6,4}+W_{7,4} \quad (103)$$

$$W'_{6,5}=W_{6,5}+W_{7,5} \quad (104)$$

$$W'_{6,7}=W_{6,7}+W_{7,7} \quad (105)$$

$$W'_{6,8}=W_{6,8}+W_{7,8} \quad (106)$$

$$W'_{7,1}=W_{7,1}+W_{9,1}+W_{10,1}+W_{20,1} \quad (107)$$

$$W'_{7,2}=W_{7,2}+W_{9,2}+W_{10,2}+W_{20,2} \quad (108)$$

$$W'_{7,4}=W_{7,4}+W_{9,4}+W_{10,4}+W_{20,4} \quad (109)$$

$$W'_{7,5}=W_{7,5}+W_{9,5}+W_{10,5}+W_{20,5} \quad (110)$$

$$W'_{7,7}=W_{7,7}+W_{9,7}+W_{10,7}+W_{20,7} \quad (111)$$

$$W'_{7,8}=W_{7,8}+W_{9,8}+W_{10,8}+W_{20,8} \quad (112)$$

$$W'_{11,1}=W_{11,1}+W_{12,1}+W_{13,1} \quad (113)$$

$$W'_{11,2}=W_{11,2}+W_{12,2}+W_{13,2} \quad (114)$$

$$W'_{11,4}=W_{11,4}+W_{12,4}+W_{13,4} \quad (115)$$

$$W'_{11,5}=W_{11,5}+W_{12,5}+W_{13,5} \quad (116)$$

$$W'_{11,7}=W_{11,7}+W_{12,7}+W_{13,7} \quad (117)$$

$$W'_{11,8}=W_{11,8}+W_{12,8}+W_{13,8} \quad (118)$$

7.4 FORMATION OF THE HAMILTONIAN

7.4.1 General Discussion

In order to utilize Portryagin's minimum principle in the application of optimal control to a plant, it is necessary to construct the Hamiltonian of the plant from the plant's state equations. If the equations describing the plant are decomposed (decoupled), the Hamiltonian is constructed from the terms of the performance index, the right hand side of the state equation and the coordination equation associated with each of the subplants defined by the particular decomposition used.

7.4.2 Hamiltonian Corresponding To Local Vertical Stabilization Control.

$$H = \sum_{i=1}^{20} \sum_{j=i}^{6} p_{i,j} + G(\phi_i^*, \theta_i^*, \psi_i^*, \omega_{ix}^*, \omega_{iy}^*, \omega_{ix}^*)$$

$$i \neq 4,5,14,15,16,17,18,19$$

$$+ \sum_{i=1}^{20} \Big\{ u_{ix}(T_{aix} - T_{aix}^*)^2 + u_{iy}(T_{aiy} - T_{aiy}^*)^2 + u_{iz}(T_{aiz} - T_{aiz}^*)^2$$

$$i \neq 4,5,14,15,16,17,18,19$$

$$+\lambda_{i,1}\hat{S}_{Rix} + \lambda_{i,2}\Big[2(a_{ix,ix,ix}\omega_{ix})_o^1 \omega_{ix}$$

$$+ \frac{(I_i')_{11}}{|I_i'|} T_{aix} + G_{Rix}(T_{eix}, F_{ix}, S_{Rix})\Big]$$

$$+\lambda_{i,3}\hat{S}_{Riy} + \lambda_{i,4}\Big[2(a_{iy,iy,iy}\omega_{iy})_o \omega_{iy}$$

[1] The subscript "o" denotes evaluation at a point of equilibrium.

C-3

$$+\frac{(I_i')_{22}}{|I_i'|}T_{aiy}+G_{Riy}(T_{eiy},F_{iy},S_{Riy})\Big]$$

$$+\lambda_{i,5}\hat{S}_{Riz}+\lambda_{i,6}\Big[2(a_{iz,iz,iz}\omega_{iz})_o\omega_{iz}$$

$$+\frac{(I_i')_{33}}{|I_i'|}T_{aiz}+G_{Riz}(T_{eiz},F_{iz},S_{Riz})\Big]$$

$$+\rho_{i,1}(\omega_{ix}+\theta_i\omega_{iz}-\hat{S}_{Rix})$$

$$+\rho_{i,2}\Big[\omega_i^T A'_{ix,i}\omega_i+\sum_{\substack{j=1\\ j\neq i}}^{20}(\omega_j^T\bar{A}_{ix,j}\omega_j+b_{ix,j}\dot{\omega}_j)$$

$$+\frac{(I_i')_{21}}{|I_i'|}T_{iy}+\frac{(I_i')_{31}}{|I_i'|}T_{iz}+g_{Rix}-S_{Rix}\Big]$$

$$+\rho_{i,3}(\omega_{iy}-\phi_i\omega_{iz}-\hat{S}_{Riy})$$

$$+\rho_{i,4}\Big[\omega_i^T A'_{iy,i}\omega_i+\sum_{\substack{j=1\\ j\neq i}}^{20}(\omega_j^T\bar{A}_{iy,j}\omega_j+b_{iy,j}\dot{\omega}_j)$$

$$+\frac{(I_i')_{12}}{|I_i'|}T_{ix}+\frac{(I_i')_{32}}{|I_i'|}T_{iz}+g_{Riy}-S_{Riy}\Big]$$

$$+\rho_{i,5}(\phi_i\omega_{iy}+\omega_{iz}-\hat{S}_{Riz})$$

$$+\rho_{i,6}\Big[\omega_i^T A'_{iz,i}\omega_i+\sum_{\substack{j=1\\ j\neq i}}^{20}(\omega_j^T\bar{A}_{iy,j}\omega_j+b_{iy,j}\dot{\omega}_j)$$

$$+\frac{(I_i')_{13}}{|I_j'|}T_{ix}+\frac{(I_i')_{23}}{|I_i'|}T_{iy}+g_{Riz}-S_{Riz}\Big]$$

$$+\beta_{i,1}(\phi_i-\phi_i^*)+\beta_{i,2}(\omega_{ix}-\omega_{ix}^*)+\beta_{i,3}(\theta_i-\theta_i^*)$$

$$+\beta_{i,4}(\omega_{iy}-\omega_{iy}^*)+\beta_{i,5}(\psi_i-\psi_i^*)+\beta_{i,6}(\omega_{iz}-\omega_{iz}^*)$$

$$+\nu_{i,1}(T_{aix}-T_{aix}^*)+\nu_{i,2}(T_{aiy}-T_{aiy}^*)+\nu_{i,3}(T_{aiz}-T_{aiz}^*) \qquad (119)$$

where $\beta_{i,j}$ and $\nu_{i,j}$,j = 1,2,...,6 are Lagrange multipliers introduced to ensure satisfaction of the following conditions:

$$\phi_i=\phi_i^* \qquad (120)$$
$$\omega_{ix}=\omega_{ix}^* \qquad (121)$$
$$\theta_i=\theta_{i*} \qquad (122)$$
$$\omega_{iy}=\omega_{iy}^* \qquad (123)$$
$$\psi_i=\psi_i \qquad (124)$$
$$\omega_{iz}=\omega_{iz}^* \qquad (125)$$
$$T_{iax}=T_{iax}^* \qquad (126)$$
$$T_{iay}=T_{iay}^* \qquad (127)$$
$$T_{iaz}=T_{iaz}^* \qquad (128)$$

and $\lambda_{i,j}$, j = 1,2,...,6 are the costate variables

The decoupled rotational state equations, (44) through (49), may be obtained from the following necessary conditions for optimality applied to the Hamiltonian.

$$\dot{\phi}_i=\frac{\partial H}{\partial \lambda_{i,1}} \qquad (129)$$

$$\dot{\omega}_{ix}=\frac{\partial H}{\partial \lambda_{i,2}} \qquad (130)$$

$$\dot{\theta}_i=\frac{\partial H}{\partial \lambda_{i,3}} \qquad (131)$$

$$\dot{\omega}_{iy} = \frac{\partial H}{\partial \lambda}_{i,4} \tag{132}$$

$$\dot{\psi}_i = \frac{\partial H}{\partial \lambda}_{i,5} \tag{133}$$

$$\dot{\omega}_{iz} = \frac{\partial H}{\partial \lambda}_{i,6} \tag{134}$$

The rotational state coordination equations, (50) through (55), may be derived from the application of the following necessary optimality conditions to the Hamiltonian.

$$\frac{\partial H}{\partial \rho}_{i,j} = 0, \quad i=1,2,\ldots,6 \tag{135}$$

7.5 Development of Costate Equations

The rotational costate equations, which are equal in number to the rotational state equations, may be obtained by application of the following necessary conditions for optimality

$$\dot{\lambda}_{i,1} = -\frac{\partial H}{\partial \phi_i} \tag{136}$$

$$\dot{\lambda}_{i,2} = -\frac{\partial H}{\partial \omega_{ix}} \tag{137}$$

$$\dot{\lambda}_{i,3} = -\frac{\partial H}{\partial \theta_i} \tag{138}$$

$$\dot{\lambda}_{i,4} = -\frac{\partial H}{\partial \omega_{iy}} \tag{139}$$

$$\dot{\lambda}_{i,5} = -\frac{\partial H}{\partial \psi_i} \tag{140}$$

$$\dot{\lambda}_{i,6} = -\frac{\partial H}{\partial \omega_{iz}} \tag{141}$$

From equations (70) through (94) and (119) the above listed necessary optimality conditions yield the following:

For i = 1,6,7,11:

$$\dot{\lambda}_{i,1} = -2W'_{i,1}\phi_i + \omega_{iz}\rho_{i,3} - \omega_{iy}\rho_{i,5} - \beta_{i,1} \tag{142}$$

For i = 2,3,8,9,10,12,13,20:

$$\dot{\lambda}_{i,1} = -2W_{i,1}\phi_i + \omega_{iz}\rho_{i,3} - \omega_{iy}\rho_{i,5} - \beta_{i,1} \tag{143}$$

$$\lambda_{i,1}(t_f) = 0 \tag{144}$$

For i = 1,6,7,11:

$$\begin{aligned}\dot{\lambda}_{i,2} = {} & -2W'_{i,2}\omega_{ix} - 2(a_{ix,ix,ix}\omega_{ix})_o\lambda_{i,2} - \rho_{i,1} \\ & -(a_{ix,ix,iy}\omega_{iy} + a_{ix,ix,iz}\omega_{iz})_o\rho_{i,2} \\ & -(2a_{iy,ix,ix}\omega_{ix} + a_{iy,ix,iy}\omega_{iy} + a_{iy,ix,iz}\omega_{iz})_o\rho_{i,4} \\ & -(2a_{iz,ix,ix}\omega_{ix} + a_{iz,ix,iy}\omega_{iy} + a_{iz,ix,iz}\omega_{iz})_o\rho_{i,6} \\ & -\beta_{i,2}\end{aligned} \tag{145}$$

For i = 2,3,8,9,10,12,13,20

$$\dot{\lambda}_{i,2} = -2W_{i,2}\omega_{ix} - 2(a_{ix,ix,ix}\omega_{ix})_o\lambda_{i,2} - \rho_{i,1}$$

$$-(a_{ix,ix,iy}\omega_{iy} + a_{ix,ix,iz}\omega_{iz})_o\rho_{i,2}$$

$$-(2a_{iy,ix,ix}\omega_{ix} + a_{iy,ix,iy}\omega_{iy} + a_{iy,ix,iz}\omega_{iz})_o\rho_{i,4}$$

$$-(2a_{iz,ix,ix}\omega_{ix} + a_{iz,ix,iy}\omega_{iy} + a_{iz,ix,iz}\omega_{iz})_o\rho_{i,6}$$

$$-\beta_{i,2} \qquad (146)$$

$$\lambda_{i,2}(t_f) = 0 \qquad (147)$$

For i = 1,6,7,11:

$$\dot{\lambda}_{i,3} = -2W'_{i,4}\theta_i - \omega_{iz}\rho_{i,1} - \beta_{i,3} \qquad (148)$$

For i = 2,3,8,9,10,12,13,20

$$\dot{\lambda}_{i,3} = -2W_{i,4}\theta_i - \omega_{iz}\rho_{i,1} - \beta_{i,3} \qquad (149)$$

$$\lambda_{i,3}(t_f) = 0 \qquad (150)$$

For i = 1,6,7,11:

$$\ddot{\lambda}_{i,4} = -2W'_{i,5}\omega_{iy} - 2(a_{iy,iy,iy}\omega_{iy})_o\lambda_{i,4}$$

$$-(a_{ix,ix,iy}\omega_{ix} + 2a_{ix,iy,iy}\omega_{iy} + a_{ix,iy,iz}\omega_{iz})_o\rho_{i,2}$$

$$-\rho_{i,3} - (a_{iy,ix,iy}\omega_{ix} + a_{iy,iy,iz}\omega_{iz})_o\rho_{i,4}$$

$$-\phi_i \rho_{i,5} \quad -\beta_{i,4}$$

$$-(a_{iz,ix,iy}\omega_{ix}+2a_{iz,iy,iy}\omega_{iy}+a_{iz,iy,iz}\omega_{iz})_o \rho_{i,6} \tag{151}$$

For i = 2,3,8,9,10,12,13,20:

$$\dot{\lambda}_{i,4} = -2W_{i,5}\omega_{iy} - 2(a_{iy,iy,iy}\omega_{iy})_o \lambda_{i,4}$$

$$-(a_{ix,ix,iy}\omega_{ix}+2a_{ix,iy,iy}\omega_{iy}+a_{ix,iy,iz}\omega_{iz})_c \rho_{i,2}$$

$$-\rho_{i,3} - (a_{iy,ix,iy}\omega_{ix}+a_{iy,iy,iz}\omega_{iz})_o \rho_{i,4}$$

$$-\phi_i \rho_{i,5} - \beta_{i,4}$$

$$-(a_{iz,ix,iy}\omega_{ix}+2a_{iz,iy,iy}\omega_{iy}+a_{iz,iy,iz}\omega_{iz})_o \rho_{i,6} \tag{152}$$

$$\lambda_{i,4}(t_f) = 0 \tag{153}$$

For i = 1,6,7,11:

$$\dot{\lambda}_{i,5} = -2W'_{i,7}\psi_i - \beta_{i,5} \tag{154}$$

For i = 2,3,8,9,10,12,13,20

$$\dot{\lambda}_{i,5} = -2W_{i,7}\psi_i - \beta_{i,5} \tag{155}$$

$$\lambda_{i,5}(t_f) = 0 \tag{156}$$

For i = 1,6,7,11:

$$\dot{\lambda}_{i,6} = -2W'_{i,8}\omega_{iz} - 2(a_{iz,iz,iz}\omega_{iz})_o\lambda_{i,6} - \theta_i\rho_{i,1}$$

$$-(a_{ix,ix,iz}\omega_{ix} + a_{ix,iy,iz}\omega_{iy} + 2a_{ix,iz,iz}\omega_{iz})_o\rho_{i,2}$$

$$+\phi_i\rho_{i,3}$$

$$-(a_{iy,ix,iz}\omega_{ix} + a_{iy,iy,iz}\omega_{iy} + 2a_{iy,iz,iz}\omega_{iz})_o\rho_{i,4}$$

$$-\rho_{i,5} - \beta_{i,6}$$

$$-(a_{iz,ix,iz}\omega_{ix} + a_{iz,iy,iz}\omega_{iy})_o\rho_{i,6} \qquad (157)$$

For i = 2,3,8,9,10,12,13,20:

$$\dot{\lambda}_{i,6} = -2W_{i,8}\omega_{iz} - 2(a_{iz,iz,iz}\omega_{iz})_o\lambda_{i,6} - \theta_i\rho_{i,1}$$

$$-(a_{ix,ix,iz}\omega_{ix} + a_{ix,iy,iz}\omega_{iy} + 2a_{ix,iz,iz}\omega_{iz})_c\rho_{i,2}$$

$$+\phi_i\rho_{i,3}$$

$$-(a_{iy,ix,iz}\omega_{ix} + a_{iy,iy,iz}\omega_{iy} + 2a_{iy,iz,iz}\omega_{iz})_o\rho_{i,4}$$

$$-\rho_{i,5} - \beta_{i,6}$$

$$-(a_{iz,ix,iz}\omega_{ix} + a_{iz,iy,iz}\omega_{iy})_o\rho_{i,6} \qquad (158$$

$$\lambda_{i,6}(t_f) = 0 \qquad (159)$$

The rotational costate coordination equations, which are equal in number to the rotational state coordination equations, may be derived from the following necessary optimality conditions

$$\frac{\partial H}{\partial \hat{S}_{Rix}} = 0 \quad \rightarrow \quad \rho_{i,1} = \lambda_{i,1} \tag{160}$$

$$\frac{\partial H}{\partial S_{Rix}} = 0 \quad \rightarrow \quad \rho_{i,2} = \lambda_{i,2} \tag{161}$$

$$\frac{\partial H}{\partial \hat{S}_{Riy}} = 0 \quad \rightarrow \quad \rho_{i,3} = \lambda_{i,3} \tag{162}$$

$$\frac{\partial H}{\partial S_{Riy}} = 0 \quad \rightarrow \quad \rho_{i,4} = \lambda_{i,4} \tag{163}$$

$$\frac{\partial H}{\partial \hat{S}_{Riz}} = 0 \quad \rightarrow \quad \rho_{i,5} = \lambda_{i,5} \tag{164}$$

$$\frac{\partial H}{\partial S_{Riz}} = 0 \quad \rightarrow \quad \rho_{i,6} = \lambda_{i,6} \tag{165}$$

7.6 DEVELOPMENT OF CONTROL ALGORITHM

The optimal control equations resulting from a gradient approach to the local vertical attitude stabilization control problem yields the following equations:

$$(T_{aix})_{r+1} = (T_{aix})_r - q_{ix} \left(\frac{\partial H}{\partial T_{aix}}\right)_r \tag{166}$$

$$(T_{aiy})_{r+1} = (T_{aiy})_r - q_{iy} \left(\frac{\partial H}{\partial T_{aiy}}\right)_r \tag{167}$$

$$(T_{aiz})_{r+1} = (T_{aiz})_r - q_{iz} \left(\frac{\partial H}{\partial T_{aiz}}\right)_r \tag{168}$$

where r is the iteration index and q_{ix}, q_{iy} and q_{iz} are constants to be chosen on the basis of the rate of approach of the control system to optimal operation.

$$\frac{\partial H}{\partial T_{aix}} = 2\, W_{i,3}\, T_{ix} + 2u_{ix}\,(T_{aix} - T^*_{aix}) + \frac{(I_i')_{11}}{|I_i'|}\ \lambda_{1,2} + \frac{(I_i')_{12}}{|I_i'|}\ \rho_{i,4} + \frac{(I_i')_{13}}{|I_i'|}\ \rho_{i,6} + \nu_{i,1} \tag{169}$$

$$\frac{\partial H}{\partial T_{iay}} = 2W_{i,6}T_{iy} + 2u_{iy}\,(T_{aiy} - T^*_{aiy}) + \frac{(I_i')_{22}}{|I_i'|}\ \lambda_{i,4} + \frac{(I_i')_{21}}{|I_i'|}\ \rho_{i,2} + \frac{(I_i')_{23}}{|I_i'|}\ \rho_{i,6} + \nu_{i,2} \tag{170}$$

$$\frac{\partial H}{\partial T_{iaz}} = 2W_{1,9}T_{iz}+2u_{iz}\,(T_{aiz}-T^*_{aiz}) + \frac{(I_i')_{33}}{|I_i'|}\,\lambda_{i,6}$$

$$+ \frac{(I_i')_{31}}{|I_i'|}\,\rho_{i,2} + \frac{(I_i')_{32}}{|I_i'|}\,\rho_{i,4} + \nu_{i,3} \qquad (171)$$

7.7 ADDITIONAL NECESSARY OPTIMALITY CONDITIONS

$$\frac{\partial H}{\partial \beta_{i,1}} = 0 \rightarrow \phi_i^* = \phi_i \qquad (172)$$

$$\frac{\partial H}{\partial \beta_{i,2}} = 0 \rightarrow \omega_{ix}^* = \omega_{ix} \qquad (173)$$

$$\frac{\partial H}{\partial \beta_{1,3}} = 0 \rightarrow \theta_i^* = \theta_i \qquad (174)$$

$$\frac{\partial H}{\partial \beta_{i,4}} = 0 \rightarrow \omega_{iy}^* = \omega_{iy} \qquad (175)$$

$$\frac{\partial H}{\partial \beta_{i,5}} = 0 \rightarrow \psi_i^* = \psi_i \qquad (176)$$

$$\frac{\partial H}{\partial \beta_{i,6}} = 0 \rightarrow \omega_{iz}^* = \omega_{iz} \qquad (177)$$

$$\frac{\partial H}{\partial \nu_{i,1}} = 0 \rightarrow T_{aix}^* = T_{aix} \qquad (178)$$

$$\frac{\partial H}{\partial \nu_{i,2}} = 0 \rightarrow T^*_{aiy} = T_{aiy} \tag{179}$$

$$\frac{\partial H}{\partial \nu_{i,3}} = 0 \rightarrow T^*_{aiz} = T_{aiz} \tag{180}$$

From $\frac{\partial H}{\partial \phi_{i*}} = 0$: (181)

For i=1,8

$$\beta_{i,1} = 2W_{i,1}\,\phi^*_i + \frac{\partial G}{\partial \phi_i *} \tag{182}$$

For i=2,3,6,7,9,10,11,12,13,20

$$\beta_{i,1} = \frac{\partial G}{\partial \phi_i *} \tag{183}$$

From $\frac{\partial H}{\partial \omega^*_{ix}} = 0$: (184)

For i=1,8

$$\beta_{i,2} = 2W_{i,2}\,\omega^*_{ix} + \frac{\partial G}{\partial \omega^*_{ix}} \tag{185}$$

For i=2,3,6,7,9,10,11,12,13,20

$$\beta_{i,2} = \frac{\partial G}{\partial \omega^*_{ix}} \tag{186}$$

From $\frac{\partial H}{\partial \Theta_i^*} = 0$: (187)

For i=1,8

$$\beta_{i,3} = 2W_{i,4}\,\Theta_i^* + \frac{\partial G}{\partial \Theta_i^*} \tag{188}$$

For i=2,3,6,7,9,10,11,12,13,20

$$\beta_{i,3} = \frac{\partial G}{\partial \Theta_i^*} \tag{189}$$

From $\frac{\partial H}{\partial \omega_{iy}^*} = 0$: (190)

For i=1,8

$$\beta_{i,4} = 2W_{i,5}\,\omega_{iy}^* + \frac{\partial G}{\partial \omega_{iy}^*} \tag{191}$$

For i=2,3,6,7,9,10,11,12,13,20

$$\beta_{i,4} = \frac{\partial G}{\partial \omega_{iy}^*} \tag{192}$$

From $\frac{\partial H}{\partial \psi_i^*} = 0$ (193)

For i=1,8

$$\beta_{i,5} = 2W_{i,7}\,\psi_i^* + \frac{\partial G}{\partial \psi_i^*} \tag{194}$$

For i=2,3,6,7,9,10,11,12,13,20

$$\beta_{i,5} = \frac{\partial G}{\partial \psi_i^*} \tag{195}$$

From $\frac{\partial H}{\partial \omega_{iz}^*} = 0$ (196)

For i=1,8

$$\beta_{i,6} = 2W_{i,8}\ \omega_{iz}^* + \frac{\partial G}{\partial \omega_{iz}^*} \tag{197}$$

For i=2,3,6,7,9,10,11,12,13,20

$$\beta_{i,6} = \frac{\partial G}{\partial \omega_{iz}^*} \tag{198}$$

From $\frac{\partial H}{\partial T_{aix}^*} = 0$: (199)

$$2u_{ix}(T_{aix}^* - T_{aix}) + \frac{(I_i')_{12}}{|I_i'|}\ \rho_{i,4} + \frac{(I_i')_{13}}{|I_i'|}\ \rho_{i,6} = \nu_{i,1} \tag{200}$$

From $\frac{\partial H}{\partial T_{aiy}^*} = 0$: (201)

$$2u_{iy}(T_{aiy}^* - T_{aiy}) + \frac{(I_i')_{21}}{|I_i'|}\ \rho_{i,2} + \frac{(I_i')_{23}}{|I_i'|}\ \rho_{i,6} = \nu_{i,2} \tag{202}$$

From $\frac{\partial H}{\partial T_{aiz}^*} = 0$: (203)

$$2u_{iz}(T_{aiz}^* - T_{aiz}) + \frac{(I_i')_{31}}{|I_i'|}\ \rho_{i,2} + \frac{(I_i')_{32}}{|I_i'|}\ \rho_{i,4} = \nu_{i,3} \tag{204}$$

7.8 CONSTRUCTION OF SUBPROBLEM HIERARCHIES

In order to effect optimal control using multilevel hierarchical techniques selected subsets of the equations presented thus far are assembled into subproblems which, in turn, are assembled into a hierarchical configuration similar in form to that depicted in Figure 7-5. The subproblem hierarchy corresponding to optimal control of the system incorporates two additional classes of subproblems to be solved on the lower level, the costate subproblems and the control subproblems. The addition of the costate subproblems to the lower level of the hierarchy increases the number of coordination equations appearing in the coordination subproblem at the apex of the hierarchy because each of the costate variables has a corresponding costate coordination variable associated with it. To simplify subsequent discussion of this hierarchy all of the subproblems of a particular type will be regarded as being grouped into a single subproblem, that is, all state subproblems into a single state subproblem, all costate subproblems into a single costate subproblem and all control subproblems into a single control problem. Then each subproblem of a particular type will consist of all equations of that type with their associated boundary conditions.

In particular, for optimal local vertical attitude stabilization, the state subproblem consists of equations (44) through (49) which are the decomposed rotational state equations of the Space Construction Base. The decomposed translational state equations, equations (1) through (12) also may be included in this subproblem although they are not essential for the feedback control equations in this case.

The costate subproblem for optimal local vertical attitude stabilization consists of equations (142) through 159) and the control subproblem consists of equations (169) through (171).

In addition to the coordination equations for the decomposed rotational state equations, equations (50) through (55) and the coordination equations for the decomposed translational stable equations, if they are included in the state subproblem, the coordination subproblem at the apex of the hierarchy also includes the costate coordination equations, equations (160) through (165) in order to effect optimal local vertical attitude control.

It should be noted that the costate equations, (142) through (159), incorporate the coordination variables, $\beta_{i,j}$, and the control equations, (169) through (171) incorporate the coordination variables $\nu_{i,1}$, $\nu_{i,2}$ and $\nu_{i,3}$. The additional equations required to define these variables are provided by equations (69), (182) through (19) and equations (200), (202) and (204). These additional equations may be incorporated in the coordination subproblem at the apex of the subproblem hierarchy. This increases the overall dimension of the coordination subproblem to a considerable extent and also greatly increases the number of coordination variables to be transmitted between the subproblems of the hierarchy with control compared with the number required for the hierarchy without control. The resulting subproblem hierarchy for the controlled system is portrayed in Figure 7-7 in which the following relationships are utilized.

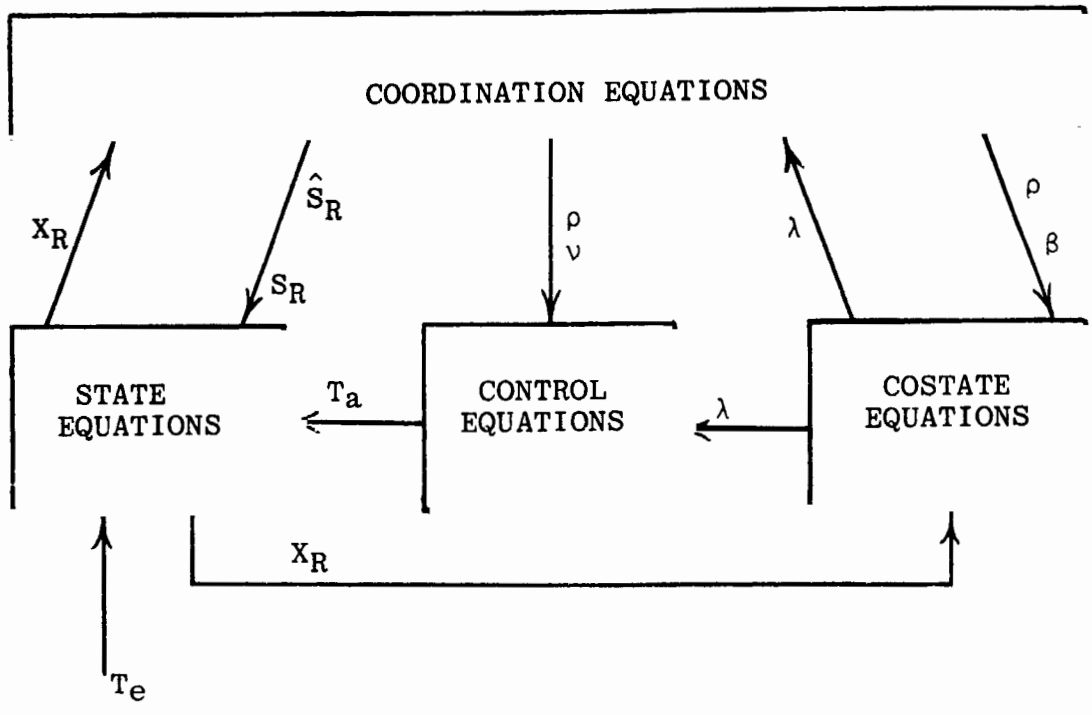

Subproblem Hierarchy For Multilevel Local Vertical Attitude Stabilization Control Without Translational Equations

FIGURE 7-7

$$X_R = (X_{R1}, X_{R2}, \ldots, X_{R20})^T \tag{205}$$

$$X_{Ri} = (\phi_i, \omega_{ix}, \theta_i, \omega_{iy}, \psi_i, \omega_{iz})^T \tag{206}$$

$$\hat{S}_R = (\hat{S}_{R1}, \hat{S}_{R2}, \ldots, \hat{S}_{R20})^T \tag{207}$$

$$\hat{S}_{Ri} = (\hat{S}_{Rix}, \hat{S}_{Riy}, \hat{S}_{Riz})^T \tag{208}$$

$$S_R = (S_{R1}, S_{R2}, \ldots S_{R20})^T \tag{209}$$

$$S_{Ri} = (S_{Rix}, S_{Riy}, S_{Riz})^T \tag{210}$$

$$T_a = (T_{a1}, T_{a2}, \ldots T_{a20})^T \tag{211}$$

$$T_{ai} = (T_{aix}, T_{aiy}, T_{aiz})^T \tag{212}$$

$$\lambda = (\lambda_1, \lambda_2, \ldots \lambda_{20})^T \tag{213}$$

$$\lambda_i = (\lambda_{i,1}, \lambda_{i,2}, \ldots, \lambda_{i,6})^T \tag{214}$$

$$\rho = (\rho_1, \rho_2, \ldots \rho_{20})^T \tag{215}$$

$$\rho_i = (\rho_{i,1}, \rho_{i,2}, \ldots \rho_{i,6})^T \tag{216}$$

$$\beta = (\beta_1, \beta_2, \ldots \beta_{20})^T \tag{217}$$

$$\beta_i = (\beta_{i,1}, \beta_{i,2}, \ldots \beta_{i,6})^T \tag{218}$$

$$\nu = (\nu_1, \nu_2, \ldots \nu_{20})^T \tag{219}$$

$$\nu_j = (\nu_{i,1}, \nu_{i,2}, \nu_{i,3})^T \tag{220}$$

$$T_e = (T_{e1}, T_{e2}, \ldots T_{e20})^T \tag{221}$$

$$T_i = T_{ai} + T_{ei} \tag{222}$$

$$T_{ei} = (T_{eix}, T_{eiy}, T_{eiz})^T \tag{223}$$

It should be noted that T_{ei} represents the external disturbance torque applied to the ith rigid body of the model and T_{ai} represents the control actuator torque applied to the same body.

If the translational state equations, (1) through (12), are added to the state subproblem and the translational coordination equations, (19) through (30), are added to the coordination subproblem of the hierarchy of Figure 7-7, it assumes the form shown in Figure 7-8. For this hierarchy, the following additional relationships are required.

$$X_T = (X_{T1}, X_{T8})^T \tag{224}$$

$$X_{Ti} = (R_{ix}, V_{Tix}, R_{iy}, V_{Tiy}, R_{iz}, V_{Tiz})^T \; ; i=1,8 \tag{225}$$

$$\hat{S}_T = (\hat{S}_{T1}, \hat{S}_{T8})^T \tag{226}$$

$$\hat{S}_{Ti} = (\hat{S}_{Tix}, \hat{S}_{Tiy}, \hat{S}_{Tiz})^T \tag{227}$$

$$S_T = (S_{T1}, S_{T8})^T \tag{228}$$

$$S_{Ti} = (S_{Tix}, S_{Tiy}, S_{Tiz})^T \tag{229}$$

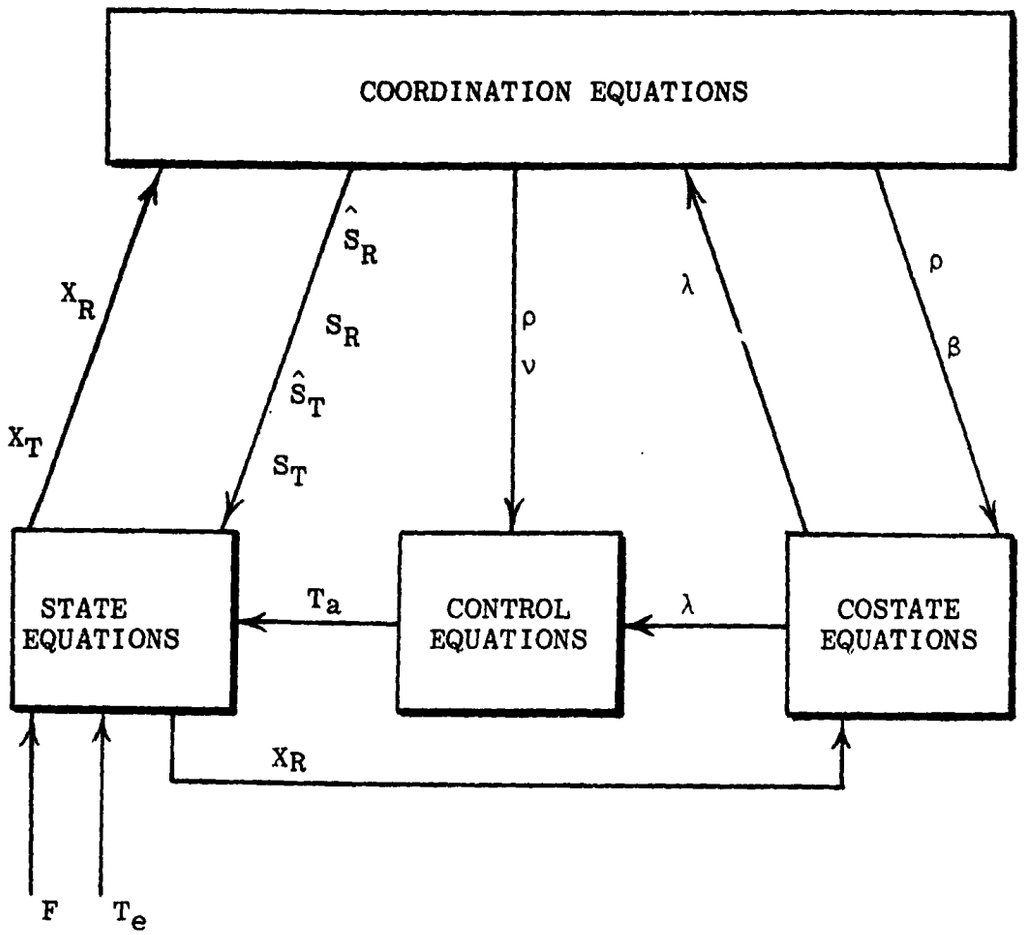

Subproblem Hierarchy for Multilevel
Local Vertical Attitude Stabilization
Control With Translational Equations

FIGURE 7-8

The coordination variables β and ν and their corresponding equations may be eliminated from the subproblem hierarchy shown in Figures 7-7 and 7-8 by expressing each of them in terms of the remaining coordination variables. Each of the resulting modified subproblem hierarchies for the controlled system contains a coordination subproblem of substantially smaller dimension and requires transmission of many fewer coordination variables than do each of the original hierarchies. This approach to the reduction of the subproblem hierarchy consists of several steps.

1. Expansion of the partial derivatives of G appearing in equations (182) through (198) defining $\beta_{i,j}$ by utilizing equation (69) which defines $G(\emptyset_i^*, \omega_{ix}^*, \theta_i^*, \omega_{iy}^*, \psi_i^*, \omega_{iz}^*)$.

2. Substitution of the results of Step 1 in equations (182) through (198).

3. Substitution of the results of step 2 in the costate equations (142) through (159).

4. Substitution of the equations defining $\nu_{i,j}$, (200), (202) and (204) into the control equations, (169) through (171).

The costate and control equations resulting from application of the steps listed above are presented in Appendix C.

Substitution of the equations of Appendix C for the corresponding costate and control equations in the subproblems of the hierarchy depicted in Figure 7-8 leads to construction of the reduced subproblem hierarchy shown in Figure 7-9. The definitions of the variables given in equations (205) through (223), except for the variables that have been eliminated, also apply to the reduced hierarchy.

For the most general Space Construction Base configuration, 12, the range of the rigid body index, i, is given by: i=1,2,3,6,7,8,9,10,11,12,13,20. The range of i is reduced correspondingly for the 11 other configurations. Table 7-3 lists the numbers of scalar state, costate, coordination and control equations to be solved for each configuration in order to effect multilevel local vertical stabilization attitude control utilizing the reduced subproblem hierarchy of Figure 7-9.

Inspection of the state equations, (1)-(12) and (44) through (49) and the costate equations of Appendix C, (C-1) through (C-48), reveals that they are ordinary first order differential equations. In general, initial conditions are known at the outset for the state variables, while final conditions are known for the costate variables. The remaining equations in the subproblem hierarchy, the state coordination equations, (19)-(30) and (50) through (55), the costate coordination equations, (160) through (165) and the control equations, (C-49) through (C-51) are algebraic.

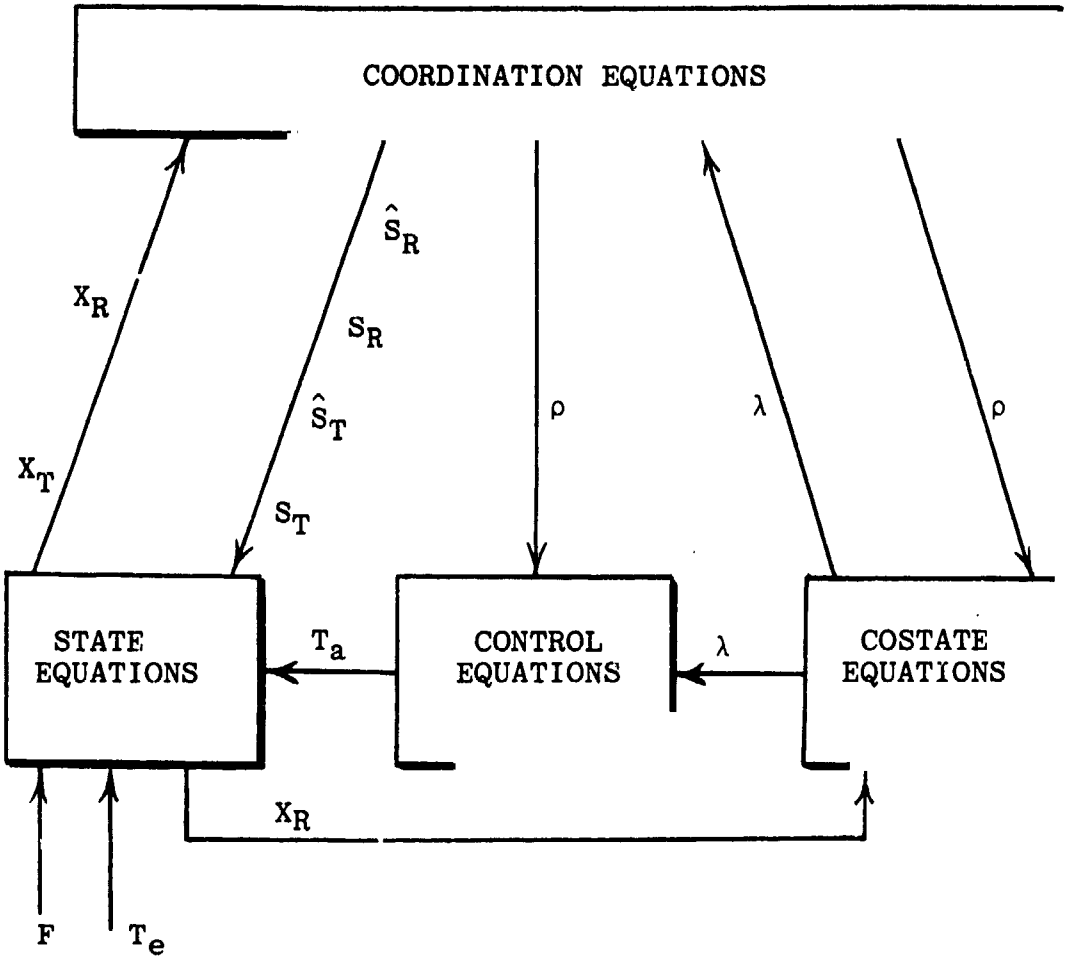

Reduced Subproblem Hierarchy for Multilevel Local Vertical Attitude Stabilization Control With Translational Equations

FIGURE 7-9

TABLE 7-3

Numbers of Scalar Equations To Be Solved For
Local Vertical Attitude Stabilization Control

CONFIGURATION	STATE	CO-STATE	COORDINATION	CONTROL	TOTAL
1	36	24	60	9	129
2	42	30	72	12	156
3	48	36	84	15	183
4	60	48	108	18	234
5	60	48	108	18	234
6	60	48	108	18	234
7	60	48	108	18	234
8	72	60	132	24	288
9	72	60	132	24	288
10	90	66	156	33	345
11	96	72	168	36	372
12	96	72	168	36	372

Due to decomposition, the coupling between the equations associated with the ith rigid body and those associated with the remaining rigid bodies in the mathematical model is suppressed. The state and costate equations associated with the ith body, however, constitute a two-point boundary value (TPBV) problem to be solved because the initial values are known for the state variables and the final values are known for the costate variable at the outset. Such a set of equations usually is discretized temporally to approximate each ordinary differential equation with a set of finite-difference equations that is more amenable to numerical solution on a digital computer. Once this step is taken, all of the equations in the subproblem hierarchy are then algebraic.

7.9 REFERENCES

7-1 Cornell, G. A., "Space Base Mathematical Model", Bendix Research Laboratories Internal Memorandum, December 14, 1977.

7-2 Chichester, F. D., "Application of Multilevel Control to a Single Axis Torsional System", The Bendix Corporation Guidance Systems Division, MT-40,808.

7-3 Porcelli, Giacomo, "Attitude Control of Flexible Space Vehicles", AIAA Journal, Volume 10, No. 6,, June 10, 1972, pp 807-812.

7-4 Hassan, M and M. G. Singh, "The Optimization of Non-Linear Systems Using a New Two Level Method", Automatica, Vol. 12, July 1976, pp 359-363.

7-5 Singh, M. G. and M. Hassan, "A Two Level Prediction Algorithm for Non-Linear Systems", Automatica, Vol. 13, January 1977, pp 95-96.

7-6 Hassan, M. F. and M. G. Singh, "A Two-Level Costate Prediction Algorithm for Non-Linear Systems", Automatica, Vol. 13, November 1977, pp 629-634.

7-7 Singh, M. G. and M. F. Hassan, "Hierarchical Optimization for Non-Linear Dynamical Systems with Non-Separable Cost Functions", Automatica, Vol. 14, January 1978, pp 99-101.

Section 8.0

8.0 Structural Analysis Task - A Method for Determining Overall Flexible Body Characteristics for a Series of Connected Substructures*

8.1 INTRODUCTION

This section summarizes two analytical methods by which a series of flexible bodies can be connected to each other. Both of the techniques presented assume that the flexible body characteristics of the individual sub-bodies comprising the total structure are known in terms of their free-free modes, assuming a discrete coordinate formulation. The first technique assumes that a single connection point exists between two adjacent bodies thus forming a topological tree configuration without any closed loops. This formulation does not require detailed modeling of the dynamics at the connection point and is particularly useful in modeling systems that have large relative angular degrees of freedom between adjacent sub-bodies (i.e., articulated antennas, etc.). The second technique allows multiple connection points between adjacent bodies and hence would also be applicable to a vehicle topological tree configuration having closed loops. In this formulation, detailed modeling of various connection points is required in order to specify the interface forces and torques between contiguous bodies at these points. Both modeling techniques are presented in terms of an illustrative

*Summarized from S. C. Rybak, "A Method For Determining Overall Flexible Body Characteristics For A Series of Connected Substructures," AAS 78-104, March 10-13, 1978.

example of a structure composed of five sub-bodies. With proper parameter values the configuration used can represent vehicles that have already flown (i.e., Saturn, Skylab) for which the characteristics of the overall structure and the individual sub-bodies comprising the structure are known. These data can then be used to determine the fidelity with which each of the two techniques presented models the specific vehicles considered.

8.2 BACKGROUND

To meet the requirements of large orbiting space stations and solar power satellites, NASA is considering a generation of satellites that are many times larger than anything considered or flown to date. Attitude control of such large satellites presents a unique and challenging problem to the control engineer, no doubt requiring the development of new and novel control techniques to achieve overall satisfactory satellite control. However, before control system design can proceed, a model of the vehicle to be controlled must be generated in order to allow the formulation of satisfactory control techniques. It is virtually a certainty that for the size of satellite being considered for a space base or solar power station, structural flexibility and its interaction with the on-board control system will be a prime consideration in its design. Due to the vehicle size overall vibration testing of the total structure in order to obtain its flexibility characteristics is not feasible. Modeling the total vehicle using a normal modal-coordinate approach, although possible, has some serious drawbacks.

although the comments made about the truncation possibility of the technique presented below are plausible, at the present state of development, they are still conjectural and additional work is required to establish their validity.

Equations of motion assuming single and multiple connections between contiguous bodies are presented. Single connection points between bodies do not require the modeling of individual connection points and hence the equations generated will apply equally to a series of connected rigid bodies or rigid bodies connected to flexible bodies. However, the system of equations is restricted to describing a topological tree configuration without any closed loops. The equations developed for multiple connection points between bodies will be applicable to topological tree configurations containing closed loops. However, in the manner in which they are formulated, they would not be applicable to the accommodation of two or more rigid bodies connected to each other within the connection chain.

Equations of motion for single and multiple connections between bodies are developed for a vehicle consisting of five substructures. With proper parameter values the structural configurations used could represent vehicles such as Saturn or Skylab for which detailed structural data are available. The analysis techniques presented can be applied to these data thus determining the degree of modeling fidelity achieved.

8.3 EQUATIONS OF MOTION FOR SINGLE CONNECTION POINT BETWEEN BODIES

Equations of motion were generated for Figure 8-1 shown below. The general procedure that was followed is described in tabular form and the resulting equations are identified. The detailed derivation and accompanying assumptions may be found in the complete paper described in the reference.

Translational Equations of Motion

a) Generate equations describing the sum of forces on each body.
b) Solve for the constraint forces between bodies.

Angular Momentum of Flexible Body

a) Derive the expression for the total angular momentum of the configuration shown in Figure 8-1.

Rotational Equations of Motion

a) Derive the expressions for the rotational equations of motion using the rate of change of angular momentum expressions for each of the five bodies in the figure.
b) Solve for the constraint torques between bodies.
c) Substitute the constraint torque equation expressions in the rate of change of angular momentum expression for body 2 and derive an overall rotational equation of motion for the vehicle system.
d) Express all terms of the overall rotational equation of motion in body 2 coordinates.

$$\dot{\omega}_4 = {}_2T_4{}^T\left[\dot{\omega}_2 + \ddot{\gamma}^2(r_8^2) + \tilde{\omega}_2\dot{\gamma}^2(r_8^2)\right] - \ddot{\gamma}^4(-r_9^4) - \left\{{}_2T_4{}^T\left[\omega_2 + \dot{\gamma}^2(r_8^2)\right]\right\}\tilde{\dot{\gamma}}^4(-r_9^4) \qquad (8\text{-}7)$$

$$\dot{\omega}_5 = {}_2T_5{}^T\left[\dot{\omega}_2 + \ddot{\gamma}^2(r_6^2) + \tilde{\omega}_2\dot{\gamma}^2(r_6^2)\right] - \ddot{\gamma}^5(-r_7^5) - \left\{{}_2T_5{}^T\left[\omega_2 + \dot{\gamma}^2(r_6^2)\right]\right\}\tilde{\dot{\gamma}}^5(-r_7^5) \qquad (8\text{-}8)$$

b) Modal Equation Set

$$\phi_{1e}^{1TN}F_{1e} + \phi_{1e}^{1RN}{}_{1e} + \phi^{1TN}(r_1^1)F_{c12} + \phi^{1RN}(r_1^1)M_{c12} = M_N^1\ddot{q}_N^1 + C_N^1\dot{q}_N^1 + K_N^1 q_N^1 \qquad (8\text{-}9)$$

$$\phi_{2e}^{2TN}F_{2e} + \phi_{2e}^{2RN}T_{2e} - \phi^{2TN}(-r_2^2)F_{c12} + \phi^{2TN}(r_3^2)F_{c23} + \phi^{2TN}(r_8^2)F_{c24} + \phi^{2TN}(r_6^2)F_{c25} - \phi^{2RN}(-r_2^2)M_{c12} + \phi^{2RN}(r_3^2)M_{c23} + \phi^{2RN}(r_8^2)M_{c24} + \phi^{2RN}(r_6^2)M_{c25} = M_N^2\ddot{q}_N^2 + C_N^2\dot{q}_N^2 + K_N^2 q_N^2 \qquad (8\text{-}10)$$

$$\phi_{3e}^{3TN}F_{3e} + \phi_{3e}^{3RN}T_{3e} - \phi^{3TN}(-r_4^3)F_{c23} - \phi^{3RN}(-r_4^3)M_{c23} =$$

$$M_N^{3..3}q_N + C_N^{3.3}q_N + K_N^3 q_N^3 \qquad (8\text{-}11)$$

$$\phi_{4e}^{4TN}F_{4e} + \phi_{4e}^{4RN}T_{4e} - \phi^{4TN}(-r_9^4)F_{c24} - \phi^{4RN}(-r_9^4)M_{c24} =$$

$$M_N^{4..4}q_N + C_N^{4.4}q_N + K_N^4 q_N^4 \qquad (8\text{-}12)$$

$$\phi_{5e}^{5TN}F_{5e} + \phi_{5e}^{5RN}T_{5e} - \phi^{5TN}(-r_7^5)F_{c25} - \phi^{5RN}(-r_7^5)M_{c25} =$$

$$M_N^{5..5}q_N + C_N^{5.5}q_N + K_N^5 q_N^5 \qquad (8\text{-}13)$$

c) Transformation equation set:

$$\mu^j(r_k^j) = \left[\phi^{jTN}(r_k^j)\right]^T q_N^j \qquad (8\text{-}14)$$

$$\gamma^j(r_k^j) = \left[\phi^{jRN}(r_k^j)\right]^T q_N^j \qquad (8\text{-}15)$$

$$\dot{\mu}^j(r_k^j) = \left[\phi^{jTN}(r_k^j)\right]^T \dot{q}_N^j \qquad (8\text{-}16)$$

$$\dot{\gamma}^j(r_k^j) = \left[\phi^{jRN}(r_k^j)\right]^T \dot{q}_N^j \qquad (8\text{-}17)$$

$$\ddot{\mu}^j(r_k^j) = \left[\phi^{jTN}(r_k^j)\right]^T \ddot{q}_N^j \qquad (8\text{-}18)$$

$$\ddot{\gamma}(r_k^j) = \left[\phi^{jRN}(r_k^j)\right]^T \ddot{q}_N^j \qquad (8\text{-}19)$$

d) Overall rotational equation of motion:

$$\sum_{j=1}^{5} {}^2T_j\, T_{je} + \sum_{j=1}^{5} {}^2T_j\, (R_{jj} - \mu_o^j)\tilde{}\, F_{je}$$

$$+ \frac{1}{M_T}\left\{(D_{21}^2 + {}^2T_1\, D_{21}^1)\tilde{}\left[\left(\sum_{j=2}^{5} m_j\right){}^2T_1\, F_{1e} - m_1 \sum_{j=2}^{5} {}^2T_j\, F_{je}\right]\right.$$

$$+(D_{23}^2 + {}^2T_3\, D_{23}^3)\tilde{}\left[\left(\sum_{\substack{j=1\\ j\neq 3}}^{5} m_j\right) {}^2T_3\, F_{3e} - m_3 \sum_{\substack{j=1\\ j\neq 3}}^{5} {}^2T_j\, F_{je}\right]$$

$$+(D_{24}^2 + {}^2T_4\, D_{24}^4)\tilde{}\left[\left(\sum_{\substack{j=1\\ j\neq 4}}^{5} m_j\right){}^2T_4\, F_{4e} - m_4 \sum_{\substack{j=1\\ j\neq 4}}^{5} {}^2T_j\, F_{je}\right]$$

$$+(D_{25}^2 + {}^2T_5\, D_{25}^5)\tilde{}\left[\left(\sum_{j=1}^{4} m_j\right) {}^2T_5\, F_{5e} - m_5 \sum_{j=1}^{4} {}^2T_j\, F_{je}\right] =$$

$$\sum_{j=1}^{5} {}^2T_j \left\{J_j\dot{\omega}_j + \sum_{k=1}^{n} J_k{}^{j*}\dot{\gamma}^j(r_k) + \tilde{\omega}_j J_j \omega_j + \tilde{\omega}_j \sum_{k=1}^{n} J_k{}^{j*}\dot{\gamma}^j(r_k)\right.$$

$$+\sum_{k=1}^{n}\left[\tilde{\dot{\gamma}}^{j}(r_k)J_k^{j*}-J^{j*}\tilde{\dot{\gamma}}^{j}(r_k)\right]\omega_j+\sum_{k=1}^{n}\tilde{\dot{\gamma}}^{j}(r_k)J_k{}^{j*}\dot{\gamma}^{j}(r_k)\Bigg\}$$

$$+\frac{1}{M_T}\left\{m_1\left(\sum_{j=2}^{5}m_j\right)(D_{21}^2+{}_2T_1\,D_{21}^1)-m_1m_3(D_{23}^2+{}_2T_3\,D_{23}^3)\right.$$

$$\left.-m_1m_4(D_{24}^3+{}_2T_4\,D_{24}^4)-m_1m_5(D_{25}^2+{}_2T_5\,D_{25}^5)\right\}^{\sim}\left\{D_{21}^2+\dot{\tilde{\omega}}_2\,D_{21}^2\right.$$

$$\left.+2\tilde{\omega}_2D_{21}^2+\tilde{\omega}_2\tilde{\omega}_2D_{21}^2+{}_2T_1\left[\ddot{D}_{21}^1+\dot{\tilde{\omega}}_1D_{21}^1+2\tilde{\omega}_1\dot{D}_{21}^1+\tilde{\omega}_1\tilde{\omega}_1D_{21}^1\right]\right\}$$

$$+\frac{m_3}{M_T}\left\{-m_1\,(D_{12}^2+{}_2T_1\,D_{12}^1)+\left(\sum_{\substack{j=1\\j\neq3}}^{5}m_j\right)(D_{23}^2+{}_2T_3\,D_{23}^3)-m_4(D_{24}^2+{}_2T_4\,D_{24}^4)\right.$$

$$\left.-m_5(D_{25}^2+{}_2T_5\,D_{25}^5)\right\}^{\sim}\left\{\ddot{D}_{23}^2+\dot{\tilde{\omega}}_2\,D_{23}^2+\tilde{\omega}_2\tilde{\omega}_3D_{23}^2+2\tilde{\omega}_2\,D_{23}^2\right.$$

$$\left.+{}_2T_3\left[\ddot{D}_{23}^2+\dot{\tilde{\omega}}_3\,D_{23}^3+2\tilde{\omega}_3\,\dot{D}_{23}^3+\tilde{\omega}_3\tilde{\omega}_3D_{23}\right]\right\}$$

$$+\frac{m_4}{M_T}\left\{-m_1(D_{21}^2+{}_2T_1D_{21}^1)-m_3(D_{23}^2+{}_2T_3D_{23}^3)+\left(\sum_{\substack{j=1\\j\neq4}}^{5}m_j\right)(D_{24}^2+{}_2T_4D_{24}^4)\right.$$

$$- m_5(D_{25}^2 + {}_2T_5 D_{25}^2)\Big\}^{\sim} \Big\{\ddot{D}_{24}^2 + \dot{\tilde{\omega}}_2 D_{24}^2 + 2\tilde{\omega}_2 \dot{D}_{24}^2 + \tilde{\omega}_2\tilde{\omega}_4 D_{24}^2$$

$$+ {}_2T_4 \left[\ddot{D}_{24}^4 + \dot{\tilde{\omega}}_4 D_{24}^4 + 2\tilde{\omega}_4 \dot{D}_{24}^4 + \tilde{\omega}_4\tilde{\omega}_4 D_{24}^4\right]\Big\}$$

$$+ \frac{m_5}{M_T}\Big\{-m_2(D_{21}^2 + {}_2T_1 D_{21}^1) - m_3(D_{23}^3 + {}_2T_3 D_{23}^3) - m_4(D_{24}^2 + {}_2T_4 D_{24}^4)$$

$$+ \left(\sum_{j=1}^{4} m_j\right)(D_{25}^2 + {}_2T_5 D_{25}^5)\Big\}^{\sim} \Big\{\ddot{D}_{25}^2 + \dot{\tilde{\omega}}_2 D_{25}^2 + 2\tilde{\omega}_2 \dot{D}_{25}^2 + \tilde{\omega}_2\tilde{\omega}_5 D_{25}^2$$

$$+ {}_2T_5 \left[\ddot{D}_{25}^2 + \dot{\tilde{\omega}}_5 D_{25}^5 + 2\tilde{\omega}_5 \dot{D}_{25}^5 + \tilde{\omega}_5\tilde{\omega}_5 D_{25}^5\right]\Big\}$$

$$+ \sum_{j=1}^{5} {}_2T_j \left[\sum_{k=1}^{n} m_k^j \left[r_k^j + \mu^j(r_k)\right]^{\sim} \left[\ddot{\mu}^j(r_k) + \dot{\tilde{\omega}}_j \mu^j(r_k) + 2\tilde{\omega}_j \dot{\mu}^j(r_k)\right.\right.$$

$$- \tilde{\omega}_j\tilde{\omega}_j \mu^j(r_k)\Big] + m_k^j \tilde{\mu}^j(r_k)\left[\dot{\tilde{\omega}}_j r_k^j + \tilde{\omega}_j\tilde{\omega}_j r_k^j\right]\Big\}$$

$$\left. - m_j \tilde{\mu}_o^j\,(\ddot{\mu}_o^j + \dot{\tilde{\omega}}_j \mu_o^j + 2\tilde{\omega}_j \dot{\mu}_o^j + \tilde{\omega}_j\tilde{\omega}_j \mu_o^j)\right] \qquad (8\text{-}20)$$

$$J_k^{j*} = {}_jT_k\, J_k^j\, {}_jT_k^T \qquad (8\text{-}21)$$

e) Modal equations with substitutions for constraint forces and torques.

$$\left[\phi_{1e}^{1RN} - \phi^{1RN}(r_1^1)\right]T_{1e} + \left[\phi_{1e}^{1TN} - \phi^{1RN}(r_1^1)(R_{11} - \mu_o^1)^{\sim}\right]F_{1e}$$

$$+ \frac{1}{M_T}\left[\phi^{1TN}(r_1^1) + \phi^{1RN}(r_1^1)\tilde{D}_{21}^1\right]\left[m_1\sum_{j=2}^{5} {}^1T_j\, F_{je} - \left(\sum_{j=2}^{5} m_j\right)F_{1e}\right] =$$

$$M_N^1\ddot{q}_N^1 + C_N^1\dot{q}_N^1 + K_N^1 q_N^1 + \frac{1}{M_T}\left\{\phi^{1TN}(r_1^1) + \phi^{1RN}(r_1^1)\,\tilde{D}_{21}^1\right\}$$

$$i\left\{m_1\left[-\left(\sum_{j=2}^{5} m_j\right)\ddot{D}_{21} + m_3\ddot{D}_{23} + m_4\ddot{D}_{24} + m_5\ddot{D}_{25}\right]\right\}$$

$$- \phi^{1RN}(r_1^1)\left\{J_1\dot{\omega}_1 + \sum_{k=1}^{n} J_k^{1*}\ddot{\gamma}^1(r_k^1) + \sum_{k=1}^{n}\left[\dot{\gamma}^1(r_k^1)J_k^{1*} - J_k^{1*}\tilde{\dot{\gamma}}^1(r_k^1)\right]\omega_1\right.$$

$$\left. + \sum_{k=1}^{n} \tilde{\dot{\gamma}}^1(r_k^1)J_k^{1*}\dot{\gamma}^1(r_k^1) + \tilde{\omega}_1 J_1\omega_1 + \tilde{\omega}_1\sum_{k=1}^{n} J_1{}^{1*}\dot{\gamma}^1(r_k^1)\right.$$

$$\left. + i\left[\sum_{k=1}^{n} m_k^1\left\{\left[r_k^1 + \mu^1(r_k^1)\right]^{\sim}\ddot{\mu}^1(r_k^1) + \tilde{\mu}^1(r_k^1)\ddot{r}_k^1\right\} - m_1\tilde{\mu}_o^1\ddot{\mu}_o^1\right]\right\}$$

(8-22)

$$\phi_{2e}^{2TN}F_{2e} + \phi_{2e}^{2RN}T_{2e} + \phi^{2RN}(-r_2^2)_2T_1\left[T_{1e} + (R_{11} - \mu_o^1)^{\sim}F_{1e}\right]$$

$$+\phi^{2RN}(r_3^2)_2T_3\left[T_{3e} + (R_{33} - \mu_o^3)^{\sim}F_{3e}\right] + \phi^{2RN}(r_8^2)_2T_4\left[T_{4e}+(R_{44} - \mu_o^4)^{\sim}F_{4e}\right]$$

$$+\phi^{2RN}(r_6^2)_2T_5\left[T_{5e} + (R_{55} - \mu_o^5)^{\sim}F_{5e}\right]$$

$$+ \frac{1}{M_T}\left\{\left[-\phi^{2RN}(-r_2^2)(_2T_1D_{21}^1)^{\sim} - \phi^{2TN}(-r_2^2)\right]\left[m_1\sum_{j=2}^{5}{}_2T_jF_{je} - \left(\sum_{j=2}^{5}m_j\right)_2T_1F_{1e}\right]\right.$$

$$+\left[\phi^{2TN}(r_3^2)+ \phi^{2RN}(r_3^2)(_2T_3D_{23}^3)^{\sim}\right]\left[\left(\sum_{\substack{j=1\\j\neq3}}^{5}m_j\right)_2T_3F_{3e} - m_3\sum_{\substack{j=1\\j\neq3}}^{5}{}_2T_jF_{je}\right]$$

$$+\left[\phi^{2TN}(r_8^2)+ \phi^{2RN}(r_8^2)(_2T_4D_{24}^4)^{\sim}\right]\left[\left(\sum_{\substack{j=1\\j\neq4}}^{5}m_j\right)_2T_4F_{4e} - m_4\sum_{\substack{j=1\\j\neq4}}^{5}{}_2T_jF_{je}\right]$$

$$\left.+\left[\phi^{2TN}(r_6^2)+ \phi^{2RN}(r_6^2)(_2T_5D_{25}^5)^{\sim}\right]\left[\left(\sum_{j=1}^{4}m_j\right)_2T_5F_{5e} - m_5\sum_{j=1}^{4}{}_2T_jF_{je}\right]\right\} =$$

$$M_N^2\ddot{q}_N^2 + C_N^2\dot{q}_N^2 + K_N^2q_N^2$$

$$+ \phi^{2RN}(-r_2^2)_2T_1\left\{J_1\dot{\omega}_1 + \sum_{k=1}^{n} J_k^{1*}\ddot{\gamma}^1(r_k^1) + \tilde{\omega}_1 J_1\omega_1 + \tilde{\omega}_1 \sum_{k=1}^{n} J_k^{1*}\dot{\gamma}^1(r_k^1)\right.$$

$$+ \sum_{k=1}^{n}\left\{\left[\tilde{\dot{\gamma}}^1(r_k^1)\ J_k^{1*} - J_k^{1*}\dot{\gamma}^1(r_k^1)\right]\omega_1 + \tilde{\dot{\gamma}}^1(r_k^1)\ J_k^{1*}\dot{\gamma}^1(r_k^1)\right\}$$

$$+\left[\sum_{k=1}^{n} m_k^1\left\{\left[r_k^1 + \mu^1(r_k^1)\right]^{\sim}\ddot{\mu}^1(r_k^1) + \tilde{\mu}^1(r_k^1)\ddot{r}_k^1\right\} - m_1\ \tilde{\mu}_o^1\ \ddot{\mu}_o^1\right]\Bigg\}$$

$$+ \phi^{2RN}(r_3^2)_2T_3\left\{J_3\dot{\omega}_3 + \sum_{k=1}^{n} J_k^{3*}\ddot{\gamma}^3(r_k^3) + \tilde{\omega}_3 J_3\omega_3 + \tilde{\omega}_3 \sum_{k=1}^{n} J_k^{3*}\dot{\gamma}^3(r_k^3)\right.$$

$$+ \sum_{k=1}^{n}\left\{\left[\tilde{\dot{\gamma}}^3(r_k^3)\ J_k^{3*} - J_k^{3*}\dot{\gamma}^3(r_k^3)\right]\omega_3 + \tilde{\dot{\gamma}}^3(r_k^3) J_k^{3*}\dot{\gamma}^3(r_k^3)\right\}$$

$$+\left[\sum_{k=1}^{n} m_k^3\left\{\left[r_k^3 + \mu^3(r_k^3)\right]^{\sim}\ddot{\mu}^3(r_k^3) + \tilde{\mu}^3(r_k^3)\ddot{r}_k^3\right\} - m_3\ \tilde{\mu}_o^3\ \ddot{\mu}_o^3\right]\Bigg\}$$

$$+ \phi^{2RN}(r_8^2)\ {}_2T_4 \left\{ J_4\dot{\omega}_4 + \sum_{k=1}^{n} J_k^{4*}\ddot{\gamma}^4(r_k^4) + \tilde{\omega}_4 J_4\omega_4 + \tilde{\omega}_4 \sum_{k=1}^{n} J_k^{4*}\dot{\gamma}^4(r_k^4) \right.$$

$$\left. + \sum_{k=1}^{n} \left\{ \left[\tilde{\dot{\gamma}}^4(r_k^4) J_k^{4*} - J_k^{4*}\dot{\gamma}^4(r_k^4) \right] \omega_4 + \tilde{\dot{\gamma}}^4(r_k^4) J_k^{4*}\dot{\gamma}^4(r_k^4) \right\} \right.$$

$$\left. + \left[\sum_{k=1}^{n} m_k^4 \left\{ \left[r_k^4 + \mu^4(r_k^4) \right]^{\sim} \ddot{\mu}^4(r_k^4) + \tilde{\mu}^4(r_k^4)\ddot{r}_k^4 \right\} - m_4 \tilde{\mu}_o^4\ \ddot{\mu}_o^4 \right] \right\}$$

$$+ \phi^{2RN}(r_6^2)\ {}_2T_5 \left\{ J_5\dot{\omega}_5 + \sum_{k=1}^{n} J_k^{5*}\ddot{\gamma}^5(r_k^5) + \tilde{\omega}_5 J_5\omega_5 + \tilde{\omega}_5 \sum_{k=1}^{n} J_k^{5*}\dot{\gamma}^5(r_k^5) \right.$$

$$\left. + \sum_{k=1}^{n} \left\{ \left[\tilde{\dot{\gamma}}^5(r_k^5) J_k^{5*} - J_k^{5*}\dot{\gamma}^5(r_k^5) \right] \omega_5 + \tilde{\dot{\gamma}}^5(r_k^5) J_k^{5*}\dot{\gamma}^5(r_k^5) \right\} \right.$$

$$\left. + \left[\sum_{k=1}^{n} m_k^5 \left\{ \left[r_k^5 + \mu^5(r_k^5) \right]^{\sim} \ddot{\mu}^5(r_k^5) + \tilde{\mu}^5(r_k^5)\ddot{r}_k^5 \right\} - m_5\ \tilde{\mu}_o^5\ \ddot{\mu}_o^5 \right] \right\}$$

$$
\begin{aligned}
&- \frac{m_1}{M_T}\left[\phi^{2RN}(-r_2^2)\left({}_2T_1 D_{21}^1\right)^{\sim} + \phi^{2TN}(-r_2^2)\right]^{i}\left[-\left(\sum_{j=2}^{5} m_j\right)\ddot{D}_{21} + m_3\,\ddot{D}_{23}\right.\\
&\left. + m_2\,\ddot{D}_{24} + m_5\,\ddot{D}_{25}\right]\\
&+ \frac{m_3}{M_T}\left[\phi^{2TN}(r_3^2) + \phi^{2RN}(r_3^2)\left({}_2T_3 D_{23}^3\right)^{\sim}\right]^{i}\left[-m_1\ddot{D}_{21} + \left(\sum_{\substack{j=1\\ j\neq 3}}^{5} m_j\right)\ddot{D}_{23}\right.\\
&\left. - m_4\,\ddot{D}_{24} - m_5\,\ddot{D}_{25}\right]\\
&+ \frac{m_4}{M_T}\left[\phi^{2TN}(r_8^2) + \phi^{2RN}(r_8^2)\left({}_2T_4\, D_{24}^4\right)^{\sim}\right]^{i}\left[-m_1\,\ddot{D}_{21} - m_3\,\ddot{D}_{23}\right.\\
&\left. + \left(\sum_{\substack{j=1\\ j\neq 4}}^{5} m_j\right)\ddot{D}_{24} - m_5\ddot{D}_{25}\right]\\
&+ \frac{m_5}{M_T}\left[\phi^{2TN}(r_6^2) + \phi^{2RN}(r_6^2)\left({}_2T_5\, D_{25}^5\right)^{\sim}\right]^{i}\left[-m_1\,\ddot{D}_{21}\right.\\
&\left. - m_3\,\ddot{D}_{23} - m_4\,\ddot{D}_{24} + \left(\sum_{j=1}^{4} m_j\right)\ddot{D}_{25}\right] \qquad (8\text{-}23)
\end{aligned}
$$

$$\left[\phi_{3e}^{3RN} - \phi^{3RN}(-r_4^3)\right] T_{3e} + \left[\phi_{3e}^{3TN} - \phi^{3RN}(-r_4^3)(R_{33} - \mu_o^3)^{\sim}\right] F_{3e}$$

$$- \frac{1}{M_T}\left[\phi^{3TN}(-r_4^3) + \phi^{3RN}(-r_4^3)\ \tilde{D}_{23}\right]\left[\left(\sum_{\substack{j=1\\ j\neq 3}}^{5} m_j\right) F_{3e} - m_3 \sum_{j=1}^{5} T_j\ F_{je}\right] =$$

$$M_N^3 \ddot{q}_N^3 + C_N^3 \dot{q}_N^3 + K_N^3 q_N^3$$

$$- \phi^{3RN}(-r_4^3)\left\{J_3\dot{\omega}_3 + \sum_{k=1}^{n} J_k^{3*}\ddot{\gamma}^3(r_k^3) + \tilde{\omega}_3 J_3 \omega_3 + \tilde{\omega}_3 \sum_{k=1}^{n} J_k^{3*}\dot{\gamma}^3(r_k^3)\right.$$

$$+ \sum_{k=1}^{n}\left\{\left[\tilde{\dot{\gamma}}^3(r_k^3)\ J_k^{3*} - J_k^{3*}\tilde{\dot{\gamma}}^3(r_k^3)\right]\omega_3 + \tilde{\dot{\gamma}}^3(r_k^3)\ J_k^{3*}\dot{\gamma}^3(r_k^3)\right\}$$

$$+ i\left[\sum_{k=1}^{n} m_k^3\left\{\left[r_k^3 + \mu^3(r_k^3)\right]^{\sim}\ddot{\mu}^3(r_k^3) + \tilde{\mu}^3(r_k^3)\ddot{r}_k^3\right\} - m_3\ \ddot{\mu}_o^3\right]\Bigg\}$$

$$+ \frac{m_3}{M_T}\left[\phi^{3TN}(-r_4^3) + \phi^{3RN}(-r_4^3)\ \tilde{D}_{23}^3\right] i\left[m_i\ddot{D}_{21} - \left(\sum_{j=1}^{5} m_j\right)\ddot{D}_{23}\right.$$

$$\left. + m_4\ \ddot{D}_{24} + m_5\ \ddot{D}_{25}\right] \qquad (8\text{-}24)$$

$$\left[\phi_{4e}^{4RN} - \phi^{4RN}(-r_9^4)\right] T_{4e} + \left[\phi^{4TN} - \phi^{4RN}(-r_9^4)(R_{44} - \mu_o^4)^{\sim}\right] F_{4e}$$

$$- \frac{1}{M_T}\left[\phi^{4TN}(-r_9^4) + \phi^{4RN}(-r_9^4)\,\tilde{D}_{24}^4\right]\left[\left(\sum_{\substack{j=1\\ j\neq 4}}^{5} m_j\right) F_{4e} - m_4 \sum_{\substack{j=1\\ j\neq 4}}^{5} {}^4T_j\, F_{je}\right] =$$

$$M_N^4 \ddot{q}_N^4 + C_N^4 \dot{q}_N^4 + K_N^4 q_N^4$$

$$- \phi^{4TN}(-r_9^4)\left\{ J_4 \dot{\omega}_4 + \sum_{k=1}^{n} J_k^{4*} \ddot{\gamma}^4(r_k^4) + \tilde{\omega}_4 J_4 \omega_4 + \tilde{\omega}_4 \sum_{k=1}^{n} J_k^{4*} \dot{\gamma}^4(r_k^4) \right.$$

$$+ \sum_{k=1}^{n}\left\{\left[\tilde{\dot{\gamma}}^4(r_k^4)\, J_K^{4*} - J_k^{4*}\dot{\gamma}^4(r_k^4)\right]\omega_4 + \tilde{\gamma}^4(r_k^4)\, J_k^{4*}\dot{\gamma}^4(r_k^4)\right\}$$

$$\left. + \left[\sum_{k=1}^{n} m_k^4 \left\{\left[r_k^4 + \mu^4(r_k^4)\right]^{\sim} \ddot{\mu}^4(r_k^4) + \tilde{\mu}^4(r_k^4)\ddot{r}_k^4\right\} - m_4\, \tilde{\mu}_o^4\, \ddot{\mu}_o^4\right]\right\}$$

$$+ \frac{m_4}{M_T}\left[\phi^{4TN}(-r_9^4) + \phi^{4RN}(-r_9^4)\,\tilde{D}_{24}^4\right]\left[m_1 \ddot{D}_{21} + m_3 \ddot{D}_{23}\right.$$

$$\left. - \left(\sum_{j=1}^{5} m_j\right)\ddot{D}_{24} + m_5 \ddot{D}_{25}\right] \qquad (8\text{-}25)$$

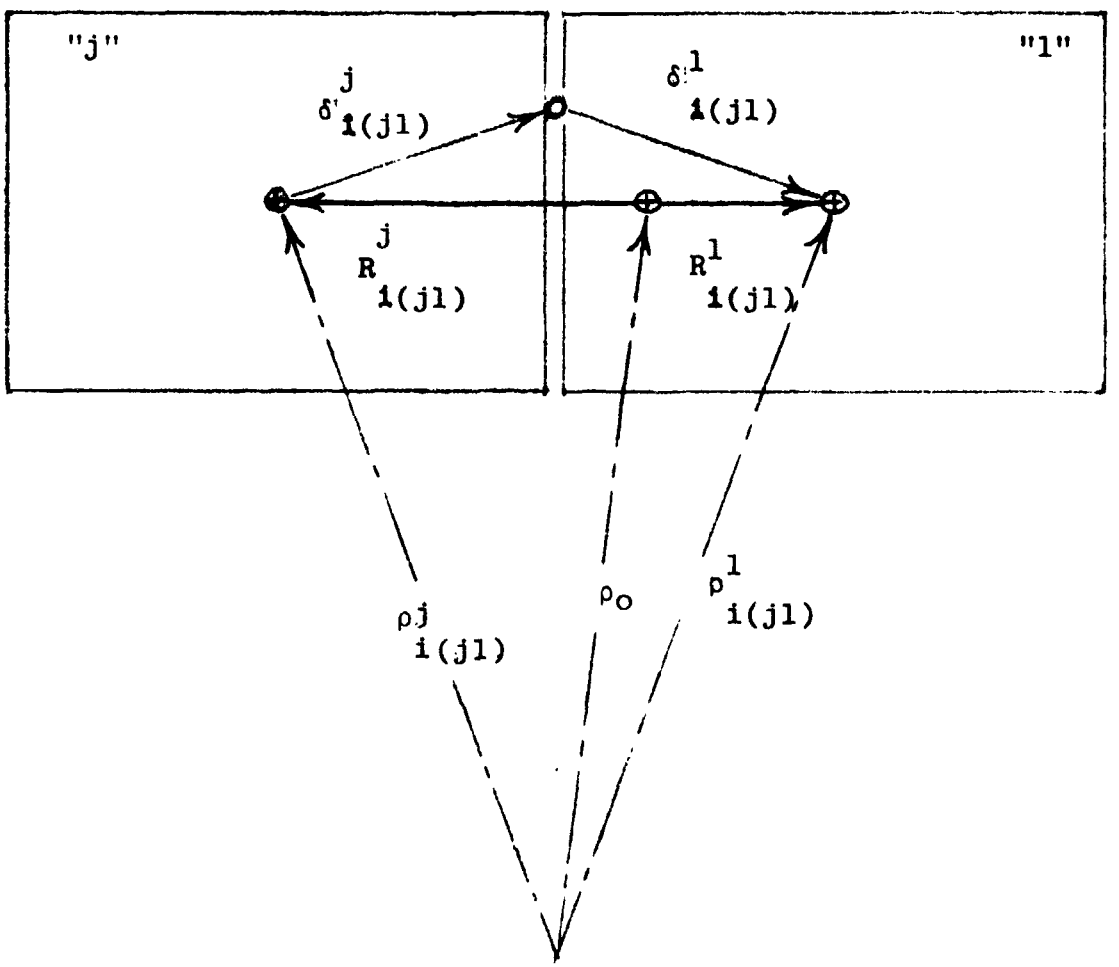

FIGURE 8-2. TYPICAL CONNECTION POINT BETWEEN BODIES "j" AND "1"

The necessary set of equations is:

a. Rate of change of angular momentum for the system.

$$\dot{H}_j = J_j\dot{\omega}_j + \sum_{k=1}^{n} J_k^{j*}\ddot{\gamma}^j(r_k) + \Bigg[\sum_{k=1}^{n}\Bigg\{\dot{\tilde{\gamma}}^j(r_k)\ {}_jT_k\ J_k^j\ {}_jT_k^T - {}_jT_k\ J_k^j\ {}_jT_k^T\ \dot{\tilde{\gamma}}^j(r_k)\Bigg\}\Bigg]\omega_j + \tilde{\omega}_j\Big[J_j\omega_j + \sum_{k=1}^{n} J_j^{j*}\dot{\gamma}^j(r_k)\Big]$$

$$+ \sum_{k=1}^{n}\Big[\dot{\tilde{\gamma}}^j(r_k)\ {}_jT_k\ J_k^j\ {}_jT_k^T\ \dot{\gamma}^j(r_k)\Big] + \Bigg[\sum_{k=1}^{n} m_k^j\Big\{\Big[r_k^j+\mu^j(r_k)\Big]\times\ddot{\mu}^j(r_k) + \mu^j(r_k)\times\ddot{r}_k^j\Big\} - m_j\ \mu_o^j\times\ddot{\mu}^j\Bigg] \qquad (8\text{-}27)$$

b. The transformation equations as defined in (8-14) through (8-19).

c. The interface force equation in "j" rigid body coordinates.

$$F_{i(jl)}|_j = \left(\frac{1}{m_{i(jl)}^j + m_{i(jl)}^l}\right)\Big\{-m_{i(jl)}^j f_i^j(\mu^j;\dot{\mu}^j;\dot{\gamma}^j;\dot{\gamma}^j) + m_{i(jl)}^l\ {}_jT_l f_i^l(\mu^l;\dot{\mu}^l;\gamma^l;\dot{\gamma}^l) - m_{i(jl)}^j m_{i(jl)}^l\Big[\ddot{\gamma}_{i(jl)}^j + \dot{\tilde{\omega}}_j + 2\tilde{\omega}_j\cdot\dot{\tilde{\gamma}}_{i(jl)}^j + \tilde{\omega}_j\tilde{\omega}_j\Big]\ {}_jT_{k(r_i)}\ \Big(\delta_{i(jl)}^j + \delta_{i(jl)}^l\Big)\Big\} \qquad (8\text{-}28)$$

d. Interface torque equation in "j" rigid body coordinates.

$$M_{i(j1)}|_j = \frac{1}{2}\Bigg\{ {}_jT_1 L_i^1(\mu_;^1 \dot{\mu}_;^1 \gamma_;^1 \dot{\gamma}^1) - L_i^j(\mu_;^j \dot{\mu}_;^j \gamma_;^j \dot{\gamma}^j)$$

$$+(J_i^{j*} - J_i^{1*})(\dot{\omega}_j + \ddot{\gamma}^j_{i(j1)}) + \tilde{\omega}_j (J_i^{j*} - J_i^{1*})(\omega_j + \dot{\gamma}^j_{i(j1)})$$

$$\left[\tilde{\dot{\gamma}}^j_{i(j1)}(J_i^{j*} - J_i^{1*}) - (J_i^{j*} - J_i^{1*})\tilde{\dot{\gamma}}^j_{i(j1)}\right] \omega_j + \tilde{\dot{\gamma}}^j_{i(j1)}(J_i^{j*} - J_i^{1*})\dot{\gamma}^j_{i(j1)}$$

$$\left(\frac{1}{m^j_{i(j1)} + m^1_{i(j1)}}\right) \left[T_k(r_i)\ \left(\delta^j_{i(j1)} - \delta^1_{i(j1)}\right)\right]^{\sim}$$

$$\left[m^1_{i(j1)}\ {}_jT_1 f_i^1\ (\mu_;^1 \dot{\mu}_;^1 \gamma_;^1 \dot{\gamma}^1) - m^j_{i(j1)} f_i^j(\mu_;^j \dot{\mu}_;^j \gamma_;^j \dot{\gamma}^j)\right.$$

$$-m^j_{i(j1)} m^1_{i(j1)} \left[\ddot{\gamma}^j_{i(j1)} + \tilde{\dot{\gamma}}^j_{i(j1)} \dot{\gamma}^j_{i(j1)} + \tilde{\dot{\omega}}_j + 2\tilde{\omega}_j \tilde{\dot{\gamma}}^j_{i(j1)} + \tilde{\omega}_j \tilde{\omega}_j\right]$$

$$\left.{}_jT_{k(r_i)}\ \left(\delta^j_{i(j1)} + \delta^1_{i(j1)}\right)\right]\Bigg\} \qquad (8\text{-}29)$$

where:

$$\omega = \omega_j + \dot{\gamma}^j_{i(j1)} \qquad (8\text{-}30)$$

e. System rotational equations of motion.

$$T_{1e}+(R_{11}-\mu_o^1)^{\sim}F_{1e}+\sum_{i=1}^{k}\left\{(r^1_{i(12)}-\mu_o^1+\mu^1_{i(12)}+\tilde{\delta}^1_{i(12)})F_{i(12)}|_1+M_{i(12)}|_1\right\}$$

$$=\frac{{}^{i}dH_1}{dt} \qquad (8\text{-}31)$$

$$T_{2e}+(R_{22}-\mu_o^2)^{\sim}F_{2e}-\sum_{i=1}^{k}\left\{(r^2_{i(12)}-\mu_o^2+\mu^2_{i(12)}+\delta^2_{i(12)})^{\sim}{}_2T_1\ F_{i(12)}|_1\right.$$

$$\left.+{}_2T_1\ M_{1(12)}|_1\right\}+\sum_{i=1}^{k}\left\{(r^2_{i(23)}-\mu_o^2+\mu^2_{i(23)}+\delta_{i(23)})^{\sim}F_{i(23)}|_2+M_{i(23)}|_2\right\}$$

$$+\sum_{i=1}^{k}\left\{(r^2_{i(24)}-\mu_o^2+\mu_{i(24)}+\delta^2_{i(24)})^{\sim}\ F_{i(24)}|_2+M_{i(24)}|_2\right\}$$

$$+\sum_{i=1}^{k}\left\{(r^2_{i(25)}-\mu_o^2+\mu^2_{i(25)}+\delta^2_{i(25)})^{\sim}\ F_{i(25)}|_2+M_{i(25)}|_2\right\}=\frac{{}^{i}dH_2}{dt}$$

(8-32)

$$T_{3e}+(R_{33}-\mu_o^3)^{\sim} F_{3e}-\sum_{i=1}^{k}\left\{(r^3_{i(23)}-\mu_o^3+\mu^3_{i(23)})^{\sim}{}_3T_2\ F_{i(23)}|_2\right.$$

$$\left.+{}_3T_2\ M_{i(23)}|_2\right\} = \frac{{}^{i}dH_3}{dt} \qquad (8\text{-}33)$$

$$T_{4e}+(R_{44}-\mu_o^4)^{\sim} F_{4e}-\sum_{i=1}^{k}\left\{(r^4_{i(24)}-\mu_o^4+\mu^4_{i(24)}-\delta^4_{i(24)})^{\sim}{}_4T_2\ F_{i(24)}|_2\right.$$

$$\left.+{}_4T_2\ M_{i(24)}|_2\right\} = \frac{{}^{i}dH_4}{dt} \qquad (8\text{-}34)$$

$$T_{5e}+(R_{55}-\mu_o^5)^{\sim}F_{5e}-\sum_{i=1}^{k}\left\{(r^5_{i(25)}-\mu_o^5+\mu^5_{i(25)}-\delta^5_{i(25)})_5T_2\ F_{i(25)}|_2\right.$$

$$\left.-\ {}_5T_2\ M_{i(25)}|_2\right\} = \frac{{}^{i}dH_5}{dt} \qquad (8\text{-}35)$$

f. System modal equations.

$$\phi^{1RN}_{1e}\ T_{1e}+\phi^{1TN}_{1e}\ F_{1e}+\sum_{i=1}^{k}\left\{\phi^{1TN}\ (r^1_{i(12)}F_{i(12)}|_1+\phi^{1RN}(r^1_{i(12)})M_{i(12)}|_1\right\}$$

$$= M^1_N\ \ddot{q}^1_N + C^1_N\ \dot{q}^1_N + K^1_N\ q^1_N \qquad (8\text{-}36)$$

$$\phi_{2e}^{2RN}\, T_{2e} + \phi_{2e}^{2TN}\, F_{2e} - \sum_{i=1}^{k} \left\{ \phi^{2TN}(r_{i(12)}^2)_2 T_1\, F_{i(12)}|_1 + {}_2T_1 M_{i(12)}|_1 \right\}$$

$$+ \sum_{i=1}^{k} \left\{ \phi^{2TN}(r_{i(23)}^2) F_{i(23)}|_2 + \phi^{2RN}(r_{i(23)}^2) M_{i(23)}|_2 \right\}$$

$$+ \sum_{i=1}^{k} \left\{ \phi^{2TN}(r_{i(24)}^2) F_{i(24)}|_2 + \phi^{2RN}(r_{i(24)}^2) M_{i(24)}|_2 \right\}$$

$$+ \sum_{i=1}^{k} \left\{ \phi^{2TN}(r_{i(25)}^2 F_{i(25)}|_2 + \phi^{2RN}(r_{i(25)}^2) M_{i(25)}|_2 \right\} =$$

$$M_N^2\, \ddot{q}_N^2 + C_N^2\, \dot{q}_N^2 + K_N^2\, q_N^2 \qquad (8\text{-}37)$$

$$\phi_{3e}^{3RN}\, T_{3e} + \phi_{3e}^{3TN}\, F_{3e} - \sum_{i=1}^{k} \left\{ \phi^{3TN}(r_{i(23)}^3)_3 T_2\, F_{i(23)}|_2 \right.$$

$$\left. + \phi^{3RN}(r_{i(23)}^3)_3 T_2\, M_{i(23)}|_2 \right\} = M_N^3\, \ddot{q}_N^3 + C_N^3\, \dot{q}_N^3 + K_N^3\, q_N^3$$

$$(8\text{-}38)$$

$$\phi_{4e}^{4RN}\ T_{4e}+\phi_{4e}^{4TN}\ F_{4e}-\sum_{i=1}^{k}\left\{\phi^{4TN}(r^4_{i(24)}\ {}_4T_2\ F_{i(24)}|_2\right.$$

$$\left.+\phi^{4TN}(r^4_{i(24)})\ {}_4T_2\ M_{i(24)}|_2\right\}=M_N^4\ \ddot{q}_N^4+C_N^4\ \dot{q}_N^4+K_N^4\ q_N^4 \qquad (8\text{-}39)$$

$$\phi_{5e}^{5RN}\ T_{5e}+\phi_{5e}^{5TN}\ F_{5e}-\sum_{i=1}^{k}\left\{\phi^{5TN}(r^5_{i(25)})\ {}_5T_2\ F_{i(25)}|_2\right.$$

$$\left.+\phi^{5TN}(r^5_{i(25)})\ {}_5T_2\ M_{i(25)}|_2\right\}=M_N^5\ \ddot{q}_N^5+C_N^5\ \dot{q}_N^5+K_N^5\ q_N^5 \qquad (8\text{-}40)$$

8.5 NOMENCLATURE

ρ_j = Vector from inertial point to instantaneous center (C.M.) of body j j - 1,2,...5

ρ_o = Vector from inertial point to instantaneous C.M. of vehicle system

R_j = Vector from center of mass of total vehicle system to the instantaneous C.M. of body j j = 1,2,...5

r_1^1 = Vector from rigid body C.M. of body 1 to C.M. of the connection subelement between bodies 1 and 2 contained in body 1 when it is in an undeformed state

r_2^2 = Vector from the C.M. of the connection subelement between bodies 1 and 2 contained in body 2 to the C.M. of body 2 when it is in an undeformed state

r_3^2 = Vector from the C.M. of body 2 to the C.M. of the connection subelement between bodies 2 and 3 contained in body 2 when in an undeformed state

r_4^3 = Vector from the C.M. of the connection subelement between bodies 2 and 3 contained in body 3 to the C.M. of body 3 when it is in an undeformed state

r_6^2 = Vector from the C.M. of body 2 to the connection subelement between bodies 2 and 5 contained in body 2 when it is in an undeformed state

r_7^5 = Vector from the C.M. of the connection subelement between bodies 2 and 5 contained in body 5 to the C.M. of body 5 when it is in undeformed state

r_8^2 = Vector from the C.M. of body 2 to the C.M. of the connection subelement between bodies 2 and 4 contained in body 2 when it is in an undeformed state

r_9^4 = Vector from the C.M. of the connection subelement between bodies 2 and 4 contained in body 4 to the C.M. of body 4 when it is in its undeformed state

$\mu^j(r_k)$ = Linear deformation of body "j" at the r_k location in body "j" referenced to the C.M. of body "j" when in an undeformed state

μ_o^j = Vector from the C.M. of body j when in an undeformed state to the instantaneous C.M. of body "j"

δ_{jl}^j = Vector from the C.M. of the connection subelement between bodies "j" and "l" contained in body "j" to the actual connection point between the two bodies

$\dot{\gamma}^j(r_k)$ = Angular rate due to deformation of body "j" at location r_k

This rate is expressed in rigid body coordinates of body "j"

m_j = Mass of body j

m_k^j = Mass of k^{th} subelement of body j

j^Tk = Transformation from the k^{th} subelement coordinates to rigid body coordinates (i.e., when body j is undeformed) of body j

$^{j}T_{l}$ = Transformation from rigid body coordinates of body "l" to rigid body coordinates of body "j"

F_{je} = External force applied to body "j"

T_{je} = External torque applied to body "j"

$\phi^{jRN}_{(r_k)}$ = Nx3 matrix of rotational modal gains of body "j" at location r_k

$\phi^{jTN}(r_k)$ = Nx3 matrix of translational modal gains of body "j" at location r_k

M^{j}_{N} = NxN diagonal mass matrix for body "j"

C^{j}_{N} = NxN diagonal damping matrix for body "j"

K^{J}_{N} = NxN diagonal stiffness matrix for body "j"

q^{j}_{N} = N^{th} modal coordinate for body "j"

M_{cjl} = Constraint torque between bodies "j" and "l"

F_{cjl} = Constraint force between bodies "j" and "l"

D_{2j} = Distance from the instantaneous C.M. of body 2 to the instantaneous C.M. of body "j"

ω_k = Inertial rate of subelement k

δ^{j}_{k} = Vector from C.M. of subelement "k" to differential mass located in subelement k

$\rho^{j}_{i(jl)}$ = Distance from inertial point to the C.M. of the connection subelement at the i^{th} connection point between bodies "j" and "l" contained in body "j"

$\rho^{l}_{i(jl)}$ = Distance from inertial point to the C.M. of the connection subelement at the i^{th} connection point between bodies "j" and "l" contained in body "l"

$\delta^{j}_{i(jl)}$ = Distance from C.M. of the connection subelement contained in body "j" at the i^{th} connection point between bodies "j" and "l" to the actual point of connection between the two bodies

$\delta^{l}_{i(jl)}$ = Distance from C.M. of the connection subelement contained in body "l" at the i^{th} connection point between bodies "j" and "l" to the actual point of connection between the two bodies

$R^{j}_{i(jl)}$ = Distance from the composite C.M. of the connection subelements contained in bodies "j" and "l" at the i^{th} connection point to the C.M. of the connection subelement contained in body "j"

$R^{l}_{i(jl)}$ = Distance from the composite C.M. of the connection subelements contained in bodies "j" and "l" at the i^{th} connection point to the C.M. of the connection subelement contained in body "l"

$\mu^{j}_{i(jl)}$ = Linear motion of the C.M. of the connection subelement contained in body "j" at the i^{th} connection point between bodies "j" and "l" due to structural deformation

$\mu^{l}_{i(jl)}$ = Linear motion of the C.M. of the connection subelement contained in body "l" at the i^{th} connection point between bodies "j" and "l" due to structural deformation

$\gamma^{j}_{i(jl)}$ = Angular rotation of the connection subelement contained in body "j" at the i^{th} connection point between bodies "j" and "l" due to structural deformation

$\gamma^{l}_{i(jl)}$ = Angular rotation of the connection subelement contained in body "l" at the i^{th} connection point between bodies "j" and "l" due to structural deformation

$r^{j}_{i(jl)}$ = Location of the C.M. of the connection subelement contained in body "j" at the i^{th} connection point between bodies "j" and "l" with respect to the rigid body C.M. of body "j"

SECTION 9

9.0 CONCLUSIONS AND RECOMMENDATIONS

9.1 INTRODUCTION

A brief summary of conclusions and recommendations are condensed in the following paragraphs.

9.2 MISSION PROFILE

A mission profile, defining module locations and mass properties, was supplied in the RFQ. Operational requirements of the Space Construction Base were non-existent in this data package and certain assumptions were made regarding its operation and performance requirements. These many requirements are tabulated in section 2 and were used as a baseline for subsequent studies described in sections 3 through 8.

9.3 ACTUATOR SIZING

Skylab-type double-gimbal control moment gyro (DG CMG) units are recommended as the primary actuators. When using minimum angular momentum orientations in each configuration, the maximum number of DG CMG's is 24 (see Table 3-12). This is true when the alternate "non-rolling" approach is used for solar pointing the panels during the X local vertical orientation of configuration 12. Figure 3-7 indicates that the minimum average solar power efficiency would be 80.8%, when β = 36.1 degrees.

9.4 MOMENTUM DESATURATION

A momentum management approach is recommended which utilizes magnetic torquing as the primary desaturation system for configurations 1 through 9M, with an RCS system available for backup desaturation during configurations 8M and 9M (see Table 4-5).

In configurations 10M and 11M, the RCS system will take over as the primary desaturation system, and the magnetic torquing system previously available will be usable for assistance. This prevents the addition of extremely heavy supplementary magnetic torquing coils.

For the local vertical oriented configuration 12M, a fixed tilt gravity gradient desaturation approach eliminates the addition of heavier desaturation equipment. The RCS and magnetic torquing systems used during configurations 10M and 11M will then be available for assistance and backup desaturation at this point in the mission.

9.5 CONTROL SYSTEM APPROACH

Review of control system requirements has pinpointed certain features which will require special attention during the remainder of the study. These include: (1) low sensitivity to model uncertainty; (2) adaptability to configuration changes; (3) intermodule statability; and (4) high system integrity with respect to component failures. The functions of: (1) control coordination and (2) intermodule and appendage control require special attention due to their uniqueness in this application.

Study conclusions relative to concept studies are:

1. Much of the control system for the Space Construction Base will consist of elements similar to other satellites. However, there are two parts which are quite different: module and appendage stability control and the vehicle control coordinator.
2. Coupling control should include two modes: artificial stiffening for use during a maneuver and decoupling for use in stabilizing a given attitude.
3. Coupling control should be used selectively based on the payoff in performance improvement and the impact on actuator requirements.
4. Rotary torquers may be used for coupling control actuators - including locations where CMGs may not be used.
5. Artificial damping of structural modes may be difficult to achieve, considering model uncertainty. If this feature is required, it may be necessary to include adaptive notch or bandpass filters in the design in order to achieve significant damping over the range of structural dynamics.
6. Redundant sensors will be required due to the shifting of structural modes during buildup.
7. A vehicle control coordinator will be required to select sensors and adjust control parameters as the configuration changes.

The recommendations are: (1) continuation of this study should place emphasis on the vehicle control coordinator and the appendage and module stabilizing control with particular attention to minimizing sensitivity to modeling errors, and (2) there should be a separate effort to evaluate simple sensors such as strain gages and optical devices for measuring relative angles and angle rates.

9.6 DIGITAL SIMULATION

Two models are being simulated on a digital computer. One is a three dimensional representation of Configuration 1 of the Space Construction Base. The other is a much simpler one dimensional model. Although a hybrid coordinate model may be useful with uncontrolled flexible appendages, it would not be appropriate for coupling control studies. The selected models are satisfactory for the present work.

9.7 MULTILEVEL CONTROL

9.7.1 Results

1. The 12 configurations of the Space Construction Base mathematical model developed by Bendix Research Laboratories have been recast into decomposed state variable forms each of which consists of a set of decoupled scalar first order ordinary differential equations and a set of algebraic equations.

2. The decomposed state variable form of the mathematical model representing each of the configurations of the Space Construction Base without control is comprised of two sets of equations: translational equations and rotational equations.

4. The requirement that each of the state variables be either observable or reconstructed should be investigated with respect to its effect on required computer capacity.

5. Should the required computer capacity be excessive, a new set of models for the 12 configurations of the Space Construction Base may have to be developed. One of the more promising approaches appears to involve the combination of hybrid coordinates with multilevel control techniques.

6. The multilevel control algorithms developed for the decomposed state variable model of the Space Construction Base should be transformed in such a way that they may be applied to the discrete rigid body simulation model at Bendix Research Laboratories.

7. Expansion of the elements of the quadratic coefficient matrices appearing in the coordination equations involves large numbers of terms. More efficient algebraic methods for such expansions need to be developed.

9.8 STRUCTURAL ANALYSIS OF FLEXIBLE BODY CHARACTERISTICS

The flexible body characteristics for a series of interconnected bodies have been modelled in a free-free modal form that permits large angular rotations between contiguous bodies to accommodate large deflections during deployment and operations. The technique applied provides a basis for generation of a more efficient computer program with a higher degree of fidelity than those

presently being used. The unique feature of this technique is that the overall characteristics of a large space vehicle may be determined by combining the measured (or derived) characteristics of the smaller modules of which it is comprised. The method developed also should allow truncation of substructure modes before assembly of the total vehicle model.

Recommendations concerning the developed mathematical model using the above technique are the following:

a. Investigate the validity of truncation of modes.
b. Establish criteria by which satisfactory truncations can be accomplished.
c. Validate the model by applying it to a known space vehicle such as Skylab or Saturn.
d. Continue to develop the model in such a way that the application to any N-body spacecraft will be simple and modular.
e. Develop a general computer program for the model.

Pgs. 9-5, [illegible]

APPENDIX A

DETAILED DESCRIPTION OF N-BODY MODEL

Prepared by: G. A. Cornell
Bendix Research Laboratories
Bendix Center
Southfield, Michigan 48076

December 1977

Internal
Memorandum

Bendix Research Laboratories

Date December 14, 1977 Letter No.

Southfield, Michigan

To K. C. Smith

From G. A. Cornell

Subject Space Base Mathematical Model

ABSTRACT

This memorandum presents a sixty-six degree of freedom mathematical model of the space base incorporating all twelve buildup configurations. A computer simulation of this model is being developed for use in designing and evaluating feasible space base control systems.

1.0 INTRODUCTION

1.1 Background

This memorandum is written under the Bendix Research Laboratories (BRL) tactical program, "Space Base Support," Project 7648, Work Order Number 7318, Simulation Model Development. The memorandum documents the effort accomplished to date in developing a mathematical model of the space base. A computer simulation will be defined from this mathematical model to aid in the development and evaluation of feasible space base control systems.

1.2 Objectives

The objective of the Simulation Model Development effort is to define the equations for a digital computer simulation. The model may be used to examine the stabilization and control of the buildup and assembly phase. A specific objective is to structure the model so as to allow, by appropriate parameter inputs, any of the twelve interim vehicle configurations to be studied. The model must be capable of distributing sensors and actuators about the space base and of including short-term external disturbances such as those caused

by docking. Vehicle flexibility must also be incorporated in the model. For purposes of studying vernier control system one module must be loosely coupled via a six degree of freedom suspension to the remainder of the space base.

1.3 Scope

This memorandum derives the equations of motion of the twelve space base configurations. It is assumed that each configuration consists of a series of rigid bodies connected by a spring hinge suspension. The flexibility of the solar wings are included by this method.

Each Space Base configuration is defined in terms of the number of rigid bodies assumed, the modules contained in each rigid body, and the location of the spring hinges.

The suspension equations are defined and provisions are made for external forces and torques on each body. Actuator forces and torques on each body are also provided but the control system equations are not included as they are yet to be developed.

2.0 NOTATION

The notation used in this memorandum is defined below.

Symbol	Definition
a_{ij}	Elements on the left side of the equations of motion matrix.
b_i	Elements on the right side of the equations of motion matrix.
C_{Sij}	Spring damping coefficient of the suspension torque vector of body j on body i.

Symbol	Definition
F_{ai}	Actuator force vector on body i.
F_{ei}	External force vector on body i
F_i	$F_i = F_{ai} + F_{ei}$
$\dot{h}_i$	Time derivative of the angular momentum vector of body i.
I_i	Inertia tensor of body i.
I_{Xi}, I_{Yi}, I_{Zi}	Moments of inertia of body i.
I_{XYi}, I_{XZi}, I_{YZi}	Products of inertia of body i.
I_{XM}, I_{YM}, I_{ZM}	Moments of inertia of the space base modules.
K_{Sij}	Spring stiffness coefficient of the suspension torque vector of body i on body j.
K_{Sijx}, K_{Sijx}, K_{Sijy}	Components of spring stiffness coefficient.
L	Quantity in the equations of motion that is a function of only m_i, R_{ij}, and $\dot{\omega}_i$.
m_i	Mass of body i.
m_M	Mass of a space base module.
Σm	Total mass of space base.
N	Quantity in the equation of motion that is a function of only m_i, R_{ij} and ω_i.
P_j	Hinge point j.
P_{jx}, P_{jy}, P_{jz}	Coordinates of the j^{th} hinge point with respect to the space base coordinate system.

Symbol	Definition
R_{ai}	Position vector from the center of mass of body i to the point of application of the actuator force.
R_{ei}	Position vector from the center of mass of body i to the point of application of the external force.
$\ddot{R}_i$	Linear acceleration vector of body i with respect to inertial space.
R_{ij}	Position vector of hinge point j with respect to the center of mass of body i.
R_{ijx}, R_{ijy}, R_{ijz}	Components of the R_{ij} position vector in the body i coordinate system.
S_{ij}	Suspension force vector of body j on body i.
T_{ai}	Actuator torque vector on body i.
T_{ei}	External torque vector on body i.
T_i	Moments resulting from the external and actuator forces and moments.
T_{Sij}	Suspension torque vector of body j on body i.
T_{SijM}	Torque motor input.
${}_jT_i$	Coordinate transformation from body i to body j.
x_i, y_i, z_i	Components of the position vector of the composite center of mass of body i measured with respect to the space base coordinate system.

Symbol	Definition
x_M, y_M, z_M	Components of the position vector of the center of mass a space base module measured with respect to the space base coordinate system.
α_{ij}	$\dot{\omega}_i \times R_{ij}$
β_{ij}	$\omega_i \times (\omega_i \times R_{ij})$
$\Delta\omega_{ij}$	Angular velocity vector of body j measured with respect to body i.
$\Delta\omega_{ijx}, \Delta\omega_{ijy}, \Delta\omega_{ijz}$	Components of the vector $\Delta\omega_{ij}$ in the body j coordinate system.
$\Delta\phi_{ij}, \Delta\theta_{ij}, \Delta\psi_{ij}$	Euler angles of body j measured with respect to body i.
$\dot{\Delta}\phi_{ij}, \dot{\Delta}\theta_{ij}, \dot{\Delta}\psi_{ij}$	Euler angle rates of body j with respect to body i.
ϕ_i, θ_i, ψ_i	Euler angles of body i measured with respect to inertial space.
$\dot{\phi}_i, \dot{\theta}_i, \dot{\psi}_i$	Euler angle rates of body i measured with respect to inertial space.
ω_i	Angular rate vector of body i.
$\dot{\omega}_i$	Angular acceleration vector of body i.
$\omega_{ix}, \omega_{iy}, \omega_{iz}$	Components of vector ω_i in body i coordinates.
$\dot{\omega}_{ix}, \dot{\omega}_{iy}, \dot{\omega}_{iz}$	Components of vector $\dot{\omega}_i$ in body i coordinates.

Symbol	Definition
BFMi	Beam Fabrication Module i.
CCM	Construction Control Module i.
DMi	Docking Module i.
ETi	External Tank i.
HMi	Habitability Module i.
KWA	150 KW Solar Wing A
KWB	150 KW Solar Wing B.
KWS	150 KW Subsystem.
LMi	Logistics Module i.
MPi	Manipulator i.
MSM	Mission Support Module.
Pi	Pallet i.
PSP	Public Service Plate.
SMi	Subsystem Module i.
SPM	Space Processing Module.
SWA	Solar Wing A.
SWB	Solar Wing B.
TAi	Turret Assembly i.

3.0 DERIVATION OF EQUATIONS

3.1 General

The Space Base is assumed to be divided up in a group of rigid bodies connected by spring hinge suspensions. It is assembled, starting with the baseline Configuration 1, by adding on additional modules. As other modules are added, a total of twelve configurations are defined. This section defines for each configuration the number of rigid bodies assumed in model derivation, the modules comprising each rigid body, and the location of the spring hinges.

The degrees of freedom are also defined in this section along with derivation of the equations of motion. Coordinate transformations relating vector components to the various body coordinate systems are defined. Euler angle rate and suspension equations are also presented.

A block diagram of the overall mathematical model is shown in Figure 1.

3.2 Description of the Configurations

The Space Base buildup consists of a series of twelve configurations. Each configuration is divided up into a group of rigid bodies. Table 1 lists the number of rigid bodies assumed for each configuration.

Each rigid body is a collection of modules or part of a module. For example, solar wing A is divided into two rigid bodies. Table 2 defines the breakdown of the rigid bodies and modules for each configuration.

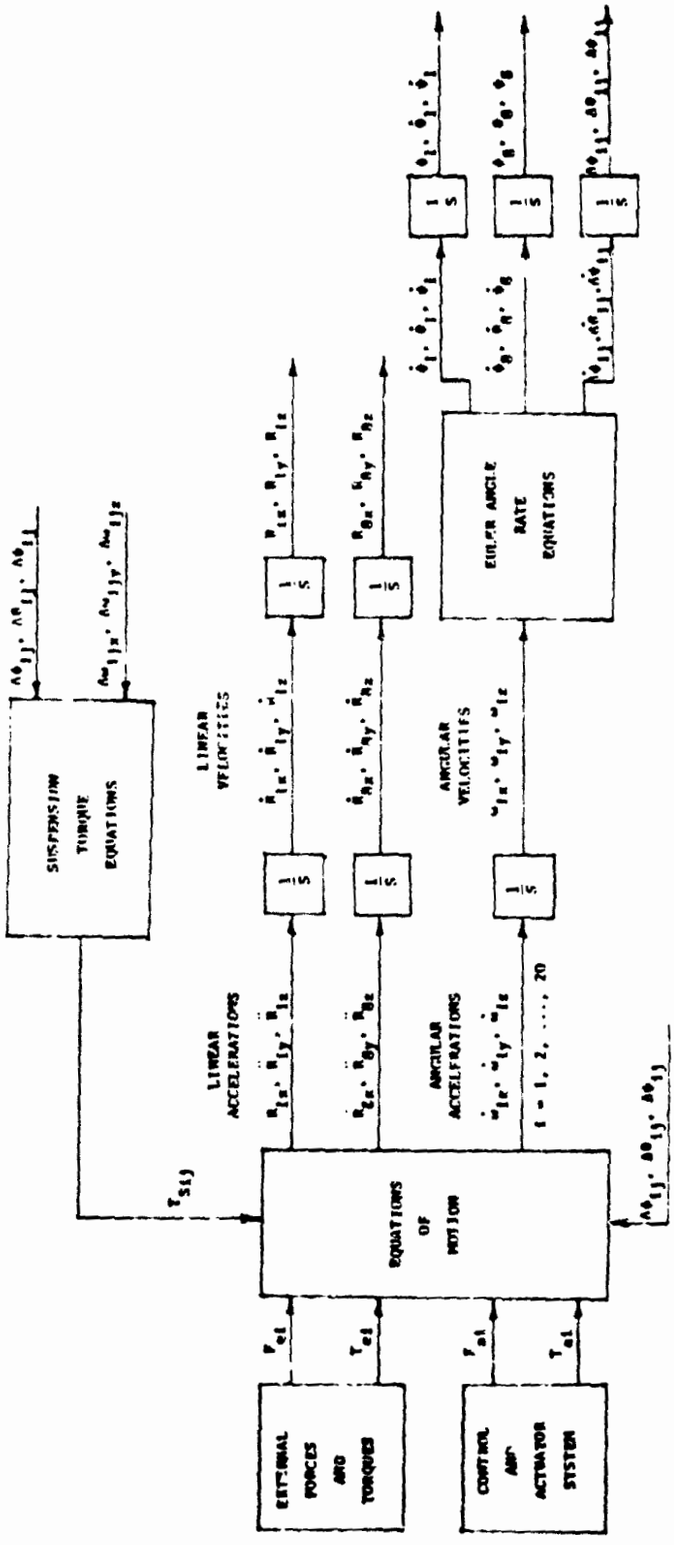

Figure 1 - Overall Mathematical Model of the Space Base

Table 1

Configuration	Number of Rigid Bodies
1	5
2	6
3	7
4	8
5	8
6	8
7	8
8	10
9	10
10	19
11	20
12	20

Figure 2 presents a topological tree that shows how the rigid bodies are connected. A single line drawn between bodies indicates a three degree of freedom spring hinge suspension. A double line indicates a six degree of freedom suspension.

Figure 3 shows a sketch of the space base and locates all of the spring hinges.

3.3 Degrees of Freedom

As shown in Figure 2, a three degree of freedom hinge is assumed between each body except bodies 1 and 8. These two bodies are assumed to be connected by a six degree of freedom suspension. As a result, the total degrees of freedom for each configuration are defined as shown in Table 3.

Table 2 - Breakdown of Space Base Modules and Bodies

Configuration	Rigid Bodies													
	1	264	365	6	7	8	9	10	11	12,14 16,18	13,15 17,19	20		
1	SM1 TA1 HM1 DM1	SMA	SMB	---	---	---	---	---	---	---	---	---		
2	Same +LM1	Same	Same	MSM DM2	---	---	---	---	---	---	---	---		
3	Same	Same	Same	Same	SPM	---	---	---	---	---	---	---		
4	Same +P1	Same	Same	Same	Same	P2	---	---	---	---	---	---		
5	Same	Same	Same	Same +LM2 LM3	Same	Same	---	---	---	---	---	---		
6	Same +SM2 SM3 HM2 HM3	Same	Same	Same	Same	Same	---	---	---	---	---	---		
7	Same	Same	Same	Same	Same +CCM	Same	---	---	---	---	---	---		
8	Same	Same	Same	Same	Same +DM3	Same	DM5 TA3 MT2 ET1	DM4 TA2 MT1	---	---	---	---		
9	Same	Same	Same	Same	Same	Same	Same +RFM1	Same +ET2	---	---	---	---		
10	Same	Same	Same	Same	Same	Same	Same +RFM2	Same	KWS	KWA	KWR	---		
11	Same	Same	Same	Same	Same	Same	Same	Same	Same	Same	Same	LM4		
12	Same	Same	Same	Same	Same	Same	Same (RFM's in diff position)	Same	Same	Same	Same	Same -LM4 +PSP		

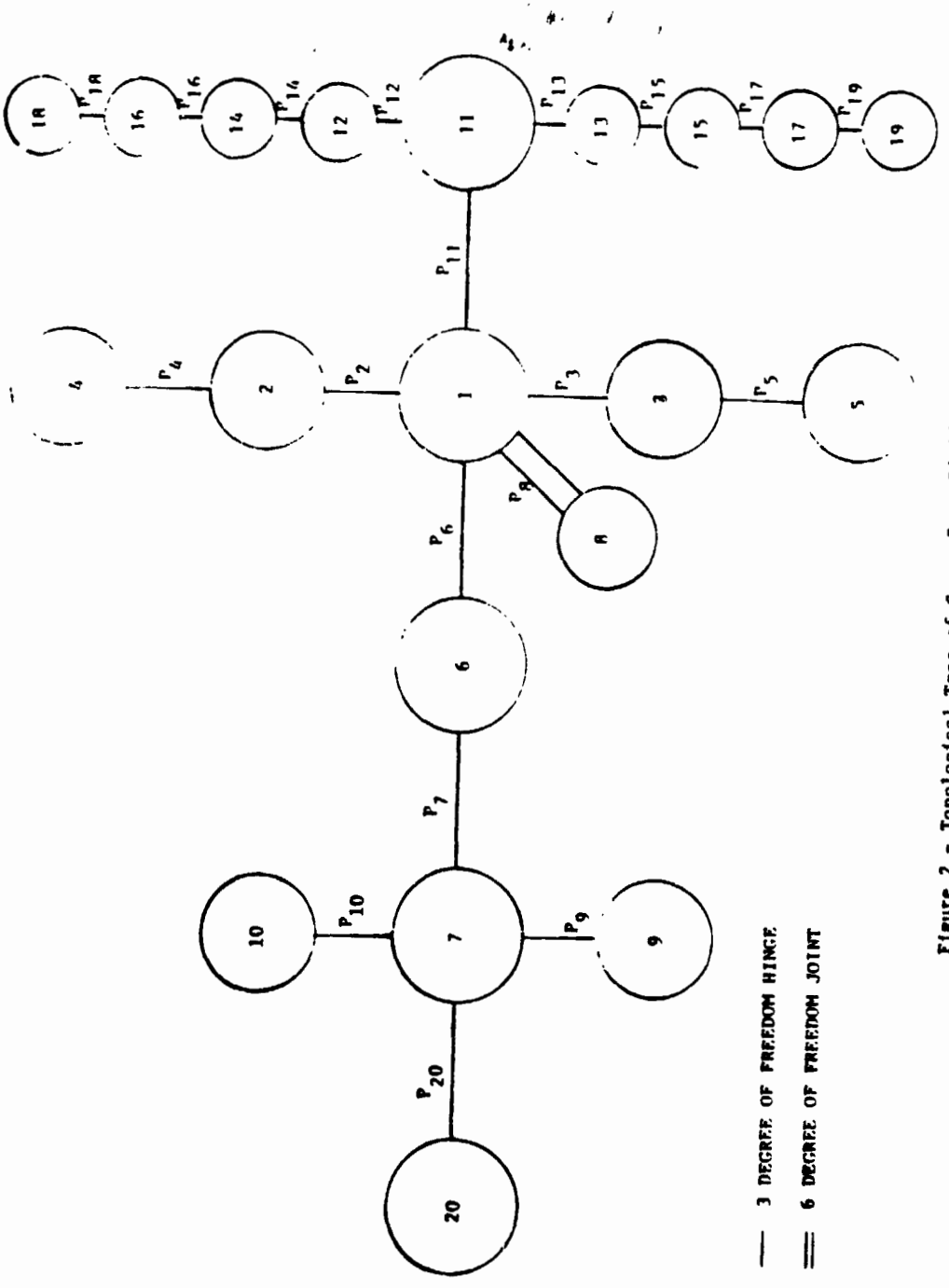

Figure 2 - Topological Tree of Space Base Rigid Bodies

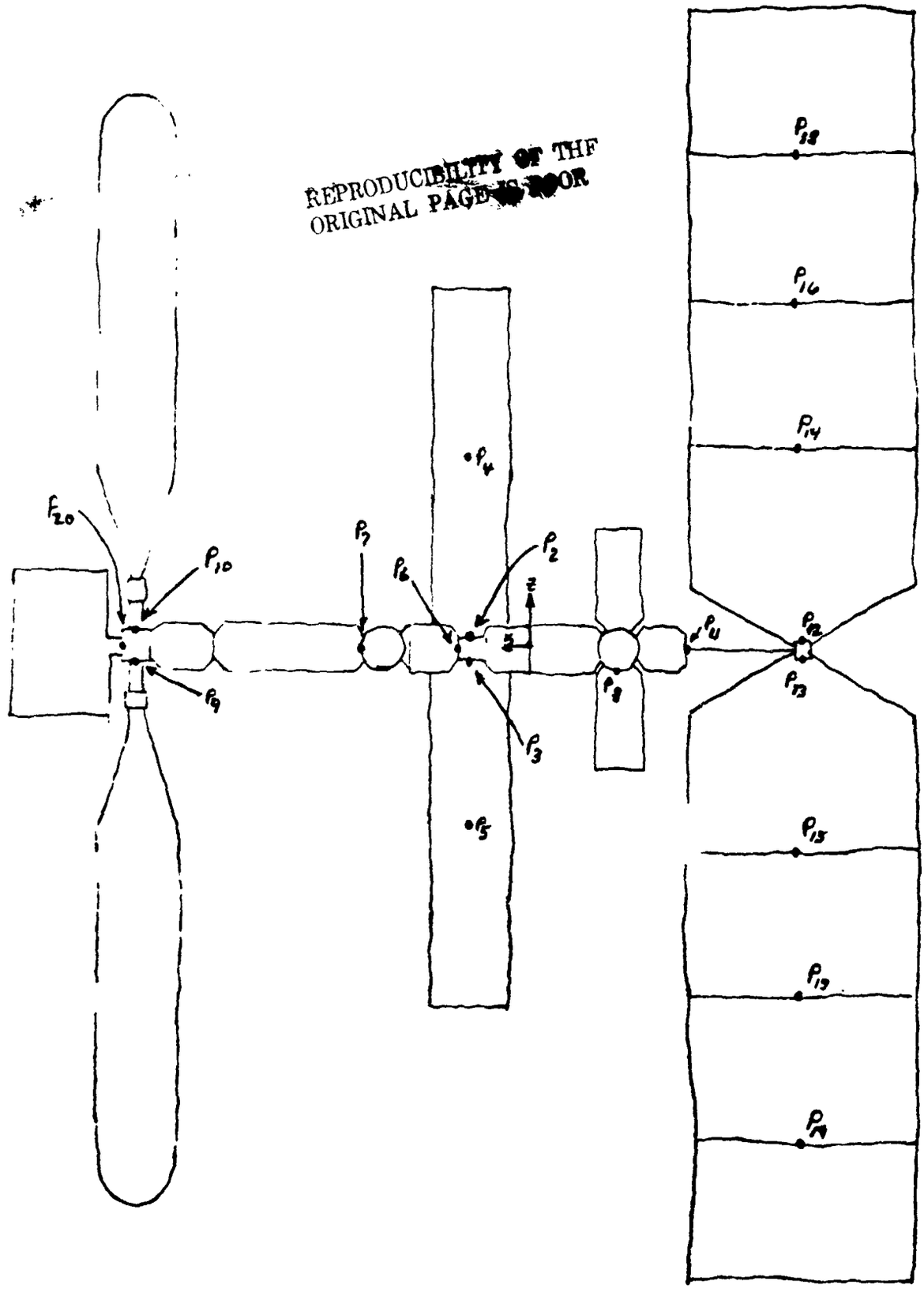

Figure 3 - Location of Hinge Points

Table 3 - Degrees of Freed

Configuration	Degrees of Freedom		
	Translational	Rotational	Total
1	3	15	18
2	3	18	21
3	3	21	24
4	6	24	30
5	6	24	30
6	6	24	30
7	6	24	30
8	6	30	36
9	6	30	36
10	6	57	63
11	6	60	66
12	6	60	66

3.4 Equations of Motion

3.4.1 Translational Equations

The translational equations of motion for each rigid body is derived by equating the mass m_i times the linear acceleration vector $\ddot{R}_i$ to the sum of the force vectors (suspension forces S_{ij} and external F_{ei} and actuator F_{ai} forces; $F_i = F_{ei} + F_{ai}$) acting on the body. Hence,

$$m_1 \ddot{R}_1 = -S_{12} - S_{13} - S_{16} - S_{18} - S_{1,11} + F_1 \quad (1)$$

$$m_2 \ddot{R}_2 = S_{12} - S_{24} + F_2 \quad (2)$$

$$m_3 \ddot{R}_3 = S_{13} - S_{35} + F_3$$

$$m_4 \ddot{R}_4 = S_{24} + F_4 \qquad (3)$$

$$m_5 \ddot{R}_5 = S_{35} + F_5 \qquad (4)$$

$$m_6 \ddot{R}_6 = S_{16} - S_{67} + F_6 \qquad (5)$$

$$m_7 \ddot{R}_7 = S_{67} - S_{79} - S_{7,10} - S_{7,20} + F_7 \qquad (6)$$

$$m_8 \ddot{R}_8 = S_{18} + F_8 \qquad (7)$$

$$m_9 \ddot{R}_9 = S_{79} + F_9 \qquad (8)$$

$$m_{10} \ddot{R}_{10} = S_{7,10} + F_{10} \qquad (9)$$

$$m_{11} \ddot{R}_{11} = S_{1,11} - S_{11,12} - S_{11,13} + F_{11} \qquad (10)$$

$$m_{12} \ddot{R}_{12} = S_{11,12} - S_{12,14} + F_{12} \qquad (11)$$

$$m_{13} \ddot{R}_{13} = S_{11,13} - S_{13,15} + F_{13} \qquad (12)$$

$$m_{14} \ddot{R}_{14} = S_{12,14} - S_{14,16} + F_{14} \qquad (13)$$

$$m_{15} \ddot{R}_{15} = S_{13,15} - S_{15,17} + F_{15} \qquad (14)$$

$$m_{16} \ddot{R}_{16} = S_{14,16} - S_{16,18} + F_{16} \qquad (15)$$

$$m_{17} \ddot{R}_{17} = S_{15,17} - S_{17,19} + F_{17} \qquad (16)$$

(17)

$$m_{18} \ddot{R}_{18} = S_{16,18} + F_{18} \tag{18}$$

$$m_{19} \ddot{R}_{19} = S_{17,19} + F_{19} \tag{19}$$

$$m_{20} \ddot{R}_{20} = S_{7,20} + F_{20} \tag{20}$$

The linear acceleration of body 2 ($\ddot{R}_2$) can be expressed in terms of the linear acceleration of body 1 ($\ddot{R}_1$) and the angular accelerations of body 1 ($\dot{\omega}_1$) and body 2 ($\dot{\omega}_2$), i.e.,

$$\ddot{R}_2 = \ddot{R}_1 + \dot{\omega}_1 \times R_{12} - \dot{\omega}_2 \times R_{22} + \omega_1 \times (\omega_1 \times R_{12}) - \omega_2 \times (\omega_2 \times R_{22}) \tag{21}$$

where R_{ij} is the vector from the center of mass of body i to the j^{th} hinge point. The linear acceleration of the other bodies can be expressed in the same manner.

Summing equations (1) through (20) excluding (8) and substituting equations like (21) yields an expression for $\ddot{R}_1$, i.e.,

$$\ddot{R}_1 = \frac{1}{\Sigma M} [\Sigma F - S_{18} - N - L] - \tag{22}$$

where

$$\Sigma M = \sum_{i=1}^{20} m_i - m_8 \tag{23}$$

$$\Sigma F = \sum_{i=1}^{20} F_i - F_8 \tag{24}$$

Let

$$\alpha_{ij} = \dot{\omega}_i \times R_{ij} \tag{25}$$

and

$$\beta_{ij} = \omega_j \times (\omega_i \times R_{ij}) \tag{26}$$

Then L and N are functions of m_i, α_{ij}, and β_{ij}, i.e.,

$$L = f(m_i, \alpha_{ij}) \tag{27}$$

$$N = f(m_i, \beta_{ij}) \tag{28}$$

As a result, the linear acceleration $\ddot{R}_1$ can be written in terms of m_i, R_{ij}, F_{ei}, F_{ai}, S_{18}, $\dot{\omega}_i$, and ω_i. The quantities m_i and R_{ij} are given constants, F_{ei} is a given external input, F_{ai} is control system output, S_{18} is a suspension force output, ω_i is the integral of $\dot{\omega}_i$, and finally $\dot{\omega}_i$ is determined in the following section which derives the rotational equations of motion.

The suspension forces S_{ij} are needed for the rotational equations of motion. They are given by

$$S_{ij} = f(m_i, F_i, \alpha_{ij}, \beta_{ij}) \tag{29}$$

The linear acceleration of body 8 is given v

$$\ddot{R}_8 = \frac{1}{m_8} [S_{18} + F_8] \tag{30}$$

3.4.2 Rotational Equations

The rotational equations of motion for each rigid body is derived by equating the rate of change of angular momentum to the sum of the moment vectors acting on each body. The rate of change of angular momentum $\dot{h}_i$ is defined by

$$\dot{h}_i = I_i \dot{\omega}_i + \omega_2 \times I_i \omega_i \tag{31}$$

where I_i is the inertia tensor

$$I_i = \begin{pmatrix} I_{Xi} & -I_{XYi} & -I_{XZi} \\ -I_{XYi} & I_{Yi} & -I_{YZi} \\ -I_{XZi} & -I_{YZi} & I_{Zi} \end{pmatrix} \tag{32}$$

Then for each body

$$\dot{h}_1 = -R_{12} \times S_{12} - R_{13} \times S_{13} - R_{1,11} \times S_{1,11} - R_{16} \times S_{16} - R_{18} \times S_{18} - T_{S12} - T_{S13} - T_{S16} - T_{S1,11} - T_{S18} + T_1 \tag{33}$$

$$\dot{h}_2 = R_{22} \times S_{12} - R_{24} \times S_{24} + T_{S12} - T_{S24} + T_2 \tag{34}$$

$$\dot{h}_3 = R_{33} \times S_{13} - R_{35} \times S_{35} + T_{S13} - T_{S35} + T_3 \tag{35}$$

$$\dot{h}_4 = R_{44} \times S_{24} + T_{S24} + T_4 \tag{36}$$

$$\dot{h}_5 = R_{55} \times S_{35} + T_{S35} + T_5 \tag{37}$$

$$\dot{h}_6 = R_{66} \times S_{16} - R_{67} \times S_{67} + T_{S16} - T_{S67} + T_6 \quad (38)$$

$$\dot{h}_7 = R_{77} \times S_{67} - R_{79} \times S_{79} - R_{7,10} \times S_{7,10} - R_{7,20} \times S_{7,20} + T_{S67} - T_{S79} - T_{S7,10} - T_{S7,20} + T_7 \quad (39)$$

$$\dot{h}_8 = R_{88} \times S_{18} + T_{S18} + T_8 \quad (40)$$

$$\dot{h}_9 = R_{99} \times S_{79} + T_{S79} + T_9 \quad (41)$$

$$\dot{h}_{10} = R_{10,10} \times S_{7,10} + T_{S7,10} + T_{10} \quad (42)$$

$$\dot{h}_{11} = R_{11,11} \times S_{1,11} - R_{11,12} \times S_{11,12} - R_{11,13} \times S_{11,13} + T_{S1,11} - T_{S11,12} - T_{S11,13} + T_{11} \quad (43)$$

$$\dot{h}_{12} = R_{12,12} \times S_{11,12} - R_{12,14} \times S_{12,14} + T_{S11,12} - T_{S12,14} + T_{12} \quad (44)$$

$$\dot{h}_{13} = R_{13,13} \times S_{11,13} - R_{13,15} \times S_{13,15} + T_{S11,13} - T_{S13,15} + T_{13} \quad (45)$$

$$\dot{h}_{14} = R_{14,14} \times S_{12,14} - R_{14,16} \times S_{14,16} + T_{S12,14} - T_{S14,16} + T_{14} \quad (46)$$

$$\dot{h}_{15} = R_{15,15} \times S_{13,15} - R_{15,17} \times S_{15,17} + T_{S13,15} - T_{S15,17} + T_{15} \quad (47)$$

$$\dot{h}_{16} = R_{16,16} \times S_{14,16} - R_{16,18} \times S_{16,18} + T_{S14,16} - T_{S16,18} + T_{16} \quad (48)$$

$$\dot{h}_{17} = R_{17,17} \times S_{15,17} - R_{17,19} \times S_{17,19} + T_{S15,17} - T_{S17,19} + T_{17} \quad (49)$$

$$\dot{h}_{18} = R_{18,18} \times S_{16,18} + T_{S16,18} + T_{18} \quad (50)$$

$$\dot{h}_{19} = R_{19,19} \times S_{17,19} + T_{S17,19} + T_{19} \quad (51)$$

$$\dot{h}_{20} = R_{20,20} \times S_{7,20} + T_{S7,20} + T_{20} \quad (52)$$

where T_i are moments resulting from the external and actuator forces and moments, i.e.,

$$T_i = R_{ei} \times F_{ei} + R_{ai} \times F_{ai} + T_{ai} + T_{ei} \quad (53)$$

and where T_{Sij} is the spring hinge torque vector of body j on body i.

These equations can be manipulated into a scalar matrix of the following form:

$$\begin{bmatrix} a_{11} & a_{12} & \cdots & a_{1,57} \\ a_{21} & a_{22} & \cdots & \cdot \\ a_{31} & \cdot & \cdots & \cdot \\ \cdot & \cdot & \cdots & \cdot \\ \cdot & \cdot & \cdots & \cdot \\ \cdot & \cdot & \cdots & \cdot \\ \cdot & \cdot & \cdots & \cdot \\ \cdot & \cdot & \cdots & \cdot \\ \cdot & \cdot & \cdots & \cdot \\ \cdot & \cdot & \cdots & \cdot \\ \cdot & \cdot & \cdots & \cdot \\ \cdot & \cdot & \cdots & \cdot \\ \cdot & \cdot & \cdots & \cdot \\ \cdot & \cdot & \cdots & \cdot \\ a_{57,1} & \cdot & \cdots & a_{57,57} \end{bmatrix} \begin{bmatrix} \dot{\omega}_{1x} \\ \dot{\omega}_{1y} \\ \dot{\omega}_{1z} \\ \cdot \\ \cdot \\ \dot{\omega}_{7x} \\ \dot{\omega}_{7y} \\ \dot{\omega}_{7z} \\ \dot{\omega}_{9x} \\ \dot{\omega}_{9y} \\ \dot{\omega}_{9z} \\ \cdot \\ \dot{\omega}_{20x} \\ \dot{\omega}_{20y} \\ \dot{\omega}_{20z} \end{bmatrix} = \begin{bmatrix} b_1 \\ b_2 \\ b_3 \\ \cdot \\ \cdot \\ \cdot \\ \cdot \\ \cdot \\ \cdot \\ \cdot \\ \cdot \\ \cdot \\ \cdot \\ \cdot \\ b_{57} \end{bmatrix} \qquad (54)$$

where the elements a_{ij} are functions of m_i, R_{ij}, I_{Xi}, I_{Yi}, I_{Zi}, I_{XYi}, I_{XZI}, I_{YZi}, ϕ_i, θ_i, and ψ_i. The quantities ϕ_i, θ_i, and ψ_i are the Euler angles of body i.

The elements b_i are functions of the same quantities as a_{ij} along with F_{ei}, F_{ai}, T_{ei}, T_{ai}, S_{18}, ω_i, T_{Sij}, R_{ai}, and R_{ei}.

Inverting the matrix provides the solution for the components of angular-acceleration ($\dot{\omega}_{ix}$, $\dot{\omega}_{iy}$, $\dot{\omega}_{iz}$) for all the bodies except body 8. The equation for the angular acceleration of body 8 is given by

$$I_8 \dot{\omega}_8 = R_{88} \times S_{18} + T_{S18} + T_8 - \omega_8 \times I_8 \omega_8 \qquad (55)$$

3.5 Transformation of Coordinates

In order to expand the vector equations of motion, derived in the previous section, into scaler equations all the vectors in an equation must be expressed in a common coordinate system. As a result, provisions must be made to transform vector components from one body coordinate system to another. This is accomplished using the notation

$$\begin{bmatrix} \text{Vector Components in Body j Coordinates} \end{bmatrix} = {}_j T_i \begin{bmatrix} \text{Vector Components in Body i Coordinates} \end{bmatrix} \qquad (56)$$

The transformations ${}_4T_2$, ${}_5T_3$, ${}_6T_1$, ${}_8T_1$, ${}_{11}T_1$, ${}_7T_6$, ${}_9T_7$, ${}_{10}T_7$, ${}_{20}T_7$, ${}_{14}T_{12}$, ${}_{15}T_{13}$, ${}_{16}T_{14}$, ${}_{17}T_{15}$, ${}_{18}T_{16}$, and ${}_{19}T_{17}$ are all small angle transformations. Hence, they are defined by

$$j^{T}_{i} = (\Delta\phi_{ij})(\Delta\theta_{ij})(\Delta\psi_{ij}) \tag{57}$$

where

$$(\Delta\phi_{ij}) = \begin{pmatrix} 1 & 0 & 0 \\ 0 & 1 & \Delta\phi_{ij} \\ 0 & -\Delta\phi_{ij} & 1 \end{pmatrix} \tag{58}$$

$$(\Delta\theta_{ij}) = \begin{pmatrix} 1 & 0 & -\Delta\theta_{ij} \\ 0 & 1 & 0 \\ \Delta\theta_{ij} & 0 & 1 \end{pmatrix} \tag{59}$$

$$(\Delta\psi_{ij}) = \begin{pmatrix} 1 & \Delta\psi_{ij} & 0 \\ -\Delta\psi_{ij} & 1 & 0 \\ 0 & 0 & 1 \end{pmatrix} \tag{60}$$

and where $\Delta\psi_{ij}$, $\Delta\theta_{ij}$, and $\Delta\phi_{ij}$ are the Euler angles of body j with respect to body i. Expanding

$$j^{T}_{i} = \begin{pmatrix} 1 & \Delta\psi_{ij} & -\Delta\theta_{ij} \\ -\Delta\psi_{ij} & 1 & \Delta\phi_{ij} \\ \Delta\theta_{ij} & -\Delta\theta_{ij} & 1 \end{pmatrix} \tag{61}$$

For bodies having a large angle articulation a different transformation is required. Hence the transformations ${}_{2}T_{1}$, ${}_{3}T_{1}$, ${}_{12}T_{11}$ and ${}_{13}T_{11}$ are defined by

$$ {}_{j}T_{i} = \begin{pmatrix} \cos \Delta\psi_{ij} & \sin \Delta\psi_{ij} & -\Delta\theta_{ij} \\ -\sin \Delta\psi_{ij} & \cos \Delta\psi_{ij} & \Delta\phi_{ij} \\ \Delta\theta_{ij} \cos \Delta\psi_{ij} + \Delta\phi_{ij} \sin \Delta\psi_{ij} & \Delta\theta_{ij} \sin \Delta\psi_{ij} - \Delta\phi_{ij} \cos \Delta\psi_{ij} & 1 \end{pmatrix} \tag{62} $$

All other transformations can be derived from those defined above.

3.6 Euler Angle Rate Equations

The Euler angle rates ($\dot{\Delta\psi}_{ij}$, $\dot{\Delta\theta}_{ij}$, $\dot{\Delta\phi}_{ij}$) are related to the body angular rates $\Delta\omega_{ij}$ by the vector equation

$$ \Delta\omega_{ij} = (\Delta\phi_{ij})(\Delta\theta_{ij})\, \dot{\Delta\psi}_{ij} + (\Delta\phi_{ij})\, \dot{\Delta\theta}_{ij} + \dot{\Delta\phi}_{ij} \tag{63} $$

Expanding into scalars

$$ \begin{bmatrix} \Delta\omega_{ijx} \\ \Delta\omega_{ijy} \\ \Delta\omega_{ijz} \end{bmatrix} = \begin{pmatrix} 1 & 0 & -\Delta\theta_{ij} \\ 0 & 1 & \Delta\phi_{ij} \\ \Delta\theta_{ij} & -\Delta\phi_{ij} & 1 \end{pmatrix} \begin{bmatrix} 0 \\ 0 \\ \dot{\Delta\psi}_{ij} \end{bmatrix} + \begin{pmatrix} 1 & 0 & 0 \\ 0 & 1 & \Delta\phi_{ij} \\ 0 & -\Delta\phi_{ij} & 1 \end{pmatrix} \begin{bmatrix} 0 \\ \dot{\Delta\theta}_{ij} \\ 0 \end{bmatrix} + \begin{bmatrix} \dot{\Delta\phi}_{ij} \\ 0 \\ 0 \end{bmatrix} \tag{64} $$

Solving for the Euler angle rates yield

$$\dot{\Delta\phi}_{ij} = \Delta\omega_{ijx} + \Delta\theta_{ij}\ \Delta\omega_{ijz} \tag{65}$$

$$\dot{\Delta\theta}_{ij} = \Delta\omega_{ijy} - \Delta\phi_{ij}\ \Delta\omega_{ijz} \tag{66}$$

$$\dot{\Delta\psi}_{ij} = \Delta\phi_{ij}\ \Delta\omega_{ijy} + \Delta\omega_{ijz} \tag{67}$$

where

$$\Delta\omega_{ij} = \omega_j - {}_jT_i\ \omega_i \tag{68}$$

For body 1

$$\dot{\phi}_1 = \omega_{1x} + \theta_1\ \omega_{1z} \tag{69}$$

$$\dot{\theta}_1 = \omega_{1y} - \phi_1\ \omega_{1z} \tag{70}$$

$$\dot{\psi}_1 = \phi_1\ \omega_{1y} + \omega_{1z} \tag{71}$$

3.7 Suspension Equations

The suspension torques T_{Sij} generated by each of the spring hinges are assumed to be linear functions of the Euler angles ($\Delta\psi_{ij}$, $\Delta\theta_{ij}$, $\Delta\phi_{ij}$) and the rates ($\Delta\omega_{ijx}$, $\Delta\omega_{ijy}$, $\Delta\omega_{ijz}$), i.e.,

$$T_{Sijx} = K_{Sijx}\ \Delta\phi_{ij} + C_{Sijx}\ \Delta\omega_{ijx} \tag{72}$$

$$T_{Sijy} = K_{Sijy}\,\Delta\theta_{ij} + C_{Sijy}\,\Delta\omega_{ijy} \tag{73}$$

$$T_{Sijz} = K_{Sijz}\,\Delta\psi_{ij} + C_{Sijz}\,\Delta\omega_{ijz} \tag{74}$$

where K_{Sij} and C_{Sij} are the spring and damping constants.

For the bodies that have large articulation angles about the z axis, the suspension torque is given by a torque motor, i.e.,

$$T_{Sijz} = T_{Sijm} \tag{75}$$

where T_{Sijm} is a torque motor input.

3.8 Equations for Computing the Composite

3.8.1 Composite Masses

The composite masses of the rigid bodies are computed simply by summing the masses m_M of the modules comprising the rigid body, i.e.,

$$m_i = \Sigma\, m_M \tag{76}$$

3.8.2 Inertia Tensor

The elements of the inertia tensor are computed as follows:

$$I_{Xi} = \Sigma\, I_{XM} + \Sigma\, m_M \left[\left(y_M - y_i\right)^2 + \left(z_M - z_i\right)^2\right] \tag{77}$$

$$I_{Yi} = \Sigma\, I_{YM} + \Sigma\, m_M \left[\left(x_M - x_i\right)^2 + \left(z_M - z_i\right)^2\right] \tag{78}$$

$$I_{Zi} = \Sigma\, I_{ZM} + \Sigma\, m_M \left[\left(x_M - x_i\right)^2 + \left(y_M - y_i\right)^2 \right] \tag{79}$$

$$I_{XYi} = \Sigma\, m_M \left(x_M - x_i\right)\left(y_M - y_i\right) \tag{80}$$

$$I_{XZi} = \Sigma\, m_M \left(x_m - x_i\right)\left(z_M - z_i\right) \tag{81}$$

$$I_{YZi} = \Sigma\, m_M \left(y_M - y_i\right)\left(z_M - z_i\right) \tag{82}$$

where x_M, y_M, z_M are the coordinates of the center of mass of module M measured in the space base coordinate system and x_i, y_i, z_i are the coordinates of the composite center of mass of body i measured in the space base coordinates.

3.8.3 Hinge Points

The hinge point components R_{ijx}, R_{ijy}, R_{ijz} locate the hinge points P_j with respect to the center of mass m_i of the composite rigid body. The components are computed by

$$R_{ijx} = P_{jx} - x_i \tag{83}$$

$$R_{ijy} = P_{jy} - y_i \tag{84}$$

$$R_{ijz} = P_{jz} - z_i \tag{85}$$

3.8.4 Composite Center of Mass

The location of the composite center of mass of each body must be computed. The components x_i, y_i, z_i are computed by:

$$x_i = \frac{1}{m_i} \Sigma\, m_M\, x_M \qquad (86)$$

$$y_i = \frac{1}{m_i} \Sigma\, m_M\, y_M \qquad (87)$$

$$z_i = \frac{1}{m_i} \Sigma\, m_M\, z_M \qquad (88)$$

GAC:glp

Distribution:

G. A. Cornell (3)
R. W. Duncan
J. G. Elliott
S. I. Lieberman (2)
D. B. Lipski
A. K. Nakashima
K. C. Smith
N. O. Tiffany
A. B. Van Rennes

J. Jennings (3) - GSD
R. Kaczynski - GSD
D. Zomick - GSD

C. Rybak - BEEI

APPENDIX B

ALTERNATE FREQUENCY DOMAIN DESIGN METHODS FOR THE ATTITUDE CONTROL OF A FLEXIBLE SPACE VEHICLE

Prepared for: Bendix Research Laboratories
Bendix Center
Southfield, Michigan 48076

Prepared by: Dr. Gary Leininger
Engineering Consultant
4546 Vicksburg Drive
Sylvania, Ohio

May 1978

SUMMARY

This interim report describes some preliminary results concerning the application of the Multivariable Nyquist Array method to the design of an attitude control system for a flexible space vehicle. The system used in the study is the lightly damped, three body model developed by Porcelli. With the exception of the open loop model description, the parameters resulting from the MNA design were obtained independent of the Porcelli control configuration. For design comparative purposes, an alternate single loop elimination design was made using root locus and Bode methods.

An initial application of the MNA program to the full order model of the space vehicle suggests a decoupling of the control objectives. This result was confirmed by a CSMP study of the open loop dynamics as well as by physical considerations. Using this result, a reduced order model was developed for the design of the control units for the flexible appendages. Application of the MNA program to the reduced order model clearly indicates a need for phase lead compensation in each control loop. A CSMP simulation of the full order model with the decoupled control system design demonstrates the utility of the MNA design method for flexible space vehicle systems.

Section 1. INTRODUCTION

A recent paper by Porcelli [1] details a multi-loop attitude control system design for a flexible space vehicle using a three body model representation. Using the con ept of mode separability, Porcelli shows that when some of the lightly damped closed loop dynamic modes are contained within the control system bandwidth, sustained oscillations may occur in the flexible appendages during transient operations. To improve the dynamic response, a pair of auxiliary control loops are established to increase the structural damping by active means.

Since the main control loop is designed in accordance with the attitude control specifications, the auxiliary control loops may be designed independently. The design approach proposed by Porcelli initially ignores the flexible connections between the vehicle bodies. Each auxiliary loop design is then based upon the rigid body dynamics of the component body to which it is directly related. Recognizing the conservative aspects of this design approach, the auxiliary loop bandwidth is progressively decreased until an acceptable design is obtained. For the examples in [1], auxiliary loop bandwidths one decade below the bandwidth of the main control loop proved satisfactory.

The Porcelli method is useful when all dynamic modes attributed to the flexible appendages are either within or exterior to the control bandwidth. The examples in [1] demonstrate both cases. Situations may arise, however, where some of the modes associated with the appendages are within the main control bandwidth while other modes are exterior. In this situation, the design approach may not be quite as clear as in the former cases. Here it may be desirable to have an appendage control unit which utilizes sensor

information from each body simultaneously. This is particularly true if physical considerations limit the position and number of appendage control units. Further considerations regarding N-body models may prove to be untractable using the Porcelli method. This would certainly be the case, for example, if the structural modes were highly interactive. Here the flexible members could not be ignored in favor of a rigid body analysis and design, as required by the Porcelli method.

As an alternative to the Porcelli method, a Multivariable Nyquist Array (MNA) design was initiated for the three body models in [1]. One distinctive feature of the MNA method is the utilization of the complete system model at each stage of the design procedure. Any simplifying assumptions in the model order or system characteristics, if any, are based exclusively on physical considerations. Thus, in terms of the satellite model, all flexible appendage modes are retained and accounted for.

The next section develops the mathematical model for the three body system. Section 3 briefly reviews the open loop dynamic conditions from a root locus viewpoint and outlines an alternative classical control design procedure by successive loop reductions. The CSMP runs using the Porcelli control configuration are also presented and compared with the alternate designs. Section 4 describes the MNA design for the lightly damped case.

Section 2. MATHEMATICAL MODEL

The system model for the flexible space vehicle is presented in Figure 1 where all system components represented are considered to be ideal elements.

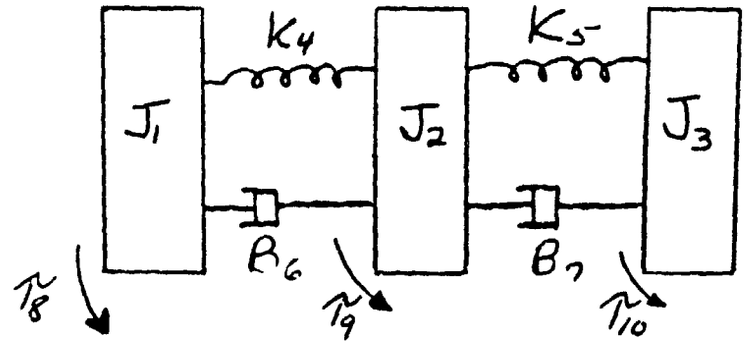

Figure 1: Full Order Model for Attitude Control

The system inputs are represented by torque drivers $\tau_8(t)$, $\tau_9(t)$, and $\tau_{10}(t)$ with $\theta_1(t)$, $\theta_2(t)$, and $\theta_3(t)$ selected as the measurable set of system outputs. Using the systems graph approach, Figure 2, the following set of circuit and cutset equations are obtained:

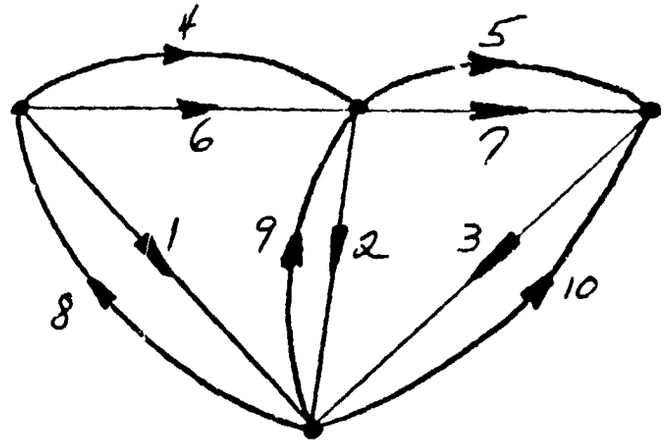

Figure 2: System Graph

Circuit Equations	Cutset Equations
$\dot{\varphi}_8 + \dot{\varphi}_1 = 0$	$\tau_1 + \tau_4 + \tau_6 - \tau_8 = 0$
$\dot{\varphi}_9 + \dot{\varphi}_2 = 0$	$\tau_2 + \tau_5 + \tau_7 - \tau_9 - \tau_4 - \tau_6 = 0$
$\dot{\varphi}_{10} + \dot{\varphi}_3 = 0$	$\tau_3 - \tau_5 - \tau_7 - \tau_{10} = 0$
$\dot{\varphi}_4 + \dot{\varphi}_2 - \dot{\varphi}_1 = 0$	(1)
$\dot{\varphi}_5 + \dot{\varphi}_3 - \dot{\varphi}_2 = 0$	
$\dot{\varphi}_6 + \dot{\varphi}_2 - \dot{\varphi}_1 = 0$	
$\dot{\varphi}_7 + \dot{\varphi}_3 - \dot{\varphi}_2 = 0$	

The component equations corresponding to Figure 1 are:

$$J_i \frac{d\theta_i}{dt} = \tau_i \qquad i = 1, 2, 3. \tag{2}$$

$$\frac{d\tau_i}{dt} = K_i \dot{\theta}_i \qquad i = 4, 5 \tag{3}$$

$$\tau_i = B_i \dot{\theta}_i \qquad i = 6, 7 \tag{4}$$

$$\tau_i \text{ - drivers} \qquad i = 8, 9, 10 \tag{5}$$

Selecting the state variables as $\dot{\theta}_1$, $\dot{\theta}_2$, $\dot{\theta}_3$, τ_4, τ_5 and θ_1, the following state equations are obtained

$$\frac{d\dot{\theta}_1}{dt} = \frac{\tau_1}{J_1} = \frac{1}{J_1}[\tau_8 - \tau_4 - \tau_6] = \frac{1}{J_1}[\tau_8 - \tau_4 - B_6(\dot{\varphi}_1 - \dot{\varphi}_2)]$$

$$\frac{d\dot{\varphi}_2}{dt} = \frac{\tau_2}{J_2} = \frac{1}{J_2}[\tau_9 + \tau_4 + \tau_6 - \tau_5 - \tau_7]$$

$$= \frac{1}{J_2}[\tau_9 + \tau_4 - \tau_5 + B_6(\dot{\theta}_1 - \dot{\varphi}_2) - B_7(\dot{\theta}_2 - \dot{\theta}_3)] \tag{6}$$

$$\frac{d\dot{\theta}_3}{dt} = \frac{\tau_3}{J_3} = \frac{1}{J_3}[\tau_{10} + \tau_5 + \tau_7] = \frac{1}{J_3}[\tau_{10} + \tau_5 + B_7(\dot{\theta}_2 - \dot{\theta}_3)]$$

$$\frac{d\tau_4}{dt} = K_4 (\dot{\theta}_1 - \dot{\theta}_2)$$

$$\frac{d\tau_5}{dt} = K_5 (\dot{\theta}_2 - \dot{\theta}_3)$$

$$\frac{d\theta_1}{dt} = \dot{\theta}_1$$

with output equations

$$\begin{aligned} \theta_1 &= \theta_1 \\ \theta_2 &= \theta_1 - \frac{\tau_4}{K_4} \\ \theta_3 &= \theta_1 - \frac{\tau_4}{K_4} - \frac{\tau_5}{K_5} \end{aligned} \tag{7}$$

In vector form the above equations become

$$\dot{x} = Ax + Bu \tag{8}$$

$$y = Cx \tag{9}$$

where

$$A = \begin{bmatrix} -\frac{B_6}{J_1} & \frac{B_6}{J_1} & 0 & -\frac{1}{J_1} & 0 & 0 \\ \frac{B_6}{J_2} & -\left(\frac{B_5+B_7}{J_2}\right) & \frac{B_7}{J_2} & \frac{1}{J_2} & -\frac{1}{J_2} & \\ 0 & \frac{B_7}{J_3} & -\frac{B_7}{J_3} & 0 & \frac{1}{J_3} & 0 \\ K_4 & -K_4 & 0 & 0 & 0 & 0 \\ 0 & K_5 & -K_5 & 0 & 0 & 0 \\ 1 & 0 & 0 & 0 & 0 & 0 \end{bmatrix} \tag{10}$$

$$B = \begin{bmatrix} \frac{1}{J_1} & 0 & 0 \\ 0 & \frac{1}{J_2} & 0 \\ 0 & 0 & \frac{1}{J_3} \\ 0 & 0 & 0 \\ 0 & 0 & 0 \\ 0 & 0 & 0 \end{bmatrix} \tag{11}$$

$$C = \begin{bmatrix} 0 & 0 & 0 & 0 & 0 & 1 \\ 0 & 0 & 0 & \frac{1}{K_4} & 0 & 1 \\ 0 & 0 & 0 & -\frac{1}{K_4} & -\frac{1}{K_5} & 1 \end{bmatrix} \tag{12}$$

and

$$x = \begin{bmatrix} \dot{\theta}_1 \\ \dot{\theta}_2 \\ \dot{\theta}_3 \\ \tau_4 \\ \tau_5 \\ \theta_1 \end{bmatrix} \qquad u = \begin{bmatrix} \tau_8 \\ \tau_9 \\ \tau_{10} \end{bmatrix} \qquad y = \begin{bmatrix} \theta_1 \\ \theta_2 \\ \theta_3 \end{bmatrix} \tag{13}$$

From [1] the model parameters for the lightly damped case ara

$$J_1 = 1 \qquad J_2 = .5 \qquad J_3 = .25$$

$$K_4 = K_5 = .0001 \tag{14}$$

$$B_6 = B_7 = .0001$$

Using the Q - R algorithm, the eigenvalues of the open loop system are obtained as:

$$
\begin{aligned}
\lambda_1 &= 0 \\
\lambda_2 &= 0 \\
\lambda_3, \lambda_4 &= -.0001 \pm j\ .01414 \\
\lambda_5, \lambda_6 &= -.00035 + j\ .0265
\end{aligned}
\tag{15}
$$

The periods of the lightly damped modes are, respectively,

$$
\begin{aligned}
\omega_1 &= .01414 \qquad & T_1 &= 444.36 \text{ secs} \\
\omega_2 &= .0265 \qquad & T_2 &= 240.46 \text{ secs}
\end{aligned}
\tag{16}
$$

In the next section, the results of Porcelli are compared with an alternate syrthesis approach using single loop elimination.

Section 3. CLASSICAL DESIGN APPROACH

For the state variable equations of Section 2, the open loop transfer functions of Appendix A were obtained from the application of Danielevsky's method [2]. It is interesting to examine the transfer function relating the angular displacement of mass J_1 with the input to mass 1 in closer detail. This transfer function is repeated here as

$$\frac{\theta_1(s)}{\tau_8(s)} = G_{11}(s) = \frac{s^4 + .0008s^3 + .0008s^2 + .16E\text{-}6s + .8E\text{-}7}{s^2(s^4 + .0009s^3 + .0009s^2 + .28E\text{-}6s + .14E\text{-}6)} \tag{17}$$

The poles and zeros of $G_{11}(s)$ are obtained as

Zeros	Poles
$z_1, z_2 = -.0000586 \pm j\ .01082$	$p_1, p_2 = -.0001 \pm j\ .01414$
$z_3, z_4 = -.00034 \pm j\ .0261$	$p_3, p_4 = -.00035 \pm j\ .0265$
	$p_5 = 0.0$
	$p_6 = 0.0$

(18)

With this pole-zero arrangement it is apparent that the complex zeros virtually cancel the complex poles and the transfer function could be reasonably approximated by

$$\frac{\theta_1(s)}{\tau_8(s)} = G_{11}(s) \approx \frac{1}{s^2} \tag{19}$$

Figure 3 contains a sketch of the root locus for the uncompensated system. Figure 4 provides the Nyquist diagram for the full order model. The large loops in Figure 4 are due to the resonant frequencies associated with the appendages. Note that these Nyquist loops do not effect the stability issue for the overall system.

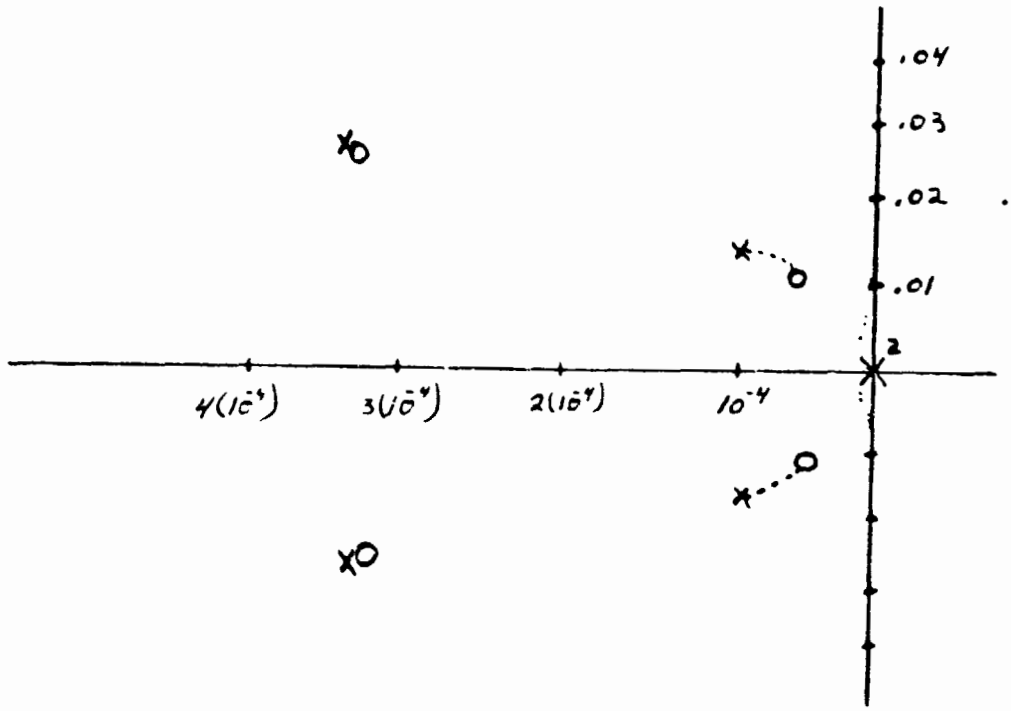

Figure 3: Root Locus for Full Order Model

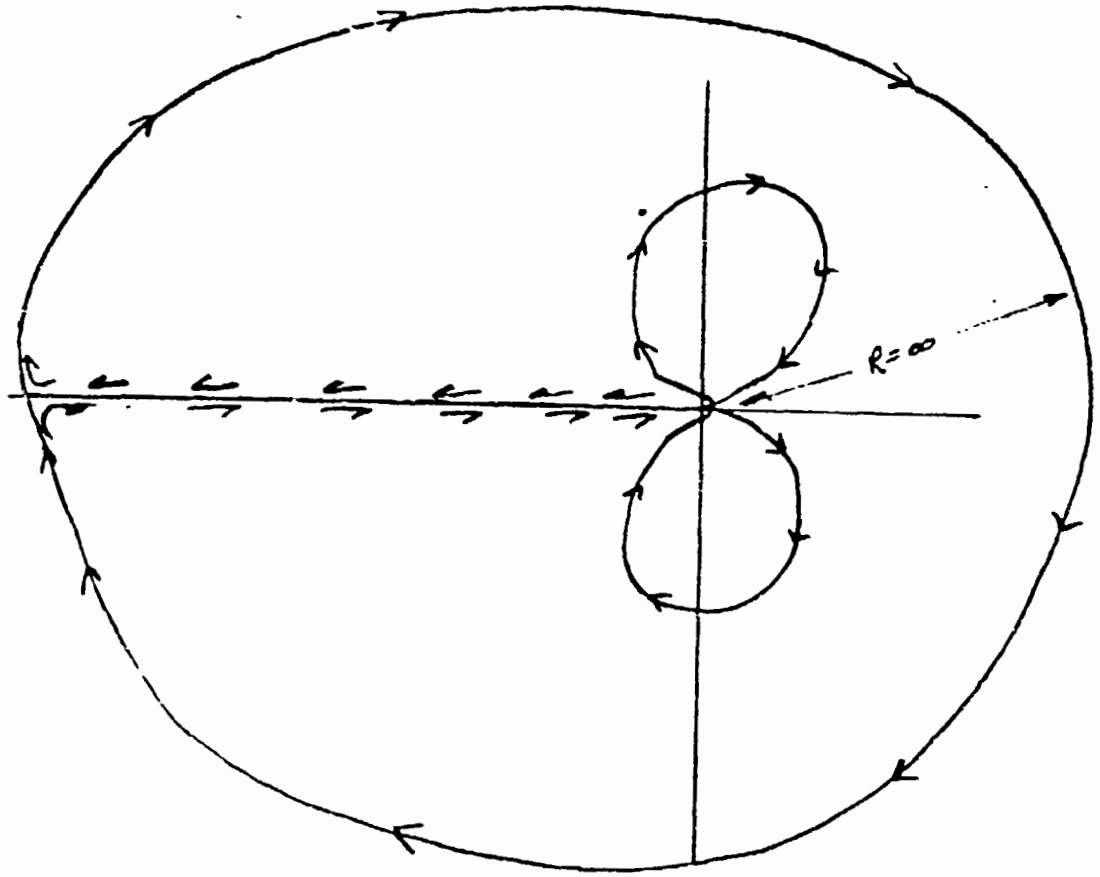

Figure 4: Nyquist Diagram for Uncompensated Full Order Model

Clearly to stabilize the system for high gain and to obtain the closed loop dynamic response desired, it is necessary to inject phase lead compensation. For all practical design purposes the control design from the terminals $\{\theta_1, \tau_8\}$ can proceed using the approximation in (19).

Following standard phase lead design procedures, a Bode plot of

$$G(s) = \frac{1}{s^2} \tag{20}$$

is made and appears in Figure 5a.

The phase lead compensator has the form

$$G_c(s) = \alpha\left(\frac{1 + TS}{1 + \alpha TS}\right) \tag{21}$$

Selecting $\alpha = .1$ to inject a large amount of phase lead at the gain crossover point

$$\text{Sin } \phi_m = \frac{1 - \alpha}{1 + \alpha} \quad \text{or} \quad \phi_m = 54.9^\circ \tag{22}$$

Since the magnitude curve is also adjusted when the phase is modified, the new crossover frequency is obtained from the $-20 \log_{10}(1/\sqrt{\alpha})$ point on the magnitude curve, i.e.,

$$-20 \log_{10}(1/\sqrt{\alpha}) = -10 \text{ db} \tag{23}$$

$$\omega_m = 1.779 \tag{24}$$

The zero and pole location for the compensator are obtained from

$$\frac{1}{T} = \sqrt{\alpha}\, \omega_m = .562 \tag{25}$$

$$\frac{1}{\alpha T} = 5.62 \tag{26}$$

Thus

$$G_c(s) = .1\left[\frac{1 + 1.779S}{1 + .1779S}\right] \tag{27}$$

or

```
        B O D E    D E S I G N    P R O G R A M
        - - - -    - - - - - -    - - - - - - -
*** PROBLEM I.D. : SAT
*** FORWARD TRANSFER FUNCTION IN POLYNOMIAL FORM ? : Y
    HIGHEST POWER OF 'S' IN NUMERATOR : 0
       COEFFICIENT OF S**0 : 1
    HIGHEST POWER OF 'S' IN DENOMINATOR : 2
       COEFFICIENT OF S**2 : 1
       COEFFICIENT OF S**1 : 0
       COEFFICIENT OF S**0 : 0
*** COMPENSATION FUNCTION IN POLYNOMIAL FORM ? : Y
*** INITIAL, FINAL RADIAN FREQUENCY  : .01,10
    MIN =-40.00      DB AT  180.0 DEG AT F = 10.00
    MAX = 80.00      DB AT  180.0 DEG AT F =0.1000E-01
    MIN, MAX FREQUENCY TO BE DISPLAYED : .01,10
    EXAMINE A POINT AND LABEL WITH :
*** REDRAW WITH INITIAL, FINAL FREQUENCY :
*** REDRAW WITH NEW COMPENSATION ? : Y
*** COMPENSATION FUNCTION IN POLYNOMIAL FORM ? : Y
    HIGHEST POWER OF 'S' IN NUMERATOR : 1
       COEFFICIENT OF S**1 : 10
       COEFFICIENT OF S**0 : 5.62
    HIGHEST POWER OF 'S' IN DENOMINATOR : 1
       COEFFICIENT OF S**1 : 1
       COEFFICIENT OF S**0 : 5.62
*** INITIAL, FINAL RADIAN FREQUENCY  : .01,10
    MIN =-21.18      DB AT -153.9 DEG AT F = 10.00
    MAX = 80.00      DB AT -179.1 DEG AT F =0.1000E-01
    EXAMINE A POINT AND LABEL WITH :
*** REDRAW WITH INITIAL, FINAL FREQUENCY :
*** REDRAW WITH NEW COMPENSATION ? :
*** END OF PROBLEM....MAKE A HARD COPY ? : Y
*** RESTART WITH A NEW FUNCTION AND PAGE ? :
```

Figure 5a: Bode Plot for $G(s) = 1/s^2$ with Compensation

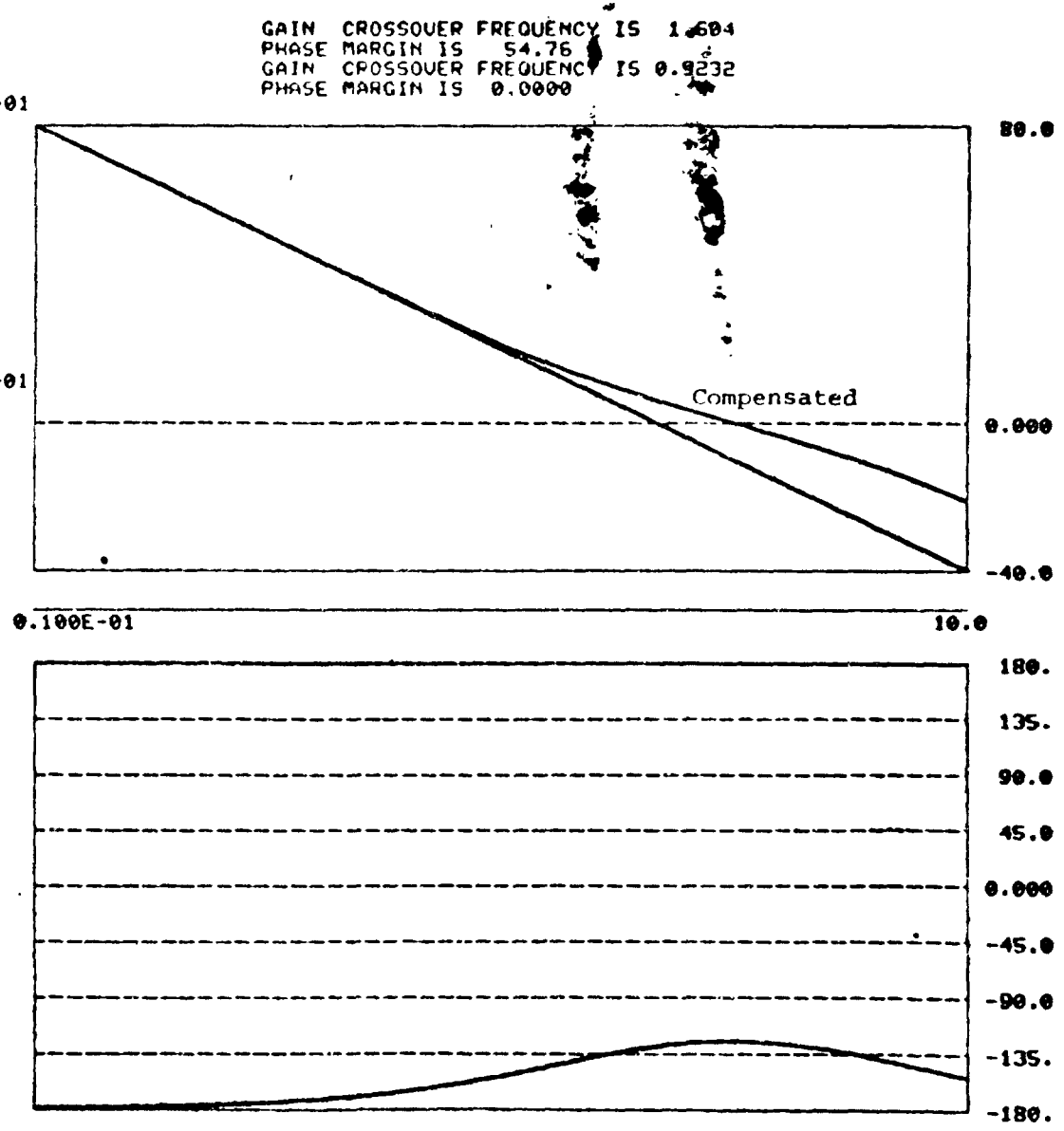

Figure 5b: Bode Plot for Full Order Model with Compensation

```
      B O D E    D E S I G N    P R O G R A M
      - - - -    - - - - - -    - - - - - - -
 ### PROBLEM I.D. : SATFOM
 ### FORWARD TRANSFER FUNCTION IN POLYNOMIAL FORM ? : Y
     HIGHEST POWER OF 'S' IN NUMERATOR : 4
        COEFFICIENT OF S##4 : 1
        COEFFICIENT OF S##3 : .0008
        COEFFICIENT OF S##2 : .0008
        COEFFICIENT OF S##1 : .16E-06
        COEFFICIENT OF S##0 : .8E-07
     HIGHEST POWER OF 'S' IN DENOMINATOR : 6
        COEFFICIENT OF S##6 : 1.
        COEFFICIENT OF S##5 : .0009
        COEFFICIENT OF S##4 : .0009
        COEFFICIENT OF S##3 : .28E-06
        COEFFICIENT OF S##2 : .14E-06
        COEFFICIENT OF S##1 : 0
        COEFFICIENT OF S##0 : 0
 ### COMPENSATION FUNCTION IN POLYNOMIAL FORM ? : 1
 ### INITIAL, FINAL RADIAN FREQUENCY  : .001,10
     MIN =-40.00      DB AT -180.0 DEG AT F = 10.00
     MAX = 115.1      DB AT -180.0 DEG AT F =0.1000E-02
     MIN, MAX FREQUENCY TO BE DISPLAYED : .001,10
     EXAMINE A POINT AND LABEL WITH : 0001
 ^U  EXAMINE A POINT AND LABEL WITH : 0002
     EXAMINE A POINT AND LABEL WITH :
 ### REDRAW WITH INITIAL, FINAL FREQUENCY :
 ### REDRAW WITH NEW COMPENSATION ? : Y
 ### COMPENSATION FUNCTION IN POLYNOMIAL FORM ? : Y
     HIGHEST POWER OF 'S' IN NUMERATOR : 1
 ^U     COEFFICIENT OF S##1 : 10
        COEFFICIENT OF S##0 : 5.62
     HIGHEST POWER OF 'S' IN DENOMINATOR : 1
        COEFFICIENT OF S##1 : 1
        COEFFICIENT OF S##0 : 5.62
 ### INITIAL, FINAL RADIAN FREQUENCY  : .001,10
     MIN =-21.13      DB AT -153.9 DEG AT F = 10.00
     MAX = 115.1      DB AT -179.3 DEG AT F =0.1000E-02
     EXAMINE A POINT AND LABEL WITH : COMP
     EXAMINE A POINT AND LABEL WITH :
```

```
[ COMP ] =    5.883      DB AT F = 0.9850
GAIN  CROSSOVER FREQUENCY IS  1.586
PHASE MARGIN IS   54.73
[ 0002 ] =   49.75       DB AT F = 0.1060E-01
[ 0001 ] =   93.03       DB AT F = 0.1422E-01
GAIN  CROSSOVER FREQUENCY IS 0.9129
PHASE MARGIN IS  0.6287E-02
```

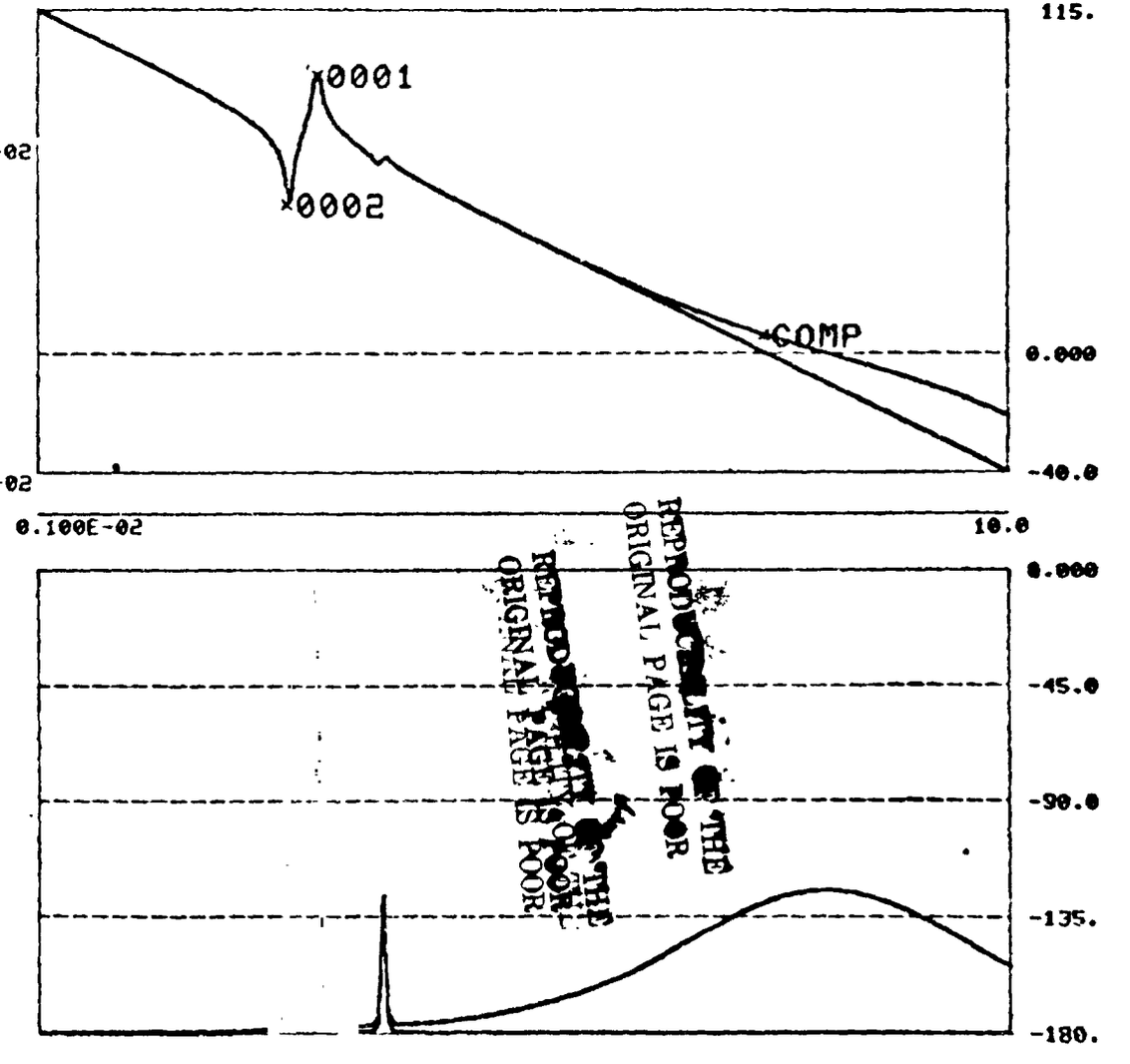

$$G_c(s) = \frac{S + .562}{S + 5.62} \tag{28}$$

The compensated system is indicated in Figures 5a and 5b. Figure 6 contains the Nyquist diagram for the compensated G(s) in (17).

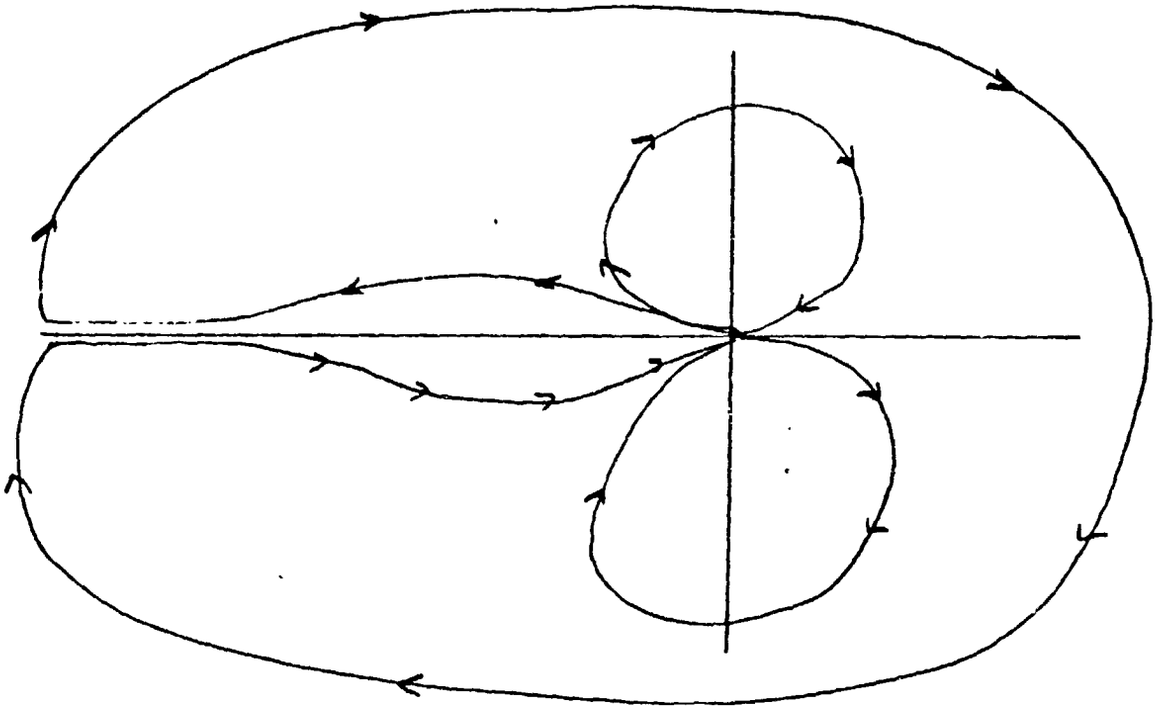

Figure 6: Compensated Nyquist Diagram

For time domain analysis, the compensator of (28) is represented by

$$\dot{X}_7 = -5.62\ X_7 - 5.058\ \theta_1(t) \tag{29}$$

$$\tau_8(t) = X_7(t) + \theta_1(t) \tag{30}$$

A CSMP run using the state equations in (8) and (9) with the main control unit developed above provided a 0.1% settling time, T_s, for the vehicle of

$$T_s = 3.9 \quad \text{seconds} \tag{31}$$

With no control on the appendages slowly damped oscillations remained significant at t = 5000 seconds. Using Porcelli's compensator for the main control unit the 0.1% settling time is

$$T_s = 10.9 \text{ seconds} \quad (32)$$

with similar oscillations occurring in the appendages. In each case, an initial offset of .02 radians was assumed for all vehicle bodies.

Based upon the above analysis, it can be concluded that the main control unit for the satellite is only concerned with the dynamics of the large mass. This is further supported by the CSMP runs wherein the angular displacements associated with the appendage masses at t = 3.9 seconds remain within 1.3% and .01% of their initial offsets, respectively (Appendix C). Thus for the design of the appendage control units, it can be assumed that the main body has been returned to the equilibrium point (the origin).

Ignoring the main body is equivalently reflected in Figure 7.

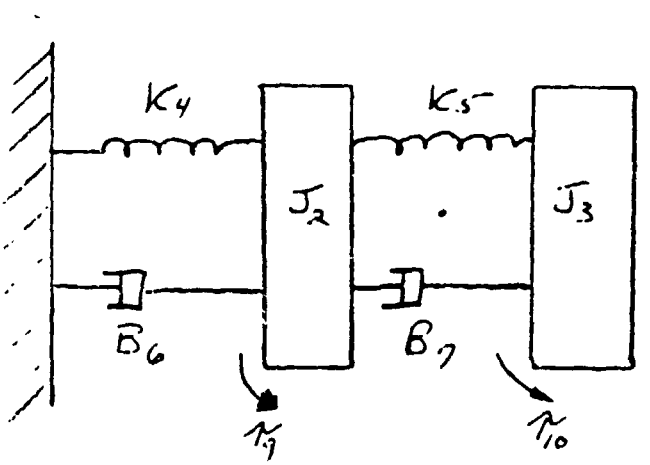

Figure 7: Reduced Order Model

Following a development similar to the full order model (FOM) the state equations for the reduced order model (ROM) are obtained as

$$\dot{x} = Ax + Bu \quad (33)$$

$$y = Cx \quad (34)$$

where

Matrix Form: $\dot{x} = Ax + Bu \qquad y = Cx$

$$A = \begin{bmatrix} -\left(\frac{B_6 + B_7}{J_2}\right) & \frac{B_7}{J_2} & \frac{1}{J_2} & -\frac{1}{J_2} \\ \frac{B_7}{J_3} & -\frac{B_7}{J_3} & 0 & \frac{1}{J_3} \\ -K_4 & 0 & 0 & 0 \\ K_5 & -K_5 & 0 & 0 \end{bmatrix} \tag{35}$$

$$B = \begin{bmatrix} \frac{1}{J_2} & 0 \\ 0 & \frac{1}{J_3} \\ 0 & 0 \\ 0 & 0 \end{bmatrix} \tag{36}$$

$$C = \begin{bmatrix} 0 & 0 & -\frac{1}{K_4} & 0 \\ 0 & 0 & -\frac{1}{K_4} & -\frac{1}{K_5} \end{bmatrix} \tag{37}$$

and

$$x(t) = \begin{bmatrix} \dot{\theta}_2 \\ \dot{\theta}_3 \\ \tau_4 \\ \tau_5 \end{bmatrix} \qquad y = \begin{bmatrix} \theta_2 \\ \theta_3 \end{bmatrix} \qquad u = \begin{bmatrix} \tau_9 \\ \tau_{10} \end{bmatrix} \tag{38}$$

The transfer functions for the reduced order model appear in Appendix B. An examination of the transfer function relating $\theta_2(t)/\tau_9(t)$ with $\tau_{10}(t) = 0$ reveals the pole-zero configuration

Zeros	Poles
$z_1, z_2 = -.0002 \pm .019998$	$p_1, p_2 = -.0000586 \pm j\ .010824$
	$p_3, p_4 = -.0003414 \pm j\ .02613$

(39)

as indicated in Figure 8 with the Bode for the ROM in Figure 9.

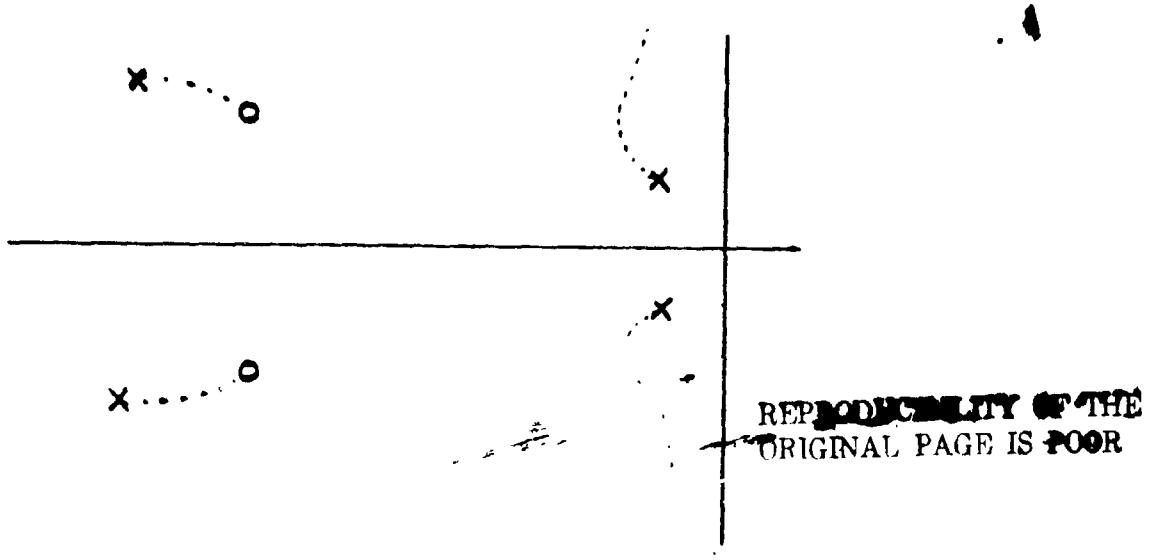

Figure 8: Root Locus for Reduced Order Model

For this model, pole-zero cancellations may once again be assumed with the result

$$\frac{\theta_2(s)}{\tau_9(s)} \approx \frac{K}{S^2 + 1.172(10^{-4})S + 1.1716(10^{-4})} \tag{40}$$

With a one percent steady state error specification

$$\lim_{s \to 0} \frac{1}{1 + G(s)} = .01 \tag{41}$$

from which the open loop gain is obtained as

$$K = 1.16(10^{-2}) \tag{42}$$

Based upon the transfer relationship in (40) it would appear that a bridged-T-compensator would be significantly more effective than the simple lead compensator used by Porcelli. For the coefficients in (40), the bridged-T-compensator has the form

$$G_c(s) = \frac{S^2 + 1.172(10^{-4})S + 1.172(10^{-4})}{S(S + .9888)} \tag{43}$$

```
    B O D E    D E S I G N    P R O G R A M
    - - - -    - - - - - -    - - - - - - -
*** PROBLEM I.D. : SAT
*** FORWARD TRANSFER FUNCTION IN POLYNOMIAL FORM ? : Y
    HIGHEST POWER OF 'S' IN NUMERATOR : 2
       COEFFICIENT OF S**2 : .00132
       COEFFICIENT OF S**1 : .55873E-05
       COEFFICIENT OF S**0 : .00015616
    HIGHEST POWER OF 'S' IN DENOMINATOR : 4
       COEFFICIENT OF S**4 : 1
       COEFFICIENT OF S**3 : .0132
       COEFFICIENT OF S**2 : 1.1025
       COEFFICIENT OF S**1 : .004224
       COEFFICIENT OF S**0 : .1024
*** COMPENSATION FUNCTION IN POLYNOMIAL FORM ? : 1
*** INITIAL, FINAL RADIAN FREQUENCY  : .001,10
    MIN =-97.50      DB AT -179.9 DEG AT F = 10.00
    MAX =-17.74      DB AT  -89.6 DEG AT F = 1.000
    MIN, MAX FREQUENCY TO BE DISPLAYED : .001,10
    EXAMINE A POINT AND LABEL WITH :
```


Figure 9: Bode Diagram for Reduced Order Model

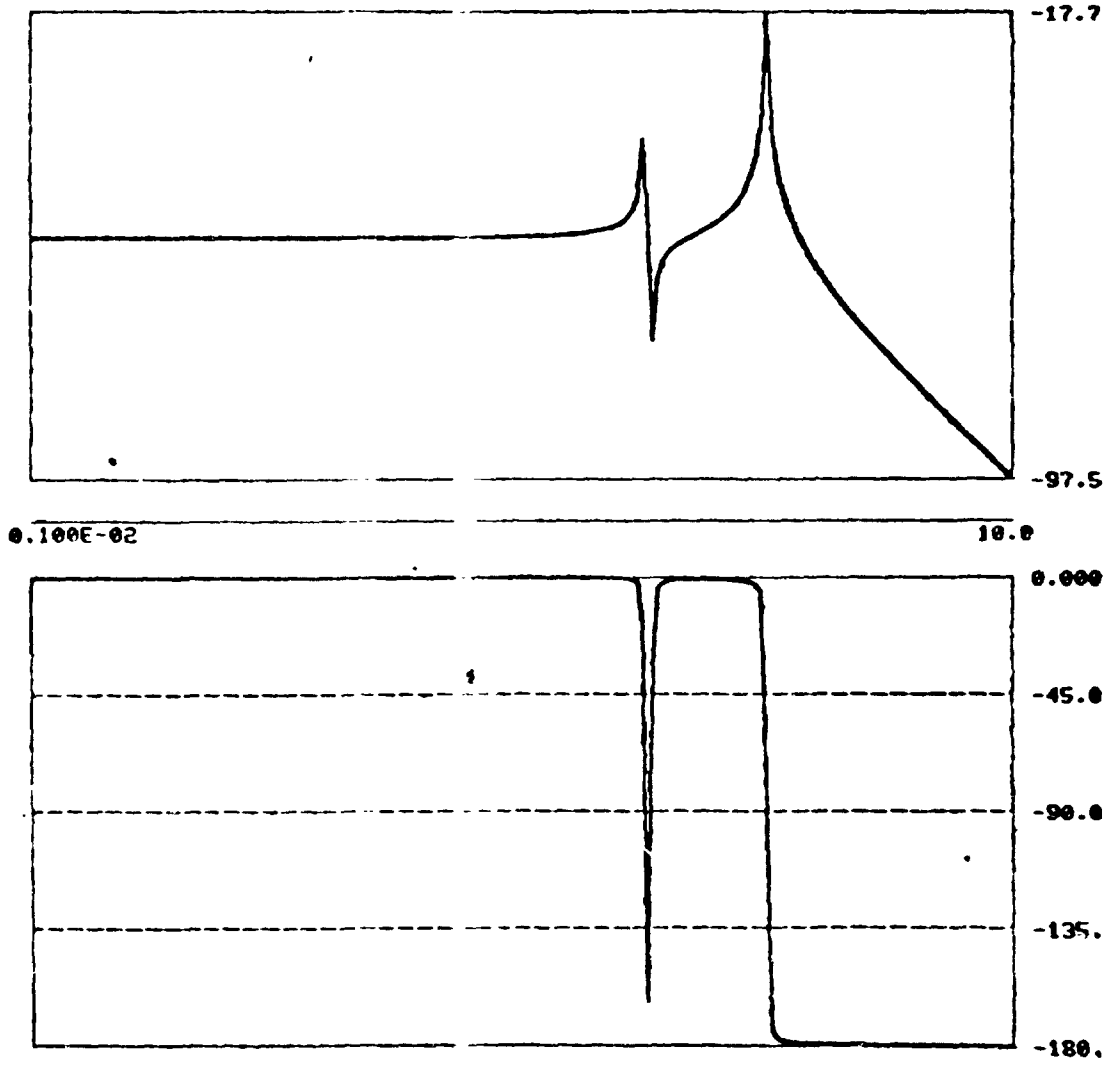

which yields the open loop transfer function

$$G_c(s)G(s) = \frac{K}{S(S + .9888)} \qquad (44)$$

The gain K in (44) could be chosen in correspondence with a steady state error specification to a ramp input or to obtain a desired set of closed loop poles with specified damping characteristics. To modify the dynamic characteristics further, a lead-lag network could be cascaded with the bridged-T network.

At this point in the design, a new state model would be developed for the space vehicle with both control loops closed. Using Danielevski's method, the system transfer function from $\theta_3(s)/\tau_{10}(s)$ could be obtained. The feedback design could then be completed in a manner similar to the design procedures above. CSMP runs could then be used to evaluate the dynamic response and adjust the appropriate compensator to correspond to the practical requirements of the vehicle.

From an examination of the transfer function for $\theta_3(s)/\tau_{10}(s)$ in Appendix B, it is clear that the analysis above would apply directly to the design of the feedback control for the third body. Experience suggests, however, that feedback control designs obtained for each loop independently may have a deleterious effect on the dynamic behavior when all loops are closed simultaneously. This condition is due primarily to the effects of system interaction among the control loops which were not incorporated into the above designs. To obtain a measure of the interaction levels for the control designs proposed above as well as those due to Porcelli, Davison's Interaction Index [3] could be used.

The concerns cited above for control system designs obtained by ignoring the interaction effects are relieved when the Multivariable Nyquist Array

method is employed since interaction levels are used in the design procedure. The next sections present a preliminary design for the flexible space vehicle using the MNA design method.

Section 4. MULTIVARIABLE NYQUIST ARRAY METHOD

The fundamental objective of the MNA design method is to decrease cross-coupled system interaction to such an extent that the closed loop system design reduces to a set of independent single loop design problems. Although simply stated, the actual reduction procedure proposed by Rosenbrock [4] and implemented by Munro [5] requires a high degree of designer intervention and is fundamentally a trial and error process.

In Figure 10, G(s) is an mxm transfer matrix representing the coupling of m inputs and m outputs.

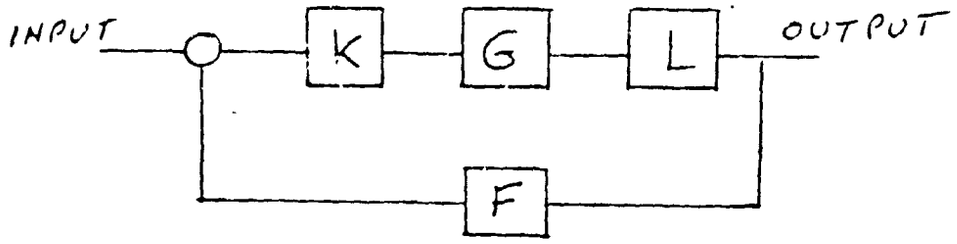

Figure 10: Multivariable System Configuration

The pre- and post-compensator matrices K and L, respectively, are each of dimension mxm. The feedback gain matrix, F, is assumed to be diagonal and of similar dimensions. Clearly, if

$$Q(S) = LG(s)K \tag{45}$$

is diagonal, loop closure may proceed on an individual loop basis with a guarantee of zero loop interaction. It is this premise upon which the MNA design philosophy is based. The adherence to strict diagonalization is relaxed, however, with the substitution and exploitation of the concept of diagonal dominant matrices.

Definition

A matrix Z(s) is diagonal dominant if either or both of the following conditions are present for all s:

$$\text{a.} \quad \sum_{\substack{j=1 \\ i \neq j}}^{m} |z_{ij}(s)|/|z_{ii}(s)| \leq \theta_i < 1 \text{ for all } i=1,2,\ldots,m \tag{46}$$

$$\text{b.} \quad \sum_{\substack{j=1 \\ j \neq i}}^{m} |z_{ji}(s)|/|z_{ii}(s)| \leq \theta_i < 1 \text{ for all } i=1,2,\ldots,m \tag{47}$$

Equation (46) defines row dominance while (47) defines the column dominance condition where θ_i is the level of dominance obtained for the ith diagonal element.

Before the design process can proceed further, Q(s) for the DNA method or $Q^{-1}(s)$ in the INA method must be made dominant by manipulation of the elements of the compensator matrices. Once dominance is achieved the design process is completed using single loop theory to select the diagonal elements of F. This selection process is enhanced through application of the Gershgorin and the Ostrowski theorems for dominant matrices.

The Gershgorin theorem [4] states that the eigenvalues of a matrix (either Q(s) or $Q^{-1}(s)$) are located in the union of the bands centered about the diagonal elements with widths determined by the sum of the moduli of the off diagonal elements by row or by column. Using the envelope procedure developed by Crossley [6] and considering each control loop separately, a graphical display of open loop system interaction results. Figures 11 and 12 indicate a typical display for an INA and DNA design formats respectively. The feedback gain selection for control loop i is then made in correspondence with the generalized Nyquist criterion and the stability theorems of Rosenbrock [4].

The Ostrowski theorem may be used to further shrink the Gershgorin bands, thereby reducing the area of uncertainty in each loop. This set of bands is frequently referred to as a set of "fuzzy" Nyquist plots (or inverse Nyquist plots for the INA). Using the innermost band as a conservative estimate of the Nyquist contour in each loop, the design proceeds on a single loop basis. Feedback gain selection must be made exterior to the Gershgorin (Ostrowski) band. Thus, phase margin, gain margin and dynamic compensation may be used to evaluate and/or improve the loop design with a guarantee of low interaction from the closure of the remaining loops.

Diagonal dominance for the Direct Nyquist Array method requires the selection of pre- and post-compensator matrix parameters so that (46) is satisfied when (45) represents the open loop transfer matrix. For the Inverse Nyquist Array method $Q^{-1}(s)$ is used and the parameters of K^{-1} and L^{-1} must be selected.

An efficient and reliable method for the evaluation of the matrix coefficients is described in [7]. The dominance algorithm uses a conjugate direction function minimization algorithm to adjust the parameter set until a performance index composed of the dominance definitions in (46) and (47) is minimized. For the INA method in a row dominance mode, the optimization problem can be separated into three independent optimization efforts; one for each row. Here the performance index by row is

$$J_i(K_{ij}) = \max_{w} \sum_{\substack{j=1 \\ i \neq j}}^{m} |\hat{q}_{ij}(s)| / |\hat{q}_{ij}(s)| \qquad i=1,2,\ldots,m \tag{48}$$

where $\hat{q}_{ij}(s)$ is an element of $Q^{-1}(s)$. For each i, the ith row of K^{-1} is adjusted until $J_i(K_{ij})$ is minimized. In practice, the ratio in (48) is computed for each discrete frequency point in the range of interest. This

array is then scanned to identify the maximum ratio. Adjusting the elements of row i in K^{-1} yields a set of final dominance levels

$$\theta_i = \min_{K_{ij}} J_i(K_{ij}) \tag{49}$$

If the dominance levels in (49) are less than unity, diagonal dominance has been achieved. In the event that some of the dominance levels are greater than one, the designer may initiate a dominance sharing search or restart the program using new starting values for the unspecified compensator parameters.

The concept of dominance sharing is detailed in [8]. It is fundamentally a rescaling of the compensator matrices to the extent that low dominance levels may be intentionally increased to a point where the previous non-dominant levels may be shifted to a range of acceptability. This procedure has been automated in the latest version of the dominance algorithm and is initiated by the designer after the final set of dominance levels have been evaluated.

Once a set of coefficients have been determined for dominance of the open loop transfer matrix, each control loop may be treated independently using single-input single-output control theory. The dominance algorithm briefly outlined above shifts the burden of establishing the dominance condition from the designer to an automated procedure. Thus designer intervention is only required during the actual design process and is no longer needed to establish the requisite dominance condition. Experience with the algorithm suggests that dominance may often be obtained within several CPU minutes or less depending upon the characteristics of G(s).

Section 5: MNA DESIGN

The Multivariable Nyquist Array method described in Section 4 was applied to the full order model of the space vehicle. Based upon an evaluation of these results, the reduced order model was used subsequent to the design of a control unit for the large mass. Although the design described herein is of a preliminary evaluation for space vehicles, the results clearly demonstrate the utility of the MNA method to flexible vehicle control system design.

Using the transfer matrix of Appendix A as the frequency domain representative for the full order satellite model, a DNA design run was initiated. For this DNA design the postcompensator matrix was prespecified as the identity matrix with the precompensator matrix to be selected in accordance with the algorithm in [7]. Figure 11 indicates the closed loop diagram for the satellite with

$$Q(s) = LG(s)K \tag{50}$$

representing the open loop transfer matrix.

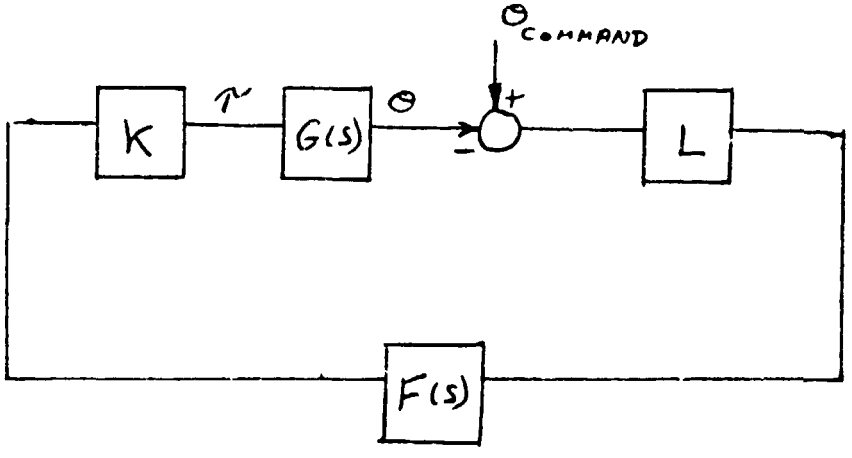

Figure 11: Closed Loop Satellite Control Design

Direct application of the DNA method to the FOM without regard to the simplifying conditions described in Section 3 produced a non-dominant condition for Q(s) in (50). Using a frequency range of

$$.005 \leq \omega \leq .03$$

for dominance evaluations, it is evident from the computer printout that dominance for each column of Q(s) is lost in the frequency range near the resonant frequencies associated with the flexible appendages. Since this design effort is using the DNA column objective, loss of dominance is not particularly significant providing that feedback gains could be selected external to the corresponding Gershgorin bands. This condition, however, is non-existent for loop 1 as the Nyquist band is coincident with the negative real axis. This condition immediately relates the dominating influence of the two open loop poles of Q(s) at the origin (i.e. pnase angle of 180°). Thus a confirmation of the single loop analysis from Section 3 is obtained directly from the DNA diagram for column 1 of Q(s) (see Figure 4). With a Nyquist diagram of this form, phase lead compensation is required to provide an adequate phase margin for the main control loop.

Using the phase compensator designed in Section 3, the angular displacement of mass J_1, is returned to the equilibrium point (origin) before any significant motion of the appendages takes place. Hence the model configuration can be modified to the reduced order model previously developed.

Application of the MNA program to the ROM over the frequency interval

$$0 \leq \omega \leq .03 \text{ radians} \qquad (51)$$

yields a dominant condition for each column of the ROM transfer matrix Q(s). Here the matrix G(s) in Appendix B provides the frequency domain description when mass J_1 is clamped.

The dominance producing compensators are

$$K = \begin{bmatrix} 1.0034 & -.94747 \\ -.70949 & .66997 \end{bmatrix} \quad (52)$$

$$L = \begin{bmatrix} 1.7174 & 0 \\ 0 & 1.2128 \end{bmatrix} \quad (53)$$

Figures 12 and 13 display the direct Nyquist diagrams for columns one and two respectively. The envelope of the Gershgorin bands are indicated in each figure.

Since the feedback gains must be selected exterior to the Gershgorin bands, it is clear from the DNA diagrams that some form of phase lead compensation is required. This form of compensation will effectively swing the DNA bands down and away from the negative real axis, thus providing an improved phase and gain margin design. This procedure will then allow for an increase in the system gain space for each control loop.

Alternatively, a bridged-T compensator could be used in each control loop to eliminate the lightly damped modes, in favor of two poles on the negative real axis. The system gain could then be selected to correspond to the desired degree of damping in each loop.

Following either compensator design procedure identified above, an effective closed loop design for the appendage control units would be obtained. For purposes of illustration, each control loop was configured with a phase lead compensator of the form

$$G_c(s) = \alpha \frac{TS + 1}{\alpha TS + 1} \quad (54)$$

with $\alpha = .1$ and $T = 30$. A CSMP run for the ROM indicates that with an initial angular off-set of .02 radians for each mass, the system was returned to their respective equilibrium points within 250 seconds as indicated in

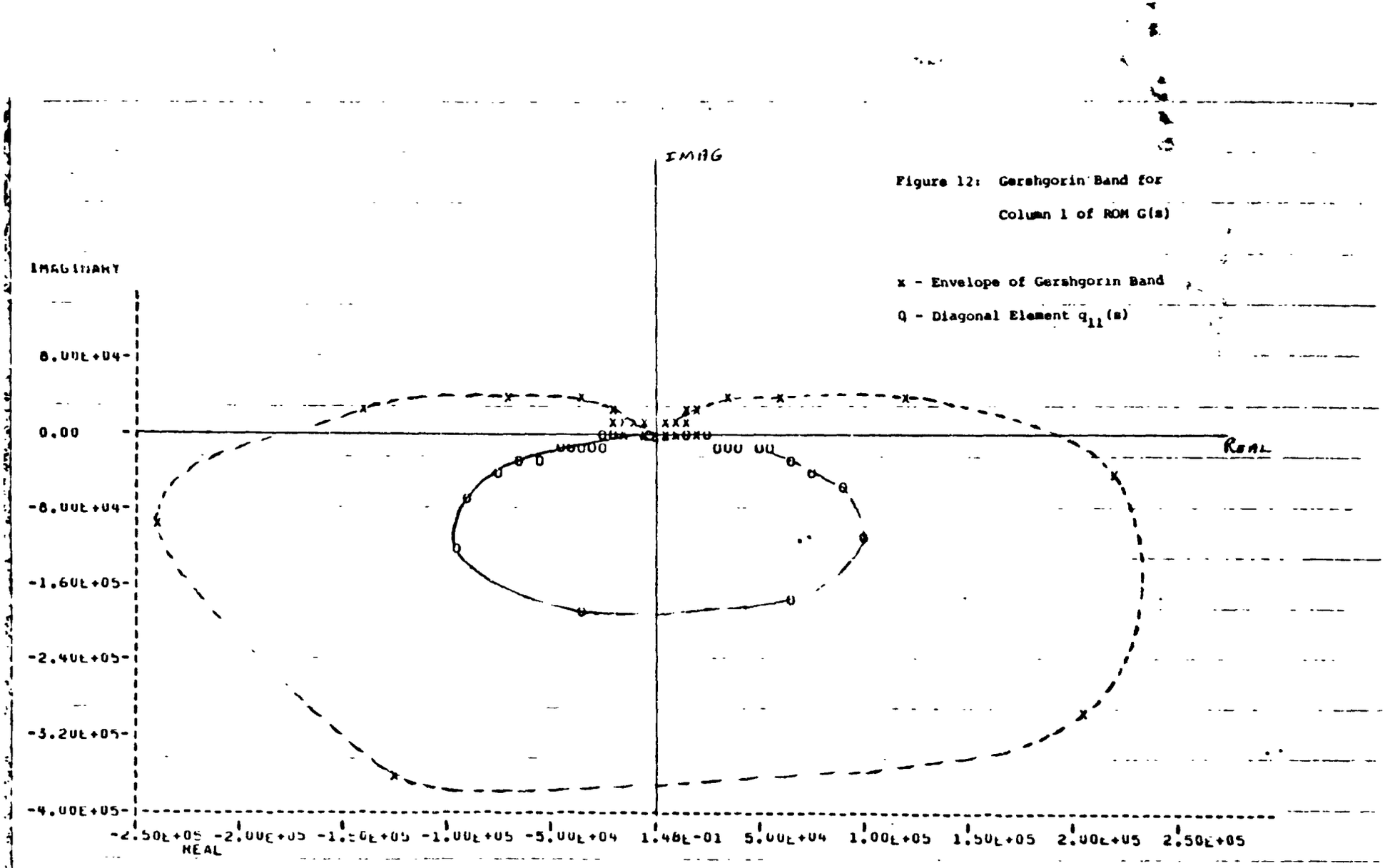

Figure 12: Gershgorin Band for Column 1 of ROM G(s)

x - Envelope of Gershgorin Band

Q - Diagonal Element $q_{11}(s)$

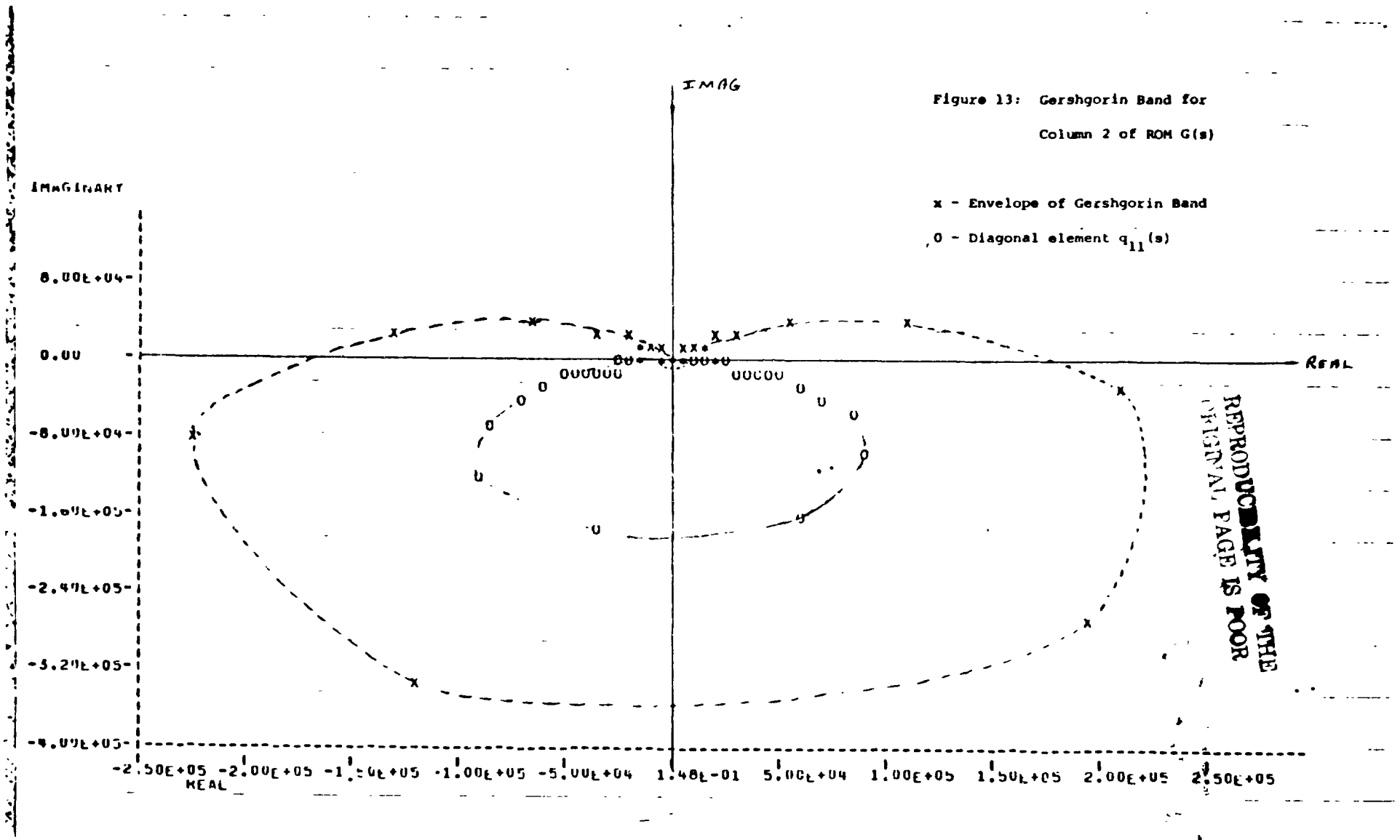

Figure 13: Gershgorin Band for Column 2 of ROM G(s)

x - Envelope of Gershgorin Band

0 - Diagonal element $q_{11}(s)$

Appendix D. Faster responses could be obtained by adjusting the pole-zero positions in (54) or by an increase in compensator gains.

In contrast to the Porcelli control units where $\tau_9(t)$ and $\tau_{10}(t)$ are only functions of $\theta_2(t)$ and $\theta_3(t)$, respectively, the MNA control configuration is of the form

$$\tau_9(t) = C_1\ \theta_2(t) + C_2\ \theta_3(t) \tag{55}$$

$$\tau_{10}(t) = C_3\ \theta_2(t) + C_4\ \theta_3(t) \tag{56}$$

The main control unit, however, is in correspondence with the Porcelli model, i.e.,

$$\tau_8(t) = C_5\ \theta_1(t) \tag{57}$$

where C_1 through C_5 are constants determined from K, L and F(s).

In view of the above preliminary results using the MNA design philosophy, the following comments are in order:

1. The MNA design method is an effective design tool for flexible space vehicles.

2. The MNA method applied without consideration of the physical properties of the system, identifies the need for system decomposition.

3. For highly interactive systems of the ROM form, the MNA method clearly demonstrates the need for a design which incorporates the interaction into the control configuration rather than ignoring its presence.

4. As a frequency domain technique for multivariable systems, the MNA method identifies the need for compensation in the proper control loops and also indicates the form of compensation required.

5. The MNA design is readily adapted to higher order models and could be easily applied to more sophisticated satellite design configurations. This is not necessarily true of the Porcelli method of design.

Section 6: CONCLUSIONS

It was the intent of this report to demonstrate the feasibility of the multivariable Nyquist array design method to the attitude control design of flexible space vehicles. Using a three body model for the vehicle with coefficients specified in the Porcelli paper, three design approaches were considered:

1. Standard single loop elimination design by classical procedures.
2. MNA design for the full order model.
3. MNA design for the reduced order model.

In each case, the design configuration independently confirm the results of Porcelli.

The first method conforms more directly to the standard compensator design approach identified in the traditional control texts. It is this design approach which is most likely to be used in the MNA compensator design. From the single loop elimination design in Section 3, it is readily apparent that this approach compares favorably with the Porcelli method. The root locus for the FOM $G_{11}(s)$ transfer function clearly delineates the control problem and bandwidth considerations which must be taken into account in the design of the main control unit. An additional feature of this single loop approach lies in the recognition of subsystem interactions associated with the appendage control design as well as the utilization of bridged-T compensation. This form of compensation does not appear in Porcelli's paper.

The second design approach ignored any previous information pertaining to the pole-zero locations in the FOM. Although system dominance was not obtained in the MNA form, subsequent analysis revealed the problem to be associated with the rigid body dynamics. This condition presented itself

in the Nyquist diagram as a 180° phase for all frequencies not associated with the resonant frequencies of the appendages. Analysis of the remaining MNA diagrams clearly indicates the need for lead compensation.

To simplify the design for the appendage control units, the first mass was assumed to be at the equilibrium point. This assumption is easily justified from the time domain analysis via CSMP. An MNA design for the ROM was made with results supportive of the FOM run. Lead compensation is clearly required for the control unit design.

Section 7: REFERENCES

1. Porcelli, G., "Attitude Control of Flexible Space Vehicles," AIAA Journal, Vol. 10, No. 6, June 1972.

2. Faddeeva, V. N., Computational Methods of Linear Algebra, Dover, Chapter 3, 1959.

3. Davison, E. J., "Interaction Index for Multivariable Control Systems," Proc. IEE, Vol. 117, No. 2, 1970.

4. Rosenbrock, H. H., Computer-Aided Control System Design, Academic Press (London), 1974.

5. Munro, N., "Conversational Mode CAD of Control Systems," IEE Int. Conf. on Computer Aided Design, England, 1972.

6. Crossley, T. R., "Envelope Curves to Inverse Nyquist Array Diagrams," Int. J. Control, Vol. 22, No. 1, 1975.

7. Leininger, G. G., "Diagonal Dominance Using Function Minimization Algorithms," 1977 IFAC MVTS Symposium, New Brunswick, Canada.

8. Leininger, G. G., "The MNA--The Concept of Dominance Sharing," NEC Int. Forum on Alternatives for Linear Multivariable Control, Chicago, Oct. 1977.

APPENDIX A

Transfer Matrix for Full Order Model

$$G_{11}(s) = (S^4 + .0008S^3 + .0008S^2 + .16E\text{-}6S + .8E\text{-}7)/\Delta$$

$$G_{12}(s) = (.0002S^3 + .0002S^2 + .16E\text{-}6S + .8E\text{-}7)/\Delta$$

$$G_{13}(s) = (.8E\text{-}7S^2 + .16E\text{-}6S + .8E\text{-}7)/\Delta$$

$$G_{21}(s) = (.4E\text{-}6S^4 + .0002S^3 + .0002S^2 + .16E\text{-}6S + .8E\text{-}7)/\Delta$$

$$G_{22}(s) = (2S^4 + .001S^3 + .001S^2 + .16E\text{-}6S + .8E\text{-}7)/\Delta$$

$$G_{23}(s) = (.0008S^3 + .0008S^2 + .16E\text{-}6S + .8E\text{-}7)/\Delta$$

$$G_{31}(s) = (.4E\text{-}6S^4 + .32E\text{-}9S^3 + .8032E\text{-}7S^2 + .16E\text{-}6S + .8E\text{-}7)/\Delta$$

$$G_{32}(s) = (.0008S^3 + 0008S^2 + .16E\text{-}6S + .8E\text{-}7)/\Delta$$

$$G_{33}(s) = (4S^4 + .002S^3 + .002S^2 + .16E\text{-}6S + .8E\text{-}7)/\Delta$$

$$\Delta = S^6 + .0009S^5 + .0009S^4 + .28E\text{-}6S^3 + .14E\text{-}6S^2$$

APPENDIX B

Transfer Matrix for Reduced Order Model

$$G_{11}(s) = (2s^2 + .0008s + .0008)/\Delta$$

$$G_{12}(s) = (.0008s + .0008)/\Delta$$

$$G_{21}(s) = G_{12}(s)$$

$$G_{22}(s) = (4s^2 + .0016s + .0016)/\Delta$$

$$\Delta = s^4 + .0008s^3 + .0008s^2 + .16(10^{-3})s + .8(10^{-7})$$

APPENDIX C

Full order model under main loop control using compensator developed in Section 3.

$$\tau_9(t) = \tau_{10}(t) = 0.0$$

Theta 1 Time Response

$0 \leq t \leq 20$

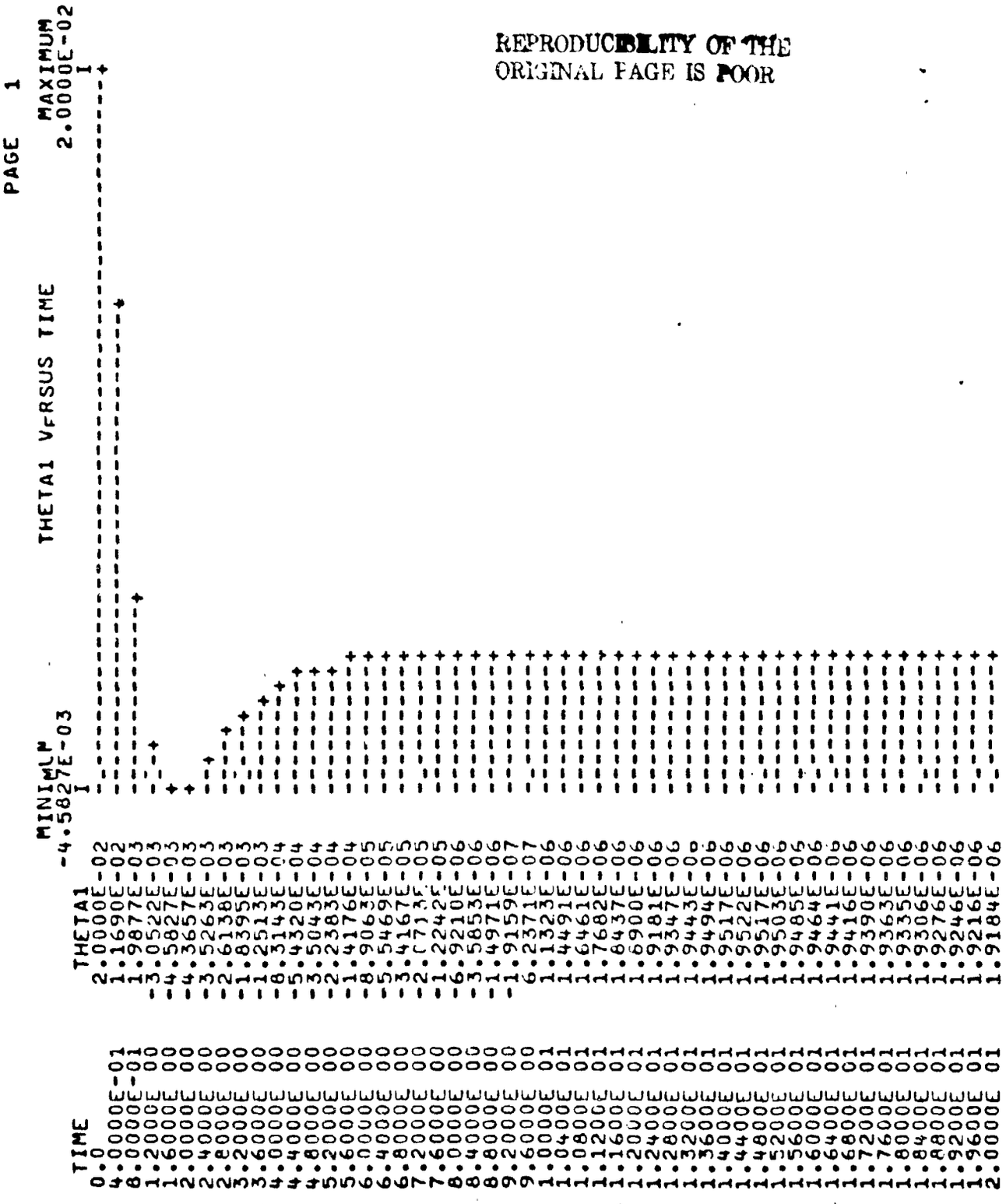

Theta 2 Time Response

$0 \leq t \leq 20$

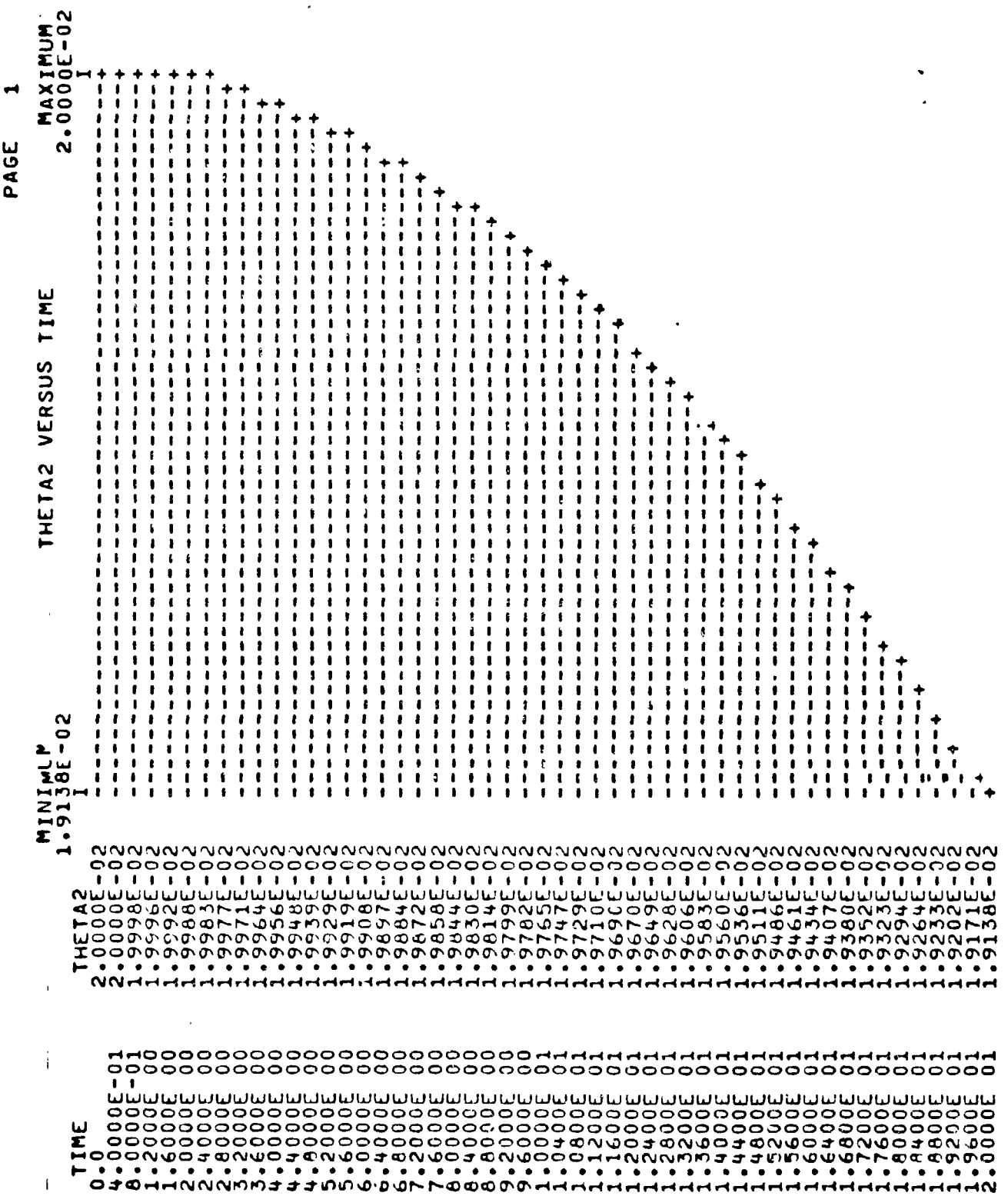

Theta 3 Time Response

$0 \leq t \leq 20$

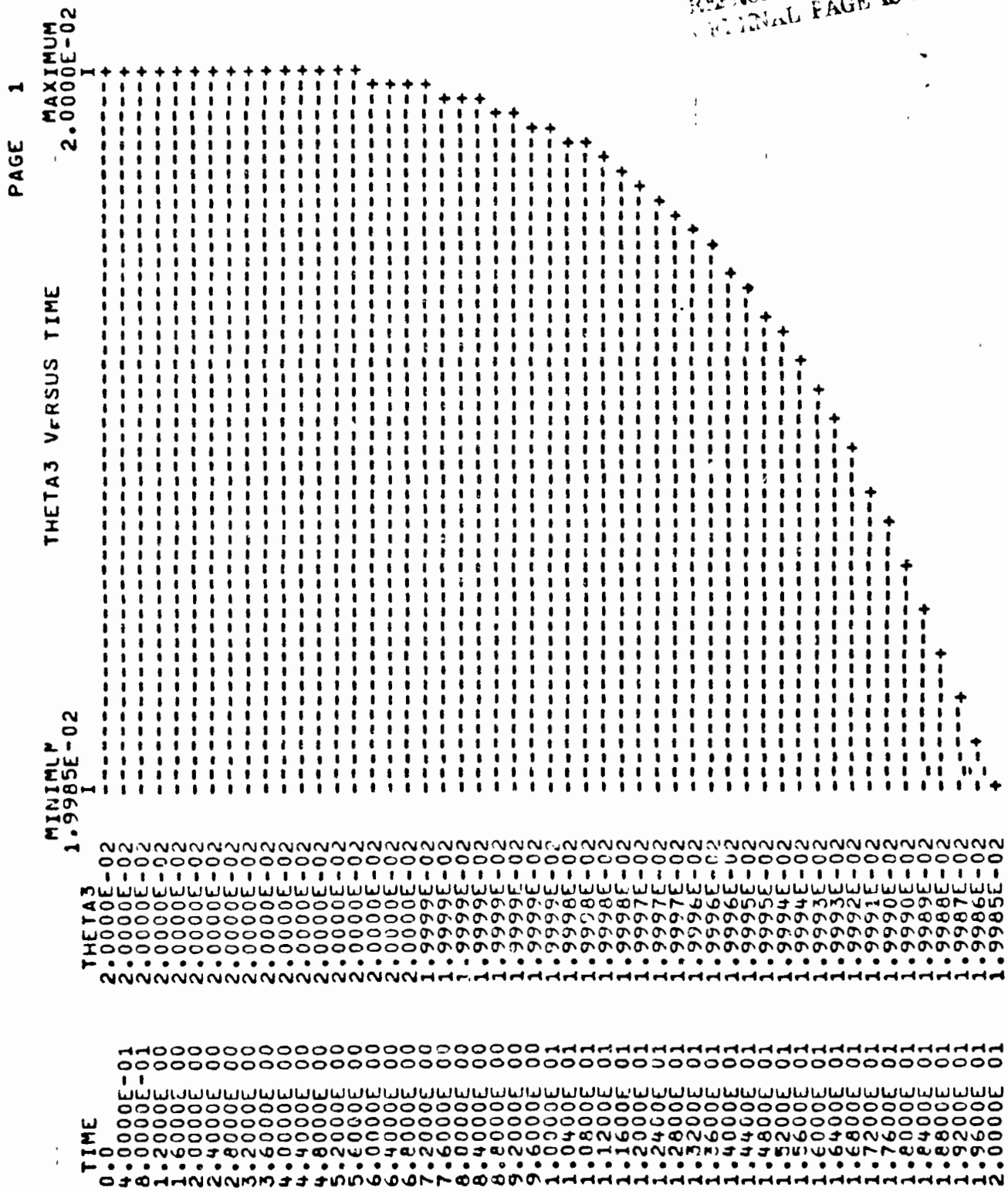

MINIMUM TAU8 VERSUS TIME MAXIMUM
-2.0000E-01 3.1841E-02

TIME	TAU8
0.0	-2.0000E-01
4.0000E-01	4.8782E-03
8.0000E-01	3.1841E-02
1.2000E 00	2.1906E-02
1.6000E 00	1.0514E-02
2.0000E 00	3.5827E-03
2.4000E 00	2.8518E-04
2.8000E 00	-9.4474E-04
3.2000E 00	-1.1958E-03
3.6000E 00	-1.0619E-03
4.0000E 00	-8.2339E-04
4.4000E 00	-5.9462E-04
4.8000E 00	-4.1143E-04
5.2000E 00	-2.7694E-04
5.6000E 00	-1.8306E-04
6.0000E 00	-1.1959E-04
6.4000E 00	-7.7595E-05
6.8000E 00	-5.0236E-05
7.2000E 00	-3.2604E-05
7.6000E 00	-2.1333E-05
8.0000E 00	-1.4170E-05
8.4000E 00	-9.6386E-06
8.8000E 00	-6.7815E-06
9.2000E 00	-4.9845E-06
9.6000E 00	-3.8563E-06
1.0000E 01	-3.1487E-06
1.0400E 01	-2.7052E-06
1.0800E 01	-2.4272E-06
1.1200E 01	-2.2526E-06
1.1600E 01	-2.1428E-06
1.2000E 01	-2.0734E-06
1.2400E 01	-2.0293E-06
1.2800E 01	-2.0008E-06
1.3200E 01	-1.9822E-06
1.3600E 01	-1.9696E-06
1.4000E 01	-1.9608E-06
1.4400E 01	-1.9543E-06
1.4800E 01	-1.9492E-06
1.5200E 01	-1.9450E-06
1.5600E 01	-1.9413E-06
1.6000E 01	-1.9379E-06
1.6400E 01	-1.9347E-06
1.6800E 01	-1.9316E-06
1.7200E 01	-1.9285E-06
1.7600E 01	-1.9254E-06
1.8000E 01	-1.9223E-06
1.8400E 01	-1.9191E-06
1.8800E 01	-1.9159E-06
1.9200E 01	-1.9126E-06
1.9600E 01	-1.9093E-06
2.0000E 01	-1.9059E-06

Tau 8 Time Response

$0 \leq t \leq 20$

Theta 2 Time Response

$0 \leq t \leq 1500$

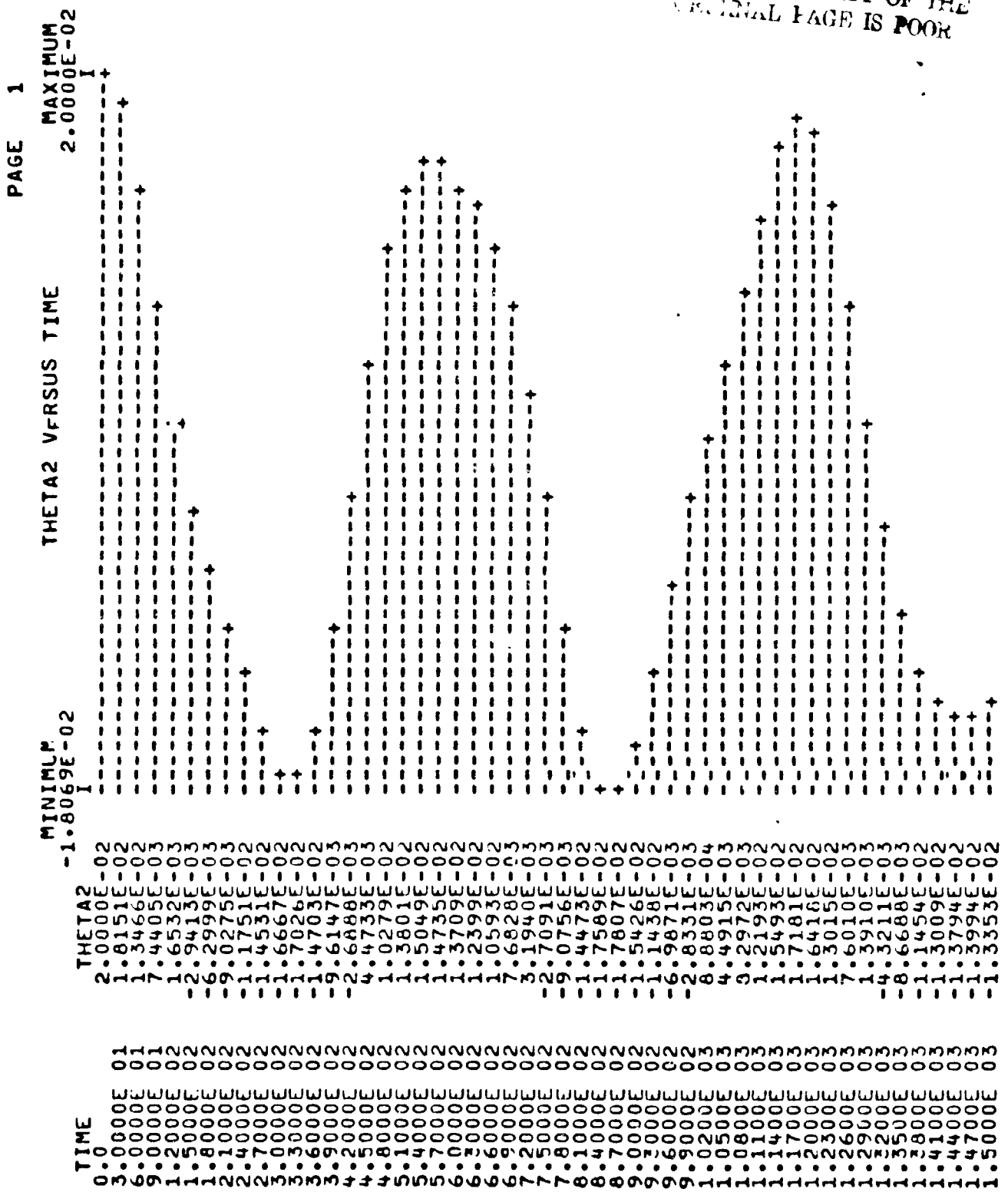

Theta 2 Time Response

$1530 \leq t \leq 3000$

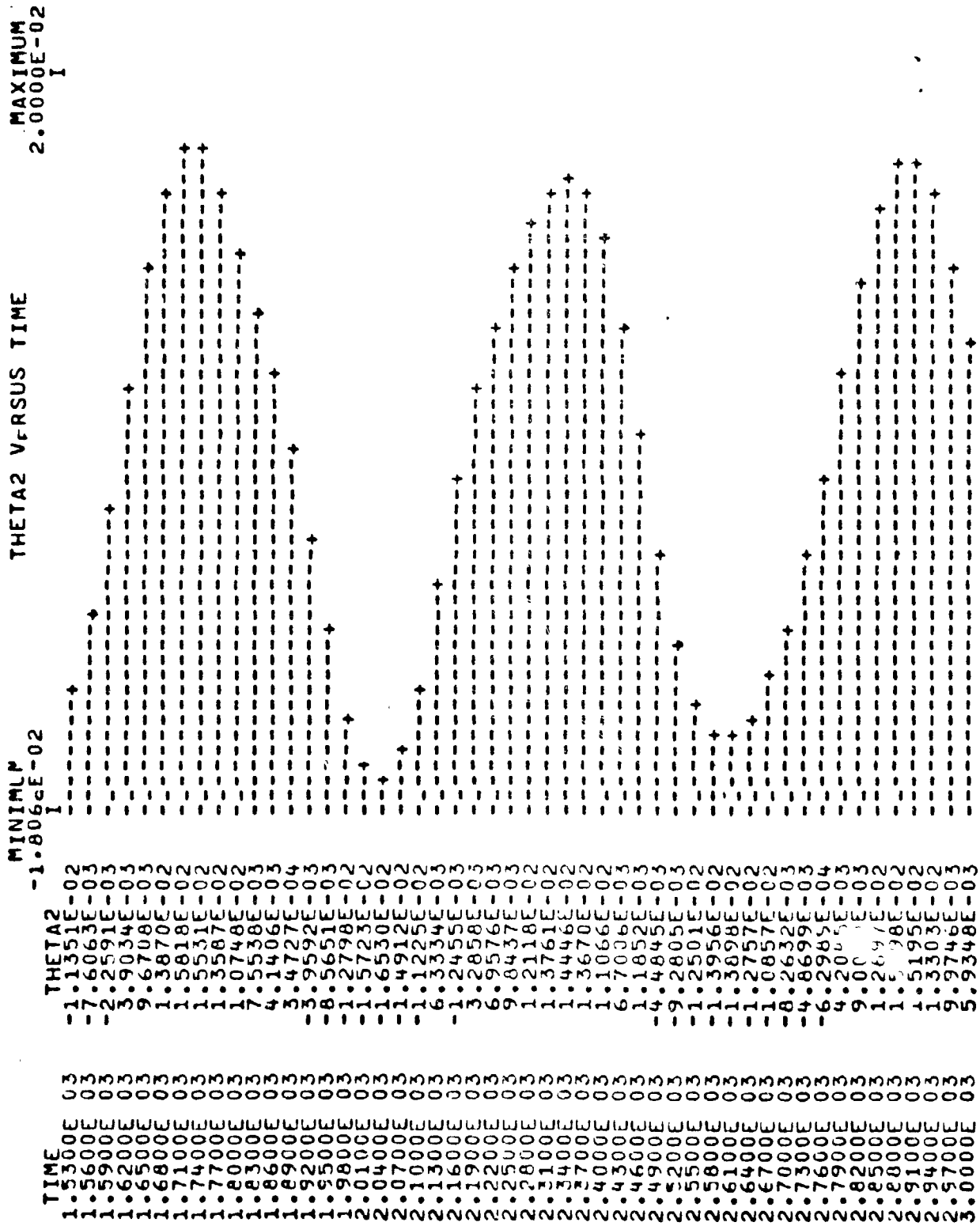

Theta 3 Time Response

$0 \leq t \leq 1500$

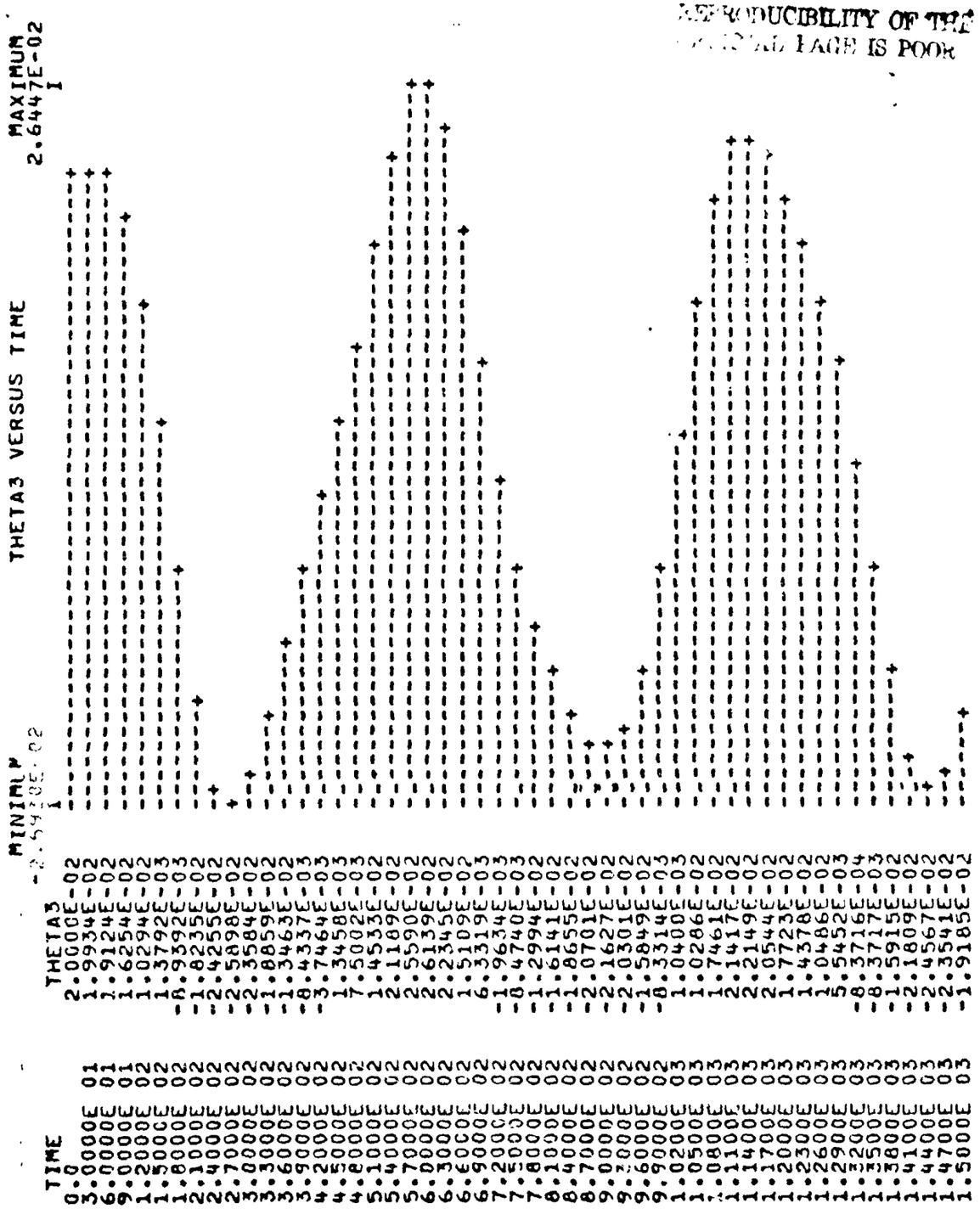

Theta 3 Time Response

$1530 \leq t \leq 3000$

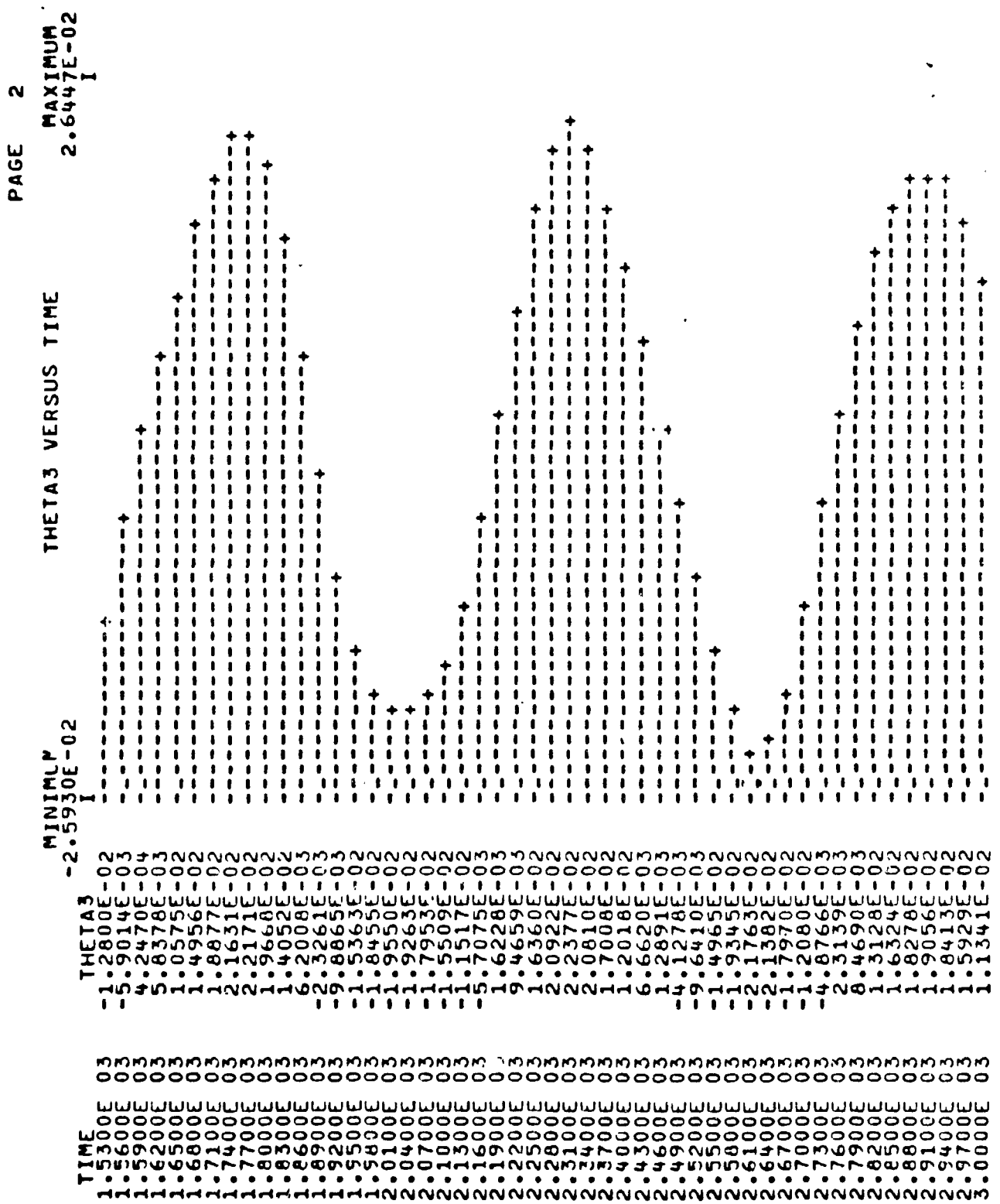

APPENDIX D

Full Order Model with Control Units

$\tau_8(t)$ from Section 3

$\tau_9(t)$, $\tau_{10}(t)$ from MNA design

Notation:

$$s\omega\phi = \begin{cases} 1 & \tau_8(t) \quad \text{activated} \\ 0 & \tau_8(t) = 0 \end{cases}$$

$$s\omega 1 = \begin{cases} 1 & \tau_9(t) \quad \text{activated} \\ 0 & \tau_9(t) = 0 \end{cases}$$

$$s\omega 2 = \begin{cases} 1 & \tau_{10}(t) \quad \text{activated} \\ 0 & \tau_{10}(t) = 0 \end{cases}$$

$$F = \begin{bmatrix} 100 & 0 \\ 0 & 100 \end{bmatrix}$$

THETA1 VERSUS TIME

MINIMUM -1.0255E-02 | MAXIMUM 2.0000E-02

TIME	THETA1
0.0	2.0000E-02
3.0000E 01	-1.7812E-03
6.0000E 01	1.4883E-04
9.0000E 01	-2.0306E-05
1.2000E 02	-4.0506E-06
1.5000E 02	-1.1807E-06
1.8000E 02	1.7465E-06
2.1000E 02	2.3585E-06
2.4000E 02	1.4164E-06
2.7000E 02	1.2074E-07
3.0000E 02	-6.6278E-07
3.3000E 02	-7.3262E-07
3.6000E 02	-3.7218E-07
3.9000E 02	3.0168E-08
4.2000E 02	2.3661E-07
4.5000E 02	2.2196E-07
4.8000E 02	9.2838E-08
5.1000E 02	-2.9215E-08
5.4000E 02	-8.0894E-08
5.7000E 02	-6.5173E-08
6.0000E 02	-2.0805E-08
6.3000E 02	1.5077E-08
6.6000E 02	2.7042E-08
6.9000E 02	1.8865E-08
7.2000E 02	4.1458E-09
7.5000E 02	-6.3036E-09
7.8000E 02	-8.5975E-09
8.1000E 02	-5.2372E-09
8.4000E 02	-9.4114E-10
8.7000E 02	1.7918E-09
9.0000E 02	2.4638E-09
9.3000E 02	1.2087E-09
9.6000E 02	5.6611E-11
9.9000E 02	-5.7982E-10
1.0200E 03	-6.1412E-10
1.0500E 03	-5.6034E-10
1.0800E 03	-2.8058E-10
1.1100E 03	-4.4974E-11
1.1400E 03	-2.0299E-12
1.1700E 03	4.8324E-11
1.2000E 03	2.9178E-11
1.2300E 03	-3.0204E-11
1.2600E 03	8.1656E-12
1.2900E 03	3.0074E-10
1.3200E 03	1.8525E-10
1.3500E 03	1.3005E-11
1.3800E 03	-7.4960E-11
1.4100E 03	-1.5146E-10
1.4400E 03	-4.4959E-11
1.4700E 03	-1.6663E-11
1.5000E 03	-2.6144E-11

Theta 1 Time Response

sw0 = sw1 = sw2 = 1

MNA Design

$0 \leq t \leq 1500$

Theta 2 Time Response

$s\omega 0 = s\omega 1 = s\omega 2 = 1$

MNA Design

$0 \leq t \leq 1500$

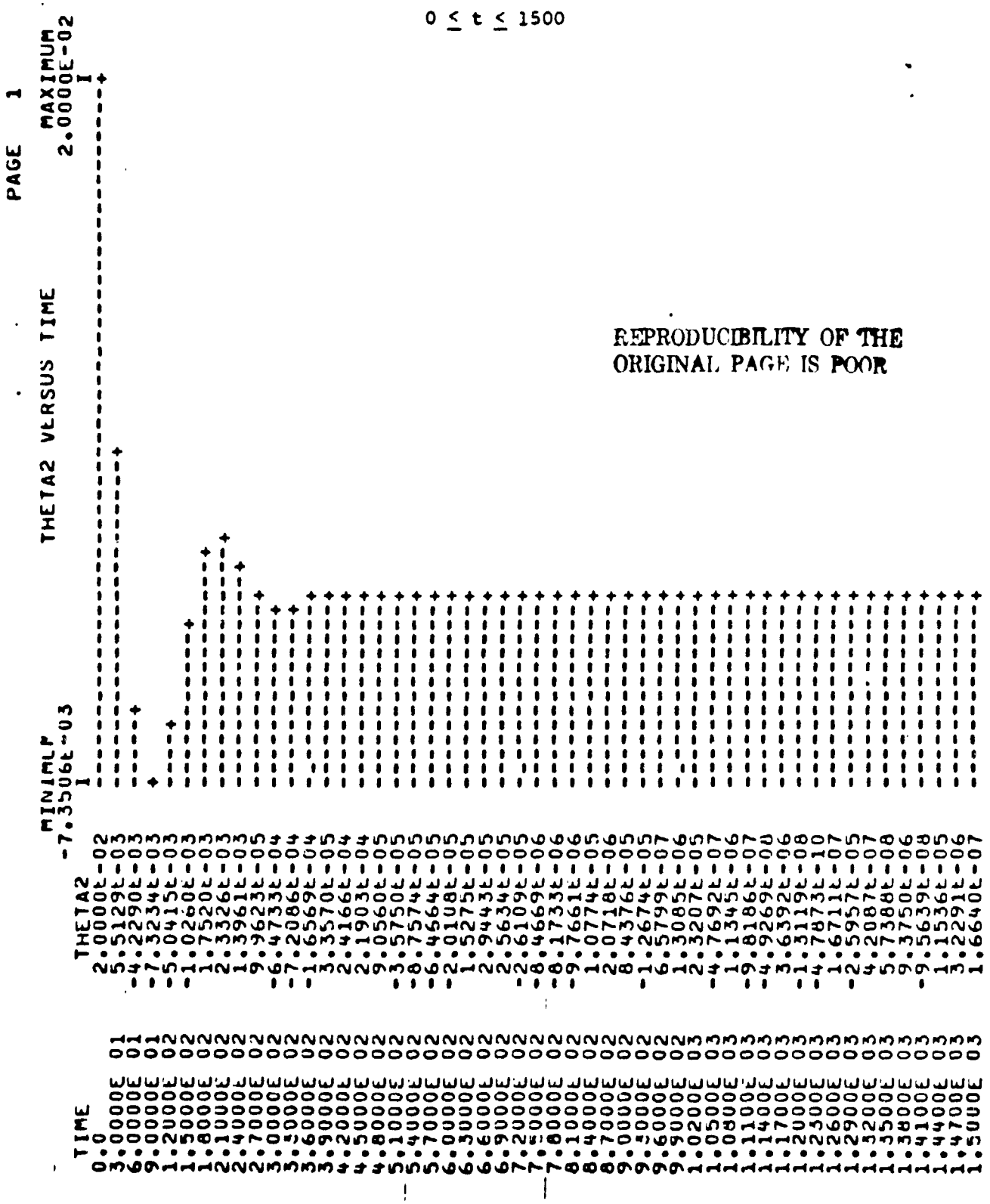

Theta 3 Time Response

$s\omega 0 = s\omega 1 = s\omega 2 = 1$

$0 \leq t \leq 1500$

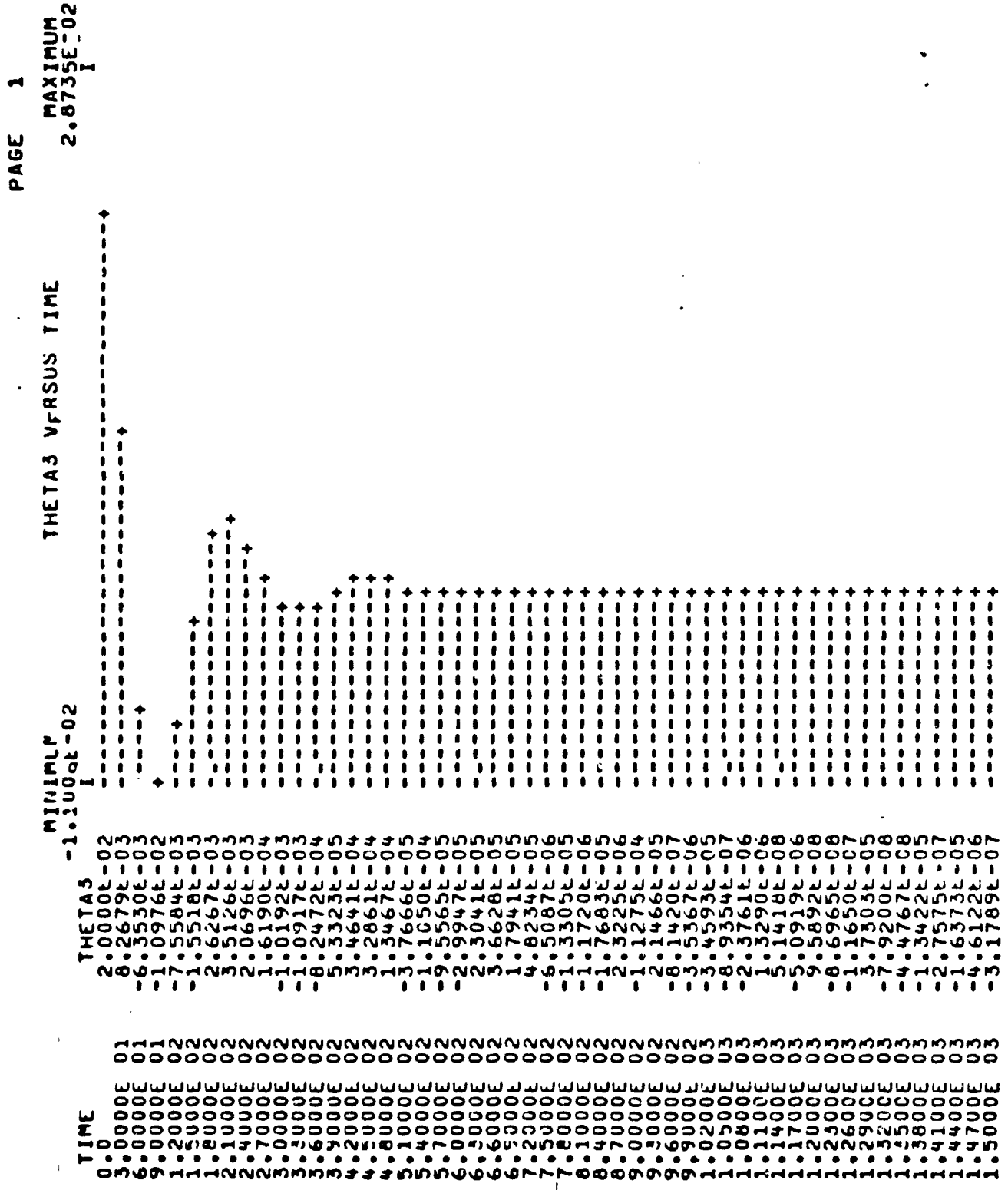

Theta 1 Time Response

$0 \leq t \leq 1500$

$s\omega 0 = 0$
$s\omega 1 = 1$
$s\omega 2 = 1$

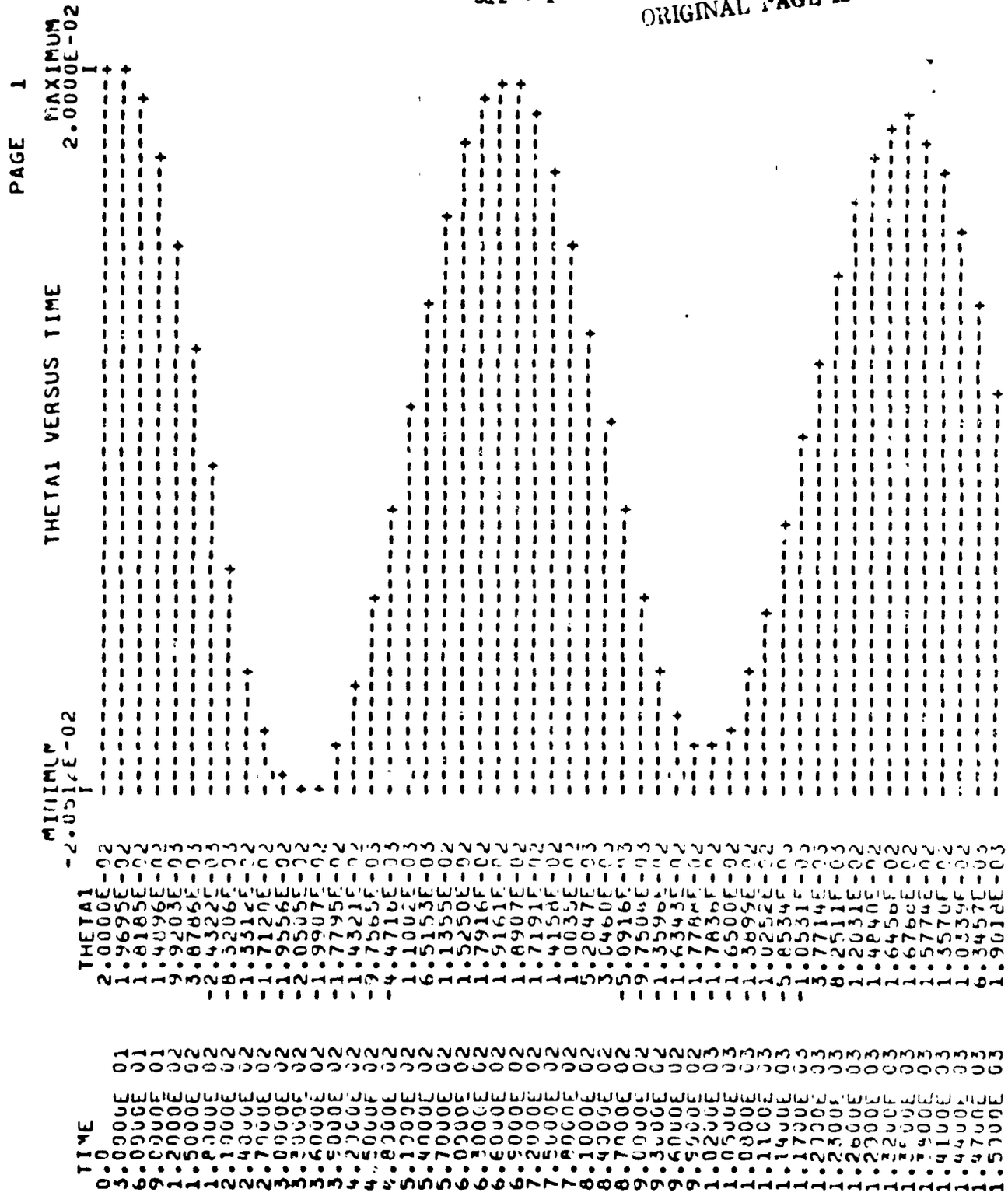

Theta 1 Time Response

$1530 \leq t \leq 3000$

sω0 = 0
sω1 = 1
sω2 = 1

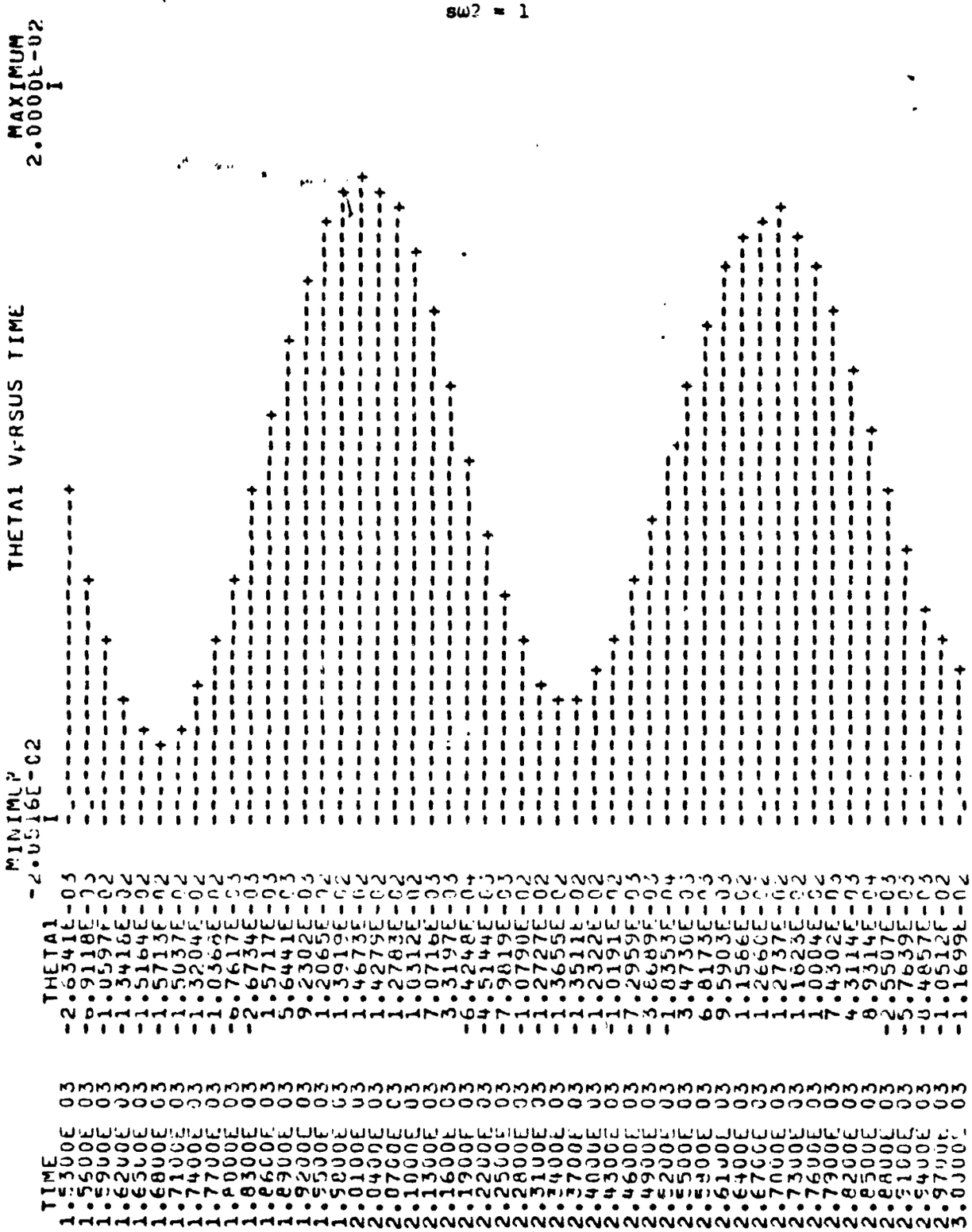

Theta 2 Time Response

$0 \leq t \leq 1500$

sw0 = 0
sw1 = 1
sw2 = 1

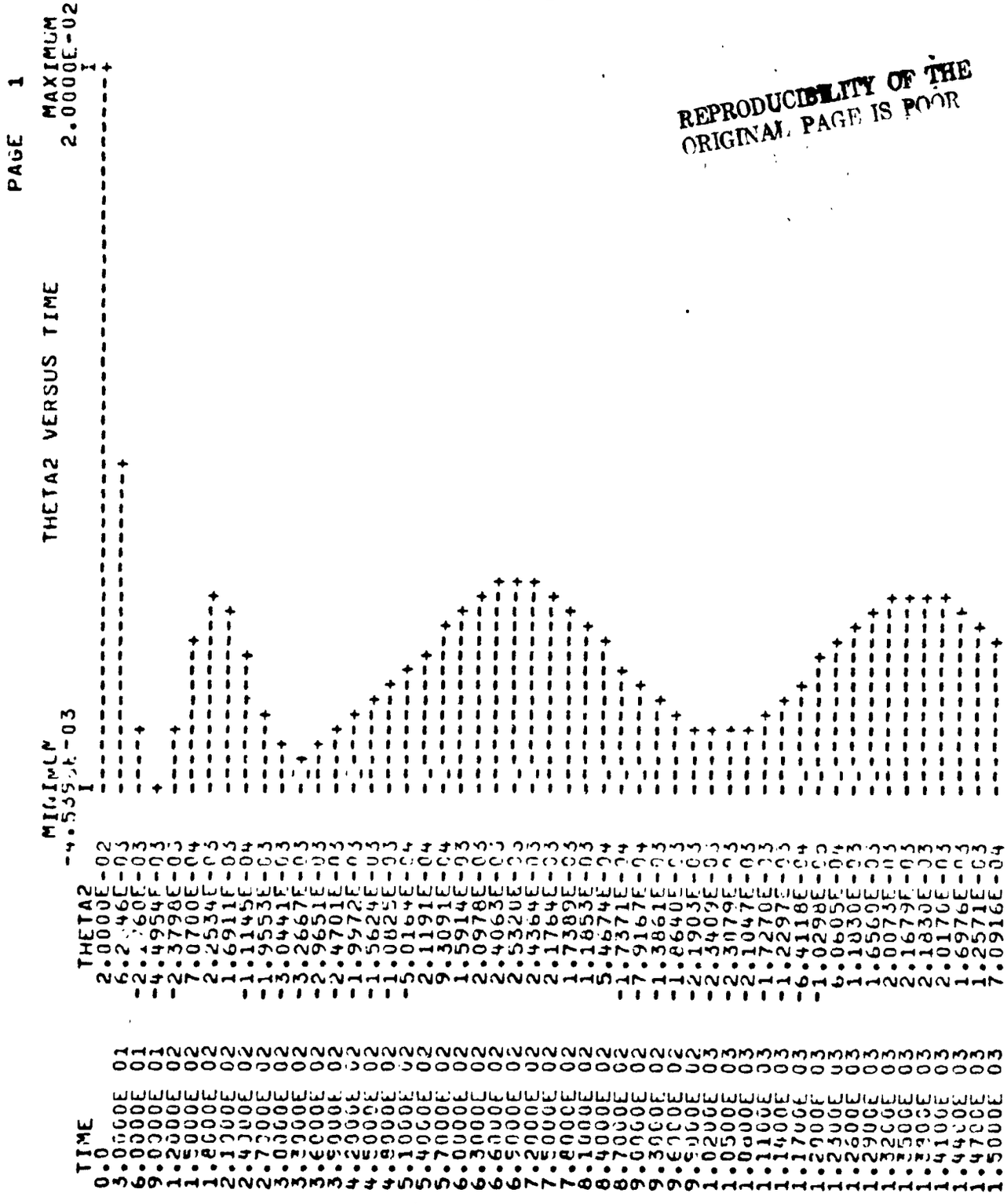

MINIMUM -8.8298E-03 THETA3 VERSUS TIME MAXIMUM 2.8735E-02

TIME	THETA3
0.0	2.0000E-02
3.0000E 01	9.3950E-03
6.0000E 01	-3.2742E-03
9.0000E 01	-6.7422E-03
1.2000E 02	-3.5667E-03
1.5000E 02	1.0588E-03
1.8000E 02	3.3737E-03
2.1000E 02	2.5359E-03
2.4000E 02	-1.6808E-04
2.7000E 02	-2.8925E-03
3.0000E 02	-4.5185E-03
3.3000E 02	-4.8910E-03
3.6000E 02	-4.4140E-03
3.9000E 02	-3.6677E-03
4.2000E 02	-2.9939E-03
4.5000E 02	-2.3444E-03
4.8000E 02	-1.6200E-03
5.1000E 02	-7.1706E-04
5.4000E 02	2.9629E-04
5.7000E 02	1.3904E-03
6.0000E 02	2.3761E-03
6.3000E 02	3.1497E-03
6.6000E 02	3.6399E-03
6.9000E 02	3.7673E-03
7.2000E 02	3.6672E-03
7.5000E 02	3.2478E-03
7.8000E 02	2.6121E-03
8.1000E 02	1.7793E-03
8.4000E 02	8.1989E-04
8.7000E 02	-1.3575E-04
9.0000E 02	-1.1864E-03
9.3000E 02	-2.0741E-03
9.6000E 02	-2.7949E-03
9.9000E 02	-3.2844E-03
1.0200E 03	-3.5125E-03
1.0500E 03	-3.4662E-03
1.0800E 03	-3.1408E-03
1.1100E 03	-2.5958E-03
1.1400E 03	-1.8434E-03
1.1700E 03	-9.6101E-04
1.2000E 03	-1.4095E-05
1.2300E 03	9.3536E-04
1.2600E 03	1.7814E-03
1.2900E 03	2.4916E-03
1.3200E 03	2.9781E-03
1.3500E 03	3.2648E-03
1.3800E 03	3.2603E-03
1.4100E 03	3.0195E-03
1.4400E 03	2.5462E-03
1.4700E 03	1.8711E-03
1.5000E 03	1.0809E-03

Theta 3 Time Response

0 ≤ t ≤ 1500

sw0 = 0

sw1 = 1

sw2 = 1

Appendix C

Costate and Control Equations For Modified Subproblem Hierarchy With Local Vertical Attitude Stabilization Control

$$\dot{\lambda}_{1,1} = 2 \sum_{i=1,2,3,6,11} W_{i,1} (\phi_i^* - \phi_1) + \omega_{1z} \rho_{1,3} - \omega_{1y} \rho_{1,5} \qquad (C-1)$$

For $i = 2,3$

$$\dot{\lambda}_{i,1} = 2 W_{i,1} (\phi_i^* - \phi_i) + \omega_{iz} \rho_{i,3} - \omega_{iy} \rho_{i,5} \qquad (C-2)$$

$$\dot{\lambda}_{6,1} = 2 [W_{6,1} (\phi_1^* - \phi_6) + W_{7,1} (\phi_7^* - \phi_6)] + \omega_{6z} \rho_{6,3}$$

$$- \omega_{6y} \rho_{6,5} \qquad (C-3)$$

$$\dot{\lambda}_{7,1} = 2 [W_{7,1} (\phi_6^* - \phi_7) + \sum_{i=9,10,20} W_{i,1} (\phi_i^* - \phi_7)]$$

$$+ \omega_{7z} \rho_{7,3} - \omega_{7y} \rho_{7,5} \qquad (C-4)$$

$$\dot{\lambda}_{8,1} = 2 W_{8,1} (\phi_8^* - \phi_8) + \omega_{8z} \rho_{8,3} - \omega_{8y} \rho_{8,5} \qquad (C-5)$$

For $i = 9, 10, 20$

$$\dot{\lambda}_{i,1} = 2 W_{i,1} (\phi_7^* - \phi_i) + \omega_{iz} \rho_{i,3} - \omega_{iy} \rho_{i,5} \qquad (C-6)$$

$$\dot{\lambda}_{11,1} = 2[W_{11,1}(\phi_1^* - \phi_{11}) + W_{12,1}(\phi_{12}^* - \phi_{11}) + W_{13,1}(\phi_{13}^* - \phi_{11})]$$

$$+ \omega_{11z}\rho_{11,3} - \omega_{11y}\rho_{11,5} \qquad (C\text{-}7)$$

For $i = 12, 13$

$$\dot{\lambda}_{i,1} = 2W_{i,1}(\phi_{11}^* - \phi_i) + \omega_{iz}\rho_{i,3} - \omega_{iy}\rho_{i,5} \qquad (C\text{-}8)$$

$$\dot{\lambda}_{1,2} = 2\sum_{i=1,2,3,6,11} W_{i,2}(\omega_{ix}^* - \omega_{1x}) - 2(a_{1x,1x,1x}\omega_{1x})_0\lambda_{1,2}$$

$$-\rho_{1,1} - (a_{1x,1x,1y}\omega_{1y} + a_{1x,1x,1z}\omega_{1z})_0\rho_{1,2}$$

$$-(a_{1y,1x,1x}\omega_{1x} + a_{1y,1x,1y}\omega_{1y} + a_{1y,1x,1z}\omega_{1z})_0\rho_{1,4}$$

$$-(2a_{1z,1x,1x}\omega_{1x} + a_{1z,1x,1y}\omega_{1y} + a_{1z,1x,1z}\omega_{1z})_0\rho_{1,6}$$

$$(C\text{-}9)$$

For $i = 2, 3$

$$\dot{\lambda}_{i,2} = 2W_{i,2}(\omega_{ix}^{*} - \omega_{ix}) - 2(a_{ix,ix,ix}\omega_{ix})_0 \lambda_{i,2} - \rho_{i,1}$$
$$- (a_{ix,ix,iy}\omega_{iy} + a_{ix,ix,iz}\omega_{iz})_0 \rho_{i,2}$$
$$- (2a_{iy,ix,ix}\omega_{ix} + a_{iy,ix,iy}\omega_{iy} + a_{iy,ix,iz}\omega_{iz})_0 \rho_{i,4}$$
$$- (2a_{iz,ix,ix}\omega_{ix} + a_{iz,ix,iy}\omega_{iy} + a_{iz,ix,iz}\omega_{iz})_0 \rho_{i,6}$$

(C-10)

$$\dot{\lambda}_{6,2} = 2[W_{6,2}(\omega_{1x}^{*} - \omega_{6x}) + W_{7,2}(\omega_{7x}^{*} - \omega_{6x})]$$
$$- 2(a_{6x,6x,6x}\omega_{6x})_0 \lambda_{6,2} - \rho_{6,1}$$
$$- (a_{6x,6x,6y}\omega_{6y} + a_{6x,6x,6z}\omega_{6z})_0 \rho_{6,2}$$
$$- (2a_{6y,6x,6x}\omega_{6x} + a_{6y,6x,6y}\omega_{6y} + a_{6y,6x,6z}\omega_{6z})_0 \rho_{6,4}$$
$$- (2a_{6z,6x,6x}\omega_{6x} + a_{6z,6x,6y}\omega_{6y} + a_{6z,6x,6z}\omega_{6z})_0 \rho_{6,6}$$

(C-11)

$$\dot{\lambda}_{7,2} = 2\left[W_{7,2}\left(\omega^*_{6x} - \omega_{7x}\right) + \sum_{i=9,10,20} W_{i,2}\left(\omega^*_{ix} - \omega_{7x}\right)\right]$$

$$-2\left(a_{7x,7x,7x}\omega_{7x}\right)_0 \lambda_{7,2} - \rho_{7,1}$$

$$-\left(a_{7x,7x,7y}\omega_{7y} + a_{7x,7x,7z}\omega_{7z}\right)_0 \rho_{7,2}$$

$$-\left(2a_{7y,7x,7x}\omega_{7x} + a_{7y,7x,7y}\omega_{7y} + a_{7y,7x,7z}\omega_{7z}\right)_0 \rho_{7,4}$$

$$-\left(2a_{7z,7x,7x}\omega_{7x} + a_{7z,7x,7y}\omega_{7y} + a_{7z,7x,7z}\omega_{7z}\right)_0 \rho_{7,6}$$

(C-12)

$$\dot{\lambda}_{8,2} = 2W_{8,2}\left(\omega^*_{8x} - \omega_{8x}\right) - 2\left(a_{8x,8x,8x}\omega_{8x}\right)_0 \lambda_{8,2} - \rho_{8,1}$$

$$-\left(a_{8x,8x,8y}\omega_{8y} + a_{8x,8x,8z}\omega_{8z}\right)_0 \rho_{8,2}$$

$$-\left(2a_{8y,8x,8x}\omega_{8x} + a_{8y,8x,8y}\omega_{8y} + a_{8y,8x,8z}\omega_{8z}\right)_0 \rho_{8,4}$$

$$-\left(2a_{8z,8x,8x}\omega_{8x} + a_{8z,8x,8y}\omega_{8y} + a_{8z,8x,8z}\omega_{8z}\right)_0 \rho_{8,6}$$

(C-13)

For $i = 9, 10, 20$

$$\dot{\lambda}_{i,2} = 2W_{i,2}(\omega^*_{7x} - \omega_{ix}) - 2(a_{ix,ix,ix}\omega_{ix})_0 \lambda_{i,2} - \rho_{i,1}$$
$$- (a_{ix,ix,iy}\omega_{iy} + a_{ix,ix,iz}\omega_{iz})_0 \rho_{i,2}$$
$$- (2a_{iy,ix,ix}\omega_{ix} + a_{iy,ix,iy}\omega_{iy} + a_{iy,ix,iz}\omega_{iz})_0 \rho_{i,4}$$
$$- (2a_{iz,ix,ix}\omega_{ix} + a_{iz,ix,iy}\omega_{iy} + a_{iz,ix,iz}\omega_{iz})_0 \rho_{i,6}$$

(C-14)

$$\dot{\lambda}_{11,2} = 2[W_{11,2}(\omega^*_{1x} - \omega_{11x}) + W_{12,2}(\omega^*_{12x} - \omega_{11x}) + W_{13,2}(\omega^*_{13x} - \omega_{11x})]$$
$$- 2(a_{11x,11x,11x}\omega_{11x})_0 \lambda_{11,2} - \rho_{11,1}$$
$$- (a_{11x,11x,11y}\omega_{11y} + a_{11x,11x,11z}\omega_{11z})_0 \rho_{11,2}$$
$$- (2a_{11y,11x,11x}\omega_{11x} + a_{11y,11x,11y}\omega_{11y} + a_{11y,11x,11z}\omega_{11z})_0 \rho_{11,4}$$
$$- (2a_{11z,11x,11x}\omega_{11x} + a_{11z,11x,11y}\omega_{11y} + a_{11z,11x,11z}\omega_{11z})_0 \rho_{11,6}$$

(C-15)

For $i = 12, 13$

$$\dot{\lambda}_{i,2} = 2W_{i,2}(\omega_{11x}^* - \omega_{ix}) - 2(a_{ix,ix,ix}\omega_{ix})_0 \lambda_{i,2}$$
$$- \rho_{i,1} - (a_{ix,ix,iy}\omega_{iy} + a_{ix,ix,iz}\omega_{iz})_0 \rho_{i,2}$$
$$- (2a_{iy,ix,ix}\omega_{ix} + a_{iy,ix,iy}\omega_{iy} + a_{iy,ix,iz}\omega_{iz})_0 \rho_{i,4}$$
$$- (2a_{iz,ix,ix}\omega_{ix} + a_{iz,ix,iy}\omega_{iy} + a_{iz,ix,iz}\omega_{iz})_0 \rho_{i,6}$$

(C-16)

$$\dot{\lambda}_{1,3} = 2\sum_{i=1,2,3,6,11} W_{i,3}(\theta_i^* - \theta_1) - \omega_{1z}\rho_{1,1} \qquad (C-17)$$

For $i = 2, 3$

$$\dot{\lambda}_{i,3} = 2W_{1,4}(\theta_1^* - \theta_i) - \omega_{iz}\rho_{i,1} \qquad (C-18)$$

$$\dot{\lambda}_{6,3} = 2[\bar{W}_{6,4}(\theta_1^* - \theta_6) + \bar{W}_{7,4}(\theta_7^* - \theta_6)] - \omega_{6,3}\rho_{6,1}$$

(C-19)

$$\dot{\lambda}_{7,3} = 2\left[W_{7,4}(\theta_6^* - \theta_7) + \sum_{i=9,10,20} W_{i,4}(\theta_i^* - \theta_7)\right] - \omega_{7,3}\rho_{7,1}$$

(C-20)

$$\dot{\lambda}_{8,3} = 2W_{8,4}(\theta_8^* - \theta_8) - \omega_{8,2}\rho_{8,1} \qquad (C-21)$$

For $i = 9, 10, 20$

$$\dot{\lambda}_{i,3} = 2W_{i,4}(\theta_7^* - \theta_i) - \omega_{i,2}\rho_{i,1} \qquad (C-22)$$

$$\dot{\lambda}_{11,3} = 2\left[W_{11,4}(\theta_1^* - \theta_{11}) + W_{12,4}(\theta_{12}^* - \theta_{11}) + W_{13,4}(\theta_{13}^* - \theta_{11})\right]$$

$$- \omega_{11,2}\rho_{11,1} \qquad (C-23)$$

For $i = 12, 13$

$$\dot{\lambda}_{i,3} = 2W_{i,4}(\theta_{11}^* - \theta_i) - \omega_{i,2}\rho_{i,1} \qquad (C-24)$$

$$\dot{\lambda}_{1,4} = 2\sum_{i=1,2,3,6,11} W_{i,5}\left(\omega^{*}_{iy} - \omega_{1y}\right) - 2\left(a_{1y,1y,1y}\,\omega_{1y}\right)_0 \lambda_{1,4}$$

$$-\left(a_{1x,1x,1y}\,\omega_{1x} + 2a_{1x,1y,1y}\,\omega_{1y} + a_{1x,1y,1z}\,\omega_{1z}\right)_0 \rho_{1,2}$$

$$-\rho_{1,3} - \left(a_{1y,1x,1y}\,\omega_{1x} + a_{1y,1y,1z}\,\omega_{1z}\right)_0 \rho_{1,4} - \phi_1\,\rho_{1,5}$$

$$-\left(a_{1z,1x,1y}\,\omega_{1x} + 2a_{1z,1y,1y}\,\omega_{1y} + a_{1z,1y,1z}\,\omega_{1z}\right)_0 \rho_{1,6}$$

(C-25)

For $i = 2, 3$

$$\dot{\lambda}_{i,4} = 2W_{i,5}\left(\omega^{*}_{1y} - \omega_{iy}\right) - 2\left(a_{iy,iy,iy}\,\omega_{iy}\right)_0 \lambda_{i,4}$$

$$-\left(a_{ix,ix,iy}\,\omega_{ix} + 2a_{ix,iy,iy}\,\omega_{iy} + a_{ix,iy,iz}\,\omega_{iz}\right)_0 \rho_{i,2}$$

$$-\rho_{i,3} - \left(a_{iy,ix,iy}\,\omega_{ix} + a_{iy,iy,iz}\,\omega_{iz}\right)_0 \rho_{i,4} - \phi_i\,\rho_{i,5}$$

$$-\left(a_{iz,ix,iy}\,\omega_{ix} + 2a_{iz,iy,iy}\,\omega_{iy} + a_{iz,iy,iz}\,\omega_{iz}\right)_0 \rho_{i,6}$$

(C-26)

$$\dot{\lambda}_{6,4} = 2\left[W_{6,5}\left(\omega^{*}_{1y} - \omega_{6y}\right) + W_{7,5}\left(\omega^{*}_{7y} - \omega_{6y}\right)\right]$$

$$- 2\left(a_{6y,6y,6y}\,\omega_{6y}\right)_0 \lambda_{6,4}$$

$$- \left(a_{6x,6x,6y}\,\omega_{6x} + 2a_{6x,6y,6y}\,\omega_{6y} + a_{6x,6y,6z}\,\omega_{6z}\right)_0 \rho_{6,2}$$

$$- \rho_{6,3} - \left(a_{6y,6x,6y}\,\omega_{6x} + a_{6y,6y,6z}\,\omega_{6z}\right)_0 \rho_{6,4} - \phi_6\,\rho_{6,5}$$

$$- \left(a_{6z,6x,6y}\,\omega_{6x} + 2a_{6z,6y,6y}\,\omega_{6y} + a_{6z,6y,6z}\,\omega_{6z}\right)_0 \rho_{6,6}$$

(C-27)

$$\dot{\lambda}_{7,4} = 2\left[W_{7,5}\left(\omega^{*}_{6y} - \omega_{7y}\right) + \sum_{i=9,10,20} W_{i,5}\left(\omega^{*}_{iy} - \omega_{7y}\right)\right]$$

$$- 2\left(a_{7y,7y,7y}\,\omega_{7y}\right)_0 \lambda_{7,4}$$

$$- \left(a_{7x,7x,7y}\,\omega_{7x} + 2a_{7x,7y,7y}\,\omega_{7y} + a_{7x,7y,7z}\,\omega_{7z}\right)_0 \rho_{7,2}$$

$$- \rho_{7,3} - \left(a_{7y,7x,7y}\,\omega_{7x} + a_{7y,7y,7z}\,\omega_{7z}\right)_0 \rho_{7,4}$$

$$- \phi_6\,\rho_{7,5}$$

$$- \left(a_{7z,7x,7y}\,\omega_{7x} + 2a_{7z,7y,7y}\,\omega_{7y} + a_{7z,7y,7z}\,\omega_{7z}\right)_0 \rho_{7,6}$$

(C-28)

$$\dot{\lambda}_{8,4} = 2W_{8,5}(\omega^*_{8Y} - \omega_{8Y}) - 2(a_{8Y,8Y,8Y}\omega_{8Y})_0 \lambda_{8,4}$$

$$-(a_{8X,8X,8Y}\omega_{8X} + 2a_{8X,8Y,8Y}\omega_{8Y} + a_{8X,8Y,8Z}\omega_{8Z})_0 \lambda_{8,2}$$

$$-\lambda_{8,3} - (a_{8Y,8X,8Y}\omega_{8X} + a_{8Y,8Y,8Z}\omega_{8Z})_0 \lambda_{8,4} - \phi_8 \lambda_{8,5}$$

$$-(a_{8Z,8X,8Y}\omega_{8X} + 2a_{8Z,8Y,8Y}\omega_{8Y} + a_{8Z,8Y,8Z}\omega_{8Z})_0 \lambda_{8,6}$$

(C-29)

For $i = 9, 10, 20$

$$\dot{\lambda}_{i,4} = 2W_{i,5}(\omega^*_{iY} - \omega_{iY}) - 2(a_{iY,iY,iY}\omega_{iY})_0 \lambda_{i,4}$$

$$-(a_{iX,iX,iY}\omega_{iX} + 2a_{iX,iY,iY}\omega_{iY} + a_{iX,iY,iZ}\omega_{iZ})_0 \lambda_{i,2}$$

$$-\lambda_{i,3} - (a_{iY,iX,iY}\omega_{iX} + a_{iY,iY,iZ}\omega_{iZ})_0 \lambda_{i,4} - \phi_i \lambda_{i,5}$$

$$-(a_{iZ,iX,iY}\omega_{iX} + 2a_{iZ,iY,iY}\omega_{iY} + a_{iZ,iY,iZ}\omega_{iZ})_0 \lambda_{i,6}$$

(C-30)

$$\dot{\lambda}_{11,4} = 2[W_{11,5}(\omega^*_{11y} - \omega_{11y}) + W_{12,5}(\omega^*_{12y} - \omega_{11y}) + W_{13,5}(\omega^*_{13y} - \omega_{11y})]$$

$$-2(a_{11y,11y,11y}\omega_{11y})_0 \lambda_{11,4}$$

$$-(a_{11x,11x,11y}\omega_{11x} + 2a_{11x,11y,11y}\omega_{11y} + a_{11x,11y,11z}\omega_{11z})_0 \rho_{11,4}$$

$$-\rho_{11,3} - (a_{11y,11x,11y}\omega_{11x} + a_{11y,11y,11z}\omega_{11z})_0 \rho_{11,4}$$

$$-\phi_{11}\rho_{11,5}$$

$$-(a_{11z,11x,11y}\omega_{11x} + 2a_{11z,11y,11y}\omega_{11y} + a_{11z,11y,11z}\omega_{11z})_0 \rho_{11,6}$$

(C-31)

For $i = 12, 13$

$$\dot{\lambda}_{i,4} = 2W_{i,5}(\omega^*_{11y} - \omega_{iy}) - 2(a_{iy,iy,iy}\omega_{iy})_0 \lambda_{i,4}$$

$$-(a_{ix,ix,iy}\omega_{ix} + 2a_{ix,iy,iy}\omega_{iy} + a_{ix,iy,iz}\omega_{iz})_0 \rho_{i,2}$$

$$-\rho_{i,3} - (a_{iy,ix,iy}\omega_{ix} + a_{iy,iy,iz}\omega_{iz})_0 \rho_{i,4}$$

$$-\phi_i \rho_{i,5}$$

(C-32)

$$-(a_{iz,ix,iy}\omega_{ix} + 2a_{iz,iy,iy}\omega_{iy} + a_{iz,iy\,iz}a_{iz})_0 \rho_{i,6}$$

$$\dot{\lambda}_{1,5} = 2\sum_{i=1,2,3,6,11} W_{i,7}\left(\psi_i^* - \psi_1\right) \qquad (C\text{-}33)$$

For $i = 2, 3$

$$\dot{\lambda}_{i,5} = 2W_{i,7}\left(\psi_1^* - \psi_i\right) \qquad (C\text{-}34)$$

$$\dot{\lambda}_{6,5} = 2\left[W_{6,7}\left(\psi_1^* - \psi_6\right) + W_{7,7}\left(\psi_7^* - \psi_6\right)\right] \qquad (C\text{-}35)$$

$$\dot{\lambda}_{7,5} = 2\left[W_{7,7}\left(\psi_6^* - \psi_7\right) + \sum_{i=9,10,20} W_{i,7}\left(\psi_i^* - \psi_7\right)\right] \qquad (C\text{-}36)$$

$$\dot{\lambda}_{8,5} = 2W_{8,7}\left(\psi_8^* - \psi_8\right) \qquad (C\text{-}37)$$

For $i = 9, 10, 20$

$$\dot{\lambda}_{i,5} = 2W_{i,7}\left(\psi_7^* - \psi_i\right) \qquad (C\text{-}38)$$

$$\dot{\lambda}_{11,5} = 2\left[W_{11,7}\left(\psi_1^* - \psi_i\right) + W_{12,7}\left(\psi_{12}^* - \psi_i\right) + W_{13,7}\left(\psi_{13}^* - \psi_i\right)\right] \qquad (C\text{-}39)$$

For $i = 12, 13$

$$\dot{\lambda}_{i,5} = 2W_{i,7}\left(\psi_{11}^* - \psi_i\right) \qquad (C\text{-}40)$$

$$\dot{\lambda}_{1,6} = 2\sum_{i=1,2,3,6,11} W_{i,8}(\omega^*_{iz} - \omega_{1z}) - 2(a_{1z,1z,1z}\omega_{1z})_0 \lambda_{1,6} - \theta_1 p_{1,1}$$

$$- (a_{1x,1x,1z}\omega_{1x} + a_{1x,1y,1z}\omega_{1y} + 2a_{1x,1z,1z}\omega_{1z})_0 p_{1,2} + \phi_1 p_{1,3}$$

$$- (a_{1y,1x,1z}\omega_{1x} + a_{1y,1y,1z}\omega_{1y} + 2a_{1y,1z,1z}\omega_{1z})_0 p_{1,4} - p_{1,5}$$

$$- (a_{1z,1x,1z}\omega_{1x} + a_{1z,1y,1z}\omega_{1y})_0 p_{1,6} \qquad (C\text{-}41)$$

For $i = 2, 3$

$$\dot{\lambda}_{i,6} = 2W_{i,8}(\omega^*_{1z} - \omega_{iz}) - 2(a_{iz,iz,iz}\omega_{iz})_0 \lambda_{i,6} - \theta_i p_{i,1}$$

$$- (a_{ix,ix,iz}\omega_{ix} + a_{ix,iy,iz}\omega_{iy} + 2a_{ix,iz,iz}\omega_{iz})_0 p_{i,2}$$

$$+ \phi_i p_{i,3} - (a_{iy,ix,iz}\omega_{ix} + a_{iy,iy,iz}\omega_{iy} + 2a_{iy,iz,iz}\omega_{iz})_0 p_{i,4}$$

$$- p_{i,5} - (a_{iz,ix,iz}\omega_{ix} + a_{iz,iy,iz}\omega_{iy})_0 p_{i,6}$$

$$(C\text{-}42)$$

$$\dot{\lambda}_{6,6} = 2\left[W_{6,8}\left(\omega_{12}^{*} - \omega_{6z}\right) + W_{7,8}\left(\omega_{7z}^{*} - \omega_{6z}\right)\right]$$

$$-2\left(a_{6z,6z,6z}\,\omega_{6z}\right)_0 \lambda_{6,6} - \Theta_6 P_{6,1}$$

$$-\left(a_{6x,6x,6z}\,\omega_{6x} + a_{6x,6y,6z}\,\omega_{6y} + 2a_{6x,6z,6z}\,\omega_{6z}\right)_0 P_{6,2}$$

$$+\Phi_6 P_{6,3} - \left(a_{6y,6x,6z}\,\omega_{6x} + a_{6y,6y,6z}\,\omega_{6y} + 2a_{6y,6z,6z}\,\omega_{6z}\right)_0 P_{6,4}$$

$$-P_{6,5} - \left(a_{6z,6x,6z}\,\omega_{6x} + a_{6z,6y,6z}\,\omega_{6y}\right)_0 P_{6,6} \qquad (C\text{-}43)$$

$$\dot{\lambda}_{7,6} = 2\left[W_{7,8}\left(\omega_{6z}^{*} - \omega_{7z}\right) + \sum_{i=9,10,20} W_{i,8}\left(\omega_{iz}^{*} - \omega_{7z}\right)\right]$$

$$-2\left(a_{7z,7z,7z}\,\omega_{7z}\right)_0 \lambda_{7,6} - \Theta_7 P_{7,1}$$

$$-\left(a_{7x,7x,7z}\,\omega_{7x} + a_{7x,7y,7z}\,\omega_{7y} + 2a_{7x,7z,7z}\,\omega_{7z}\right)_0 P_{7,2}$$

$$+\Phi_7 P_{7,3} - \left(a_{7y,7x,7z}\,\omega_{7x} + a_{7y,7y,7z}\,\omega_{7y} + 2a_{7y,7z,7z}\,\omega_{7z}\right)_0 P_{7,4}$$

$$-P_{7,5} - \left(a_{7z,7x,7z}\,\omega_{7x} + a_{7z,7y,7z}\,\omega_{7y}\right)_0 P_{7,6} \qquad (C\text{-}44)$$

$$\dot{\lambda}_{8,6} = 2W_{8,8}(\omega^*_{8z} - \omega_{8z}) - 2(a_{8z,8z,8z}\omega_{8z})_0 \lambda_{8,6} - \Theta_8 P_{8,1}$$

$$-(a_{8x,8x,8z}\omega_{8x} + a_{8x,8y,8z}\omega_{8y} + 2a_{8x,8z,8z}\omega_{8z})_0 P_{8,2}$$

$$+\Phi_8 P_{8,3} - (a_{8y,8x,8z}\omega_{8x} + a_{8y,8y,8z}\omega_{8y} + 2a_{8y,8z,8z}\omega_{8z})_0 P_{8,4}$$

$$-P_{8,5} - (a_{8z,8x,8z}\omega_{8x} + a_{8z,8y,8z}\omega_{8y})_0 P_{8,6} \qquad (C\text{-}45)$$

for $i = 9, 10, 20$

$$\dot{\lambda}_{i,6} = 2W_{i,8}(\omega^*_{iz} - \omega_{iz}) - 2(a_{iz,iz,iz}\omega_{iz})_0 \lambda_{i,6} - \Theta_i P_{i,1}$$

$$-(a_{ix,ix,iz}\omega_{ix} + a_{ix,iy,iz}\omega_{iy} + 2a_{ix,iz,iz}\omega_{iz})_0 P_{i,2}$$

$$+\Phi_i P_{i,3} - (a_{iy,ix,iz}\omega_{ix} + a_{iy,iy,iz}\omega_{iy} + 2a_{iy,iz,iz}\omega_{iz})_0 P_{i,4}$$

$$-P_{i,5} - (a_{iz,ix,iz}\omega_{ix} + a_{iz,iy,iz}\omega_{iy})_0 P_{i,6} \qquad (C\text{-}46)$$

$$\dot{\lambda}_{11,6} = 2[W_{11,8}(\omega^*_{12} - \omega_{11z}) + W_{12,8}(\omega^*_{12z} - \omega_{11z}) + W_{13,8}(\omega^*_{13z} - \omega_{11z})]$$

$$- 2(a_{11z,11z,11z}\omega_{11z})_o \lambda_{11,6} - \Theta_{11} P_{11,1}$$

$$-(a_{11x,11x,11z}\omega_{11x} + a_{11x,11y,11z}\omega_{11y} + 2a_{11x,11z,11z}\omega_{11z})_o I_{11,2}$$

$$+ \Phi_{11} P_{11,3}$$

$$-(a_{11y,11x,11z}\omega_{11z} + a_{11y,11y,11z}\omega_{11y} + 2a_{11y,11z,11z}\omega_{11z})_o I_{11,4}$$

$$-P_{11,5} - (a_{11z,11x,11z}\omega_{11x} + a_{11z,11y,11z}\omega_{11y})_o P_{11,6}$$

(C-47)

For $\lambda = 12, 13$

$$\dot{\lambda}_{\lambda,6} = 2W_{\lambda,8}(\omega^*_{11z} - \omega_{\lambda z}) - 2(a_{\lambda z,\lambda z,\lambda z}\omega_{\lambda z})_o \lambda_{\lambda,6} - \Theta_\lambda P_{\lambda,1}$$

$$-(a_{\lambda x,\lambda x,\lambda z}\omega_{\lambda x} + a_{\lambda x,\lambda y,\lambda z}\omega_{\lambda y} + 2a_{\lambda x,\lambda z,\lambda z}\omega_{\lambda z})_o I_{\lambda,2}$$

$$+ \Phi_\lambda P_{\lambda,3}$$

$$-(a_{\lambda y,\lambda x,\lambda z}\omega_{\lambda x} + a_{\lambda y,\lambda y,\lambda z}\omega_{\lambda y} + 2a_{\lambda y,\lambda z,\lambda z}\omega_{\lambda z})_o I_{\lambda,4}$$

$$-P_{\lambda,5} - (a_{\lambda z,\lambda x,\lambda z}\omega_{\lambda x} + a_{\lambda z,\lambda y,\lambda z}\omega_{\lambda y})_o P_{\lambda,6}$$

(C-48)

Substitution of equation (200) in equation (169) eliminates the term, $\nu_{i,1}$, from equation (169). Equation (169) may then be written in the following form.

$$\frac{\partial H}{\partial T_{aix}} = 2 W_{i,3} T_{ix} + \frac{(I_i')_{11}}{|I_i'|} \lambda_{i,2} + \frac{2(I_i')_{12}}{|I_i'|} \rho_{i,4}$$

$$+ \frac{2(I_i')_{13}}{|I_i'|} \qquad (C-49)$$

Similarly, equation (202) may be substituted into equation (170) to obtain the following

$$\frac{\partial H}{\partial T_{aiy}} = 2 W_{i,6} T_{iy} + \frac{(I_i')_{22}}{|I_i'|} \lambda_{i,4} + 2 \frac{(I_i')_{21}}{|I_i'|} \rho_{i,2}$$

$$+ \frac{2(I_i')_{23}}{|I_i'|} \rho_{i,6} \qquad (C-50)$$

Substitution of equation (204) in (171) yields.

$$\frac{\partial H}{\partial T_{a_i 2}} = 2 W_{i,9} T_{i2} + \frac{(I_i')_{33}}{|I_i'|} \lambda_{i,6} + 2 \frac{(I_i')_{31}}{|I_i'|} \rho_{i,2}$$

$$+ \frac{2 (I_i')_{32}}{|I_i'|} \rho_{i,4} \qquad (C\text{-}51)$$